Spring 5-31-2001

Predicting thermodynamic and transport parameters for metal contaminant sorption to hydrated metal oxides in aquatic systems

Paras Trivedi
New Jersey Institute of Technology

ABSTRACT

PREDICTING THERMODYNAMIC AND TRANSPORT PARAMETERS FOR METAL CONTAMINANT SORPTION TO HYDRATED METAL OXIDES IN AQUATIC SYSTEMS

by
Paras Trivedi

Hydrated oxides such as HAO, HFO, goethite, and HMO are prevalent in soils and sediments as discrete particles or as coatings. These microporous oxides have large surface areas and high affinity for metal ions, and hence they act as both a sink and a source for anthropogenically released metal contaminants. To better understand risks posed by metals in the environment and to develop effective waste management programs, mechanistic models are needed to accurately predict their fate in soils and sediments.

To achieve this objective, sorption of metal ions Sr, Cd, Zn, Ni, and Ca to these oxides were studied with macroscopic as well as spectroscopic experiments, as a function of pH, ionic strength, concentration, temperature, and reaction time. Macroscopic studies in combination with the XAS investigations suggest that the sorption of divalent metal ions to amorphous oxides is a two-step process: rapid adsorption to the external surface followed by slow intraparticle diffusion along the micropore walls. Adsorption is an endothermic physical reaction that can be represented by one average mechanism or site independent of pH and adsorbate concentration. Accordingly, the sorbed ions retain their primary hydration shell and form an outer sphere complex. Hence, adsorption enthalpies ($\Delta H°$) can be predicted from their primary hydration number (N) and the hydrated radius (R_H). The site capacities of these oxides are a function of pH and can be estimated from their surface charge densities.

On the other hand, metal ions form mononuclear inner sphere complexes with goethite. Although goethite may show a higher affinity for metal ions than HFO, its site capacity is much smaller than that of HFO. Macroscopic analyses disclosed two sets of adsorption sites on the goethite surface: a small set of high affinity sites available to transition metal ions and a large set of low affinity sites to which only alkaline earth metals bind. This limited availability of high affinity sites induces competitive adsorption between Ni and Zn, which can be described with the single-site Langmuir model.

XAS investigations of intraparticle diffusion studies revealed that the local structure of metal ions sorbed to amorphous oxides do not change with time suggesting that the internal sites are similar to the external ones. Modeling resulted in diffusivities ranging from 10^{-16} to 10^{-10} cm^2 s^{-1}. Therefore, surface diffusion of metal ions along the micropore walls may take from a few days to few years to reach equilibrium. Based on site activation theory, surface diffusivities can be estimated knowing the activation energy and site capacity. From Polanyi relation, E_A is linearly proportional to $\Delta H°$, and is comparable for adsorption of a specific metal to HAO, HFO, and HMO. Furthermore, because metals of the same group in the Periodic Table form similar sorption complexes, the Polanyi constant (α) was equivalent. Strong similarities in the local structure of Ni and Zn ions sorbed to HMO corroborate this hypothesis. Interestingly, surface diffusion was not important with goethite.

Overall this research renders an insight into the mechanisms by which hydrated metal oxides control the partitioning and bioavailability of metal contaminants. This study provides methods that can accurately predict important transport and thermodynamic parameters for describing the fate of these pollutants.

PREDICTING THERMODYNAMIC AND TRANSPORT PARAMETERS FOR METAL CONTAMINANT SORPTION TO HYDRATED METAL OXIDES IN AQUATIC SYSTEMS

by
Paras Trivedi

A Dissertation
Submitted to the Faculty of
New Jersey Institute of Technology
In Partial Fulfillment of the Requirements for the Degree of
Doctor of Philosophy in Environmental Engineering

Department of Civil and Environmental Engineering

May 2001

APPROVAL PAGE

PREDICTING THERMODYNAMIC AND TRANSPORT PARAMETERS FOR METAL CONTAMINANT SORPTION TO HYDRATED METAL OXIDES IN AQUATIC SYSTEMS

Paras Trivedi

Dr. Lisa Axe, Dissertation Advisor Associate Professor of Civil and Environmental Engineering, NJIT	Date
Dr. Robert Dresnack, Committee Member Professor of Civil and Environmental Engineering, NJIT	Date
Dr. Hsin-Neng Hsieh, Committee Member Professor of Civil and Environmental Engineering, NJIT	Date
Dr. Jay N. Meegoda, Committee Member Professor of Civil and Environmental Engineering, NJIT	Date
Dr. Kamalesh K. Sirkar, Committee Member Distinguished Professor of Chemical Engineering, NJIT	Date
Dr. Trevor A. Tyson, Committee Member Associate Professor of Physics, NJIT	Date

BIOGRAPHICAL SKETCH

Author Paras Trivedi

Degree Doctor of Philosophy

Education

2001 Ph.D. in Environmental Engineering, New Jersey Institute of Technology, Newark, NJ

1996 M.S. in Chemical Engineering, Louisiana Tech University, Ruston, LA

1992 B.E. in Chemical Engineering, University of Pune, India

Work Experience

1997-2001 Research Assistant; New Jersey Institute of Technology, Newark, NJ
Supported through an NSF Grant and a DuPont Young Professor Grant. Studied sorption of metals to hydrous Al, Fe, and Mn oxides using macroscopic and spectroscopic analyses. This research involved developing methods to predict thermodynamic and transport parameters for metal sorption to amorphous oxides. Also, conducted research on competitive adsorption of metals to goethite, including macroscopic and spectroscopic studies.

1996-1997 Graduate Assistant, New Jersey Institute of Technology
Assisted in laboratory for water and wastewater analysis classes.

1995-1996 Research Assistant, Louisiana Tech University, Ruston, LA
Conducted research on biological conversion of carbon monoxide from landfills to liquids and fuels using the anaerobic bacteria (PS-1) isolated from petroleum-contaminated soil.

1993-1995 Sales Officer/Chemical Engineer, Dearborn IEI India Pvt. Ltd., Bombay, India
Supported and managed projects dealing with chemical treatment of cooling and boiling waters. Held similar position with their subsidiary Ion Exchange.

1992-1993 Sales Officer/Chemical Engineer Trainee, Vijay Chemicals, Bombay, India
Trained on projects dealing with chemical treatment of cooling and boiling waters.

Publications

Trivedi, P., and L. Axe, 2001,Final Report on "Adsorption of Metal Ions onto Goethite: Single-Adsorbate and Competitive Systems", DuPont Engineering Technology.

Trivedi, P., Axe, L., and T. Tyson, 2001, XAS Studies of Ni and Zn Sorbed to Hydrous Manganese Oxide *in preparation.*

Axe, L., and P. Trivedi, 2001, Sorption and Attenuation of Metal Contaminants to Iron Oxides: Amorphous versus Crystalline *in preparation.*

Trivedi, P., Axe, L., and T. Tyson, 2001, An Analysis of Zinc Sorption to Amorphous versus Crystalline Iron Oxides using XAS *in preparation*

Trivedi, P., and L. Axe, 2001, Predicting Metal Sorption to Hydrous Al, Fe and Mn Oxides *Environ. Sci. Tech. Environ. Sci. Tech.* 35, 1779-1784.

Trivedi, P., Axe, L., and J. Dyer, 2001, Adsorption of Metal Ions onto Goethite: Single-Adsorbate and Competitive Systems *Special Volume of Journal of Colloids and Surfaces A: Physicochemical and Engineering Aspects,* in press.

Axe, L., Anderson P.R., and P. Trivedi, 2001, Diffusion along Oxides and Related Surfaces *Encyclopedia of Surface and Colloid Science* (A. Hubbard Ed.) Marcel Dekker, in press.

Trivedi, P., and L. Axe, 2000, Modeling Cd and Zn Sorption to Hydrous Metal Oxides *Environ. Sci. Tech.* 34, 2215-2223.

Axe, L., Tyson, T. Trivedi, P., and T. Morrison, 2000, Local Structure Analysis of Strontium Sorption to Hydrous Manganese Oxide *J. Colloid Interface Sci.* 224, 408-416.

Trivedi, P., and L. Axe, 1999, A Comparison of Strontium Sorption to Hydrous Aluminum, Iron, and Manganese Oxides *J. Colloid Interface Sci.* 218, 554-563.

Presentations

Trivedi, P., Axe, L., and T. Tyson, Zn Sorption to Hydrous Metal Oxides: An Investigation with XAS, 75th ACS Colloid and Surface Science Symposium, American Chemical Society – Carnegie Mellon University, PA; June 10-13, 2001.

Trivedi, P., Axe, L., and J. Dyer, Adsorption of Metal Ions onto Goethite: Single-Adsorbate and Competitive Systems, 75th ACS Colloid and Surface Science Symposium, American Chemical Society – Carnegie Mellon University, PA; June 10-13, 2001.

Trivedi, P., Axe, L. and T. Tyson, Macroscopic and Spectroscopic Studies of Transition Metal Sorption to Hydrous Metal Oxides in Aquatic Environments, Chemical Speciation and Reactivity in Water Chemistry and Water Technology: A Symposium in Honor of James J. Morgan, 220th American Chemical Society National Meeting - Washington D.C.; August 20-24, 2000.

Upadhya, H., Axe, L., Trivedi, P., and J. Dyer, Competitive Adsorption Studies of Ni, Zn, and Ca to Goethite: Single, Binary, and Ternary Systems, 32nd Mid-Atlantic Industrial and Hazardous Waste Conference – Rensselaer Polytechnic Institute, NY; June 26-29 2000.

Trivedi, P. and L. Axe, Predicting Nickel Sorption to Hydrous Metal Oxides, 74th Colloid and Surface Science Symposium, American Chemical Society - Lehigh University, PA; June 21-24, 2000.

Trivedi, P., and L. Axe, Modeling Cd and Zn Sorption to Hydrous Metal Oxides, presented at Colloid and Interfacial Phenomena in Aquatic Environment Symposium, 217th American Chemical Society National Meeting - Anaheim, CA; March 22-24, 1999.

Axe, L., Tyson, T. Trivedi, P., and T. Morrison, Local Structure Analysis of Strontium Sorption to Hydrous Manganese Oxide, 216th American Chemical Society National Meeting -Boston, MA; August 23-27, 1998.

Trivedi, P., and L. Axe, Characterization of Hydrous Aluminum Oxide and Sorption Studies with Sr and Cd, 72nd Colloid and Surface Science Symposium, American Chemical Society - Penn State University, PA; June 21-24, 1998.

Awards

2000-2001	DuPont Graduate Fellow
2000	Runners-up Award, Poster Presentation Competition at Chemical Speciation and Reactivity in Water Chemistry and Water

2000	Runners-up Award, Poster Presentation Competition at Chemical Speciation and Reactivity in Water Chemistry and Water Technology: A Symposium in Honor of James Morgan, 220th ACS National Meeting, Washington D.C.
1999	Certificate of Merit, Division of Environmental Chemistry; American Chemical Society National Meeting, New Orleans, LA
1998-2000	Recipient of the Graduate Student Achievement Award, NJIT
1997-2000	NSF Graduate Assistantship

"Water is the only drink for a wise man"

H. D. Thoreau, Walden, 1857

ACKNOWLEDGEMENT

The so-called journey of my life, towards this milestone, has been a great learning and a very exciting experience. I cannot stop thanking nature for this incredible experience – in short I feel fortunate to have lived this life. I feel fortunate in many ways. One of the top blessings was my association with my research advisor, Dr. Lisa Axe – a very strong force behind my success. I would like to thank her with all my heart and soul for not only providing me her valuable time, energy, and insight throughout this program, but also for giving me all the encouragement and reassurance.

I would also like to express my special gratitude to Dr. Trevor Tyson for imparting me with his knowledge on the spectroscopic studies as well as for serving on my research committee. My sincere thanks to all Dr. Robert Dresnack, Dr. Hsin-Neng Hsieh, Dr. Jay N. Meegoda, and Dr. Kamalesh Sirkar for all their valuable inputs while actively participating in my committee. I also would like to all my professors, laboratory staff, and the secretaries in the department of Civil and Environmental Engineering for constant guidance and help. I would also like to thank Dr. Kaumudi Pandya and Larry Fareria at NSLS in Brookhaven National Laboratory (N.Y.) for all the technical support. I would also like to thank Jim Dyer at DuPont Engineering Technology for all the support and input.

All my fellow graduate students also deserve recognition for their support and friendship. Special thanks to my friends Kyle, Michelle, Ames, Tony, and Mike – you made my life happier. To my family – I am glad you believed in me.

Mom, I hope I did you proud.

TABLE OF CONTENTS

TABLE OF CONTENTS
(Continued)

TABLE OF CONTENTS
(Continued)

Chapter **Page**

LIST OF TABLES

LIST OF FIGURES

LIST OF FIGURES
(Continued)

Figure **Page**

LIST OF FIGURES
(Continued)

LIST OF FIGURES
(Continued)

Figure **Page**

LIST OF FIGURES
(Continued)

Figure **Page**

LIST OF FIGURES
(Continued)

Figure **Page**

LIST OF FIGURES
(Continued)

Figure **Page**

LIST OF SYMBOLS

A	=	surface area in m^2
C	=	metal sorbed in moles g^{-1} oxide
C_t	=	maximum site capacity in moles g^{-1}
C_v	=	number of adsorption sites available in moles g^{-1}
D_s	=	surface diffusivity in $cm^2\ s^{-1}$
E_A	=	activation energy in kcal mol^{-1}
I	=	transmission flux in V
I_F	=	fluorescence flux in V
I_O	=	incident flux in V
K	=	adsorption equilibrium constant
k	=	photoelectron momentum space in $Å^{-1}$
K_d	=	linear distribution coefficient in L g^{-1}
K_F	=	Freundlich isotherm equilibrium constant
K_i	=	internal distribution coefficient in L g^{-1}
m	=	molecular weight
N	=	primary hydration number
N_i	=	coordination number (i =1,2,3…)
r	=	radial distance in cm
R	=	Universal gas constant in kcal mol^{-1} cal
R_i	=	average radial distance (i =1, 2, 3…)
Re	=	Reynolds' number
R_H	=	hydrated radius of metal ion in Å

LIST OF SYMBOLS
(Continued)

S	=	bulk aqueous metal concentration in M
S_o^2	=	amplitude reduction factor
t	=	time
T	=	temperature in K or ^oC
U	=	surface potential
Z	=	ionic charge
ΔG^o	=	Gibbs Free energy in kcal mol^{-1}
ΔH^o	=	adsorption enthalpy in kcal mol^{-1}
ΔS^o	=	entropies in kcal mol^{-1} K^{-1}
α	=	Polanyi constant
$\chi(k)$	=	interference function
δ	=	phase shift
ε	=	porosity
ϕ	=	phase of the complex electron scattering amplitude
λ	=	mean distance between the neighboring sites in cm
μ	=	ionic strength in M
θ	=	Bragg's diffraction angle in degrees
ρ	=	bulk density in cm^3 g^{-1}
ρ_n	=	radial structure function

LIST OF SYMBOLS
(Continued)

σ = surface charge density in C g^{-1}

σ^2 = Debye-Waller factor in $Å^2$

Γ_H = net proton sorption density in moles m^2

Γ_{OH} = net hydroxyl sorption density in moles m^2

LIST OF COPYRIGHT PERMITTED ARTICLES

Copyright permission has been obtained from the publishers to reproduce part or all of the contents of the following referenced articles in this dissertation:

"Sr Diffuison and Reaction within Fe Oxides: Evaluation of the Rate-Limitng Mechanism for Sorption" by Lisa Axe and Paul Anderson, from Journal of Colloid and Interface Science, Volume 175, 157-165, copyright © 1995 by Academic Press.

"Experimental and Theoretical Diffusivities of Cd and Sr in Hydrous Ferric Oxide" by Lisa Axe and Paul Anderson, from Journal of Colloid and Interface Science, Volume 185, 436-448, copyright © 1997 by Academic Press.

"A Comparison of Strontium sorption to Hydrous Aluminum, Iron, and Manganese Oxides" by Paras Trivedi and Lisa Axe, from Journal of Colloid and Interface Science, Volume 218, 554-563, copyright © 1999 by Academic Press.

"Modeling Cd and Zn Sorption to Hydrous Metal Oxides" by Paras Trivedi and Lisa Axe from *Environmental Science and Technology,* Volume 34, 2215-2223, copyright © 2000 by American Chemical Society.

"Predicting Metal Sorption to Hydrous Metal Oxides" by Paras Trivedi and Lisa Axe from *Environmental Science and Technology,* Volume 35, 1779-1784, copyright © 2001 by American Chemical Society.

CHAPTER 1

INTRODUCTION

Hydrated oxides of aluminum, iron, and manganese are ubiquitous in soils and sediments as discrete particles or as coatings. These oxides are microporous, have large surface area, and high affinity for metal ions. Hence they play an important role in controlling the mobility and bioavailability of toxic and bio-persistent contaminants in the environment.

Metals such as strontium, cadmium, zinc, and nickel that pose a serious threat to plants, animals, and humans are released into aquatic and soil environments largely from various anthropogenic activities (Carroll et al., CERCLA, 1997; 1998; U.S. EPA, 1997; Forstner, 1994; Hesterberg, 1998; Jenne, 1998; Lin, 1997; Rodger et al., 1998, NESHAPS, 1997; Rubin, 1999; Wilcke et al., 1998). 97; Rubin, 1999; Ross, 1994; Lin, 1997; Wilcke et al., 1998). For example, strontium-90 ($t_{1/2}$~ 28.8 y), a carcinogenic radionuclide frequently released from low-level radioactive waste into the environment, migrates from waste disposal and nuclear test sites contaminating adjacent aquifers and showing up as hardness in water (Clark et al. 1999; EPA, 1996, 1997; Inch and Jackson, 1989; Nilsson et al., 1985; Parkman et al., 1998; Toran et al., 1998). ^{90}Sr, in partnership with other high-yield fission products such as ^{137}Cs, has been reported to account for 97% of the penetrating radiation into the environment, which increases the risk of leukemia, bone cancer, and/or weakened immune system (Clark et al., 1999; Nilsson et al., 1985). Therefore, understanding ^{90}Sr retention and migration through sorption processes is critically important.

Likewise, releases of Cd, Ni, and Zn have occurred from industrial activities such as mining, electroplating and smelting along with poor waste handling practices (Carroll

et al., 1998; EPA, 1997; Rubin, 1999; Ross, 1994; Lin, 1997; Wilcke et al., 1998). Cadmium has a deleterious and carcinogenic effect on human beings and animals and ranks 7th amongst the top 20 hazardous substances according to the U.S. EPA (ATSDR (Cd), 1989; U.S. EPA, 1997; Hesterberg, 1998). High-level exposures of cadmium to humans and animals cause permanent damage to vital organs and the immune system, lung cancer, high blood pressure, and painful and crippling disease called 'itai-itai' (ATSDR (Cd), 1989). The U.S. EPA has established a maximum contaminant level (MCL) of 0.005 mg L^{-1} for cadmium in drinking water (U.S. EPA, 1999). On the other hand, zinc, an essential nutrient for most living organisms, can also be harmful to health at elevated concentrations (ATSDR (Zn), 1989). Long-term effects of exposure to high levels of zinc include anemia, pancreas damage, infertility, and lower levels of high-density lipoprotein cholesterol (ATSDR (Zn), 1989). Under the National Secondary Drinking Water Regulations, the MCL goal (MCLG) for zinc is 5 mg L^{-1} (U.S. EPA, 1999). Nickel, a carcinogen on the U.S. EPA persistent, bioaccumulative, and toxic (PBT) Chemicals list, is released primarily from nickel smelting/refining industry, steelworks industries, electroplating, and various other industrial processes employing nickel catalysts (U.S. EPA, 1999). Exposure to Ni results in weight-loss, dermatitis, and permanent damage to heart and lungs (ATSDR (Ni), 1989; U.S. EPA, 1997). Hence, Ni has also been regulated with *de minimis* concentration of 0.1 mg L^{-1} (U.S. EPA, 1999). Although, Ca (another alkaline earth metal) in aquatic systems, is not a threat to the environment, it is often present at high concentration levels. Hence, it is important to account for its interactions with the oxides.

Once released in the water, the retention and the mobility of these metals in soils and sediments are controlled by sorption, uptake by plants, immobilization by soil organisms, and chelation (Hesterberg, 1998; Jenne, 1968; Lion et al., 1982; Ross, 1994). Of these processes, sorption is one of the most important processes for regulating contaminant distribution and fate (Hesterberg, 1998; Jenne, 1968; Lead et al., 1999; Lion et al., 1982; Ross, 1994). To assess risks from these and other metal contaminants to the surrounding environment and to manage remedial activities requires accurate models and well-defined transport parameters. The objective of this research is to understand, model, and predict contaminant distribution mechanisms in soils and sediments. Extensive research (Anderson and Benjamin, 1990; Apak, 1998; Benjamin and Leckie, 1981; Coughlin and Stone, 1995; Dzombak and Morel, 1990; Gadde and Laitinen, 1974; Garnier and Benyahya, 1999; Green-Peddersen et al., 1997; Jenne, 1968; Kanungo, 1999; Krapiel et al., 1999; Kinniburgh et al., 1976; Lion et al., 1982; Lothenbach et al., 1999; Martinez and Mc Bride, 1999; McKenzie, 1980; Meima et al., 1999; Meng and Letterman, 1990; Morgan and Stumm, 1964; Okazaki et al., 1986; Pan and Liss, 1998; Sigg et al., 1999) has demonstrated that the mobility and bioavailability of these metals are impacted by sorption to hydrous aluminum (HAO), iron (HFO), and manganese (HMO) oxides, which are ubiquitous in soils and sediments.

These hydrous oxides exist as both coatings and discrete oxide particles in soils and sediments (Dzombak and Morel, 1990; Hesterberg, 1998; Jenne, 1968; McCarty et al., 1998; Ross, 1994; Zevenbergen et al., 1999). They have large surface areas, a high affinity for metals, and microporous structures; as a result, oxides often act as sinks for metal ions (Dzombak and Morel, 1990; Hesterberg, 1998; Jenne, 1968; Lion et al., 1999;

Meima et al., 1999; Ross, 1994). Sorption to these microporous amorphous oxides can be described as a two-step process (Axe and Anderson, 1995, 1997, 1998; Fuller et al., 1993; Misak et al., 1996; Papelis et al., 1995; Scheidegger et al., 1998; Strawn et al., 1998; Waychunas et al., 1993): a rapid and reversible adsorption reaction to the external surface including the macropores is followed by slow intraparticle diffusion along the surface sites of the micropore walls. This second step is the rate-limiting mechanism in the sorption process.

The principal adsorbent properties that influence the sorption and mobility of trace metals in soils include surface charge density, particle size distribution, surface area, site density, porosity, and pore size distribution (Dzombak and Morel, 1990; Fuller et al., 1993; Hesterberg, 1998; Jenne and Zachara, 1987; Stumm 1992). Other conditions such as background electrolytes, concentration of metal ions, temperature, the presence of organic matter, and competing ions also have significant effects on distribution and bioavailability of trace contaminants (Baltpurvins, 1998; Bolan et al., 1999; Dzombak and Morel, 1990; Hesterberg, 1998; Jenne, 1968; Lee et al., 1996; Martinez and Benyahaya; 1999; Nelson et al., 1999; Simpson et al., 1998; Sparks et al., 1998).

This research is focussed on understanding distribution mechanisms for metal contaminants in the presence of ubiquitous HAO, HFO, and HMO. In an effort to improve modeling capabilities, this research includes developing methods to predict thermodynamic and transport parameters such as site densities, equilibrium constants, adsorption enthalpies, activation energies, and surface diffusivities. Accordingly, results from physical and chemical characterization of these oxides are employed to predict site densities (C_t) from the surface charge densities (σ) in C g^{-1}. Short-term sorption studies to

the hydrous oxides were conducted to evaluate important parameters such as equilibrium constants, adsorption enthalpies, and activation energies. These parameters were used to develop and test correlations that allow parameter prediction for other metal ions. Furthermore, data from transient sorption experiments were modeled to determine intraparticle surface diffusion coefficients, which can be explained by and predicted from site activation theory.

Modeling of macroscopic data alone does not provide sufficient information about the fundamental reaction mechanism occurring at the mineral/water interface; therefore, the *in situ* spectroscopic technique, X-ray absorption spectroscopy (XAS), was employed to access this information (Brown, 1990). The macroscopic studies are complemented with XAS to develop mechanistic models based on local atomic structural information for metal adsorption to hydrous oxides.

This study includes a literature review on sorption and characteristics and properties of the hydrous metal oxides that affect sorption. In addition, the discussion includes the impact of solution chemistry, adsorption models invoked to describe the adsorption mechanism, theories proposed to explain intraparticle transport, and an introduction to XAS and its application to environmental problems. Subsequently, hypotheses are presented and experimental procedures to test those hypotheses are detailed. Finally, results from the studies are presented and followed by conclusions and future work.

CHAPTER 2

SORPTION AT THE AQUEOUS OXIDE INTERFACE

This chapter begins with a review of physical characteristics and chemical properties of hydrous metal oxides found in soils and sediments. The chapter continues with a discussion on the factors influencing sorption, which includes a literature review of metal sorption to hydrous oxides. Sorption is addressed with respect to adsorption edges, isotherms, equilibrium models, and the transient process of intraparticle surface diffusion. Subsequent to the review of macroscopic studies, the chapter concludes with an overview of the use of *in situ* XAS in evaluating atomic level adsorption mechanisms, particularly with respect to the hydrous oxide aqueous interface.

2.1 Characteristics and Properties of Hydrous Metal Oxides

2.1.1 Mineralogy

Oxides of aluminum, iron, and manganese are important components of soils and sediments and represent a major sink for metals released into the environment from a variety of anthropogenic sources (Anderson and Benjamin, 1990; Apak, 1998; Benjamin and Leckie, 1981; Carroll et al., 1998; Coughlin and Stone, 1995; Dzombak and Morel, 1990; Gadde and Laitinen, 1974; Garnier and Benyahya, 1999; Green-Peddersen et al., 1997; Hesterberg, 1998; Jenne, 1968, 1998; Kanungo, 1999; Kinniburgh et al., 1976; Krapiel et al., 1999; Lion et al., 1982; Lothenbach et al., 1997; Martinez and Mc Bride, 1999; McKenzie, 1980; Meima et al., 1999; Meng and Letterman, 1990; Morgan and Stumm, 1964; Okazaki et al., 1986; Pan and Liss, 1998; Rubin, 1999; Sigg et al., 1999). These oxides occur as discrete particles or as a coating on other mineral surfaces in

aquatic environments; they have large surface areas, microporous structure, and a high affinity for metal ions (Dzombak and Morel, 1990; Jenne, 1968; Lion et al., 1982; Stahl and James, 1991; Simpson et al., 1998).

The iron oxides are the most abundant of the metallic oxides in soils and sediments; some of the most commonly found Fe oxides are ferrihydrite, hematite, maghemite, magnetite, goethite, lepidocrocite, and feroxyhite (Schwertmann and Taylor, 1989). The basic structural unit for all of these Fe oxides is the octahedron, in which each atom is surrounded by six O atoms (Schwertmann and Taylor, 1989). Of these iron oxides, ferrihydrite is the only metastable form and the most poorly ordered Fe^{3+} oxide often referred to as amorphous ferric hydroxide. Manceau and coworkers (Manceau et al. 1992; Manceau and Charlet, 1994; Manceau and Combes, 1988) found that HFO has a layered structure similar to goethite but with a short-range order, where each Fe^{3+} ion is surrounded by three O^{-2} and three OH^- groups that are located in the alternate discontinuous layers. However, they observed shorter octahedral chains in hydrous ferric oxides as compared to goethite, which, they reasoned explains the high site density while the discontinuity clarifies the high surface area. Further, Rose et al. (1996) demonstrated that the presence of PO_4^{-3} ions hinders the crystallization of the metastable of Fe oxyhydroxide. Similarly, Spadini et al. (1994) observed that the in contrast to goethite, the local structure of two-line ferrihydrite was preserved even with Cd sorbed at a surface coverage of 1 and 100%. Golden et al. (1997) also observed that Fe oxides in League soil (Southeast Texas) remained poorly crystallized in presence of P and Si.

The metastability and the rate of transformation of amorphous oxides to crystalline forms is controlled by various factors such as the rate of oxidation, the

presence of anions and cations, pH, and temperature (Baltpurvins et al., 1996; Combes et al., 1990; Golden et al., 1997; Schwertmann et al., 1999). For example, Baltpurvins et al. (1996) observed that the transformation of ferric hydroxide to hematite was favored at pH values near the zero point of charge of ferrihydrite and at high temperatures (>90°C) whereas goethite formation was favored at pH > 12 and at low temperatures (<40°C). They also observed that the rate of transformation of ferrihydrite to its crystalline analogues was greater in the presence of nitrate ions than in the presence of chloride or sulfate ions. In a recent work, Schwertmann et al. (1999) confirmed similar results; additionally they demonstrated that a fast hydrolysis of ferric nitrate solution produced a two-line ferrihydrite, while the slow hydrolysis resulted in the six-line ferrihydrite. They also reported synthesis of a series of ferrihydrites from the two-line to the six-line varieties by oxidizing a 10^{-1} M $FeCl_2$ solution at pH 6.5 with varying Si concentrations up to 0.926 mmol L^{-1}.

The mineralogy of HMO is complicated by the large number of oxides and hydroxides formed, in which substitution of Mn^{2+} or Mn^{3+} for Mn^{4+} occurs extensively (McKenzie, 1989). Most Mn oxides are built of MnO_6 octahedra and have either a tunnel structure or a layered structure (Fritsch et al., 1997; McKenzie, 1989; Morgan and Stumm, 1964). Pyrolussite, ramsdellite, nsutite, hollandite, coronadite, and todorokite are tunnel-structured oxides formed from single, double, or wider chains of MnO_6 octahedra that are linked through corner sharing. On the other hand, manganese oxides such as birnessite, vernadite, and buserite have a layered structure (Fritsch et al., 1997; Manceau and Combes, 1988; McKenzie, 1989; Morgan and Stumm, 1964). Most Mn oxides found in soils are amorphous (Fritsch et al., 1997; McKenzie, 1989; Morgan and Stumm, 1964).

Using X-ray absorption near edge spectroscopy (XANES), Manceau et al. (1992) demonstrated that Mn atoms are generally tetravalent in most poorly crystallized hydrous manganese oxides. They also found that the structure is not strictly related to that of the subsequent, well-crystallized polymorph. Manceau et al. concluded that Mn gels most likely consist of a 3-D framework of randomly distributed edge- and corner-sharing MnO_2 octahedra that transform into a large variety of structures. Friedl et al. (1997) investigated with X-ray absorption fine structure (XAFS) spectroscopy the local structural environment of oxides with Mn in different oxidation states; they found that the first shell (Mn-O) for Mn(II) hydroxides had a greater distance than in Mn(IV) oxides. Additionally, they found in $Mn(OH)_2$ and Na-birnessite the second shell was symmetric with a single Mn atom at 2.9 Å, which they reported is consistent with a structure of edge-sharing Mn octahedra sheets. In studying Sr sorption to HMO, Axe et al. (2000) found the oxide exhibited a highly ordered short-range structure even though the long-range structure was indiscernible from X-ray diffraction (XRD). They showed that each Mn atom is surrounded by 3-4 O atoms in the first shell at an average distance of 1.89 Å, while the second shell comprises approximately three Mn atoms at an average distance of 2.86 Å. This oxide structure did not vary over 6 months of aging with or without contaminant sorbed.

A number of crystalline and non-crystalline aluminum hydroxides, oxyhydroxides, and oxides are also found in nature and are particularly common in bauxite deposits and soils (Hsu, 1989). The physical and chemical properties of aluminum oxides depend to a large extent on the temperature reached during its formation (Simpson et al., 1998). Aluminum hydroxide gel upon crystallization typically

forms monohydrate oxyhydroxide called boehmite (a rhombohedral crystal). At higher temperatures it is transformed into trihydrate bayerite, which with increasing temperature, reorders to the trihydrate form called gibbsite (Simpson et al., 1998). The crystalline polymorphs of $Al(OH)_3$ such as gibbsite, bayerite, and nordstrandite are composed of the same fundamental units: two planes of close-packed OH^- with Al^{3+} sandwiched between them (Hsu, 1989). Amorphous forms of aluminum oxides are also metastable, however, the presence of anions and clay minerals can effectively retard their crystallization (Hsu, 1989; Simpson et al., 1998). The dissociation of Al-OH polymers is the rate-limiting step in the crystallization process of $Al(OH)_3$ (Simpson et al., 1998). Because this step is very slow in near neutral conditions, naturally occurring hydrated aluminum oxides remain stable and amorphous after many years of aging under normal atmospheric conditions. Hence they play a significant role in retention, mobility, and bioavailability of heavy metals (Jackson and Inch, 1989; Jenne, 1968; Lion et al., 1982; Papelis et al., 1995; Tamura et al., 1997).

The crystallinity and the stability of the hydrous oxides used in the present research are described in Chapters 5 and 6. Other physical characteristics of these amorphous oxides that are important in the sorption process include their surface area, porosity, pore size distribution, and particle size distribution. These properties are discussed in the next sections.

2.1.2 Surface Area

Surface area is an important factor in the adsorption process (Dzombak and Morel, 1990; Gregg and Sing, 1982; Jenne, 1998). By far the most popular means of measuring surface areas for finely divided solids is the Brunaer, Emmett and Teller (BET) method (Gregg

and Sing, 1982). However, with the BET method, the surface areas are measured on freeze-dried particles, as a result, hydrated ones are expected to be much greater (Bottero et al., 1993; Dzombak and Morel, 1990; Okazaki et al., 1986). For example, Bottero et al. (1993) found large variations in surface area of amorphous aluminum oxides where using adsorbing organic molecules, areas ranged from 600 to 1000 $m^2 g^{-1}$, while using N_2 gas adsorption areas were <20 $m^2 g^{-1}$. However, when measuring the surface area of ferrihydrite, they found 135-163 $m^2 g^{-1}$ using anionic surfactants for in-situ studies and 295 $m^2 g^{-1}$ from argon adsorption isotherms on dried particles. Similarly, Okazaki et al. (1986) reported surface areas for Al and Fe hydrated oxides to be much greater when measured with glycerol method than when measured with the BET method. Even though large variations in the surface area have been reported when using one method, currently, the BET approach is the standard method recommended for evaluating sorbent surface area (Dzombak and Morel, 1990). Because the amorphous oxides are microporous, it is also important to evaluate porosity and pore size distribution.

2.1.3 Porosity and Pore Size Distribution

When a metal ion is transported through the internal pores, pore size and effective radius of the hydrated cation will determine the type of intraparticle diffusion (Axe and Anderson, 1995, 1997, 1998; Froment and Bischoff, 1990; Kärger and Ruthven, 1992; Papelis et al., 1995). Traditionally, the pore size distribution is determined by either nitrogen desorption or mercury porosimetry; porosity is assessed with mercury porosimetry as well. However, these methods are employed on freeze-dried sorbents, which may not accurately represent oxide surfaces in hydrated environments. If the pore radius is much greater than the effective radius, bulk diffusion is expected. When the

cation and pore radii are approximately equivalent, then transport is referred to as configurational or surface diffusion and occurs along the pore walls. In aquatic systems where layers of water adsorb to porous surfaces resulting in micropores, surface diffusion dominates the intraparticle transport of metal ions (Axe and Anderson, 1995, 1997, 1998; Froment and Bischoff, 1990; Kärger and Ruthven, 1992). This type of diffusion has been observed to occur in HFO (Axe and Anderson, 1995, 1997) and has not been studied to the same extent for amorphous Al and Mn oxides.

2.1.4 Particle Size Distribution

The particle size distribution (PSD) can be characterized *in situ* using light scattering techniques, such as ultra-violet radiation based particle size analyzer. When studying intraparticle diffusion, it is critical to fully understand the PSD, which is used in the modeling and fitting of the surface diffusivity (Axe and Anderson, 1995, 1997). Researchers (Murray et al. 1999; Papelis et al. 1995; Roberts and Cunningham, 1998) have observed as would be expected that the smaller sized particles resulted in faster uptake of ions.

2.1.5 Surface Charge Density

When a metal oxide is exposed to water, surface hydroxyl groups are formed by dissociative sorption of water molecules; these groups can bind and release protons (Parks and Bruyn, 1962; Morgan and Stumm, 1990; Stumm, 1992):

$$SOH_2^+ \leftrightarrow SOH^o + H^+ \qquad K_{a1}^{app} \qquad (1)$$

$$SOH^o \leftrightarrow SO^- + H^+ \qquad K_{a2}^{app} \qquad (2)$$

where SOH_2^+, SOH^o, and SO^- represent surface sites, and K_{a1}^{app} and K_{a2}^{app} are apparent equilibrium acidity constants.

Potentiometric acid-base titration, in a closed system, is the most common method for measuring the net surface charge density (σ) as a function of pH (Stumm, 1992; Morgan and Stumm, 1990; Parks and Bruyn, 1962; Dzombak and Morel, 1990):

$$\frac{\sigma}{F} = [\Gamma_H] - [\Gamma_{OH}] = \frac{1}{(A \cdot S)}\{C_A - C_B - [H^+] + [OH^-]\} \quad (3)$$

where F is the Faraday Constant (96485 C mol^{-1}), A the specific surface area of the oxide (m^2 g^{-1}), S is the oxide concentration (g L^{-1}), Γ_H is the proton sorption density (mol m^{-2}), Γ_{OH} is the hydroxyl sorption density (mol m^{-2}), C_A and C_B are the molar concentrations of acid and base added, respectively, and $[H^+]$ and $[OH^-]$ are calculated from the pH measurements. The pH at which the net positive charge equals the net negative (hence the net surface charge is zero) is called the point of zero net proton charge (pH_{pznpc}) (Sposito, 1998). For pH< pH_{pznpc}, the net surface charge will be positive and the surface is more likely to adsorb anions; while for pH> pH_{pznpc} the net surface charge is negative and cation adsorption will be favored (Dzombak and Morel, 1990).

2.1.6 Surface Site Densities

Surface sites describe any potentially reactive set of functional groups on the adsorbent surface to which the adsorbates may bind physically or chemically; the number of such active sites available per unit surface area of the adsorbent is referred as the site density (C_t) (Koretsky et al., 1998). Dzombak and Morel (1990) have classified the sorption site densities on HFO into two types: Type I sites, which corresponds to a set of high-affinity cation binding sites; and Type II sites, which are inclusive of the total reactive sites

available for sorption of protons, cations (Type I sites), and anions. In another approach, surface sites on an adsorbent have also been classified according to the number of metal atoms bonded to the surface hydroxyl groups (Koretsky et al., 1998). In Type I sites, only one metal atom is bound to the OH^- group; this type of site is considered a high energy, highly reactive or ionizable site (Koretsky et al., 1998). On the other hand, Type II sites are low energy or weak ones that result in a physical type of adsorption (Koretsky et al., 1998). Experimental determinations of C_t have been accomplished with techniques other than potentiometric titrations, including tritium-exchange method, H_2O isotherm method, and the weight loss method (Dzombak and Morel, 1990; Koretsky et al., 1998). Maximum sorption densities observed at constant pH isotherms provide a reliable estimate of C_t as well (Fogler, 1992; Koretsky et al., 1998). Cations like the alkaline earth metals are potentially good probe ions as they have very high solubilities (Axe and Anderson, 1995; Dzombak and Morel, 1990; Koretsky et al., 1998). The site densities are therefore a function of pH, which is a hypothesis that will be tested in this research. Also the surface charge at a pH is a related to the surface potential through the Poisson-Boltzmann equation. As a result, in this research, using an alkaline earth metal, a method will be presented for estimating the site density from the surface charge density.

2.2 Adsorption Affinity

The surface charge resulting from pH is probably the most important factor that affects the availability of heavy metals. As pH increases, the net negative surface charge increases and cation adsorption to the oxide surface increases (Axe and Anderson, 1995,1997; Dzombak and Morel, 1990; Gadde and Laitinen, 1974; Jenne, 1968; Johnson,

1990; Lützenkirchen, 1997; McKenzie, 1980; Mishra and Tiwary, 1995, 1998; Mishra et al., 1997; Okazaki et al., 1986; Shuman, 1977; Stahl and James, 1991; Tamura et al., 1997; Toran et al., 1998).

Several studies have revealed the adsorption affinity for metal ions to oxides follows the order of Pb>Cu>Zn>Cd>Co>Mn>Sr>Ca (Benjamin and Leckie, 1981; Gadde and Laitinen, 1974; Garnier and Benyahya, 1999; Kinniburgh et al., 1976; Lion et al., 1982; Martinez and McBride, 1999; McKenzie, 1980; Okazaki et al., 1986; Sigg et al., 1999). Pan and Liss (1998) proposed that Zn, a much harder Lewis acid than Cd^{2+}, binds more strongly to goethite. Morgan and Stumm (1964) and others (Coughlin and Stone, 1995; Garnier and Benyahya, 1999; Krapiel et al., 1999; Lothenbach et al., 1997; Tamura and Furuichi, 1997) have correlated the adsorption affinities of metal ions to their first hydrolysis constants. Wehrli et al. (1990) developed a linear free energy relation between the rate constant for water exchange and the intrinsic adsorption rate constants. Researchers (Gray, 1981; Gray and Malati, 1979; Malati, 1987) compared the trends of cation adsorption to Mn and Si oxides with Hofmeister series and showed that the adsorption affinity for alkaline earth metals and certain heavy metals follows the reverse order of their hydrated radii. For the most part, correlations developed in previous studies (Coughlin and Stone, 1995; Krapiel et al., 1999; Lothenbach et al., 1997; Morgan and Stumm, 1964) were based on one temperature; hence, the relations cannot be used for other conditions.

In a number of studies (Angove et al., 1998; Axe and Anderson, 1997; Johnson, 1990; Mishra et al., 1997; Mishra and Tiwary, 1995, 1998; Rodda et al., 1996), however, adsorption of metal ions to oxides has been modeled as a function of temperature to

obtain the adsorption enthalpies. Enthalpy is related to the bonding energy between the metal ion and the adsorbent surface and represents the relative adsorption affinity. The potential energy is sum of integrated intermolecular forces which include electrostatic ones, weak polarization forces from the dipole moments induced in atoms and molecules, and the chemical or covalent bonds that result in interaction energies greater than 200 kJ mol^{-1} (de Boer, 1968; Israelachvilli, 1997). In this research, in an effort to predict enthalpies and activation energies, two correlations are tested with one relating adsorption enthalpies and hydrated cationic radii and the other relating enthalpies and activation energies. These correlations can be used to help predict sorption behavior.

2.3 Sorption Modeling

The sorption of a contaminant to hydrous oxides is a two step process: an initial fast sorption at the mineral-water interface is followed by a much slower uptake that may continue for a period of days to years (Axe and Anderson, 1995, 1997; Froment and Bischoff; 1990; Fuller et al., 1993; Jenne, 1998; Kärger and Ruthven, 1992; Papelis et al., 1995; Raven et al., 1998; Scheidegger et al., 1998; Scheinost et al. 2001; Strawn et al., 1998; Waychunas et al., 1993; Wehrli et al., 1990). Many models have been invoked to explain the sorption process (Axe and Anderson, 1995, 1997; Barrow et al., 1981; Farley et al., 1985; Froment and Bischoff; 1990; Fuller et al., 1993; Jenne, 1998; Kärger and Ruthven, 1992; Misak et al., 1996; Morgan and Stumm; 1990; Papelis et al., 1995; Scheidegger et al., 1998; Strawn et al., 1998; Waychunas et al., 1993; Wehrli et al., 1990); modeling will be discussed in the following sections.

2.4 Short-term Adsorption

The short-term adsorption mechanisms are generally described either by surface complexation or the adsorption isotherm models (Dzombak and Morel, 1990; Morgan and Stumm, 1990). The surface complexation models including constant capacitance model, diffuse layer model, and triple layer model are based on the surface protonation - deprotonation reactions (Dzombak and Morel, 1990; Morgan and Stumm, 1990; Stumm, 1992). The differences between the models lie in the description of the electrical double layer. Adsorbed ions are considered to be part of the solid surface in the diffuse layer model and constant capacitance model. Proton transfers involving surface acid groups and the formation of surface complexes with other cations and anions determine surface charge. The abutting diffuse layer of ions from the surrounding electrolyte balances the charge. The triple layer and Stern models assign primary potential determining ions (H^+ and OH^-) to an inner plane, and include a separate, adjacent plane for specifically adsorbed ions.

The Freundlich isotherm is an example of an empirical adsorption model, which assumes that adsorption is a physical process, and has the form (Dzombak and Morel, 1990; Morgan and Stumm, 1990; Stumm, 1992):

$$C = K_F [S]^n \qquad (4)$$

where C represents the moles of adsorbed species g^{-1} of adsorbent, [S] the equilibrium concentration of species in the bulk aqueous phase (M), K_F the equilibrium constant, and n the constant related to the distribution of bond strengths. Mishra and co-workers (Mishra and Tiwary, 1995, 1998; Mishra et al., 1997) have demonstrated the applicability of Freundlich isotherms to describe the sorption of metal ions to manganese oxide over a

wide range of concentrations. They found that the values of 1/n were less than one and concluded that manganese oxide used in the studies was heterogeneous in nature with an exponential distribution of adsorption sites. According to Dzombak and Morel (1990), Freundlich isotherms with $n > 1$ are indicative of adsorbents with multiple types of sites.

The Langmuir isotherm was derived on the basis of monolayer coverage (Fogler, 1992). Each type of adsorption site is equal in energy and for one type of site the linear form of the isotherm can be written as follows:

$$\frac{1}{C} = \frac{1}{C_t} + \frac{1}{K C_t} \cdot \frac{1}{[S]} \tag{5}$$

where C represents the moles of adsorbed species g^{-1} of adsorbent, [S] the equilibrium concentration of species in the bulk aqueous phase (M), C_t is the site density ($C_t = C_v + C$, where C_v is the number of sites available), and K is the equilibrium constant. In a number of studies, the Langmuir model has been employed to describe metal sorption to oxides: Zn and Pb adsorption to goethite (Johnson et al., 1990; Rodda et al., 1996); Zn adsorption to Al and Fe hydrous oxides (Shuman, 1977); Cd adsorption to hydrous manganese oxides (Posselt and Weber, 1974); Pb adsorption to hydrous ferric oxide (Morgan and Stumm 1964); Cr(III) sorption to hydrous Fe oxides (Crawford et al., 1993); iron-cyanide adsorption onto γ-Al_2O_3 (Huang and Cheng, 1997); Cu, Cd, and Pb adsorption on red mud (a mixture of Al, Fe, Si, and Ti oxides) (Apak et al., 1998); and Pb sorption to biogenic Mn oxides (Nelson et al., 1999). Because metal contaminants are often present at trace concentrations, the site densities are approximately equivalent to the number of available sites (i.e., when $C_t >> C$, then $C_t \approx C_v$); this has been observed in a number of studies (Axe and Anderson, 1995, 1997). Under these conditions, when the

total sites are approximately equivalent to the number of available ones, the Langmuir isotherm reduces to the linear distribution model:

$$C = K\,C_t\,[S] \qquad \text{or} \qquad C = K_d\,[S] \tag{6}$$

where K_d is equal to $K \times C_t$ and is referred to as the linear distribution coefficient. Equation (6) is similar in form to the Freundlich equation with n = 1. Several studies involving adsorption of heavy metals to sediments, aluminum oxides, iron oxides, and manganese oxides are described with the help of this model (Axe and Anderson, 1995, 1997; Green-Pedersen et al., 1997;Oakley et al., 1981). All of the above sorption models are based on short contact times and at a constant temperature; these models do not account for long-term sorption processes.

2.5 Adsorption Thermodynamics

Temperature is another important factor that governs metal distribution in the ecosystems. Seasonal variations of in natural water systems including soils are not uncommon. These thermal variations influence the bioavailability of trace elements (Johnson, 1990; Ross, 1994). Thus, the effect of temperature on distribution of metals is important not only in understanding adsorption mechanisms, but also in obtaining useful thermodynamic information such as adsorption enthalpy and entropy (Angove et al., 1998; Axe and Anderson, 1997; Johnson, 1990; Rodda et al., 1996). The variation in equilibrium constant (K) with temperature can be described by the van't Hoff equation (Smith and van Ness, 1987):

$$\ln\left[\frac{K_1}{K_2}\right] = \frac{-\Delta H^\circ}{R}\left[\frac{1}{T_2} - \frac{1}{T_1}\right] \tag{7}$$

where ΔH^{o} is the change in enthalpy kcal mol^{-1}, and R is the Universal Gas Constant. From the Polyani relationship, the activation energy is related to the adsorption enthalpy (E_a) through the proportionality constant α, which is expected to be equivalent for similar types of reactions (Boudart, 1968). In this research, transition metals are hypothesized to form analogous complexes with hydrous oxide surfaces; other metal groups like alkaline earth metals are expected to behave similarly. The E_a can be used to determine the theoretical surface diffusivity based on site activation theory (Axe and Anderson, 1997; Kärger and Ruthven, 1992). A detailed description of this prediction method will be presented in the following section.

2.6 Long-term Sorption

The equilibrium models while important and useful have not been adequate in modeling contaminant mobility and bioavailability. As mentioned before, sorption is a two-step process, where the second step is the rate-limiting mechanism. Several mechanisms have been observed and/or proposed for this second and rate-limiting step of the sorption process, which include intraparticle diffusion (Axe and Anderson, 1995, 1997; Barrow, 1989; Fuller et al., 1993; Misak et al., 1996; Papelis, 1995; Papelis et al., 1995; Strawn et al., 1998;Waychunas et al., 1993; Wehrlic *et al*, 1990), surface precipitation (Farley et al., 1985), and solid solution formation (Scheidegger et al., 1998). In their kinetic studies with Cd^{2+} sorption to hydrous ferric oxide (HFO), Farley et al. (1985) modeled the slow process as surface precipitation, while Scheidegger et al. (1998) observed a mixed Ni-Al hydroxide on clay and aluminum oxide particles with increasing reaction time. However, Fuller et al. (1993) and Waychunas et al. (1993) found from their macroscopic and

spectroscopic studies that the rate of As(V) sorption to ferrihydrite was limited by intraparticle diffusion; there was no evidence of either a solid solution or precipitate formation. Similarly, others have demonstrated intraparticle diffusion as the rate-limiting mechanism: Axe and Anderson (1995, 1997) modeled Sr^{2+} and Cd^{2+} sorption to HFO; Misak et al. (1996) estimated diffusivities for Co^{2+} and Zn^{2+} in hydrous ferric, stannic, and ferric-stannic oxides; Papelis et al. (1995) assessed Cd and Se(IV) sorption to micro- and meso-porous alumina with macroscopic studies which was complemented with spectroscopic studies (Papelis, 1995); Scheinost et al. (2001) demonstrated spectroscopically that sorption of Cu and Pb ions onto ferrihydrite is controlled by intraparticle diffusion; and Strawn et al. (1998) studied Pb^{2+} sorption to γ-Al_2O_3.

Hydrous amorphous oxides of Al, Fe, and Mn have significant site capacities where sorbed concentrations are much less than the site capacity (as is the case for contaminants in the subsurface), therefore, the adsorbate does not interact with itself. For these microporous oxides, the slow sorption process of intraparticle diffusion can be systematically studied. A mathematical model has been previously developed to represent this intraparticle diffusion (Axe and Anderson, 1995, 1997). Assuming the internal sites are no different than the external ones, then for an adsorbing species at dilute concentrations (or constant diffusivities), the mass balance for spherical aggregates yields the following partial differential equation:

$$\frac{\partial C}{\partial t} = \frac{D_s}{\left[1+\left(\frac{\varepsilon}{\rho K_i}\right)\right]} \frac{1}{r^2} \frac{\partial\left(r^2 \frac{\partial C}{\partial r}\right)}{\partial r} \tag{8}$$

where C represents the moles of adsorbate metal sorbed g^{-1} of hydrous oxide, D_s is surface diffusivity in $cm^2\ s^{-1}$, ε is the porosity, ρ is the bulk density of the oxide in g cm^{-3}, r represents the radial position within the sphere, and K_i is the distribution coefficient for sorption to internal sites. From characterization and isotherm studies, porosity, bulk density, and the distribution coefficient can be determined, resulting in one unknown – surface diffusivity – the fitting parameter.

Transient studies to obtain data for modeling require a lengthy period of time, and therefore predictive methods would be useful for determining surface diffusivities. Assuming that the potential on the pore surface can be described by a sinusoidal function (where the minima represent adsorption sites and the maxima signify the energy barrier or E_A for an exothermic reaction [Axe and Anderson, 1997]), the theoretical surface diffusivity is defined as (Axe and Anderson, 1997; Kärger and Ruthven, 1992):

$$D_s = \lambda[E_A/(2m)]^{1/2} \exp[-E_A/(RT)] \qquad (9)$$

where λ is the mean distance between sites, and m is the molecular weight of the metal ion. Again, as discussed earlier, from the Polyani relationship, the activation energy (E_a) is related to the adsorption enthalpy through α (Boudart, 1968).

A general problem with macroscopic investigations of sorption phenomena is that the experimental data are only able to give indirect indication of the solid/solution interface, while many structural and mechanistic aspects of sorption processes remain unclear. Researchers such as Sposito (1986) and Brown (1990) have discussed that modeling macroscopic data alone does not provide conclusive evidence of the adsorption mechanism, and that in situ spectroscopic studies are needed to better understand distribution mechanisms at mineral/water interfaces. X-ray absorption spectroscopy is

one technique that can provide *in situ* structural information about the sorbate and its surroundings (Brown, 1990; Bunker, 1999; Stern, 1976)

Even though goethite and HFO may possess similar local structures, they have different long-range configurations. Hence they may possess different types of surface sites and their relative ratios of the high affinity to low affinity sites are different. As a result, these two iron oxides may not be able to represent one another in modeling the mobility and the bioavailability of contaminants. To better understand adsorption to the different types of sites, a comparison of metal adsorption to these two oxides (HFO and goethite) is essential.

2.7 Adsorption to Goethite

In a number of these studies (Christophi and Axe, 2000; Grossl et al., 1997; Lützenkirchen, 1997), metal adsorption to crystalline iron oxides such as goethite and hematite has been found to be independent of ionic strength, thus attributing adsorption to inner-sphere complexation. Metal adsorption to goethite has also been assessed as a function of the adsorbate concentration through isotherm studies (Ankomah, 1992; Christophi and Axe, 2000; Forbes et al., 1976; Pan and Liss, 199814-17). Johnson and coworkers (Angove et al., 1999; Johnson, 1990; Rodda et al., 1993, 1996) demonstrated from their temperature studies that adsorption of such cations as Cd, Co, Pb, and Zn to goethite involves an endothermic reaction with chemical bonding between the adsorbate and the goethite surface. Other researchers have employed techniques such as pressure-jump relaxation (Grossl et al., 1995, 1997; Grossl and Sparks, 1995) and XAS (Bargar et al., 1998; Collins et al., 1999; Schlegel et al., 1997; Spadini et al., 1994) to elucidate the

reaction kinetics and mechanisms for metal adsorption to the goethite surface. Overall, metal affinities for goethite is generally, with slight variations, found to follow the order Cu > Pb > Zn> Cd > Co > Ni > Mn > Ca > Mg (Coughlin and Stone, 1995; Mckenzie, 1980; Schwertmann and Taylor, 1989). Schwertmann and Taylor (1989) observed their trend to be consistent with electronegativity, while Christophi and Axe (2000) found it to be in agreement with the hydrated radii of the cations.

In natural systems, multiple ions are often present and compete for the adsorbent surfaces. Most research, however, is limited to the adsorption edges: competitive adsorption of Cu, Pb, Zn, and Cd in the presence of Mg, phosphate, carbonate, sulfate, and silicate (Balistrieri and Murray, 1982); competitive adsorption of arsenate with phosphate and molybdate (Manning and Goldberg, 1996); competition between Cu and Pb using amorphous iron oxide (Swallow et al., 1980); adsorption competition of Cd, Cu, Pb, and Zn onto amorphous iron oxyhydroxide (Benjamin and Leckie, 1981a,b); and, adsorption of Cd in the presence of alkaline earth metals, Ca, Mg, Ba, and Sr (Cowan et al., 1991). In these above studies, competition was examined by the shift of a metals adsorption edge when a second metal of greater concentration was added to the system. Adsorption edge shifts to greater pHs (or a decrease in adsorption) are indicative of displacement of the sorbed metal. However, competition is only observed when the total number of sites is limited. Furthermore, although a number of researchers have used edge experiments, there are some problems with this approach; surface characteristics such as site density (maximum sorption density) and net surface charge along with metal speciation and its solubility change with pH.

Using isotherms, Gadde and Laitinen (1974) studied adsorption competition between Cd, Zn, and Pb on hydrous manganese oxides. However, all metal concentrations used in these experiments exceeded solubility. Vulava et al. (2000) modeled Ca^{2+} and Na^{+} competitive adsorption to a soil comprised of clay, quartz, chlorite, and goethite using cation-exchange models. To account for surface site heterogeneity, the authors applied a discrete site affinity distribution. Vulava et al. demonstrated that valid models for complex systems can be developed without understanding molecular mechanisms and without knowledge of the site densities. In a contrast, in competition studies of Cu and Pb adsorption to hematite (Christl and Kretzschmar, 1999), potentiometric titrations were fit with a 2-pK Stern model employing a range of site densities (2.2 to 16.6 sites nm^{-2}). Christl and Kretzschmar (1999) concluded that site densities are critical in evaluating competition and that competition experiments can assist in calibrating surface complexation models. In another recent competition study of Cu and Pb as well as Zn, adsorption to goethite was evaluated with *in situ* voltammetric methods and described with the help of the constant capacitance model (Palmqvist et al., 1999). For systems close to saturating surface sites, the constant capacitance model was found to describe Cu and Zn competition; however, for Pb surface complexation, the equilibrium constant was modified to fit the data. Rather than testing each potential competition system, model calibration should be achievable with single adsorbate systems given defined site densities.

Recently, competition of copper, lead, and cadmium adsorption on goethite was studied where site density was evaluated prior to competition studies to limit the number of available sites (Christophi and Axe, 2000). Isotherm studies conducted at pH 6

revealed that a single-site model described the Cu-Cd and Pb-Cd systems within the error of the model. Furthermore, although the model provided a good fit for Pb and Cd data in the Pb-Cu and Pb-Cu-Cd systems, it underpredicted copper adsorption. The difference in site densities between copper and lead revealed a set of sites not available for competition. Using this approach where copper affinity is equivalent for both sites, the model provided a good fit for copper adsorption and competition. Manning and Goldberg (1996) have conducted studies examining arsenate, phosphate, and molybdate adsorption competition to mineral surfaces. They too could model competition from single adsorbate data where, similar fits were obtained with either a single-site or two-site approach. Therefore, among their conclusions, they recommended further experimentation in assessing surface site densities and evaluating complexation mechanisms from spectroscopic data. In this research, site densities and sorption mechanisms for goethite and HFO will be measured and compared. One hypothesis is that although amorphous oxides have extensive site densities where competition would not be observed, goethite has much less (as a function of pH), and therefore competition is expected between like metals such as Ni and Zn.

2.8 X-ray Absorption Spectroscopy (XAS)

XAS is commonly divided into XAFS (> 30 eV above the edge) and XANES (Figure 1); both have been employed in environmental research. There is no fundamental distinction between the physics of XAFS and XANES other than one of complexity of the spectra arising from the dominant electronic processes in each region. For this reason XAFS and XANES are now referred to jointly under the term XAS (Bunker, 1999). In the XANES

$$I_f / I_o \propto \sigma \tag{11}$$

As the incident x-ray energy is scanned above the absorption threshold energy of the central atom, the fluoresced radiation consists of the outgoing backscattered wave functions (Bunker, 1999; Lee et al., 1981; Wong, 1986); these may interfere constructively or destructively giving rise to oscillations (Bunker, 1999; Lee et al., 1981; Wong, 1986). The XAFS spectrum reveals the atomic structure, and for a Gaussian radial distribution the single scattering signal is given by (Bunker, 1999):

$$\chi(k) = \frac{N S_o^2}{k R^2} |f_{eff}(k,r)| \sin(2kr + 2\delta + \phi) e^{-2R/\lambda} e^{-2\sigma^2 k^2} \tag{12}$$

where $\chi(k)$ is the interference function in photoelectron momentum (k) space, S_o^2 gives a constant scale factor which accounts for the loss of coherence due to multi-electron excitations, N is the coordination number, k is the photoelectron wavevector, f_{eff} (k, r) is the effective curved wave backscattering amplitude, R is the average radial distance, δ is the phase shift of the central ion, λ is the mean free path of the electron, ϕ is the phase of the complex electron scattering amplitude for each atom, and σ^2 is the mean square variation of distances about R and accounts for static and thermal vibration in the harmonic approximation (Lee et al., 1981). The term $e^{-(2R/\lambda)}$ accounts for inelastic losses in the scattering process (Brown, 1990). For highly disordered systems, higher moments of distribution can be included, for example, the cumulants C_3 and C_4 account for the skewing and Kurtosis of the distribution (Dalba and Fornasini, 1993; Bunker, 1983). The Fourier transformation of the product $k^n\chi(k)$ in momentum (k) space over a finite k-range gives rise to a radial structural function $\rho_n(r)$ in distance (r) space (Teo, 1986, Bunker, 1999):

region, multiple scattering between the absorber and the neighboring atoms has significant contributions that can provide information about the oxidation state of an atom, the symmetry, and the local environment (Brown, 1990; Lee et al., 1981; Peterson et al., 1997). On the other hand, in the XAFS region, single scattering dominates the atomic oscillations for the first two shells (Brown, 1990; Bunker 1999). These atomic oscillations are caused by constructive and destructive interference between singly scattered outgoing and backscattered photoelectron waves (Brown, 1990; Bunker, 1999; Lee et al., 1981; Wong et al., 1986). Qualitatively, XAFS information comes from electron interference when the source and the detector of the electron are the target atom (Stern, 1976). The key features of XAS are that it is (Brown, 1990; Wong, 1986):

(i) Element specific giving information about the average local structural and compositional environment around the absorbing atom.

(ii) Applicable to dilute aqueous solutions and soil/sediment suspensions where concentrations can be probed down to parts per million.

(iii) Appropriate to systems without any long-range order.

XAFS spectra are obtained by measuring the X-ray absorption or fluorescence of a given sample as a function of the wavelength. In the transmission mode, for a homogeneous sample of uniform thickness x, the absorption coefficient (μ) is related to the incident flux (I_o) and the transmitted flux (I) by (Bunker, 1999):

$$I/I_o = \exp(-\mu x) \tag{10}$$

This absorption coefficient is a product of the cross section σ (cm^2 g) and the mass density ρ (g cm^{-3}). In the fluorescence mode, the absorption coefficient is related to the incident (I_o) and the fluorescence (I_f) fluxes as (Lee et al., 1981):

Figure 1. Schematic representation of a typical X-ray absorption spectrum (μx *vs* E) (background not subtracted) for K edge of Zn (E_0 = 9659 eV), in ZnO, collected in transmission geometry at 77 K.

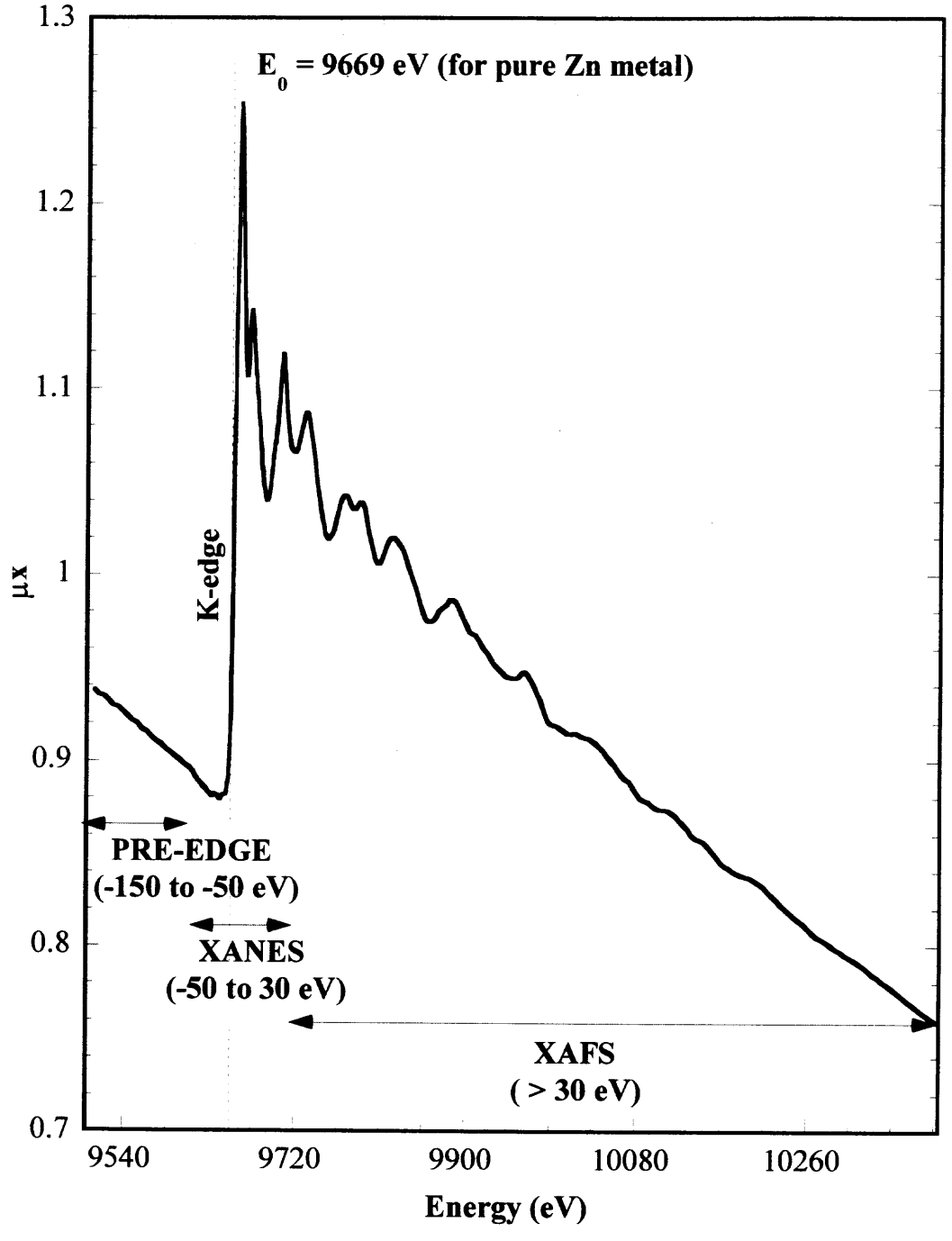

$$\rho_n(r) = \frac{1}{(2\pi)^{1/2}} \int_{k_{min}}^{k_{max}} w(k)\, k^n \chi(k)\, e^{-i2kr}\, dk \qquad (13)$$

where w(k) is a window function which defines the k range to be transformed. This Fourier transform is uncorrected for phase shifts. The modulus of $\rho_n(r)$ exhibits peaks corresponding to the various coordination shells as well as the multiscattering contributions. The position of the peak corresponds to the average frequency of the corresponding shell's XAFS, which is related to the average distance of the shell. The peak height is related to the number of atoms in the shell, the Debye Waller factor σ^2, the number of the atoms in the shell, and the k-space window chosen. In moderate to highly disordered systems, the disorder can cause significant peak shifts and hence do not correspond to the actual average distance. Analysis of the XAS data will be detailed in Experimental Procedures and Analyses Chapter. The following section will focus on the applications of XAS in environmental systems.

2.9 Role of XAS in Environmental Problems

The primary role of XAFS in the environmental field is to help elicit local structural and compositional information of metal speciation and complexation at the aqueous mineral interface. In studies of manganese and iron oxides and other related minerals, Manceau and co-workers (Friedl et al., 1997; Manceau and Combes, 1988; Manceau et al., 1992) have differentiated sorbed structures using XAFS. They have shown that most hydrous Mn gels consist of a 3-D framework of randomly distributed edge- and corner sharing MnO_2 octahedra, which allows them to transform into a large variety of structures. Further, from the XANES analysis, Manceau et al. (1992) distinguished Mn ions of

different oxidation states and also noted that in the poorly crystalline hydrous manganese oxides such as birnessite, vernadite, and absolane, Mn atoms are generally tetravalent. Axe et al. (2000) found that this structure remained stable for at least 6 months with or without Sr sorbed to it. Hydrous ferric oxides have also exhibited short-range order but with a layered structure (Manceau et al. 1992; Manceau and Charlet, 1994; Manceau and Combes, 1988). Axe et al. (1998), on the other hand, only reported that from the XANES analysis for Sr sorption to HFO that the Fe environment did not change with or without Sr sorbed for at least 6 weeks. Likewise other researchers have attempted to test the metastability of hydrous Fe oxide in the presence of anions, such as PO_4^{3-} (Rose et al., 1996) and As (V) (Waychunas et al., 1996), and have found that these anions slow down the rate of crystallization. However, there is a lack of research demonstrating the minimum concentration required to inhibit crystallization, and furthermore, when these oxides are present in heterogeneous systems, their interactions with other minerals inhibits crystallization as well. This research will attempt to further address the effect of adsorbate on metastability or inhibition of crystallization.

Extensive research efforts have involved studying heavy metal sorption to various oxide minerals of such as aluminum, iron, and silica, as well as clays including kaolinite and montmorillonite (Table 1). Metal sorption complexes include outer-sphere surface complexation where the sorbed metal ion retains its hydration shell; the inner-sphere complexation where sorbate metal ions may lose their waters of hydration and bind chemically to the surface; and surface precipitation (Brown, 1990; Stumm, 1992). Often XAS spectra reveal a "beat pattern" providing evidence of second shell contributions. However, the beat patterns do necessarily represent a particular adsorption complex as

suggested by Brown (1990). For example, Axe and co-workers (Axe et al.1998, Axe et al., 2000) have shown that despite the presence of a heavy metal such as Fe or Mn in the second shell, Sr is physically sorbed to HFO and HMO as the first shell included the waters of hydration and additional oxygen atoms from the surface. Many studies have been conducted with crystalline minerals such as γ-Al_2O_3, goethite, kaolinite, and montmorillonite; only a limited number of studies have been conducted with the ubiquitous amorphous adsorbents HFO and HMO. In addition, heterogeneous soil systems examined to date include examining the speciation of metals in contaminated systems (Carroll et al., 1998; Hesterberg et al., 1997; Manceau et al., 1996; O'Day et al., 1998; Ostergren et al., 1999; Szulczewski et al., 1997); these studies have shown that a significant fraction of the metals in these systems are associated with amorphous oxides. Clearly, there is a need for establishing molecular level information about sorption of important transition metals such as Zn and Ni to HFO and HMO. A systematic study of sorption as a function of pH and sorption density is required to better understand and model their mobility in aqueous systems.

In addition, to develop, kinetically accurate transport models, metal sorption to soils and sediments must be evaluated as a function of time. Because amorphous oxides are complicated, surface complexation mechanisms must be understood with these oxides before heterogeneous systems are studied. The effect of the contaminant on the local structure of the oxide is very important for modeling the transformation of the metastable oxide to its crystalline form. The local structure of Sr sorbed to HFO (Axe et al., 1998) and to HMO (Axe et al., 2000) did not change with time indicating that these metastable adsorbents maintain their sorption capacity for as much as six months. Similarly, Strawn

Table 1. Summary of XAS Research

System	First Shell (O)		Outer Shells			Reference
	N	R		N	R	
As(III)/α-FeOOH	3.03-3.12	1.79	Fe	2.3-2.45	3.378	Manning et al., 1998
Cd/α-FeOOH	5.5-6.2	2.3	Fe	0.6-0.6	3.24	Spadini et al., 1994
			Fe	0.6-1.2	3.46-3.51	
Cd/hyd. Fe Oxide	4.0-6.0	2.28-2.31	Fe	0.7-0.9	3.26	Spadini et al., 1994
			Fe	0.7-1.0	3.48	
Co/γ-Al_2O_3	5.9-6.1	2.07-2.08	Al	0.8-1.7	3.27-3.31	Chisholm-Brause et al., 1995
			Co	0.9-2.5	3.16-3.21	
Co/Kaolinite	5.2-5.6	2.07-2.08	Co	3.9-5.0	3.11-3.14	O'Day et al., 1994
Co/Quartz	5.3-6.0	2.06-2.08	Co	2.6-6.0	3.13-3.16	O'Day et al., 1996
Co/Smectite-Clay	6.6	2.09-2.1				Papelis and Hayes, 1996
Co/Smectite-Clay	5.6-7.4	2.1	Co	4.0-7.0	3.12-3.13	Papelis and Hayes, 1996
Co/Al_2O_3	6	2.08-2.09	Co	0.9-4.0	3.09-3.12	Towle et al., 1997
Co/TiO2 (Rutile)	5.5-6.9	1.95-1.98	Co	1.9	3.08	Towle et al., 1997
			Ti	1.3-6.0	2.96-3.0	
Co/α-Al_2O_3	5.8-7.8	2.05-2.09	Al	1.0-1.4	2.66-2.71	Towle et al., 1999
			Al	1.1-1.9	2.95-3.19	
Cr(III)/α-FeOOH			Fe, Cr	1.1-1.6	3.01	Charlet and Manceau, 1992
			Fe, Cr	0.5-0.8	3.45	
			Fe, Cr	1.2-1.9	3.99	
Cr(III)/hyd. Fe Oxide			Fe, Cr	2.61	3.05	
			Fe, Cr	0.8	3.4-3.5	
			Fe, Cr	1.5	4.03	
Cr(III)/MnOxides			Mn	2.0-4.6	2.9	Charlet and Manceau, 1992
			Cr	1.6-2.5	4.03	
Ni/Pyrophyllite	5.5-6	2.05	Ni	2.0-6.3	3.06	Scheidegger et al., 1998
			Al	1.7-4.0	3.08-3.11	
Ni/Soil clay	5.5-6.9	2.05	Ni	0.8-5.6	3.06	Roberts et al., 1999
			Al	0.9-1.8	3.06	
Pb/Al_2O_3	1.5-2.4	2.21-2.29	Al	0.4	3.28-3.32	Bargar et al., 1997
			Al	0.5-0.8	4.15-4.30	
Pb/γ-Al_2O_3	1.5-1.6	2.23	Al	0.5-0.6	3.22-3.25	Bargar et al., 1997, and
			Al	0.7	4.16	Chisholm-Brause et al., 1990
Pb/α-FeOOH	2.2-2.4	2.27-2.28	Fe	0.2-0.3	3.31-3.35	Bargar et al., 1997
Pb/Fe_2O_3	2.0-2.2	2.26-2.30	Fe	0.2-0.5	3.27-3.31	Bargar et al., 1997
Pb/Montmoriilonite	0.93-1.27	2.30-2.31	O	5.5-5.9	2.49-2.5	Strawn and Sparks, 1999
			Pb	1.1-1.3	3.76	
Pb/Montmorillonite	0.9-2.28	2.28-2.30	O	0.8	2.49	Strawn and Sparks, 1999
			Pb	1.76	3.76	
Sr/HFO	9.46-12.62	2.61-2.68	Fe	0.7-2.5	3.4-3.75	Axe et al., 1998
			Sr	7.2-11.8	3.28-3.45	
Sr/HMO	10.0-12.0	2.58	Mn	3	4.12	Axe et al., 2000
			Sr	6	3.88	
Sr/Montmorillonite	5.6-7.2	2.56-2.58				Chen et al., 1998
Sr/Kaolinite	6.0-9.0	2.56-2.58				Parkman et al., 1998
Th/SiO_2	2	2.33	O	6	2.55	Osthols et al., 1997
			Si	2	3.8-3.9	

et al. (1998) observed that for at least 23 days the local structure of lead sorbed to aluminum oxide did not change with time and hence ruled out the possibility of surface precipitation. On the other hand, Scheidegger and colleagues studied kinetics of Ni sorption to aluminum oxide (Scheidegger et al., 1998), pyrophyllite (Scheidegger et al., 1996), and to a soil clay fraction (Robberts et al., 1999) and observed the precipitation of a mixed aluminum-nickel hydroxides. Cheah et al. (1998) investigated the effect of time on copper sorption to amorphous silica, and found that Cu ions initially adsorb as monomeric species, which diffuse over time on SiO_2 surfaces to form dimers. In microporous oxides, zinc sorption to HAO, HFO, and HMO is expected to be limited by intraparticle diffusion, which will be tested in this research. Therefore, from XAFS, the adsorption complex is not expected to vary as a function of time assuming that the internal sites are equivalent to the external sites.

2.10 Summary of Literature Review

The literature review presented above invoked several queries that are the basis for the proposed hypotheses. For instance, the surface charge density calculated from potentiometric titrations and the cation site densities are both functions of pH; as a result can the site density be predicted for a given pH? Also, if metals of the same group from the Periodic Table form similar sorption complexes namely physical, can enthalpies be predicted from structural parameters. If so, then equilibrium constants and activation energies can also be predicted. Literature has demonstrated the need for such predictions but most correlations developed to date have employed experimental data recorded at one temperature and are not necessarily applicable to other conditions.

Evidence exists demonstrating sorption as a two-step process with the second step being the rate-limiting mechanism. Systematic studies with microporous hydrous oxides will be conducted to evaluate intraparticle diffusion in HAO and HMO. Assuming intraparticle diffusion is significant, can surface diffusivities be theoretically assessed using site activation theory. The two required parameters are site density and activation energy. If the correlations developed based on enthalpies and hydrated radii are proven to predict enthalpy and thus activation energy, how do the theoretical surface diffusivities compare with experimentally determined ones?

Another important question is how different are these amorphous adsorbents from crystalline ones such as goethite? Given that goethite has much smaller adsorption capacity than HFO, can competitive effects in binary metal systems be observed and predicted?

A survey of XAS studies points out that macroscopic modeling of sorption data alone is not adequate; complementary information at the atomic level is required to assist in understanding the speciation and complexation. To complete the picture, sorption of such metals as Sr, Zn, and Ni to the hydrous metal oxides needs to be examined *in situ* to fully understand contaminant distribution mechanisms. The hypotheses proposed in this research are presented in the next chapter and have been conceived from the literature review. The results are presented in Chapter 5.

CHAPTER 3

HYPOTHESES TESTED

By and large the objective of the research proposed is to better understand, model, and predict sorption of contaminants in subsurface systems. The hypotheses include establishing relations between parameters and investigating their ability to predict transport and thermodynamic parameters required to describe the sorption of other metals in similar aquatic environments. The experiments conducted developed to test the hypotheses are presented in the next chapter, and are followed by the results.

3.1 Prediction of Site Densities

The surface charge is a function of the solution pH and the zero point of charge. Site densities will be evaluated using a highly soluble probe ion, strontium. In addition, potentiometric titrations will be used to examine the pH zero point of charge and the associated surface charge above and below this point. Because oxide site densities (a sum of external and internal sites) are expected to be a function of the bulk pH, a relationship between it and surface charge will be developed.

3.2 Prediction of Sorption Parameters

In adsorption to amorphous oxides, enthalpies are expected to be less than 25.0 kcal mol^{-1}, indicating metals sorb physically to hydrous oxides in aquatic environments retaining their hydration sheath (de Boer, 1968). The physical sorption is primarily due to the electrostatic forces of attraction. Richens (1997) used structural parameters such as the primary hydration number, N, and hydrated radius, R_H, to develop a correlation for the

Coulombic energy between metal ions and each water molecule in the primary hydration shell. Typically transition metal ions have a smaller hydration number and hence a tighter hydration shell (a smaller N/R_H ratio) than alkaline earth metal ions. As a result transition metals will have a greater Coulombic energy of attraction for the amorphous oxides than alkaline earth metals. Hence, adsorption enthalpies of divalent metal ions with respect to HAO, HFO, and HMO can be written as a simplified function of their structural parameters:

$$\Delta H^\circ = f(N \times Z^2/R_H) \quad (14)$$

where Z is valence charge of a metal ion. This correlation between enthalpy and the inverse of the hydrated cation radii may elicit an estimation method for enthalpies and is presented in Chapter 5. If this correlation proves accurate, then equilibrium constants for other cations can be predicted. From this correlation, adsorption enthalpies for Ca and Ni sorption to HAO, HFO, and HMO will be estimated and compared with those determined experimentally from adsorption isotherm studies.

When metals sorb physically to HAO, HFO, and HMO, they retain their hydration sheath. Accordingly metal sorption is expected to decrease with increase in ionic strength. More importantly, as stated above, enthalpies are expected to be less than 25 kcal mol^{-1}. In addition to conducting isotherms at multiple temperatures, adsorption edge studies will be conducted at 25°C for two different ionic strengths. Furthermore, XAS studies will be conducted to determine whether two select metals, Ni and Zn, lose waters of hydration upon sorption.

For microporous hydrous oxides, intraparticle diffusion along the pore walls of the oxide is the rate-limiting mechanism for sorption. Because transient experiments to determine experimental diffusivities require lengthy periods of time, predicting them from site activation theory may be very useful. Theoretical diffusivities are a function of the activation energy (E_a) and site density (C_t). From the Polyani relationship, the activation energy is related to the adsorption enthalpy through the proportionality constant (α). One hypothesis is that the activation energy for a given metal will be comparable for all three oxides. Furthermore, for a given oxide the proportionality constant for a group of metals from the Periodic Table are expected to be equivalent due to the potential formation of similar sorption complexes. To test this hypothesis, alkaline earth and transition metals will be studied experimentally and theoretically. As part of the macroscopic experiments, metal sorption to HAO, HFO, and HMO will be investigated to determine the surface diffusivities.

According to the site activation theory, surface diffusivity is a function of the jump frequency – the product of the vibrational frequency and the Boltzmann factor (Axe and Anderson, 1997; Kärger and Ruthven, 1992). The vibrational frequency is a function of the force constant $k = d^2U/dx^2$, where U is the surface potential energy. Assuming a sinusoidal function describes this potential energy, the minima are the adsorption sites and the maxima are the barriers between sites. This energy barrier is simply the activation energy for an exothermic reaction where the metal ion desorbs to jump to the neighboring site (Axe and Anderson, 1997; Kärger and Ruthven, 1992). Therefore, activation energy can also be expressed as a function of the structural parameters of the metal ions:

$$E_A = f\left(N \times \frac{Z^2}{R_H^2}\right) \quad (15)$$

Knowing the site density and activation energy, surface diffusivity based on site activation theory can predicted.

Even though HFO and goethite are found to have similar local structures (Spadini et al., 1994) the difference in their long-range order suggests different adsorption capacities and mechanisms. Metal sorption to goethite is expected to be a chemical type of reaction and hence the adsorption enthalpies of metal ions sorbed to goethite are expected be much greater than to HFO. These hypotheses can be tested from isotherms conducted at multiple temperatures. Additionally, metals from the same group may behave alike and hence it is expected that high affinity metals like Ni and Zn will sorb to the same type of sites on the goethite surface while a lower affinity metal such as Ca sorbs to different ones, potentially of lower energy. Subsequently, in a binary metal system involving Ni and Zn, competitive effects may be observed, which can be predicted with the help of potentially the single-site Langmuir isotherm. On the other hand, in binary systems comprising one transition metal (Ni or Zn) and one alkaline earth metal (Ca), no competition is anticipated since these metals are likely sorbing to different types of sites. Adsorption studies in binary systems will be used to corroborate these hypotheses.

3.3 Local Structure of Sorption Complexes

The adsorption enthalpies represent the degree of bonding of an adsorbate to an adsorbent. Accordingly transition metals such as Ni and Zn should be more tightly bound to the oxides than an alkaline earth metal such as Sr. If this is true, the first shell radial

distances of Ni and Zn sorbed to HFO and HMO, obtained from XAS analyses, should be smaller than the first shell radial distances of Sr sorbed to HFO and HMO (Axe et al., 1998, 2000). More importantly, the XAS experiments will also confirm the supposition that metals are only physically sorbed to HFO and HMO and do not sorb chemically, undergo surface precipitation, or form solid solutions. Sorption to the microporous oxides may be limited by intraparticle diffusion. The diffusion model assumes that the sorption mechanism to the sites located along the micropore walls is no different from the ones on the external surface (Axe and Anderson, 1995; 1997). If this assumption is correct, then the local structure of metal ions (Ni and Zn) sorbed to HFO and HMO will not change with reaction time.

Contrary to the amorphous oxide systems, since metal sorption to goethite is expected to be a chemical type of reaction, sorbed Zn ions may not retain their fully hydrated structure. Additionally, because Zn ions are expected to form inner sphere adsorption complexes with goethite, it is possible to find contributions of Fe atoms in the second shell around the zinc ion. If only one type of adsorption site is available for zinc sorption on the goethite surface, then the local structure of zinc will be invariant with pH and adsorbate concentration. To verify these hypotheses, Zn sorption to goethite will be studied with the help of XAS at 298 K, as a function of pH and adsorbate concentration. If the Zn sorption to goethite is a chemical reaction then the thermal contribution to the Debye Waller factor is expected to be small; this hypothesis can be verified by conducting XAS studies on these samples at 77 K.

As seen in the literature review in Chapter 2, even though HFO and goethite have similar local structures, HFO is viewed as a mosaic of short octahedral chains resulting in larger sorption capacity and different sorption mechanisms than goethite. This hypothesis will be verified by comparing the XAS analyses of Zn-HFO systems with Zn-goethite systems. The above hypotheses are intended to achieve two main goals: one is to identify sorption mechanisms for different metal-oxide systems and the other is to establish methods for predicting important thermodynamic and transport parameters that describe the distribution and fate of metal contaminants in the presence of the hydrated oxides of Al, Fe, and Mn. Short- and long-term studies will assist in demonstrating the validity of many of these hypotheses. The others will be confirmed from the XAS studies. Experimental methods employed in this research are detailed in the Chapter 4.

CHAPTER 4

EXPERIMENTAL METHODS AND ANALYSES

This chapter reviews experimental methods used to test the hypotheses proposed in previous chapter. The chapter begins with a section on oxide preparation and is followed by physical and chemical characterization tests. The sorption experiments include batch studies for assessing the short-term adsorption process, semi-batch experiments for evaluation intraparticle diffusion, and XAS studies for the development of mechanistic models of these sorption complexes.

4.1 Syntheses and Characterization of Hydrous Metal Oxides

All chemicals used in oxide precipitation were research grade and only Millipore-Q water was employed. HAO was synthesized according to the method described by Gadde and Laitinen (1974) and others (Anderson and Benjamin, 1990; McPhail et al., 2972; Shuman, 1977), by drop-wise addition of stoichiometric amounts of NaOH to a 2.0×10^{-2} M aluminum nitrate solution under open system conditions. The 1 g L^{-1} of oxide at 6.0×10^{-2} ionic strength was aged for 4 hours prior the sorption experiments. Using the method detailed by Gadde and Laitinen (1974), 1 g L^{-1} batches of HMO were prepared by slowly adding manganese nitrate to alkaline 4.6×10^{-3} M sodium permanganate solution with a final molar ratio of 3:2. The HMO suspension was then centrifuged, rinsed, and redispersed in 1.5×10^{-2} M sodium nitrate solution at pH 7 where it was aged for 16 h. HFO was precipitated as described by Dzombak and Morel (1986). Briefly, HFO is precipitated in a carbonate-free atmosphere at 25°C where NaOH is slowly added to a

0.01 M $Fe(NO_3)_3$ solution. The suspension is aged with constant stirring for 4 hours at a pH of 7 to 7.5.

Goethite has been synthesized by modification to the Atkinson et al. (1976) method. Through drop-wise addition to ferric nitrate, 10 N NaOH was added to reach a pH of 12. The system was completely mixed ($Re > 3.0 \times 10^5$ based on a characteristic length of the stir bar diameter) for 4 h. Subsequently, the iron oxide was aged for 2 weeks at 60°C. The oxide was then rinsed with the aid of centrifugation. This process was continued until the supernatant conductivity reached background. The freeze-dried oxide was stored in a dessicator.

Characterization of the hydrous oxides included particle size analyses (PSA) using a Malvern Particle Size Analyzer, sorption studies to assess site density, potentiometric titrations to evaluate the pH point of zero net proton charge (pH_{pznpc}), and electrophoretic mobility tests for estimating the isoelectric potential (pH_{IEP}) (Sposito, 1998; Stumm, 1992). Morphology of the hydrous oxides was studied using a Phillips Electroscan 2020 environmental scanning electron microscope (ESEM). Oxide mineralogy was characterized by a Phillips X'Pert X-ray diffraction (XRD) with Ni-filtered Cu K-α radiation; in these studies, XRD was also conducted to study the influence of metal sorption on the mineralogy of the hydrous oxides.

Surface area was investigated using the Brunuaer-Emmett-Taylor (BET) nitrogen adsorption method (Gregg and Sing, 1982). This method is based on the determination of the quantity of nitrogen, which when adsorbed on the surface of a solid, completely covers the solid with a monolayer of nitrogen molecules. A volumetric procedure is then used to measure the nitrogen adsorption isotherm near its condensation point of 77 K and

to calculate the nitrogen surface area using the BET equation (Gregg and Sing, 1982). The Micrometrics ORR Surface-Area Pore-Volume Analyzer Model 2100D was employed for this analysis (IGT, 1999). Although the BET method is currently the standard method for measuring surface area, the BET area may underestimate the area available when the oxide is hydrated in an aqueous environment. Pore size distribution was assessed with mercury porosimetry (ASTM C 699) and nitrogen desorption. When mercury or nitrogen is forced into a pore, the pressure required to fill the pore completely is inversely proportional to the pore size. Calculations are based on the capillary law governing liquid penetration into small pores.

4.2 Adsorption Studies

In adsorption studies, metal solutions were tagged with ^{90}Sr, ^{109}Cd, ^{63}Ni and ^{65}Zn in nitrate-based stock solutions. The radioisotope concentrations in filtrates and suspensions were measured using a Beckmann liquid scintillation counter (Model LS 6000SE) with a liquid scintillation cocktail. Ca studies were conducted with untagged stock solutions and analyzed with the atomic absorption spectrophotometer (AA).

In general, calibration standards were run at concentrations of 10, 20, 40, 60, 80, and 100 ppb. The instrument, if necessary, automatically dilutes the original standard of 100 ppb to 20%, 40%, 60%, 80%, and 100%. The appropriate amount of matrix modifier (10 μL modifier + 10 μL sample), if needed, was added by using the auto sampler to minimize interference and increase sensitivity. The AA automatically dilutes the samples if necessary. Ca was analyzed at 422.7 nm wavelength and its detection range with AA was 2 to 100 ppb. Zn was measured at 213.9 nm with a detection range of 1 to 100 ppb.

In all sorption studies, bulk aqueous phase concentrations of metals were below saturation with respect to the most thermodynamically stable precipitate (Appendix A) (Allison et al., 1991). Also, a turbulent hydraulic regime ($Re \geq 3.0 \times 10^5$) was maintained resulting in negligible resistance to external mass transfer. Based on the mass balance, the amount sorbed was calculated. For all adsorption studies with HAO and HFO, the oxide concentration was maintained 1 g L^{-1}, while all adsorption studies with HMO were conducted with an oxide concentration of 0.1 g L^{-1}. For single adsorbate experiments with goethite, an oxide concentration of 1 g L^{-1} was used. The binary systems were studied with 0.1 g L^{-1} to limit the number of available sites. Except for adsorption edge studies, a sodium nitrate based background electrolyte was maintained at 6.0×10^{-2} M for HAO systems, 3.1×10^{-2} M for HFO systems, 1.5×10^{-2} M for HMO systems, and 1.0×10^{-3} M for goethite.

All short-term adsorption studies were conducted in Nalgene® containers (with a contact time of 4 h for amorphous oxide systems and of 2 h for goethite systems) using an LAB-LINE Orbital water bath shaker (Model 3540) (Axe and Anderson, 1995, 1997). For isotherm studies, initial metal concentrations ranged from 10^{-11} to 10^{-4} M; this broad range of concentrations allows for potentially assessing the types of sites present on the oxide surface. In the isotherm studies with amorphous oxides (Axe and Anderson, 1995, 1997), contact times from less than 1 hour to 168 hours revealed no change in the amount sorbed, indicating an equilibrium or pseudo-equilibrium between metal adsorbed to the external surface and that in the bulk aqueous phase. Likewise with the oxides used in this research, studies demonstrated that there was no difference in the amount sorbed when contact time ranged from 2 to 4 hours. Adsorption edge studies were conducted at room

temperature (~ 25°C) and two ionic strengths. Isotherms were conducted at multiple temperatures (4°C≥T≥25°C) and three pH values to evaluate equilibrium constants, site densities, and enthalpies (Angove et al., 1998; Axe and Anderson, 1997; Johnson, 1990; Mishra et al., 1997; Mishra and Tiwary, 1995, 1998, 1999; Rodda et al., 1996).

Constant boundary condition (CBC) experiments were designed to study the slow sorption process of intraparticle surface diffusion in a convenient time frame (Axe and Anderson, 1995, 1997). In short-term studies the adsorbate concentration gradient, which was the driving force, decreased with time. In CBC studies, the surface concentration was maintained constant by monitoring and maintaining the bulk aqueous concentration of metal ion constant (Axe and Anderson, 1995, 1997) (Figure 2). The CBC experiments were conducted in 1 L Nalgene® containers at room temperature and lasted from 2 -110 days.

Prior to studying competitive adsorption, experiments were conducted to investigate reversibility. For this purpose, in one set of experiments, 2×10^{-4} M Ni was added to the system and allowed to equilibrate with goethite for 2 h at pH 7 and 25°C. Then variable quantities of Zn were added and the systems were allowed to reequilibrate for an additional 2 h at a constant pH of 7. In another set of studies, the sequence of addition of these metals was reversed.

All the competition studies (for Ni-Zn, Ni-Ca, and Zn-Ca binary systems) were conducted at 25°C and 10^{-3} ionic strength with simultaneous equimolar additions over the entire adsorbate concentration range and with a 2 h contact time. For each binary system, competition was studied at pH 5, 6, and 7 with the goethite concentration maintained at 0.1 g L^{-1}. The range of adsorbate concentrations was the same as the ones selected for the

Figure 2. Constant Boundary Condition (CBC) Experiments: Intraparticle diffusion of metal contaminants along the micropore walls of amorphous oxides. Grey spherical area represents the amorphous oxide particle with micropores and dark points represent the metal adsorbate.

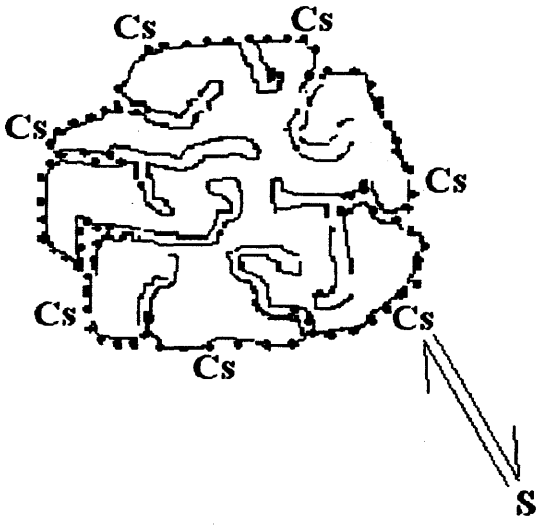

S (bulk aqueous metal concentration) - - maintained constant

Therefore C_s (amount of metal sorbed on external surface) - - maintained constant

single adsorbate experiments. Also, for the Ni-Ca and Zn-Ca systems, additional molar ratios of 1:10 and 1:100 were employed. Each binary system was conducted in duplicate sets, such that one metal was tagged and the other was untagged. Ni and Zn analyses were conducted with the liquid scintillation counter as described for the single adsorbate experiments. All Ca studies were conducted with untagged stock solutions and analyzed with the AA (Greenberg et al., 1995).

4.3 XAS Studies

Adsorption samples were prepared at pH 7 and 25°C for the following sorption densities: 1×10^{-3} and 1×10^{-2} moles of Zn g^{-1} HFO. To understand the sorption mechanism as a function of pH, samples with a sorption density of 1×10^{-3} moles of Zn g^{-1} HFO were studied at pH 6 and 8. Finally, the local structure of Zn^{2+} was also examined in a Zn-HFO coprecipitate sample prepared at pH 7 and 25°C; the zinc concentration in this sample was 1×10^{-3} moles of Zn g^{-1} HFO. Zinc adsorption to goethite was studied at the maximum loading of 1.2×10^{-5} moles of Zn g^{-1} goethite at pH 6 and 2.0×10^{-5} moles of Zn g^{-1} goethite at pH 7. Also, adsorption samples were prepared at pH 7 and 25°C for the following sorption densities: 1×10^{-4}, 1×10^{-3}, and 1×10^{-2} moles of Zn g^{-1} HMO. To understand the sorption mechanism as a function of pH, samples with a sorption density 1×10^{-2} moles of Zn g^{-1} HMO were also prepared at pH 3.5 and pH 5.0. Additionally, to test the hypothesis that metal sorption to this microporous oxide is limited by intraparticle diffusion, where the adsorption mechanism on the micropore walls is similar to that on the external surface, a 32 day old sample was also studied. The sorption density of this sample was 4×10^{-3} moles Zn g^{-1} HMO (where 1.2×10^{-3} moles were sorbed internally).

Nickel adsorption to HMO was synthesized at pH 5 and 7 and 25°C for the following sorption densities: 1×10^{-3} and 1×10^{-2} moles of Ni g^{-1} HMO. To understand the kinetics of Ni sorption to HMO, samples from a Ni-HMO CBC system, maintained at pH 7 and 25°C, were collected for XAS studies after contact times of 20 and 110 days. Ni sorption densities after 20 days and 110 days were 9.8×10^{-3} moles of Ni g^{-1} HMO (8.9×10^{-3} moles sorbed internally) and 9.9×10^{-3} moles of Ni g^{-1} HMO (8.9×10^{-3} moles sorbed internally), respectively.

The sorbed metal concentrations were measured using ^{65}Zn and ^{63}Ni as tracers in duplicate studies (see Chapter 4), where the activity was measured with a Beckman LS6000SE liquid scintillation counter. Except where otherwise stated, adsorption samples were equilibrated for 4 h under turbulent hydraulic conditions ($Re \geq 3.0 \times 10^5$ with respect to the reactor length) before the solid phase was separated from the supernatant by centrifuging at 8000 rpm for 20 minutes. These wet pastes were loaded into aluminum or acrylic cells and sealed with mylar windows to prevent the loss of moisture. Nickel oxide (NiO), nickel carbonate hydrate ($NiCO_3 \cdot nH_2O$), and a 1×10^{-3} M $Ni(NO_3)_2$ solution at pH 1 were used as standards. For zinc, reference compounds, with well known structures, included zinc carbonate hydrate or hydrozincite ($ZnCO_3 \cdot nH_2O$), zincite or zinc oxide (ZnO), zinc oxide hydrate ($ZnO \cdot nH_2O$), zinc ferrite ($ZnFe_2O_4$), and a 1×10^{-3} M $Zn(NO_3)_2$ solution at pH 1.

XAS data were acquired on beamline X-11A at the National Synchrotron Light Source (NSLS), Brookhaven National Laboratory where the electron beam energy was 2.528 and 2.8 GeV with an average beam current of 180 mA. The XAS data of the Ni-HMO adsorption samples were collected at Ni K-edge over the energy range of 8183 –

9082 eV in fluorescence mode using a Lytle detector filled with Ar gas, while those of the Zn-HMO and Zn-HFO samples were collected at Zn K-edge over the energy range of 9509 – 10408 eV under similar experimental settings. The samples were placed 45° to the incident beam. For minimizing the scattered background without attenuating the signal significantly the following filters were placed between the sample and the soller slits: a 3μm Co filter (Z-1 filter) plus one aluminum foil for Ni studies and a 6 μm Cu filter (Z-1 filter) with one aluminum foil for Zn studies. The soller slits were placed in front of the detector to block most of the filter refluorescence. Harmonic rejection was achieved by detuning the monochromator by 20% of I_o. For Zn-goethite adsorption samples, XAS spectra were collected in fluorescence mode using a multielement Ge solid-state detector, with detector elements tuned to measure Zn. For these samples, the monochromator was detuned to 70% of the fully tune Io in order to operate the detector in linear regime.

The XAS data of the reference compounds were collected at the respective K-edges over the same energy range in transmission mode at room temperature (298K) and 77 K. Prior to data collection, the energy was calibrated to the first inflection of the metal foil standards (E_o = 8.333 keV for Ni and E_o = 9.659 keV for Zn).

The XAS spectra were analyzed using WinXAS 97 (Version 1.0). For each scan, the background X-ray absorbance was subtracted by fitting a linear polynomial through the pre-edge region. The edge jump of a background corrected XAS spectrum was normalized with a zero order polynomial fit between -150 and -50 eV from the K-edge. The threshold energy (E_o) of each spectrum was determined from the first inflection point in the edge region and was used to convert the spectra from energy to k-space. An advanced spline function was employed to account for the atomic absorption in the

absence of backscattering contributions. This isolated function produced the XAFS function ($\chi(k)$), which was then weighted by k^3 to enhance the higher k-space data. The chi plots were Fourier transformed using the Bessel window function to produce the radial structural function (RSF). The atomic shells from these RSFs are fitted either in isolation or together to a model structure (of the reference compound) that was generated using FEFF7. The resulting fits provide the local coordination of metal ions sorbed to the oxides.

CHAPTER 5

ADSORPTION TO AMORPHOUS OXIDES

The hypotheses described in Chapter 3 were conceived from literature. The first two sections begin with characterization of the hydrous metal oxides, and are followed by adsorption of alkaline earth metal (Sr) and transition metals (Cd and Zn) to these oxides. The sorption experiments include short- and long-term experiments for evaluating adsorption and intraparticle diffusion. Subsequently, sorption studies conducted with Ni and Ca to test correlations developed from theory and based on experimental results.

5.1 Oxide Characteristics and Properties

Using standard methods for characterization of adsorbents as described by Gregg and Sing (1992), the surface area, porosity, and pore size distribution were evaluated on freeze-dried particles of HAO and HMO by the Institute of Gas Technology (1997) (Appendix B). Accordingly, the surface area of HAO was approximately 411 $m^2 g^{-1}$ and that of HMO was approximately 359 $m^2 g^{-1}$ (IGT Report, 1997). Because these surface areas are measured on freeze-dried particles, hydrated ones are expected to be much greater (Bottero et al., 1993; Dzombak and Morel, 1990; Meng and Letterman, 1993; Okazaki et al., 1986; Scheidegger et al., 1998). As discussed earlier for example, Bottero et al. (1993) found large variations in surface area of amorphous aluminum oxides where using adsorbing organic molecules, areas ranged from 600 to 1000 $m^2 g^{-1}$, while using N_2 gas adsorption areas were <20 $m^2 g^{-1}$. However, when measuring the surface area of ferrihydrite, they found 135-163 $m^2 g^{-1}$ using anionic surfactants for in-situ studies and 295 $m^2 g^{-1}$ from argon adsorption isotherms on dried particles. The porosity of HAO and

HMO based on pore diameters less than 250 Å was 0.4 and 0.3, respectively (IGT Report, 1997). The associated pore size distribution of HAO was monomodal with mean pore radius of 1.9 nm; while that of HMO was bimodal with two dominant pore radii of 2.1 and 6.1 nm. Thus, in aqueous systems where layers of water adsorb on the pore walls, HAO and HMO like HFO (with mean radius 3.8 nm) are microporous oxides (Axe and Anderson, 1995; Bottero et al., 1993; Kärger and Ruthven, 1992).

The in-situ technique of ESEM revealed irregular topographies for the porous aggregated particles of freshly precipitated HAO and HMO (Figure 3). The particle size distributions (PSDs) of HAO and HMO (Figure 4) are monomodal with particle diameters ranging between 1 and 500 μm; these distributions were measured under the same hydraulic regime used in sorption studies. The PSDs are almost independent of pH within the solubility range, and similar to HFO (Figure 4 [Axe and Anderson, 1995]). Given intraparticle diffusion as the rate-limiting mechanism, the time required to reach equilibrium is a function of the PSD (Axe and Anderson, 1995, 1997).

From potentiometric titrations, the pH_{pznpc} of HAO was approximately 8.98 ± 0.02 (Figure 5), which is in good agreement with others (Anderson and Benjamin, 1990; Lo and Leckie, 1993; Manning and Goldberg; 1997; Stumm, 1992). The pH_{pznpc} of HMO is approximately 2.60 ±0.05, which lies in the range of pH 1.5 to 3.0 reported by others (Mishra and Tiwary, 1995; Morgan and Stumm, 1964; Stumm, 1992). The pH_{pznpc} is 7.60 ± 0.5 for HFO, which is consistent with others (Anderson and Benjamin, 1990; Bottero *et al.*, 1993; Dzombak and Morel, 1990).

Figure 3. ESEM photographs of HAO (top) and HMO (bottom) reveal the spherical shape and the rough topography of the aggregated particles.

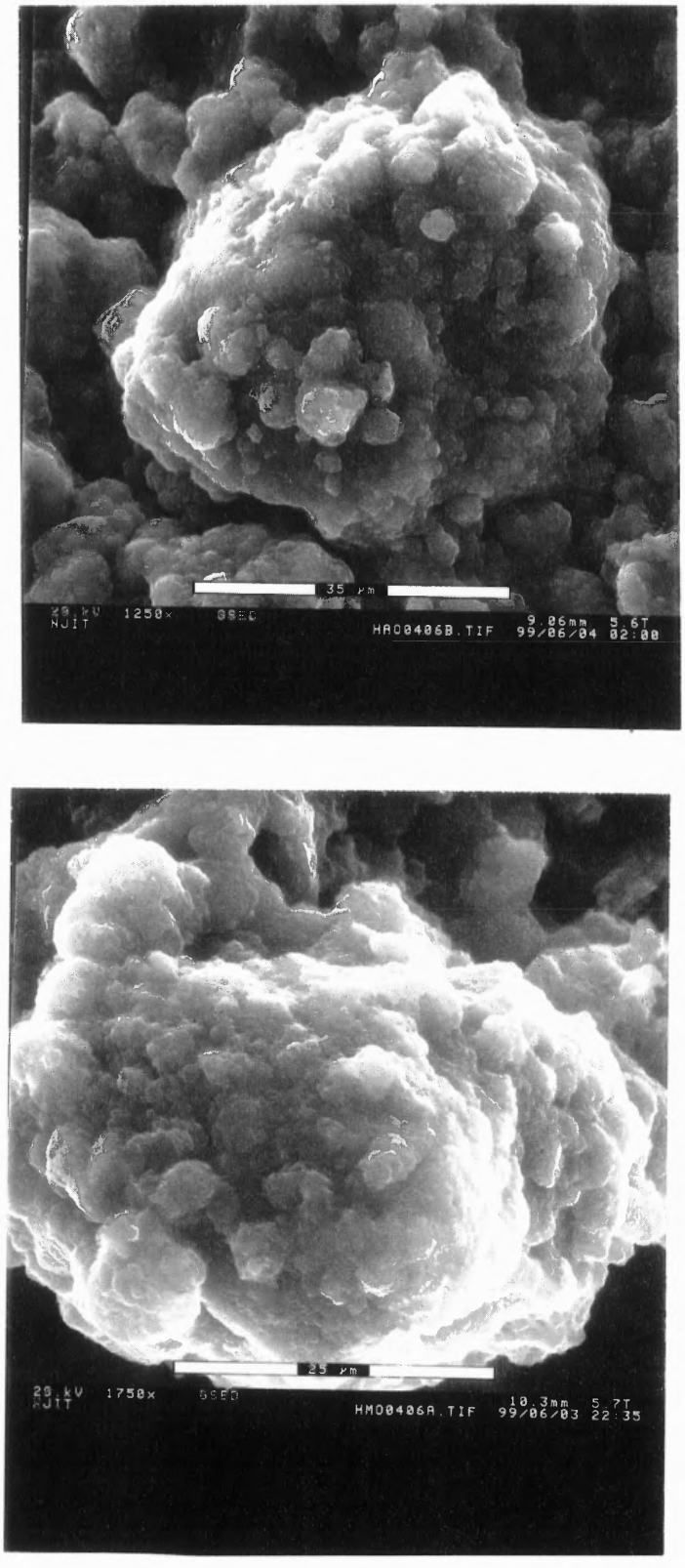

Figure 4. Particle size distributions of freshly precipitated hydrous metal oxides at 25°C are independent of suspension pH.

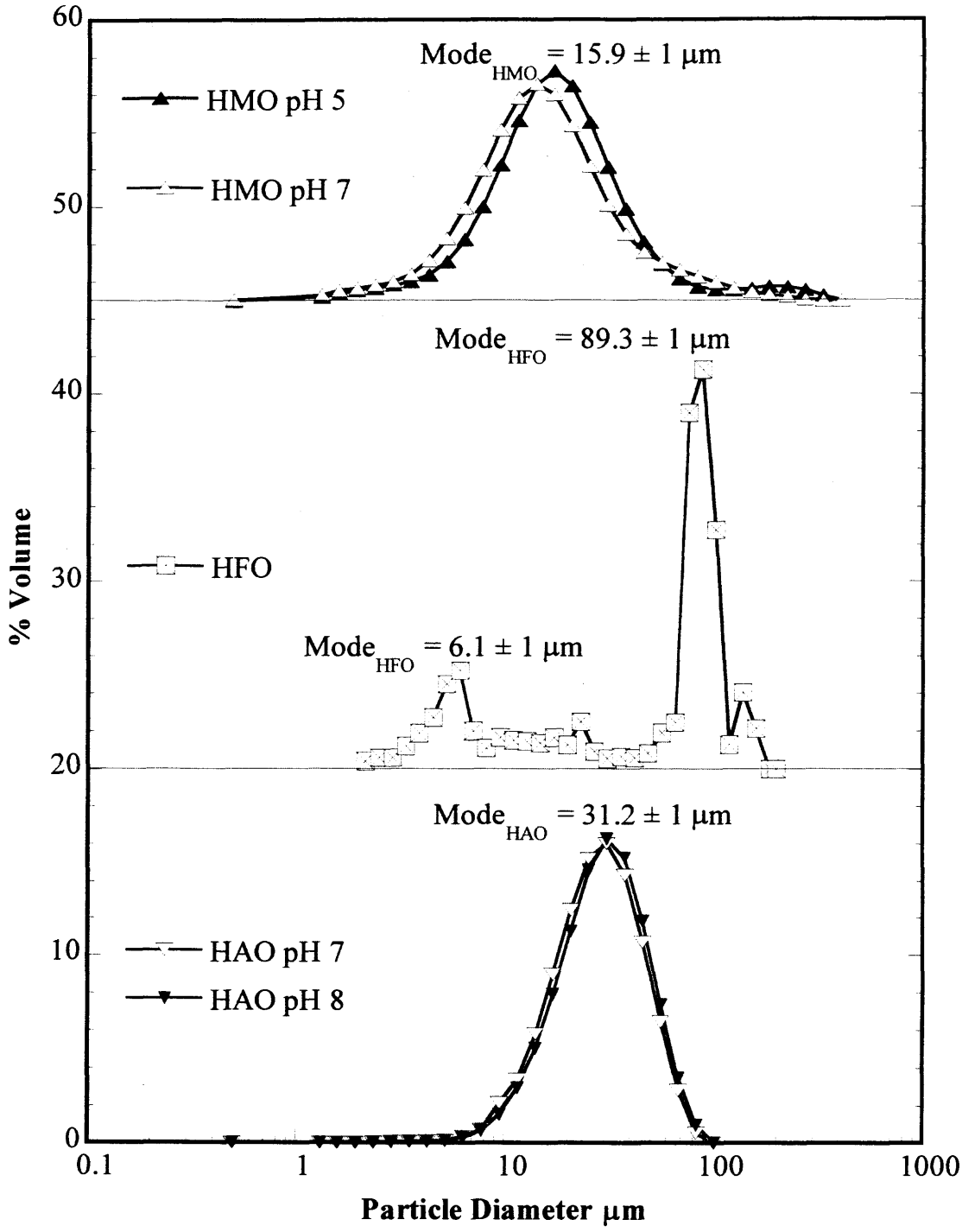

Figure 5. Potentiometric titrations of hydrous metal oxides at 25°C: Determination of pH_{PZNPC}.

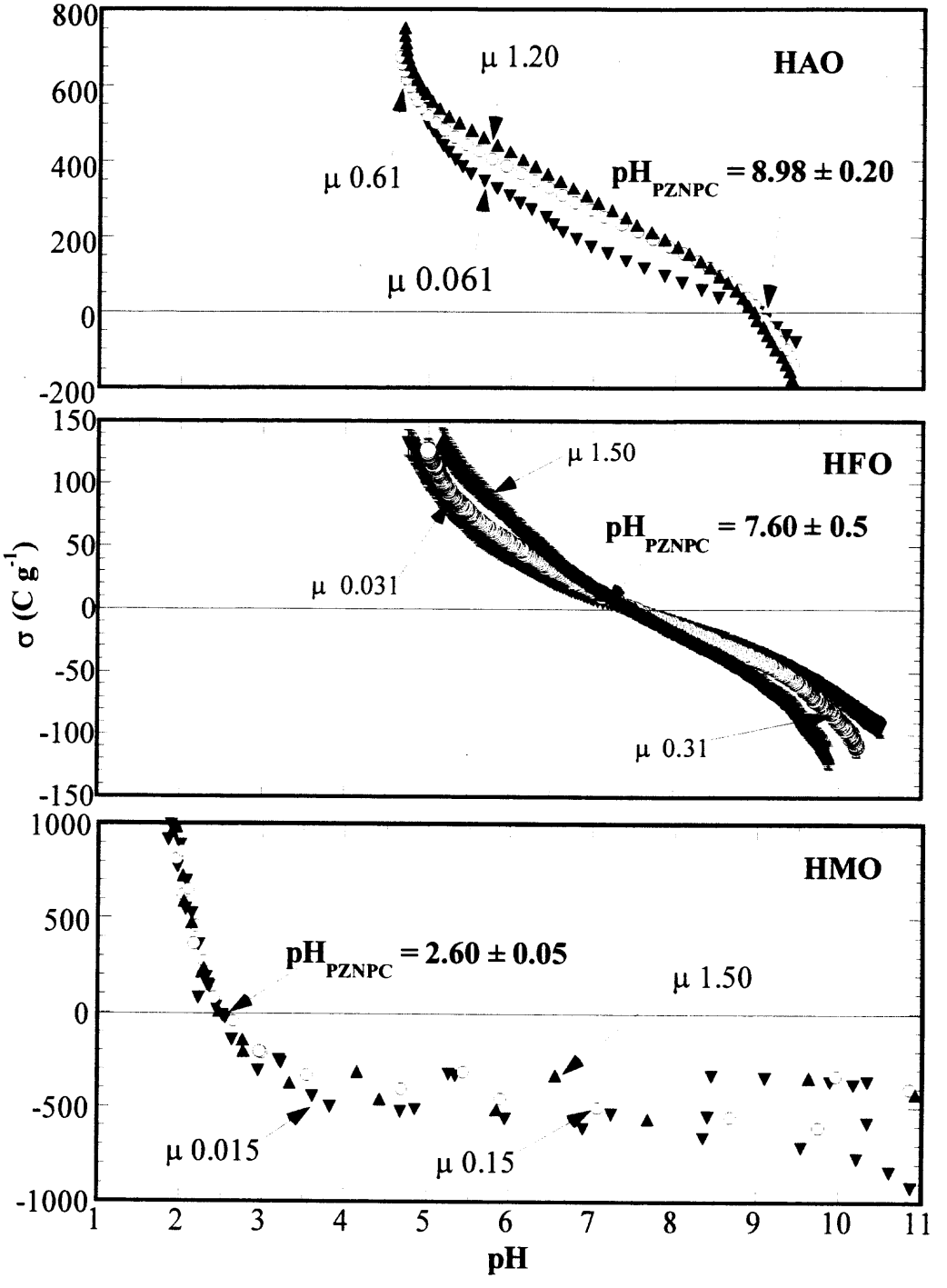

Using Sr^{2+} as the probe ion and under closed conditions, the site densities (C_t) of HAO, which account for external and internal surface sites, were in the order of 10^{-2} to 1.8×10^{-2} moles Sr g^{-1} between pH 6.0 and 8.0, while those for HMO ranged from 3.7×10^{-3} to 3.4×10^{-2} moles Sr g^{-1} between pH 3.5 and 7.0. Likewise, the site density of HFO increased from 5.7×10^{-3} moles Sr g^{-1} at pH 5.0 to 2.5×10^{-2} mol Sr g^{-1} at pH 7. Tamura et al. (1997) determined similar orders of magnitude of site densities for various aluminum, iron, manganese, and titanium oxides by Grignard reaction of surface hydroxyl groups. The difference in site densities between results presented here and others (e.g., a compilation for HFO in Dzombak and Morel, 1990) may be explained in part by the method used for measurement; in this research, assessment included both external and internal sites using the probe ion Sr that has a high solubility (Allison et al., 1991).

Figure 6 illustrates the linear relationship between site density and the external surface charge determined from potentiometric titrations. The first term on the right hand-side of the equations shown in Figure 6 relates the surface potential to charge (Murray, 1974). The intercept represents the natural log of the site density at the pH_{pznpc}. According to this relation, the site density of HFO at its pH_{pznpc} is 2.8×10^{-2} moles Sr g^{-1}. The actual site density of HFO measured at its pH_{pznpc} was 3.0×10^{-2} moles Sr g^{-1}, which falls within the model and data errors based on the propagation of errors (Ku, 1966). This result confirms the first hypothesis that site density is a function of pH and hence can be estimated from the surface charge density. Overall, characteristics and properties of the hydrous oxides are summarized in Table 2.

Figure 6. Site densities (C_t moles Sr g^{-1}) of hydrous metal oxides correlated to the surface charge density (σ) at 25°C. The legend shows the ionic strengths at which the C_t were measured

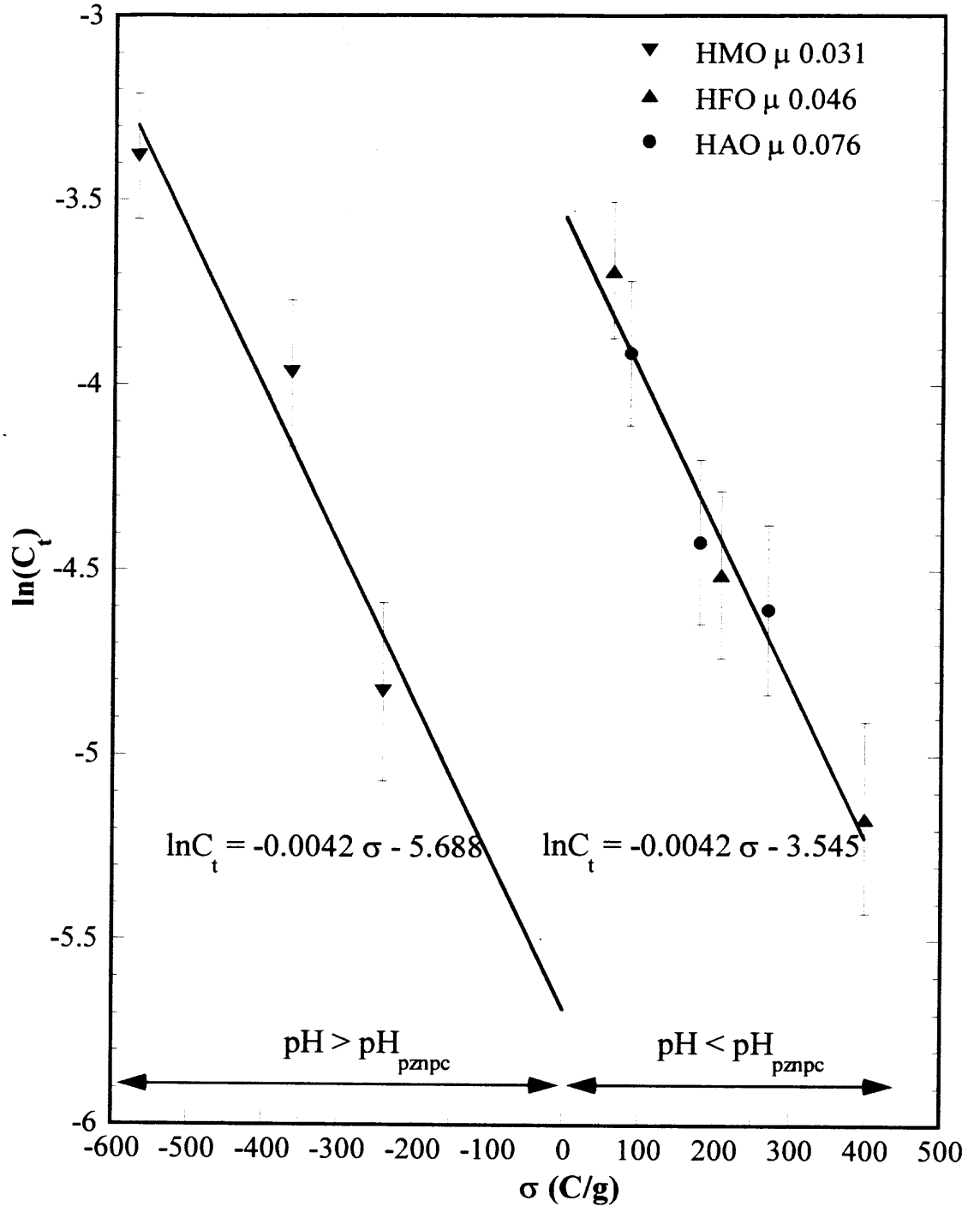

Table 2. Characteristics and Properties of Hydrous Oxides

Characteristics	HAO	HFO**	HMO
Mean Particle Diameter (μm)	30.0	40.0	20.0
Surface Area (m^2/g) *	411	36.6	359
Mean Pore Radii (nm) *	1.9	3.8	2.1, 6.1 (Bimodal)
Porosity *	0.45	0.50	0.35
pH_{ZPC}	8.98	7.60	2.55
σ ($C\ g^{-1}$) ‡	160.9	67.1	-564.1
Site Density (mole Sr g^{-1}) ‡	0.012	0.025	0.034
sites nm^{-2}	16.0	41.0	59.0

* Analyses performed by IGT
** HFO data obtained from Axe and Anderson (1995)
‡ Values estimated at pH 7

5.2 Sorption Studies with Sr, Cd, and Zn

X-ray diffraction (XRD) was conducted to assess the oxide crystallinity (or lack of) and potentially the type of sorption at higher loadings. The patterns of freshly precipitated HAO and HMO (Figure 7) indicate that oxides were amorphous. XRD of HFO as studied by Axe and Anderson (1995) also revealed broad flat patterns indicative of the amorphous oxide, ferrihydrite, which was stable up to 6 months. Furthermore, XRD studies with Sr sorbed at mole ratios of 1:1 Sr:oxide metal (Al or Mn) showed no evidence of a strontium precipitate or strontium solid solution with the oxide surface; these amorphous oxides were stable for at least 6 months. X-ray diffraction profiles of hydrous metal oxides (Figure 8) revealed that these oxides remain amorphous when Cd or Zn was sorbed to their surfaces. There was no evidence of a surface precipitate or solid solution formation in metal sorption to the hydrous oxides. The diffraction studies showed that HAO and HMO aged 6 months with and without the adsorbate remained amorphous. Many other studies (Axe and Anderson, 1995; Baltpurvins et al., 1996; Fuller et al., 1993; Golden et al., 1997; Jenne, 1968; Waychunas et al., 1993) have found that sorption may inhibit oxide crystallization; however, for the duration of studies, no crystallization was observed, with or without contaminant sorbed (Figures 7 and 8).

As seen in Figure 9, adsorption edges used to study Sr adsorption as a function of pH are broad and typical of alkaline earth metals (Axe and Anderson, 1995; Dzombak and Morel, 1990; Kinniburgh et al., 1976; Lützenkirchen, 1997; Mishra and Tiwary, 1995). Adsorption edges for Cd and Zn adsorption to hydrous metal oxides (Figure 10) illustrate the sigmoid curve characteristic of transition metals (Anderson and Benjamin,

Figure 7. X-ray diffraction profiles of HAO and HMO with and without Sr sorbed reveal these potentially nanocrystalline oxides remain amorphous for at least 6 months.

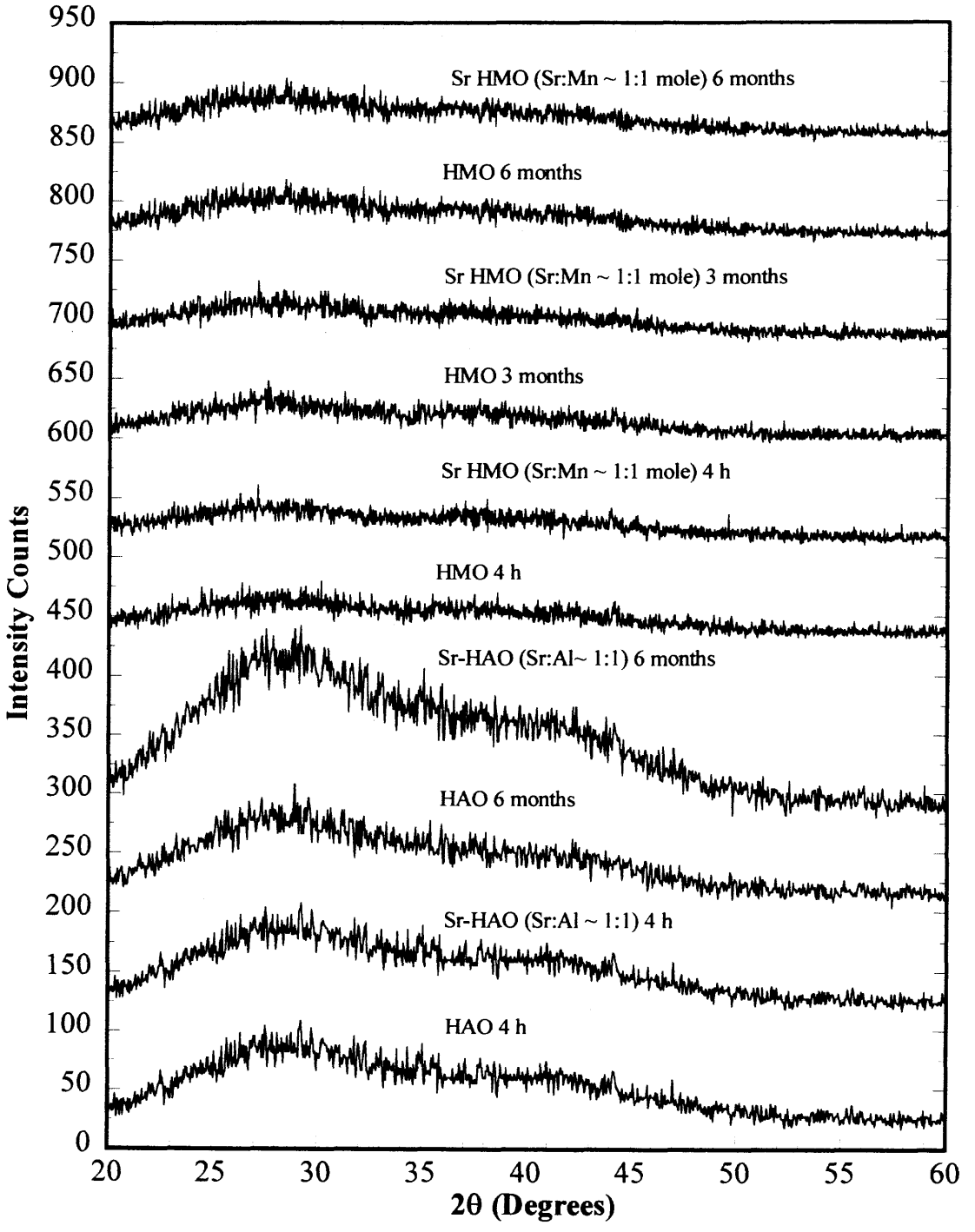

Figure 8. X-ray diffraction profiles of HAO and HMO with and without metal contaminants sorbed demonstrate that these potentially nanocrystalline oxides remain amorphous for at least 6 months.

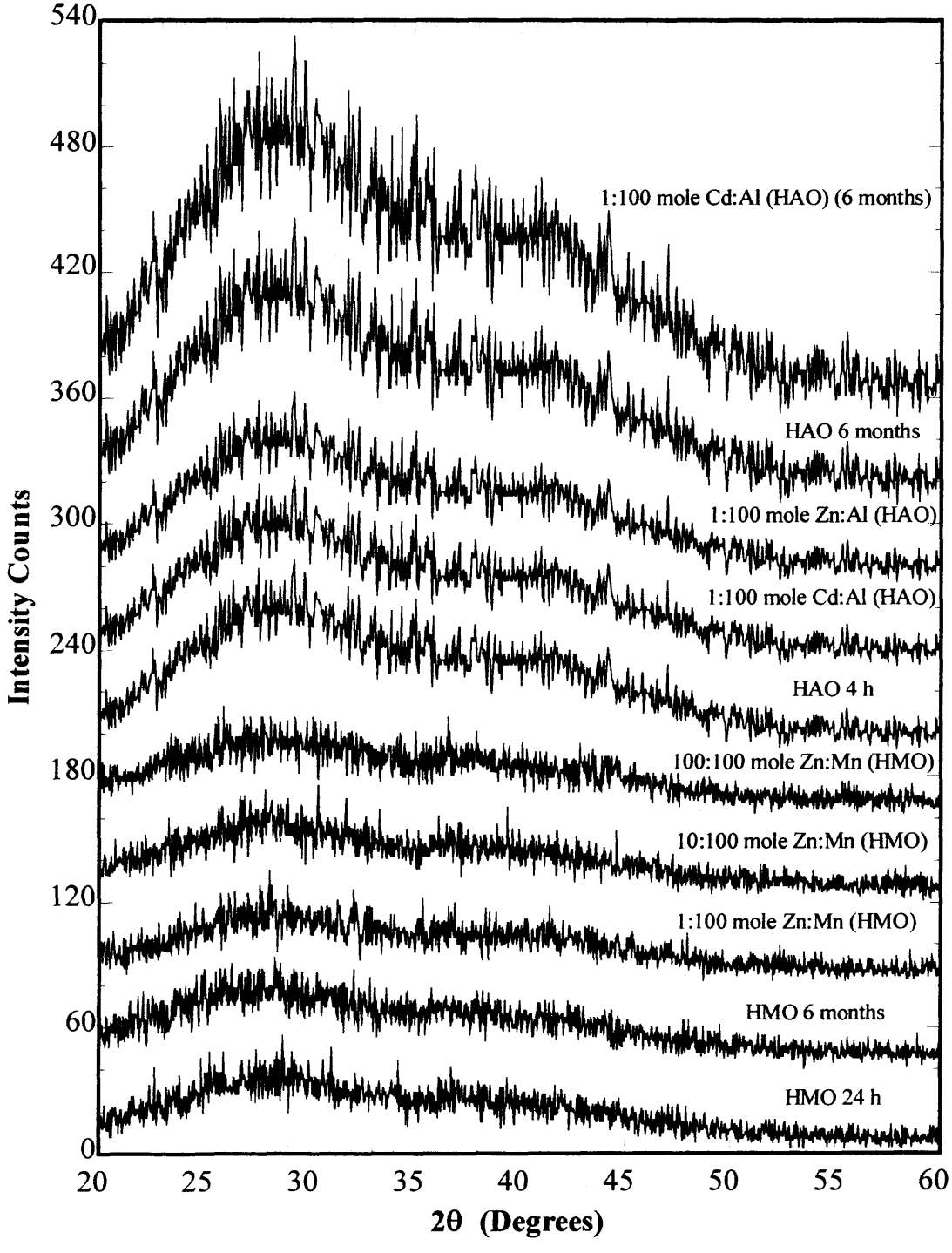

Figure 9. Adsorption edges of Sr sorption to 1 g L^{-1} hydrous metal oxides at 25°C: effect of ionic strengths. For HAO and HMO, $[Sr]_o = 5 \times 10^{-5}$ M and for HFO, $[Sr]_o = 1 \times 10^{-4}$ M.

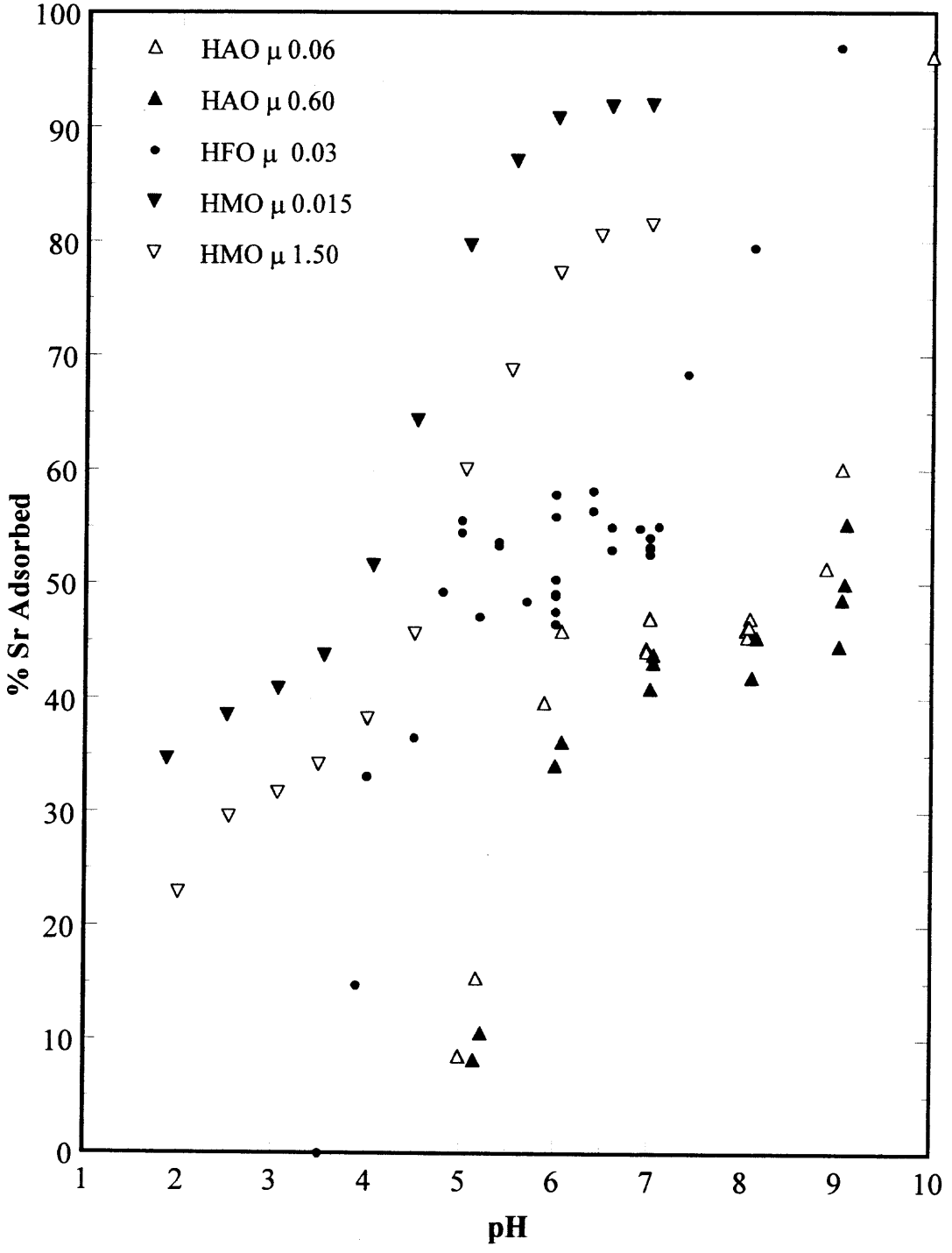

Figure 10. Adsorption edges of Cd and Zn adsorption to hydrous metal oxides at 25°C: effect of ionic strengths. For all studies, $[Cd]_o = 5 \times 10^{-5}$ M and $[Zn]_o = 5 \times 10^{-5}$ M (except for HFO -- 2×10^{-7}).

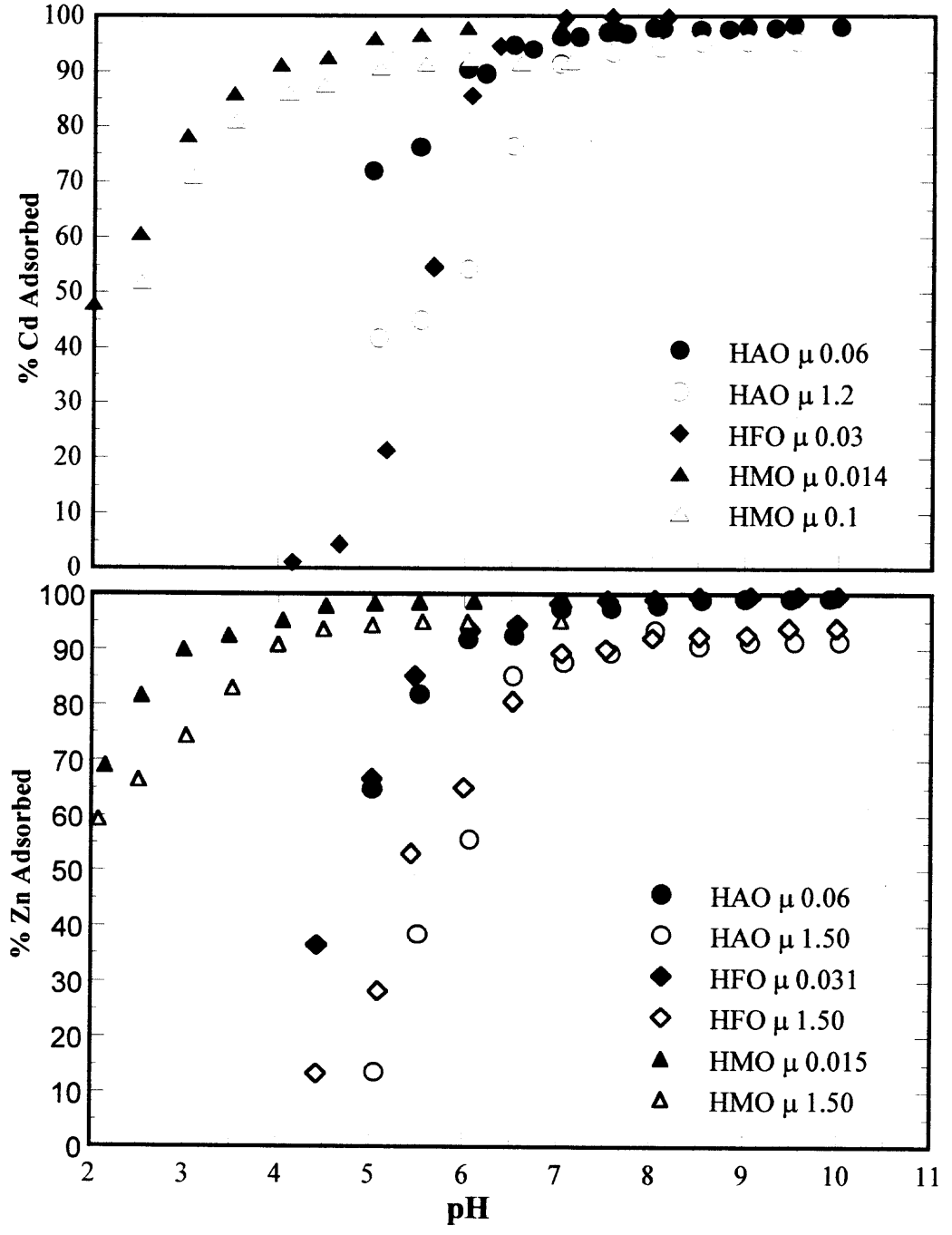

1990; Apak et al., 1995; Axe and Anderson, 1997; Crawford et al., 1993; Dzombak and Morel, 1990; Gadde and Laitinen, 1974; Kinniburgh et al., 1976; Lützenkirchen, 1997; Meng and Letterman, 1993; Misak et al., 1996; Mishra et al., 1997; Mishra and Tiwary, 1998: Shuman, 1977; Tamura et al., 1996). Regardless of metal, a comparison of adsorption edges for HAO, HFO, and HMO shows that the degree of adsorption is consistent with the pH_{pznpc} following the order of HMO > HFO > HAO; this result is in agreement with others (Anderson and Benjamin, 1990; Gadde and Laitinen, 1974; Misak et al., 1996; Tamura et al., 1997). The adsorption affinity of cations to hydrous metal oxides follows the trend of Zn > Cd > Sr, and is consistent with that observed by others (as discussed in Chapter 2).

For any hydrous oxide system, the amount of Sr^{2+}, Cd^{2+}, and Zn^{2+} sorbed decreased with increase in ionic strength, which is suggestive of physical adsorption where the waters of hydration are not lost upon sorption (Lützenkirchen, 1997; Misak et al., 1996). Misak et al. (1996) demonstrated that the decrease in the activity coefficient with increase in ionic strength could explain the adsorption edge shift to the right. However, in the present study, this change could not describe the decrease in adsorption.

Isotherms for strontium adsorption to HAO and HMO studied at 25°C and at different pH values reveal a linear relationship between the sorbed and the bulk aqueous phase concentrations over five orders of magnitude (Figure 11). This linear relationship suggests that the range of surface sites can be described with one average type of site. Isotherm fits resulted in $r^2 \geq 0.97$. Because no change in pH was observed during the adsorption studies at even the greatest loading of 10^{-2} mole g^{-1} oxide, Sr^{2+} may not displace protons and is likely held electrostatically to the surface. Similarly, isotherms for

Figure 11. Isotherms of Sr sorption to 1 g L^{-1} HAO and HMO at 25°C as a function of pH. Solid lines represent linear distribution model; K_d (L g^{-1}) is the distribution coefficient ($K \times C_t$).

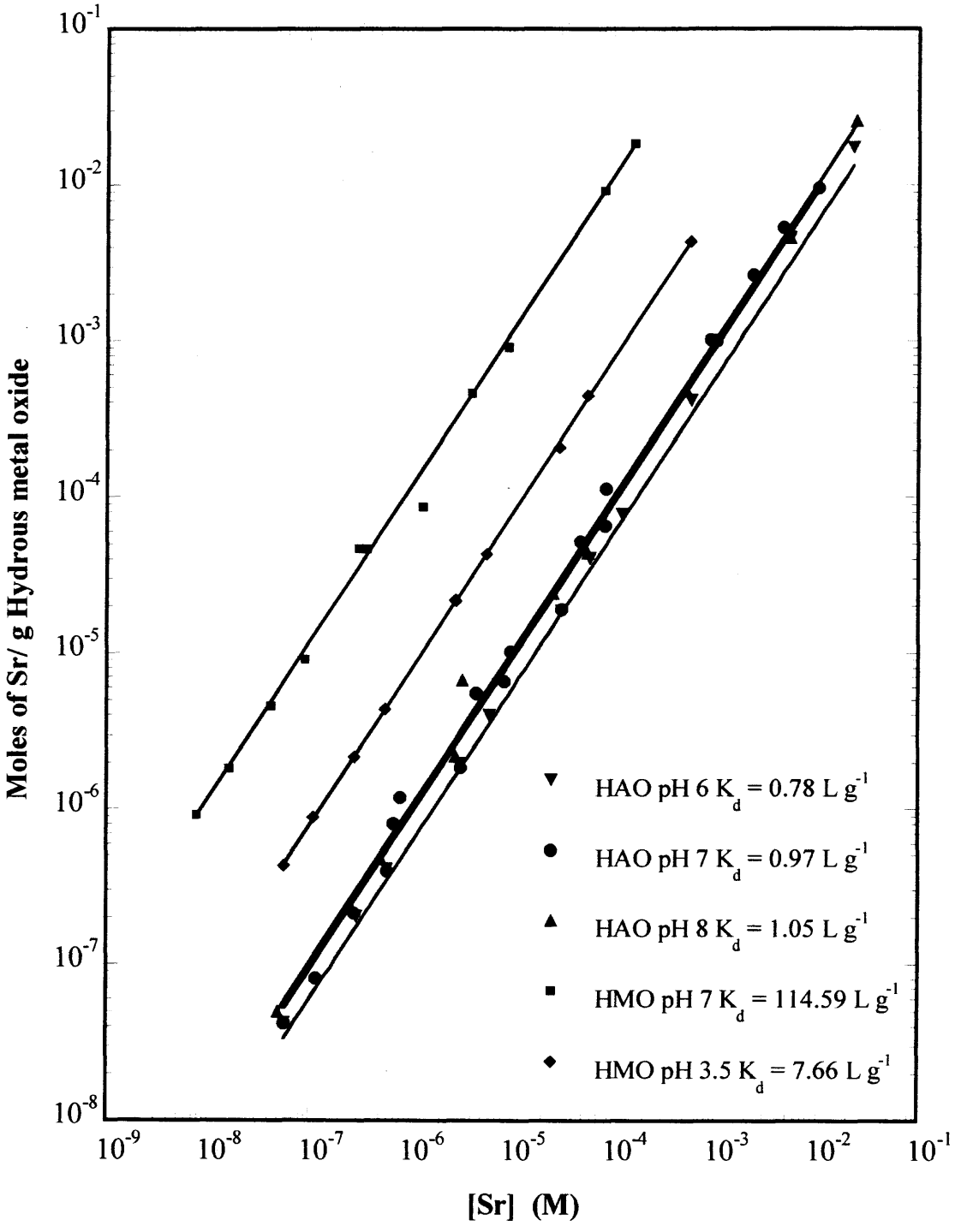

adsorption studies at even the greatest loading of 10^{-2} mole g^{-1} oxide, Sr^{2+} may not displace protons and is likely held electrostatically to the surface. Similarly, isotherms for Cd and Zn adsorption to hydrous oxides (Figure 12) demonstrated linear relationships ($r^2 \geq 0.96$) between the sorbed and the bulk aqueous concentrations. Generally for physical sorption the adsorbate should replace some cation in the diffuse layer. If protons were released, they could have been re-adsorbed back onto the oxide surface. In working with trace metal concentrations, the site densities of HAO, HFO, and HMO are approximately equivalent to the number of sites available, $C_T \approx C_V$ (Axe and Anderson, 1997), as such the Langmuir isotherm reduces to the linear distribution model. Based on Langmuir-Hinshelwood kinetics, the distribution coefficient K_d (L^{-1} g) is simply the product of the equilibrium constant and site density, $K \times C_T$ (Axe and Anderson, 1995, 1997; Fogler, 1992).

In a number of studies, the Langmuir model has been employed to describe metal sorption to oxides: Zn and Pb adsorption to goethite (Johnson, 1990; Rodda *et al*, 1996); Zn adsorption to Al and Fe hydrous oxides (Shuman, 1977); Cd adsorption to hydrous manganese oxides (Posselt and Weber, 1974); Pb adsorption to hydrous ferric oxide (Gadde and Laitinen, 1973); Cr(III) sorption to hydrous Fe oxides (Charlet and Manceau, 1992); Sr sorption to ferrihydrite (Černík and Borkovec., 1996); iron-cyanide adsorption onto γ-Al_2O_3 (Huang and Cheng, 1997); Cu, Cd, and Pb adsorption on red mud (a mixture of Al, Fe, Si, and Ti oxides) (Apak et al., 1998); and Pb sorption to biogenic Mn oxides (Nelson et al., 1999). Isotherms were also conducted for all three metals at two other temperatures besides 25°C viz. 4°C and 11°C. Data and fits ($r^2 \geq 0.95$) are consistent with results at 25°C (Table 3). Adsorption enthalpies based on the van't Hoff

Figure 12. Isotherms of Cd and Zn sorption to hydrous metal oxides at 25°C and different pH values. Solid lines are the linear distribution model and K_d is the distribution coefficient. HAO and HFO concentrations were 1 g L^{-1} and HMO was 0.1 g L^{-1}.

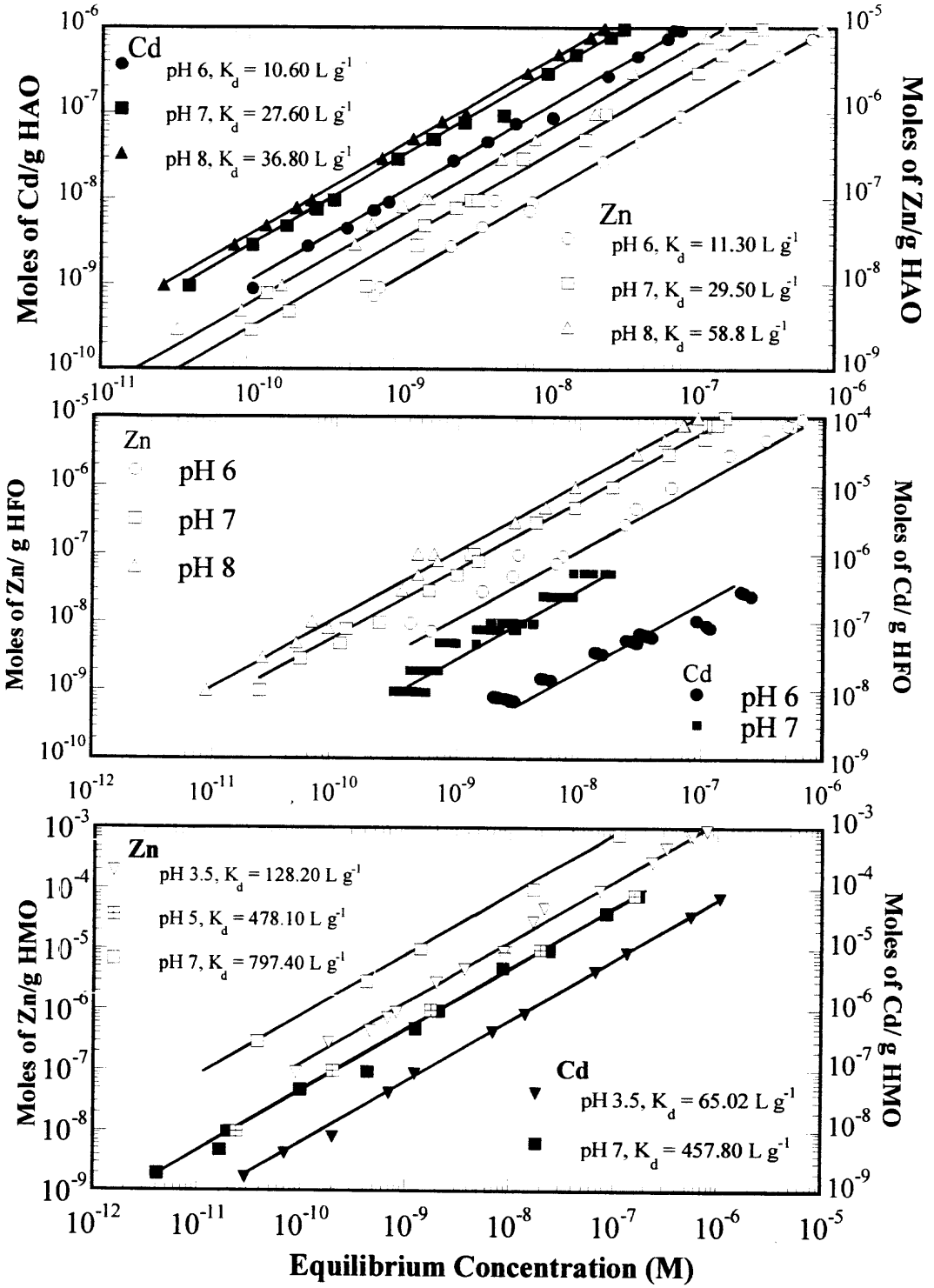

Table 3. Distribution Coefficients (K_d L g^{-1}) of Hydrous Metal Oxides

Metal	Oxide	pH	25°C	14°C	4°C
Sr	HAO	6.0	0.78	0.67	0.58
		7.0	0.97	0.76	0.64
		8.0	1.05	0.85	0.65
	HFO	7.0	0.90	0.64	0.25
	HMO	3.5	7.66	4.31	1.56
		7.0	114.59	51.61	22.50
Cd	HAO	6.0	10.56	5.20	1.20
		7.0	27.56	16.99	2.99
		8.0	36.77	18.15	4.52
	HFO	6.0	1.10	0.20	0.10
		7.0	39.00	12.00	1.30
	HMO	3.5	65.10	17.34	3.41
		7.0	457.82	107.73	24.26
Zn	HAO	6.0	11.30	4.60	1.01
		7.0	29.50	12.70	2.80
		8.0	58.80	23.70	5.40
	HFO	6.0	14.40	5.80	0.80
		7.0	59.90	20.30	3.70
		8.0	109.00	34.00	7.00
	HMO	3.5	128.20	26.34	5.30
		5.0	478.10	77.16	18.11
		7.0	797.40	194.21	34.68

* Estimated parameters have a ± 10% error

equation (Figures 13 and 14, and Table 4) demonstrate results from temperature studies conducted at pH 6.0 and 8.0 for HAO and pH 3.5 and 7 for HMO. Metal adsorption to the hydrous oxides increased with increase in temperature, indicating an entropically driven, endothermic adsorption reaction. Also, from adsorption enthalpies, metal affinity to the oxide increases in the order of HAO < HFO < HMO. Other adsorption studies have revealed endothermic reactions: Sr sorption to hydrous manganese oxide (Mishra and Tiwary, 1995); Sr and Cd sorption to HFO (Axe and Anderson, 1997); and Cd, Pb, and Zn sorption to goethite (Johnson, 1990; Rodda et al., 1996; Angove et al., 1998).

In this study as well as in the above systems, the adsorption enthalpies were less than 25 kcal $mole^{-1}$ indicative of physical forces (de Boer, 1968). Adsorption affinities of metal ions have been correlated to their first hydrolysis constants through Linear Free Energy Relation (LFER) (Hachiya et al., 1984). Richens (1997) used structural parameters such as the primary hydration number, N, and hydrated radius, R_H, to develop correlations including one for the coulombic energy between the metal ion and a water molecule in the primary hydration shell. These structural parameters for some of the environmentally important divalent metal ions (Table 5) are a result of various experiments including diffraction and scattering techniques, XAS, infrared and Raman spectroscopy, mass spectrometry, nuclear magnetic resonance spectroscopy, and various *ab initio* approaches. The criteria for selecting structural parameters in this work included using the most recently obtained data from dilute nitrate or perchlorate based solutions (Magini et al., 1988; Richens, 1997). Transition metals typically have a smaller primary hydration number (N = 4-6) and hence a tighter hydration shell (smaller R_H) as compared to alkaline earth metals for which N ranges from 7 to 10. Accordingly, hydrated metal

Figure 13. Effect of temperature on Sr sorption to hydrous metal oxides. Solid lines represent the van't Hoff model and reported values are experimental adsorption enthalpies.

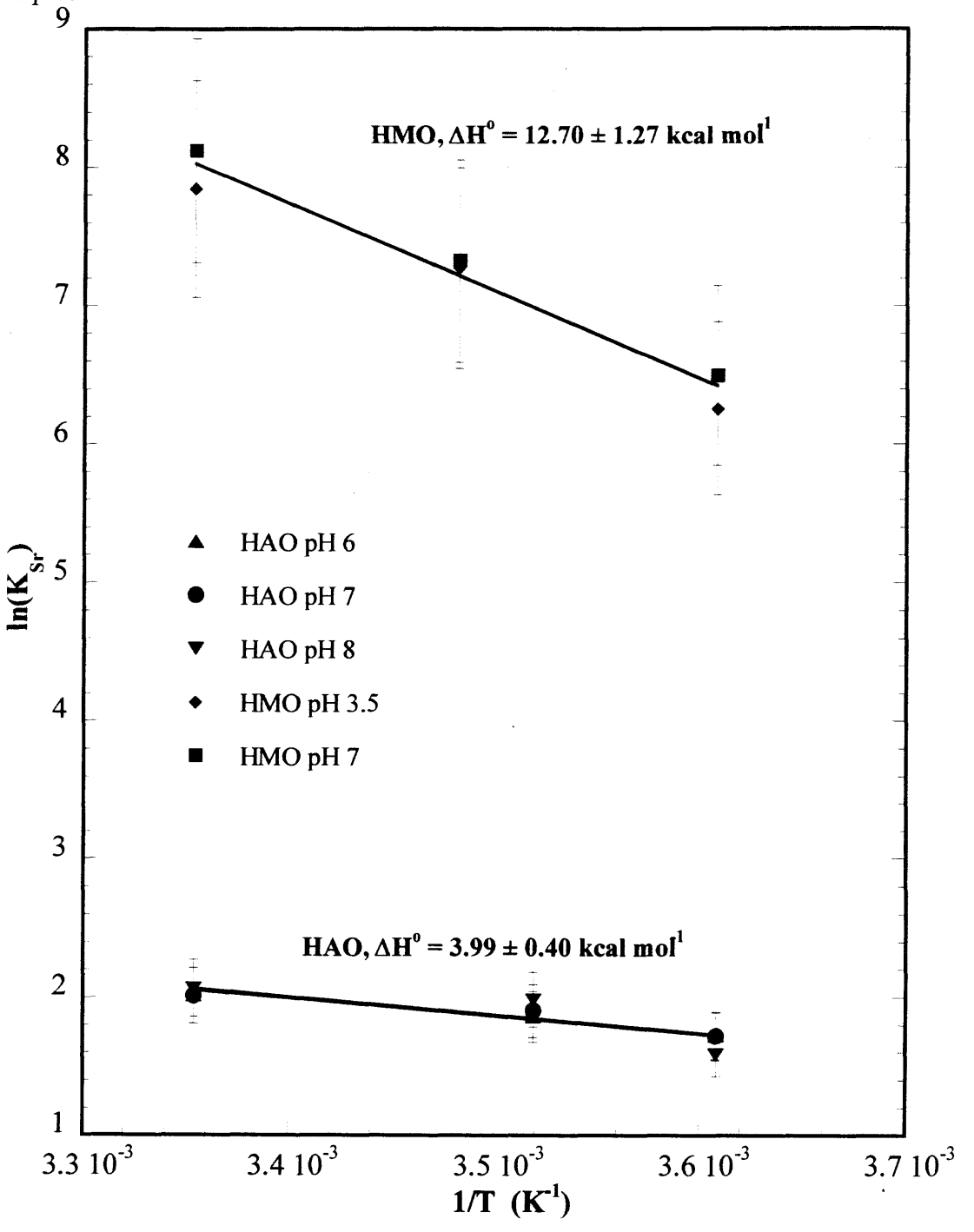

Figure 14. Effect of temperature on Cd and Zn sorption to hydrous metal oxides. Solid lines represent the van't Hoff model and reported values are experimental adsorption enthalpies.

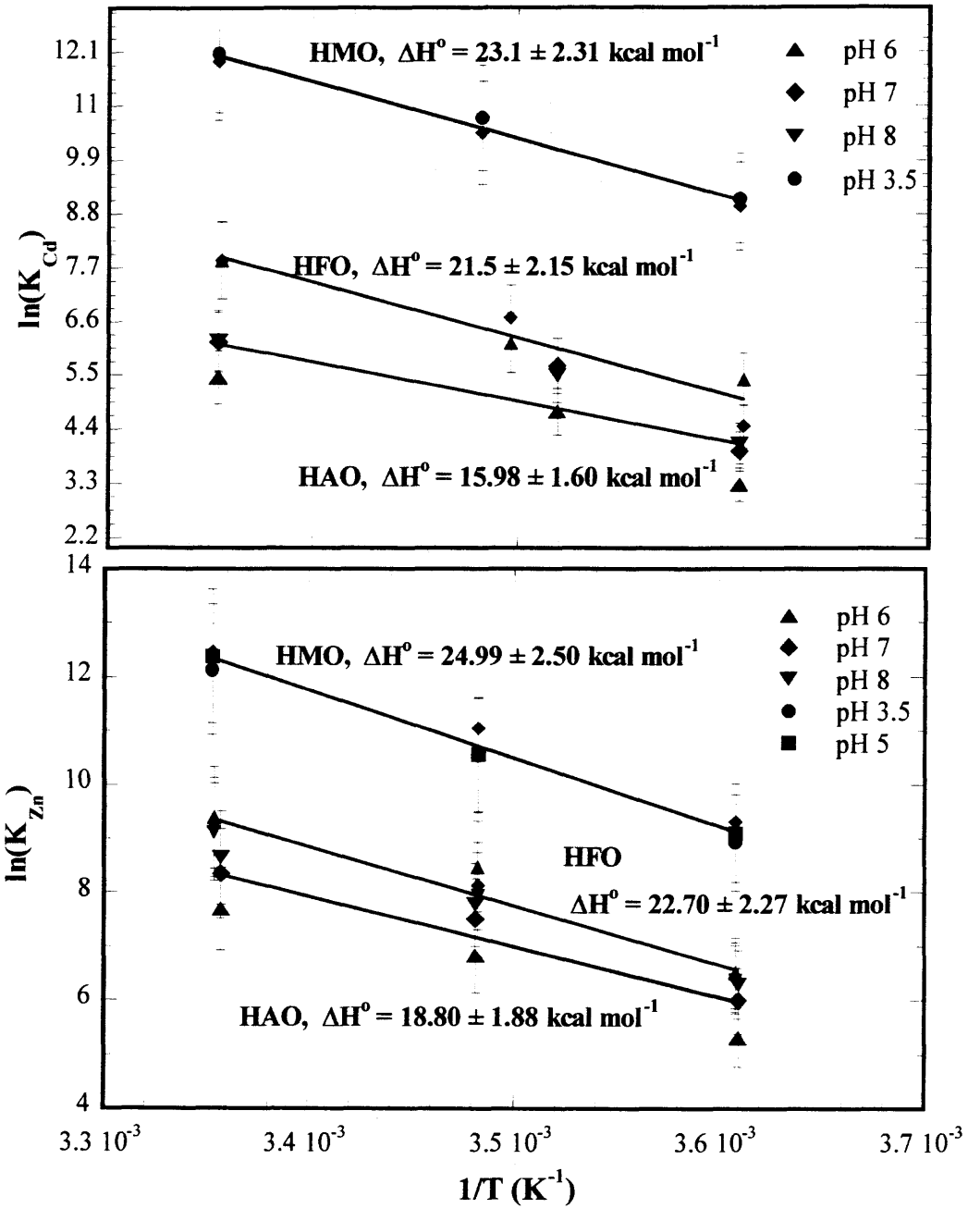

Table 4. Sorption Parameters for Different Metal- Hydrous Oxide Systems at pH 7.0

Parameters	HAO Sr	HAO Cd	HAO Zn	HFO Sr †	HFO Cd †	HFO Zn	HMO Sr	HMO Cd	HMO Zn
C_t moles Sr/g	0.012	0.012	0.012	0.025	0.025	0.025	0.034	0.034	0.034
K	162	5011	5364	60	2600	4000	2265	134653	234529
ΔG° kcal/mol	−1.20	-5.03	-5.07	-2.10	-4.64	-4.90	-5.10	-6.97	-7.30
ΔS° kcal/mol K *	0.02	0.07	0.08	0.04	0.09	0.09	0.06	0.10	0.11
ΔH° kcal/mol	3.99	15.98	18.80	9.90	21.50	22.70	12.00	23.10	24.99
E_a kcal/mol‡	11.00	13.10	14.50	8.71	15.0	15.70	12.70	13.35	15.20
α	2.75	0.82	0.77	1.30	0.70	0.69	1.00	0.58	0.61
Theor. D_s cm^2/s	1.30×10^{-11}	2.51×10^{-13}	5.41×10^{-14}	3.8×10^{-13}	1.2×10^{-14}	8.53×10^{-16}	8.9×10^{-12}	1.19×10^{-13}	9.65×10^{-15}
Expt. D_s cm^2/s	1.50×10^{-11}	2.5×10^{-13}	5.4×10^{-14}	4.0×10^{-13}	1.0×10^{-14}	8.49×10^{-16}	8.0×10^{-12}	1.14×10^{-13}	9.5×10^{-15}

Estimated parameters have a ± 10% error. All parameters are based on 25°C except the enthalpy. *ΔS° is calculated from the thermodynamic relation, $\Delta G^\circ = \Delta H^\circ - T\,\Delta S^\circ$. † Data obtained from reference [Axe and Anderson, 1997]. ‡$E_a = \alpha\,\Delta H^\circ$ where α represents the Polanyi relation constant.

Table 5. Structural Parameters of Hydrated Divalent Metal Ions

Metal	N	R_H (Å)	N/R_H
Ca*	9.0	2.53	3.56
Mg*	6.0	2.09	2.93
Be*	4.0	1.67	2.40
Sr*	9.0	2.63	3.42
Ba*	9.7	2.81	3.45
Ra*	8.0	2.87	2.79
Pb*	4.0	2.74	1.46
Co*	6.0	2.09	2.87
Ni†	6.6	2.06	3.20
Zn*	6.0	2.17	2.76
Cd†	6.0	2.28	2.63
Hg*	6.0	2.37	2.53
Mn*	6.0	2.18	2.75
Fe*	6.0	2.13	2.82
Cu†	6.0	2.07	2.90

*Richens (1997) † Magini et al. (1988).
Error associated with these parameters is 20%.
In addition to these two compilations, the above parameters are in agreement with recent XAS studies including Pb (Bargar et al., 1997, 1998; Manceau et al., 1996), Zn (Schlegel et al., 1997; Trainor et al., 2000), Hg (Collins et al., 1999), and Sr (Axe et al., 1998; O'Day et al., 2000).

ions with smaller N/R_H ratios will have a greater coulombic energy of attraction for the amorphous oxide surfaces than the ones with larger ratios. Consequently, adsorption enthalpies for divalent metal ions with respect to HAO, HFO, and HMO may be predicted knowing their structural parameters (as shown in Equation 14):

$$\Delta H^{o} = f\left(N \times \frac{Z^2}{R_H} \right) \tag{14}$$

The adsorption enthalpy-affinity correlation for each oxide is presented in Figure 15. This correlation is unique from that of Richens in that it represents the interaction between the hydrated ion and the oxide surface; it may prove useful for predicting other metal enthalpies as well as predicting activation energies based on the Polanyi relation. The predictive capabilities are tested in this research once the Polanyi constant, α, is defined. Therefore, this constant was first studied for Sr, Zn, and Cd, based on surface diffusivities fitted from experimental data and application of site activation theory in estimating theoretical surface diffusion coefficients.

To study intraparticle surface diffusion in a convenient time frame, CBC studies were conducted where the adsorbate concentration in the bulk aqueous phase was monitored and maintained constant. The initial amount of metal sorbed corresponded to the isotherm results representing adsorption to the external surface, which does not significantly change initially (Figures16 a, 17 a, 18 a, and 19 a and c). With time, the amount of metal ion sorbed to the oxide gradually increased due to intraparticle surface diffusion. In HAO, transient sorption accounts for 50% of the sites (Figures 16a and 17a). Likewise, in the CBC studies conducted to assess sorption to HMO, equilibration with the external surface was followed by the slow intraparticle diffusion that accounted for approximately 90% of the sorption sites (Figure 18a).

Figure 15. Correlation between adsorption enthalpy and the structure parameters of the hydrated metal ions (Table 5). Open points represent the experimental values (with ± 2 S.D.) from which the correlations (solid lines) were developed for each oxide. Solid points represent the predictions for other divalent metals.

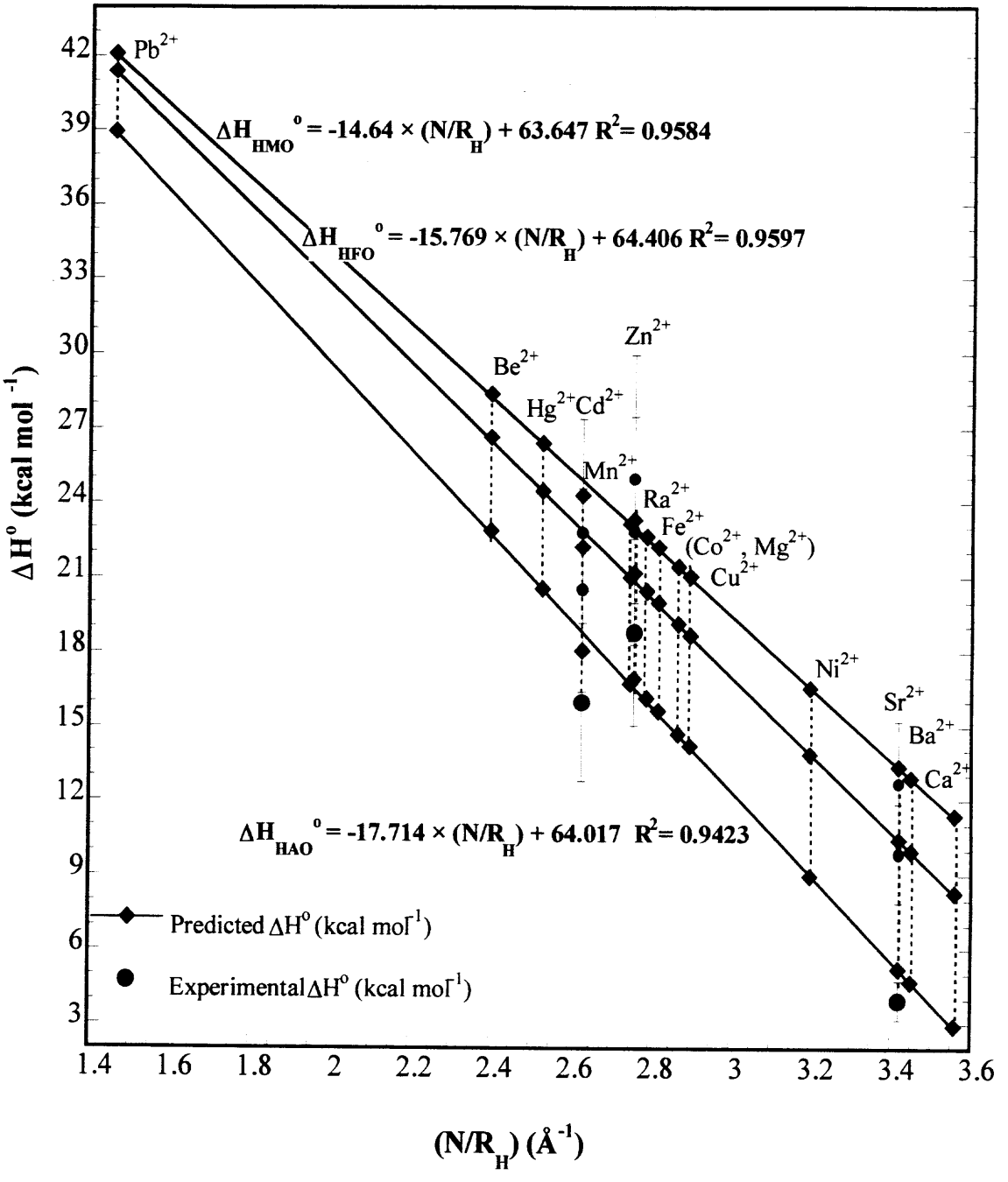

Figure 16. CBC studies of Sr sorption to 1g/L HAO at pH 7 and 25°C: (a) Experimental data and (b) Internal sorption modeled. $[Sr]_{bulk} = 2.6 \times 10^{-5}$ M maintained constant.

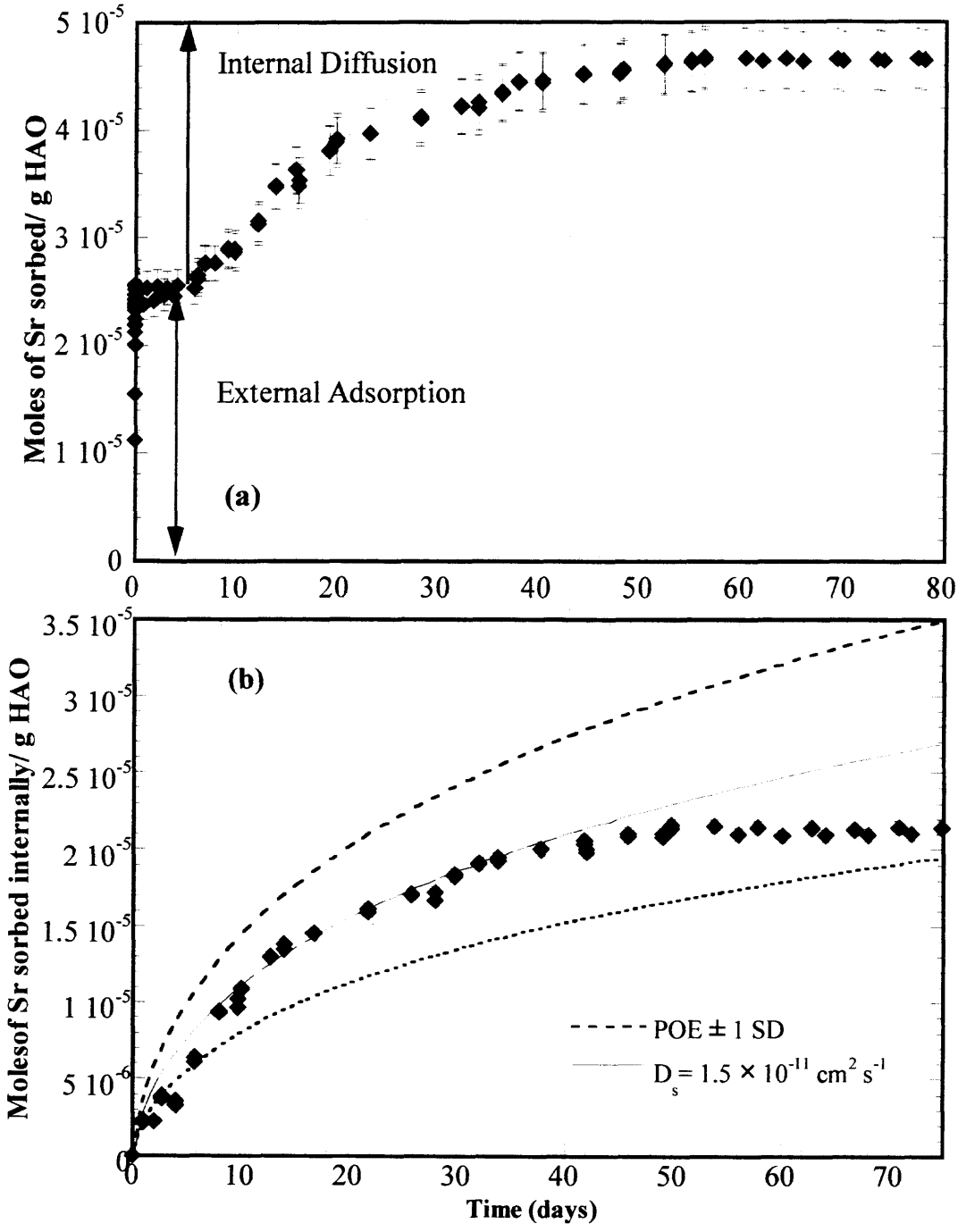

Figure 17. CBC studies of Sr sorption to 1g/L HAO at pH 8 and 25°C: (a) Experimental data and (b) Internal sorption modeled. $[Sr]_{bulk} = 2.6 \times 10^{-5}$ M maintained constant.

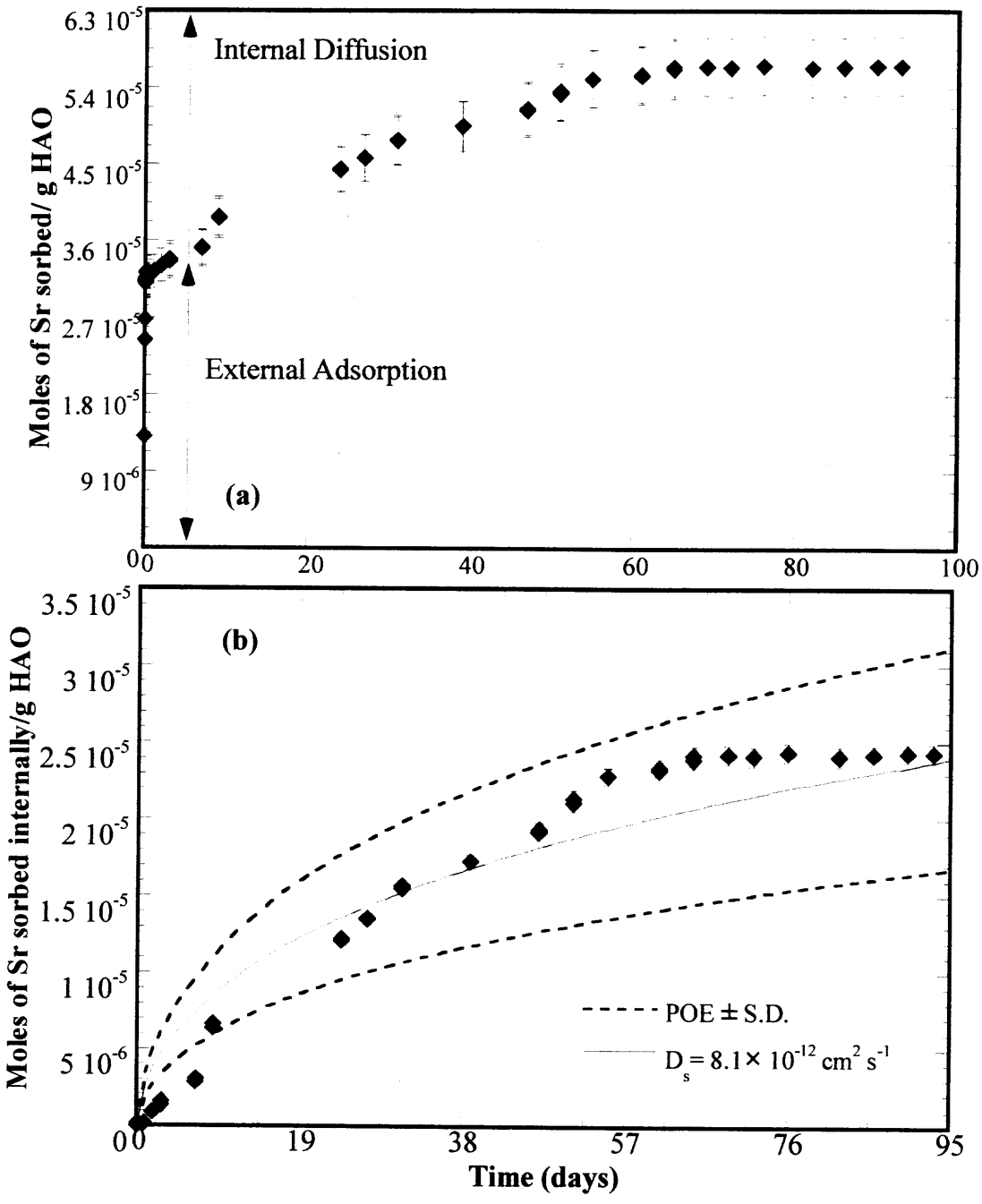

Figure 18. CBC studies of Sr sorption to 1g/L HMO at pH 7 and 25°C: (a) Experimental data and (b) Internal sorption modeled. $[Sr]_{bulk} = 8.7 \times 10^{-5}$ M maintained constant.

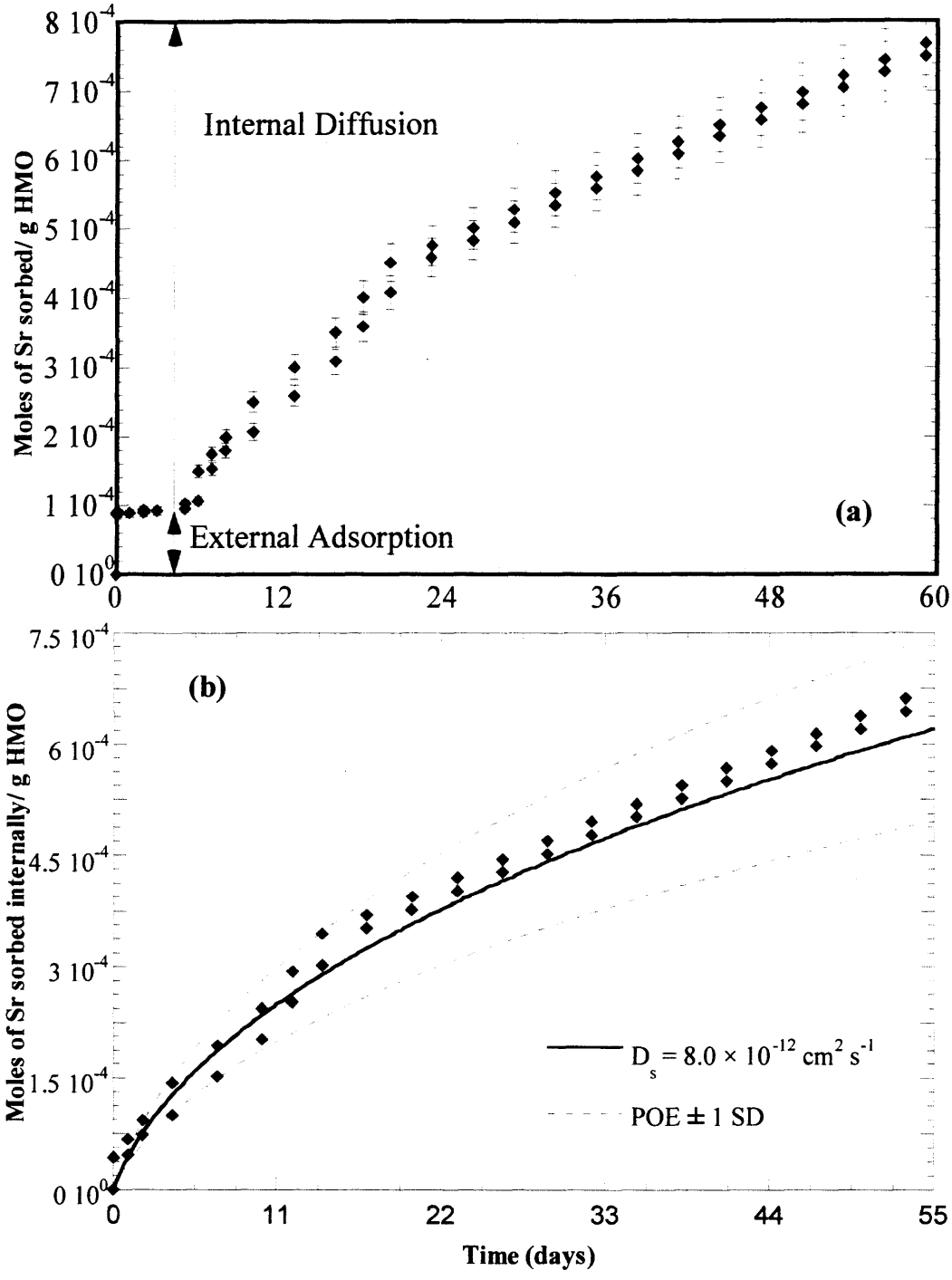

Figure 19. CBC studies with 1 g/L HAO at pH 7 and 25°C: (a) Experimental data of Cd sorption $[Cd]_{bulk} = 1.5 \times 10^{-8}$ M, (b) Cd internal sorption modeled, (c) Experimental data of Zn sorption $[Zn]_{bulk} = 1.3 \times 10^{-9}$ M, and (d) Zn internal sorption modeled.

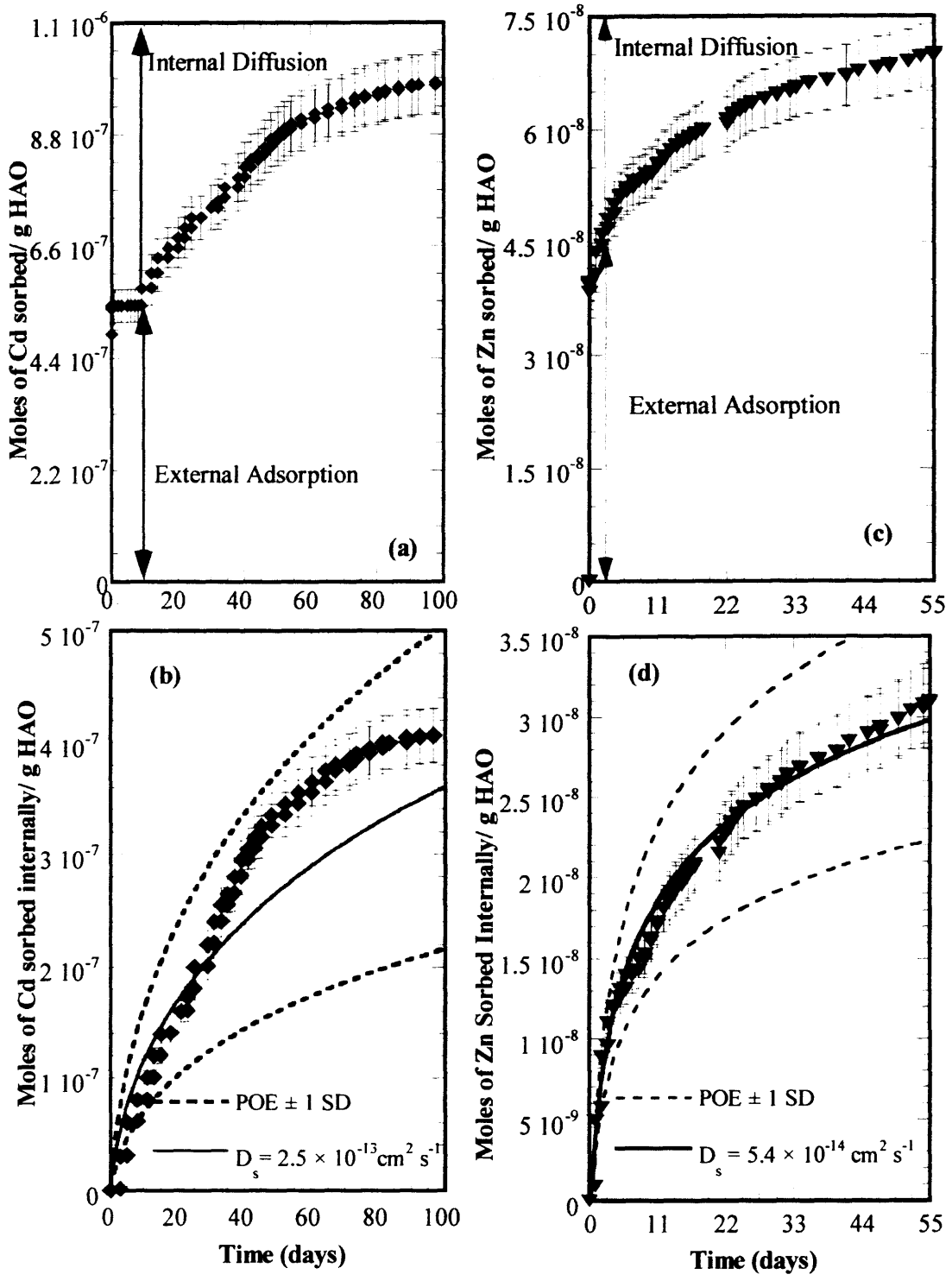

Figure 20. Modeled CBC studies at pH 7 and 25°C where the externally sorbed contribution has been subtracted: (a) Cd internal sorption to HFO with $[Cd]_{bulk} = 1.0 \times 10^{-8}$ M, (b) Zn internal sorption to HFO with $[Zn]_{bulk} = 1.5 \times 10^{-8}$ M, (c) Cd internal sorption to HMO with $[Cd]_{bulk} = 1.5 \times 10^{-9}$ M, and (d) Zn internal sorption to HMO with $[Zn]_{bulk} = 1.2 \times 10^{-9}$ M.

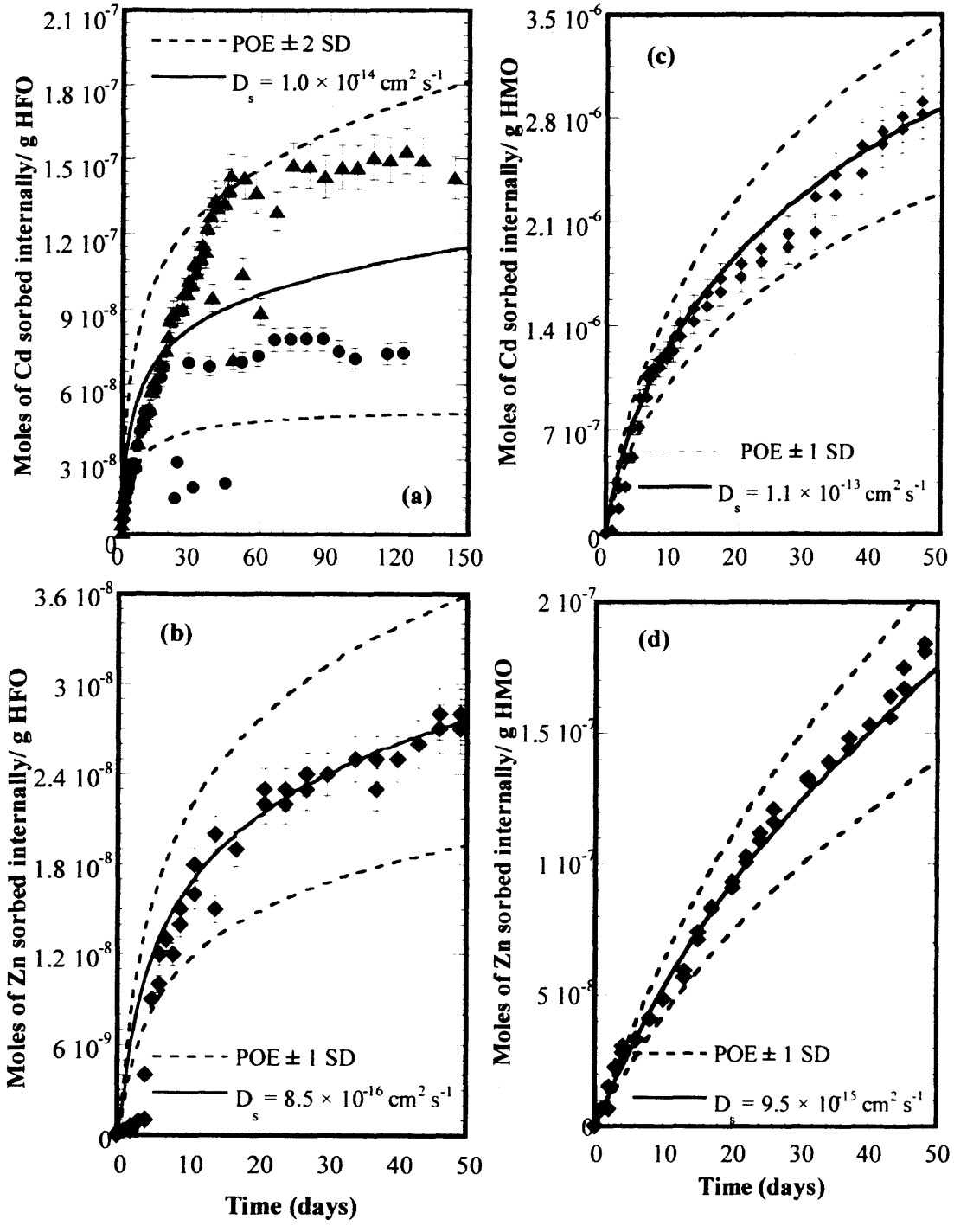

A mathematical model has been previously developed to represent this intraparticle diffusion (Axe and Anderson, 1995; 1997). Assuming the internal sites are no different than the external ones, then for spherical particles, insignificant pore diffusion (see Appendix D: pore diffusion accounts for less than 3% of all sites), dilute concentrations (or constant diffusivities), and negligible film resistance due to a turbulent hydraulic regime (Fogler, 1992), the mass balance for the adsorbate metal ion yielded Equation 8. Integrating the analytical solution to this equation over the volume of the particle (given boundary conditions including a constant surface concentration) yields the mass sorbed per particle at a specific time (Axe and Anderson, 1995, 1997; Crank, 1975):

$$\frac{M}{M_\infty} = 1 - \frac{6}{\pi^2} \sum_{n=1}^{\infty} \frac{1}{n^2} \exp\left[\frac{-D_s n^2 \pi^2 t}{R^2 \left(1 + \varepsilon_\rho K_i \right)} \right] \tag{15}$$

The diffusion coefficient, the only fitting parameter in the model, was obtained by minimizing the variance between the model and experimental mass of metal ion sorbed. For a given time, the mass sorbed internally for each particle size times the number of particles from the particle size distribution was summed to obtain the total mass of metal sorbed. This internal amount plus that sorbed to the external surface from isotherms provided the total amount sorbed. By minimizing the variance, the only fitting parameter is surface diffusivity; modeling results (Figures 16b, 17b, 18b, 19c and d, and 20; and Table 4) include Sr and Cd sorption to HFO (Axe and Anderson, 1995, 1997). For HAO and HMO, surface diffusivities ranged from 10^{-16} to 10^{-11} cm^2 s^{-1}. The model errors shown as standard deviations are based on the errors associated with the parameters determined from other experimental studies. Barrow et al. (1989) estimated diffusion parameters for Zn and Cd in goethite to be 6.5×10^{-19} cm^2 s^{-1} and 3×10^{-20} cm^2 s^{-1},

respectively. Fuller et al. (1993) evaluated effective diffusivities for As(V) in HFO, which were in the order of 10^{-11} cm^2 s^{-1}. Papelis et al. (1995) found Cd and Se(IV) diffusivities in porous aluminas ranged between 10^{-12} and 10^{-10} cm^2 s^{-1}. Axe and Anderson (1995, 1997) evaluated Cd and Sr surface diffusivities in HFO, which ranged from 10^{-14} to 10^{-13} cm^2 s^{-1}. Misak et al. (1996) reported self-diffusion coefficients of Co and Zn in hydrous Fe(III) and Sn(IV) oxides to be in the order of 10^{-11} cm^2 s^{-1}. Theis et. al (1992) found the surface diffusion coefficient, 5×10^{-9} cm^2 s^{-1}, for lead adsorption to granular iron oxide.

Moreover, as mentioned above modeling of CBC studies for HAO and HMO showed that nearly 50% to 90% of the sorption sites are located internally; however, these are not consistent with their respective porosities found on freeze dried particles. On the other hand, 40% of adsorption sites on HFO were located internally, which was consistent with its porosity (Axe and Anderson, 1995). Axe and Anderson used Hg porosimetry, which accounts for pores less than 500 Å. In these studies the porosities of HAO and HMO were measured with nitrogen desorption, and only includes pores less than 250 Å, potentially underestimating porosity.

The CBC studies suggest that hydrous oxides act as long-term sinks for metal ions introduced in soils and sediments. For each oxide and its associated particle size distribution, Figure 21 illustrates internal sorption or intraparticle surface diffusion (at pH 7) as a function of the square root of time, where sorption reaches equilibrium in approximately 3 to 4 months for Sr and 2 to 5 years for Cd. Interestingly, Zn, which has the greatest affinity for these oxides, requires approximately 5 to 10 years to reach equilibrium. Thus, in aquatic environments where the oxides are present as discrete

Figure 21. Predicting equilibrium at pH 7 and 25°C for Sr, Cd, and Zn sorption to hydrous metal oxides given their respective particle size distributions.

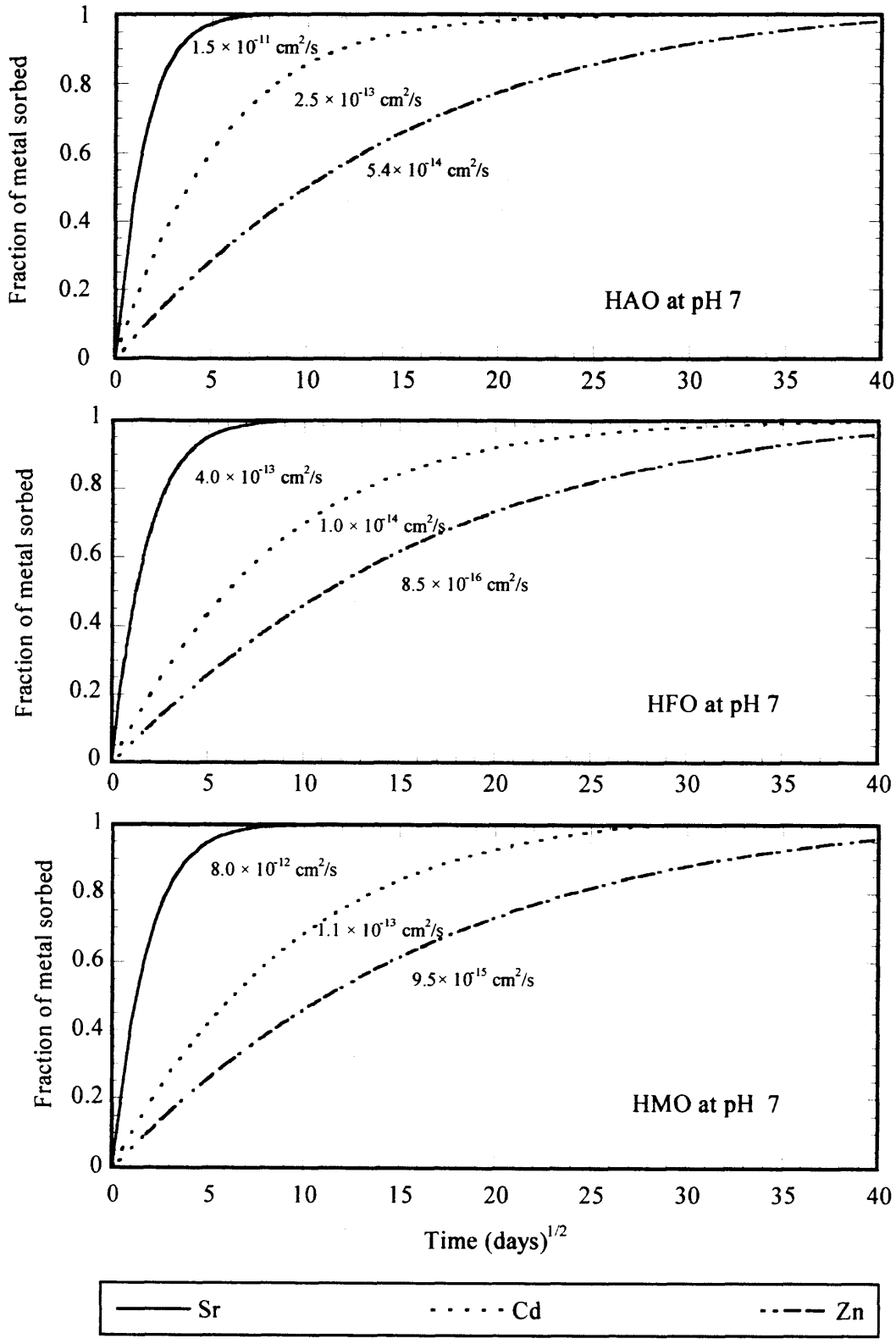

particles and coatings, amorphous aluminum, iron, and manganese oxides act as sinks for trace metal contaminants. Conversely, during desorption these amorphous oxides act as long-term source for contaminants in ecosystems. Most transport models that employ distribution coefficients and retardation factors are inadequate for describing metal and radionuclide mobility in subsurface environments (Mahara, 1993; Oakley et al., 1981; Ohtsuka et al., 1990). Because the internal sites account for as much as 90% of the total, accurate modeling requires inclusion of this contribution. However, transient studies require a lengthy period of time, and therefore predictive methods would be useful for determining surface diffusivities.

Surface diffusivities decreased with an increase in pH (Table 6), as pH increases the distance between sites decreases since the site density increases with increasing pH (Figure 5). This effect is consistent with site activation theory (Axe and Anderson, 1995, 1997; Kärger and Ruthven, 1992) (Equation 9), where the two unknowns are the distance between sites and activation energy. Because site densities are a function of pH and are related to surface charge density as shown in Figure (6), given experimental diffusivities, the only unknown is activation energy, which was estimated for the Sr, Cd, and Zn systems studied. From the Polanyi relationship, the activation energy (E_a) is related to the adsorption enthalpy through α (Boudart, 1968). Once the activation energies were determined, they were related to the enthalpy, and α was evaluated (Figure 22). For a specific metal, the activation energy was found again to be equivalent (within the error based on the propagation of errors method (Ku, 1966)) for all three oxides (Figure 22). Furthermore, for a given oxide, α was approximately equivalent for the transition metals

Table 6. Effect of pH on surface diffusivities

Metal	Oxide	pH	λ (cm)	Experimental D_s (cm^2s^{-1})
Sr	HAO	7.0	3.30×10^{-8}	1.50×10^{-11}
		8.0	2.0×10^{-8}	8.10×10^{-12}
Cd	HAO	7.0	3.30×10^{-8}	2.50×10^{-13}
		8.0	2.0×10^{-8}	2.2×10^{-13}
Cd	HFO	6.0	6.8×10^{-7}	6.0×10^{-13}
		7.0	2.0×10^{-8}	1.0×10^{-14}

λ represents the mean distance between the neighboring sites and is calculated from the site density and the surface area of the hydrated oxides. Experimental diffusivities fit the data within $\pm$ 1-2 S.D.

Figure 22. Polanyi correlations predicting activation energy from enthalpy: $E_A = \alpha\ \Delta H°$, where the Polanyi constant (α) is equivalent for a group of metals.

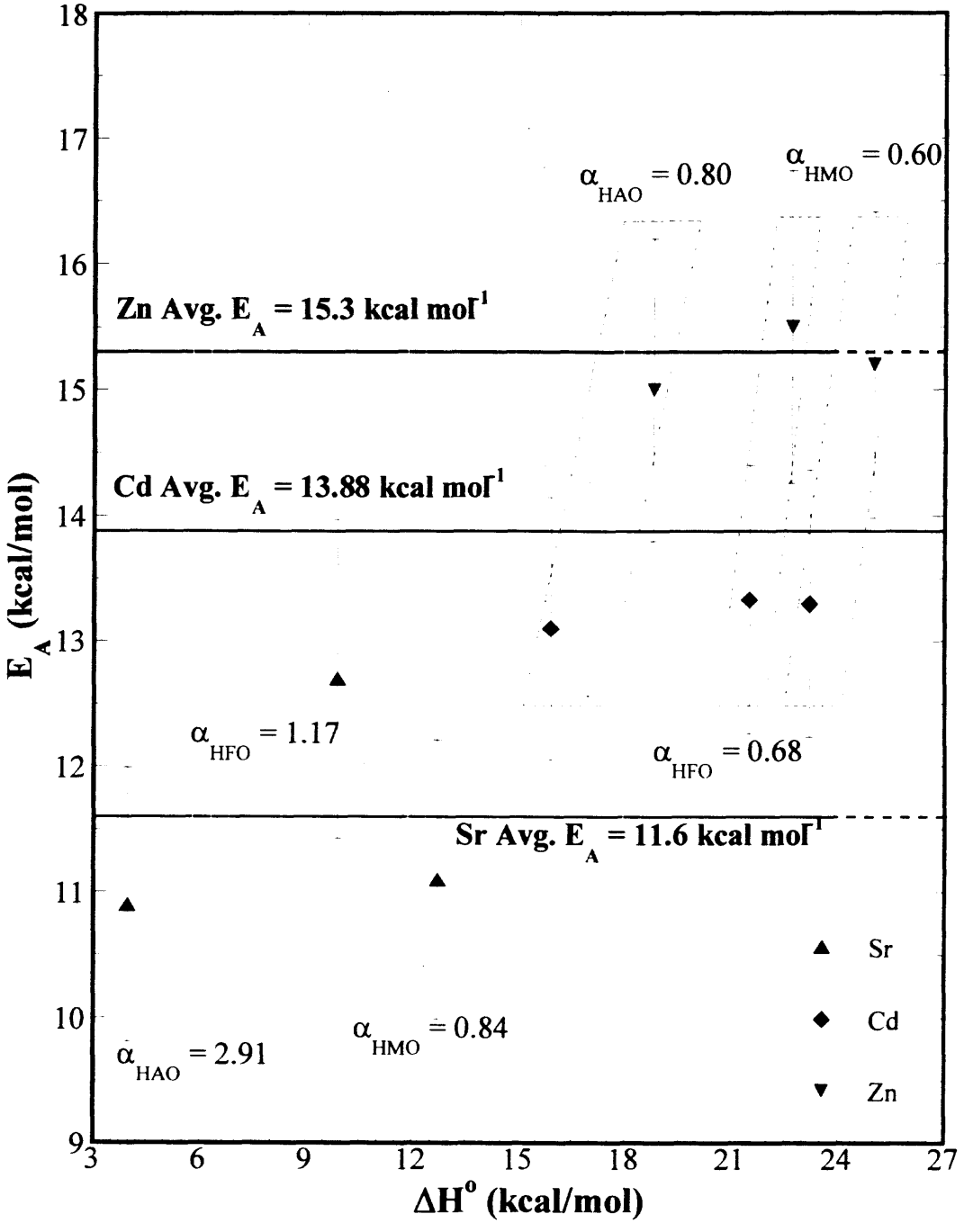

Cd and Zn (Figure 22); this suggests that metals from the same group in the Periodic Table exhibit similar sorption properties with respect to HAO, HFO, and HMO. In an effort to test the predictive capabilities of the enthalpy correlation (Figure 15) and the proportionality constant found for two groups of metals from the Periodic Table (Figure 22), sorption parameters were estimated for two ions (Table 7): Ca (an alkaline earth metal) and Ni (a transition metal). Nickel is an important transition metal that has been reported as a priority pollutant, and Ca is an alkaline earth metal that is abundant in aqueous systems. The predicted sorption parameters imply that although Ni has a much greater adsorption affinity for the oxide surfaces than Ca, the barrier or activation energies are comparable. Therefore, the diffusivities are expected to be similar resulting in analogous transport behavior.

The objective of this part of the research hence reduces to testing the effectiveness of these correlations in predicting enthalpies, activation energies, and theoretical surface diffusivities for Ni and Ca sorption to HAO, HFO, and HMO. The predicted values are then compared to experimentally determined ones in the following section.

5.3 Sorption Studies with Ni and Ca

Calcium adsorption edges (Figure 23a) to hydrous metal oxides are broad curves consistent with adsorption edges of other alkaline earth metals (Axe and Anderson, 1995; Dzombak and Morel, 1990; Lützenkirchen, 1997; Mishra and Tiwary, 1995, 1999; Meng and Letterman, 1993; Okazaki et al., 1986). On the other hand, Ni adsorption edges for these same oxides (Figure 23b) are sharp and sigmoid, consistent with other studies of Ni and transition metals (Axe and Anderson, 1997; Baumgarten and Kirchausen-Düsing,

Table 7. Predicted Sorption Parameters for Ca and Ni

Metal	Oxide	ΔH^o (kcal mol^{-1})	α	E_A (kcal mol^{-1})*	λ (nm)**	D_s (cm^2 s^{-1})
Ca	HAO	2.92	2.91	8.51	3.30	1.2×10^{-10}
	HFO	8.31	1.17	9.72	2.00	1.1×10^{-11}
	HMO	11.39	0.84	9.57	2.29	1.5×10^{-11}
Ni	HAO	8.99	0.80	7.19	3.30	7.5×10^{-10}
	HFO	13.88	0.65	9.03	2.00	1.1×10^{-11}
	HMO	16.56	0.60	9.77	2.29	7.3×10^{-11}

Estimated parameters have a ± 10% error

*$E_A = \alpha \Delta H^o$ where α is based on sorption studies of Sr, Cd, and Zn with hydrous oxides.

**λ (and therefore D_s) values are based on pH 7.

Figure 23. Adsorption edges of (a) Ca ($[Ca]_o = 1 \times 10^{-5}$ M) and (b) Ni ($[Ni]_o = 5 \times 10^{-9}$ M) at 25°C and as a function of ionic strength (μ). HAO and HFO concentrations were 1g L^{-1} and HMO was 0.1g L^{-1}.

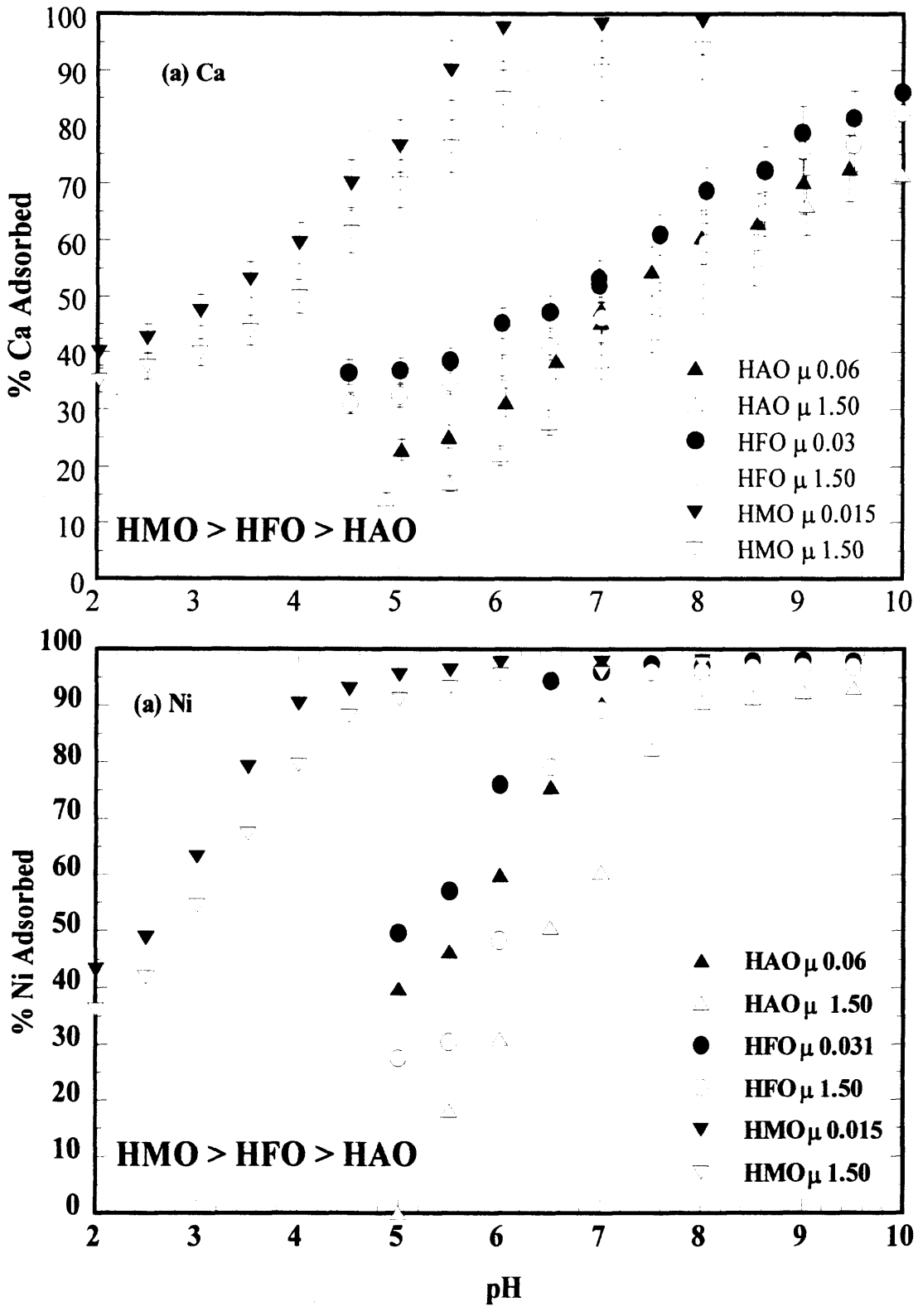

1997; Crawford et al., 1993; Dzombak and Morel, 1990; Green-Pedersen and Pind, 1997; Kanungo, 1994; McKenzie, 1980; Okazaki et al., 1986; Tamura and Furuichi, 1997). The oxides' adsorption capacities follow the order of HMO > HFO > HAO, which is in agreement with others (Anderson and Benjamin, 1990; Green-Pedersen et al., 1997; Tamura et al., 1996). Based on the present studies, for each oxide the adsorption affinity follows the trend of Zn > Cd > Ni > Sr > Ca; this result is in accord with the ones compiled in Chapter 2.

Adsorption edges also demonstrate that metal adsorption decreased with an increase in ionic strength suggesting that metal ions do not loose their waters of hydration upon adsorption (Meng and Letterman, 1993). In XAS studies, Axe and coworkers (1998, 2000) found that Sr ions remained hydrated upon adsorption, therefore sorbing physically to HFO and HMO surfaces. In other macroscopic studies, Green-Pedersen et al. (1997) observed Ni adsorption at pH 8 to MnO_2 decreased with increase in ionic strength, however they did not observe this effect in Ni adsorption to $Fe(OH)_3$ at the same pH. At pH 8, the double layer is compressed significantly with increase in ionic strength for MnO_2 but not for $Fe(OH)_3$ (Green-Pedersen et al., 1997). Interestingly, Green-Pedersen and Pind (2000) observed significant ionic strength effects for Ni adsorption to ferrihydrite-coated montmorillonite at pH 8 attributing it to a non-uniform distribution of the coating on the montmorillonite surface. On the other hand, Posselt and Weber (1974) found that Cd sorption to hydrous oxides of Al, Fe, and Mn decreased slightly with increase in ionic strength; they credited it to weak competition between Cd^{2+} and Na^{+}. In other sorption studies with clays (Green-Pedersen and Pind, 2000; Krapiel et al., 1999; Schlegel et al., 1997), a decrease in metal adsorption with an increase in ionic strength

has been attributed to an ion exchange mechanism. For many investigations with crystalline oxide surfaces (Christophi and Axe, 2000; Coughlin and Stone, 1995; Lützenkirchen, 1997), where no ionic strength effects were observed, the sorption mechanism was attributed to specific adsorption. The nature of the background electrolyte also plays an important role in metal adsorption; strong electrolytes such as NaCl can affect the degree of metal complexation resulting in pronounced ionic strength effects (Misak et al., 1996). In contrast, less reactive anions like nitrate typically only contribute to compression of the diffuse layer.

To assess the experimental adsorption enthalpies, isotherm studies for Ca (pH 7) and Ni (pH 5, 6, and 7) adsorption to hydrous oxides were conducted at 4, 14, and 25°C. For both metals, a linear relationship ($r^2 > 0.97$) was observed between the sorbed and the bulk aqueous concentrations (Figure 24), which is consistent with the single-site Langmuir isotherm (Fogler, 1992). In the subsurface where contaminants are present at trace concentrations, the total available sites (C_v) on these amorphous oxides are approximately equivalent to the site densities (C_t) and therefore as discussed earlier, based on Langmuir-Hinshelwood kinetics, the distribution coefficient, K_d, is simply equal to $K \times C_t$ (Axe and Anderson, 1995, 1997; Fogler, 1992). Previous macroscopic (Axe and Anderson, 1995;) and spectroscopic (Axe et al., 1998, 2000) research on Sr sorption to HFO and HMO have demonstrated that the local structure of Sr^{2+} is independent of adsorbate concentrations suggesting that adsorption can be modeled with one average type of site on the oxide surface. The macroscopic results are in agreement with adsorption studies of other divalent metals to HAO, HFO, and HMO (Axe and Anderson, 1995, 1997). Krapiel et al. (1999) also observed a linear trend for Zn and Ni adsorption to

Figure 24. Isotherms for (a) Ca and (b) Ni adsorption to hydrous metal oxides at 25°C and pH 7. Solid lines represent the model; K_d (L g^{-1}) = distribution coefficient. HAO and HFO concentrations were 1g L^{-1} and HMO was 0.1g L^{-1}.

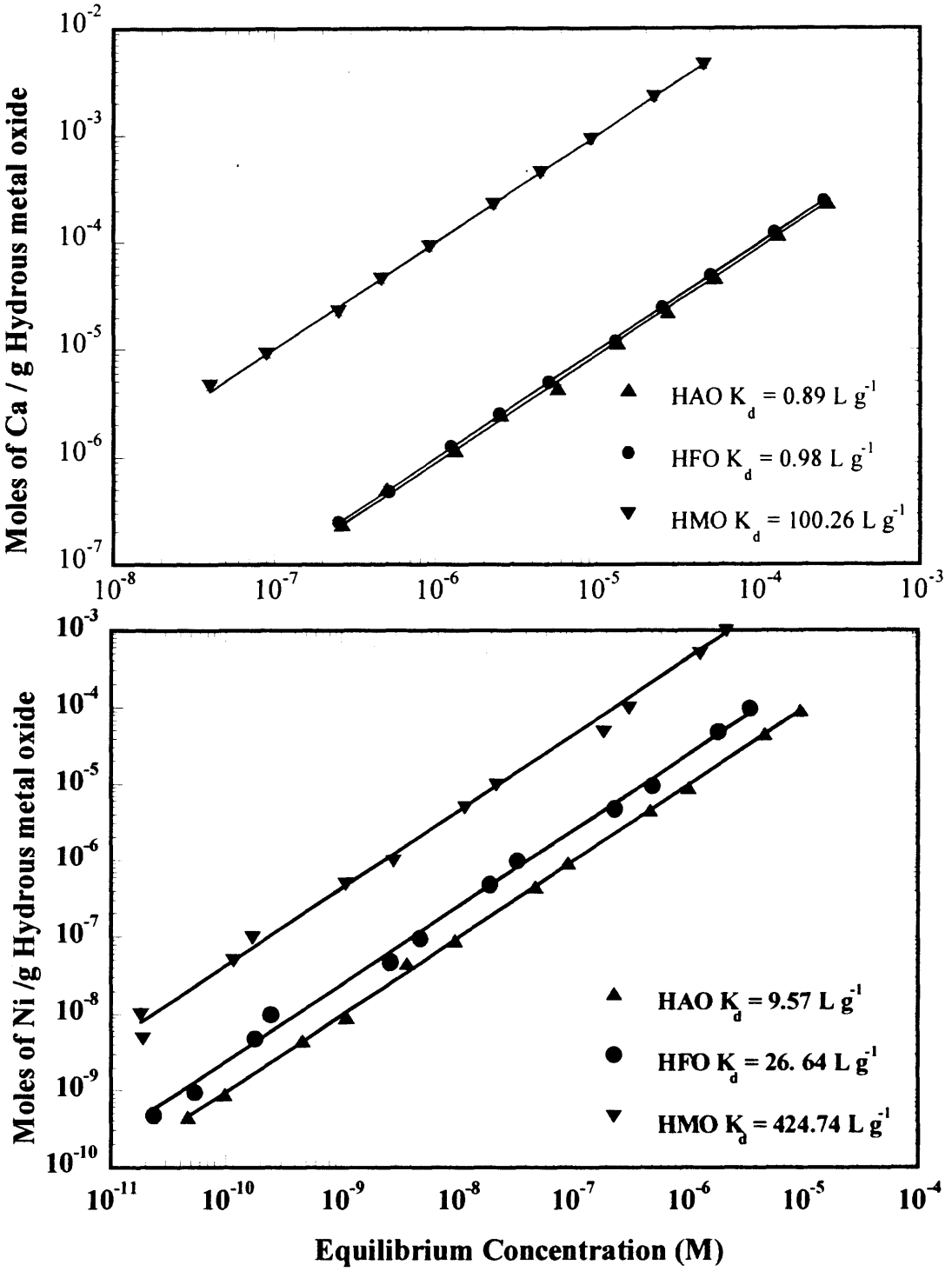

montmorillonite. Tamura and Furuichi (1997) concluded from their isotherms of numerous divalent metals including Ni to MnO_2 that since the slopes of the log-log isotherm plots did not exceed one, only monomeric ions reacted with surface. Mishra and Tiwary (1999) modeled Sr and Ba adsorption to hydrous ferric oxide with Freundlich isotherms; however their log-log slopes were close to unity suggesting that the adsorption sites may be approximated as homogeneous. In a contrast, Green-Pedersen et al. (1997) observed a linear trend for Ni adsorption to MnO_2, but not for $Fe(OH)_3$. Small et al. (1999) observed a similar linear trend for Sr sorption to ferric oxide and ferric oxide-bacteria composites.

Adsorption equilibrium constants were evaluated given the oxide site density, and adsorption enthalpies were subsequently assessed with the van't Hoff relationship (Figure 25). Consistent with other studies of divalent metals (Axe and Anderson, 1997; Johnson, 1990; Mishra and Tiwary, 1999; Rodda et al., 1996), Ca and Ni adsorption is an endothermic reaction. Furthermore, enthalpies of Ca and Ni are less than 25 kcal mol^{-1}, suggesting adsorption is due to physical forces where metal ions retain their waters of hydration (de Boer, 1968). Most importantly, the experimental adsorption enthalpies for both Ni and Ca (Figure 25) are in good agreement with the predicted ones given the error (based on one standard deviation using the propagation of errors method -- (Ku, 1966)) (Table 7). Therefore, these results suggest that adsorption enthalpies or affinities can be predicted thermodynamically (Figure 15).

Long-term sorption of Ni to hydrous oxide was studied at pH 7 applying CBC experiments (Figure 26). In these studies, Ni concentration in the bulk aqueous phase was monitored and maintained constant by measuring the activities of ^{63}Ni in the suspensions

Figure 25. Effect of temperature on Ca and Ni adsorption to hydrous oxides. Solid lines represent the van't Hoff model and data points are adsorption equilibrium constants (K) evaluated from the isotherm studies. Reported values are experimental and predicted adsorption enthalpies (kcal mol^{-1}).

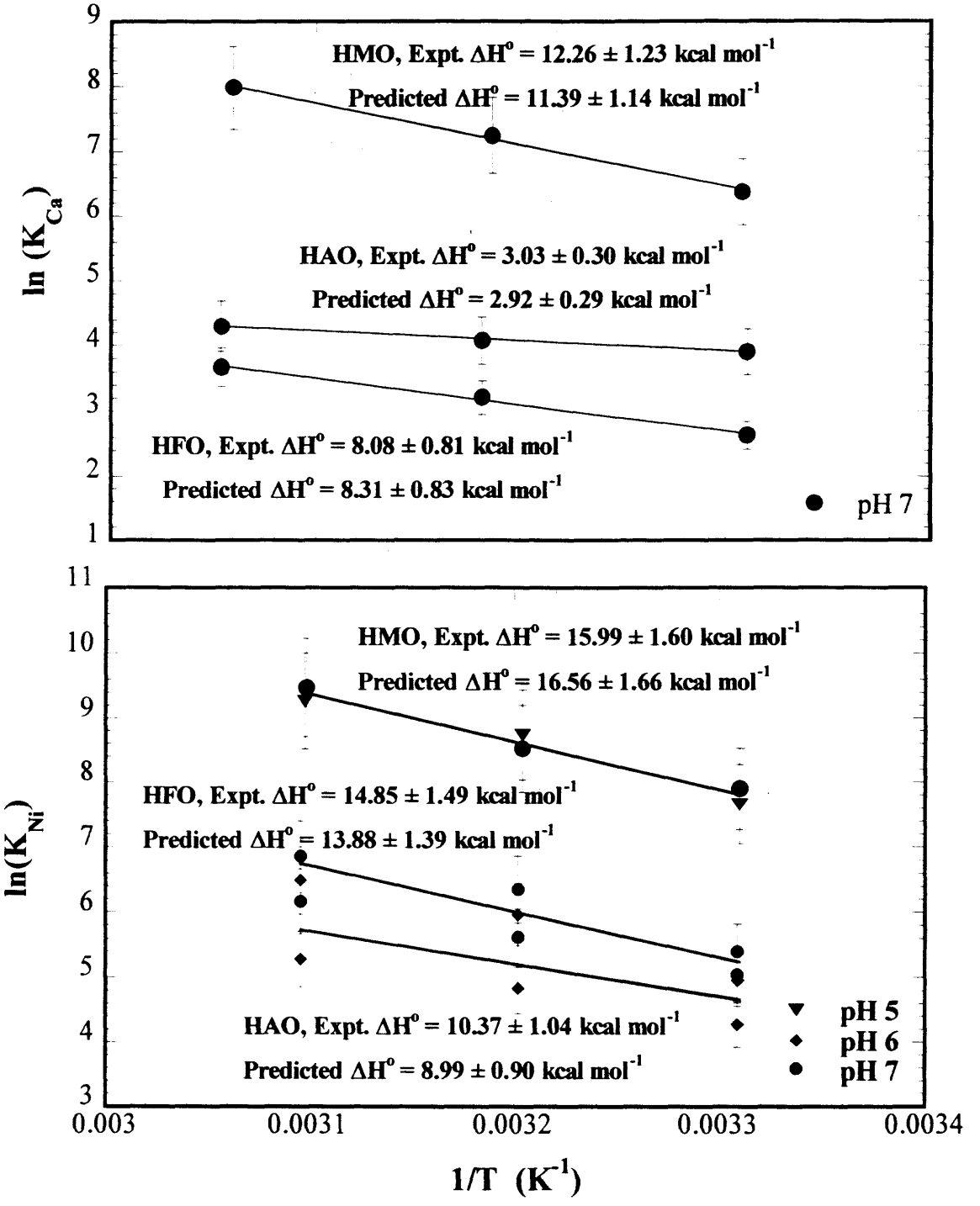

Figure 26. CBC studies at pH 7 and 25°C – modeled (solid lines) Ni internal sorption to (a) 1 g L^{-1} HAO with $[Ni]_{bulk} = 2.5 \times 10^{-8}$ M, (b) 1 g L^{-1} HFO with $[Ni]_{bulk} = 1.1 \times 10^{-7}$ M, and (c) 0.1 g L^{-1} HMO with $[Ni]_{bulk} = 3.2 \times 10^{-9}$ M. Long dashed lines represent predictions. Short dashed lines are modeling errors.

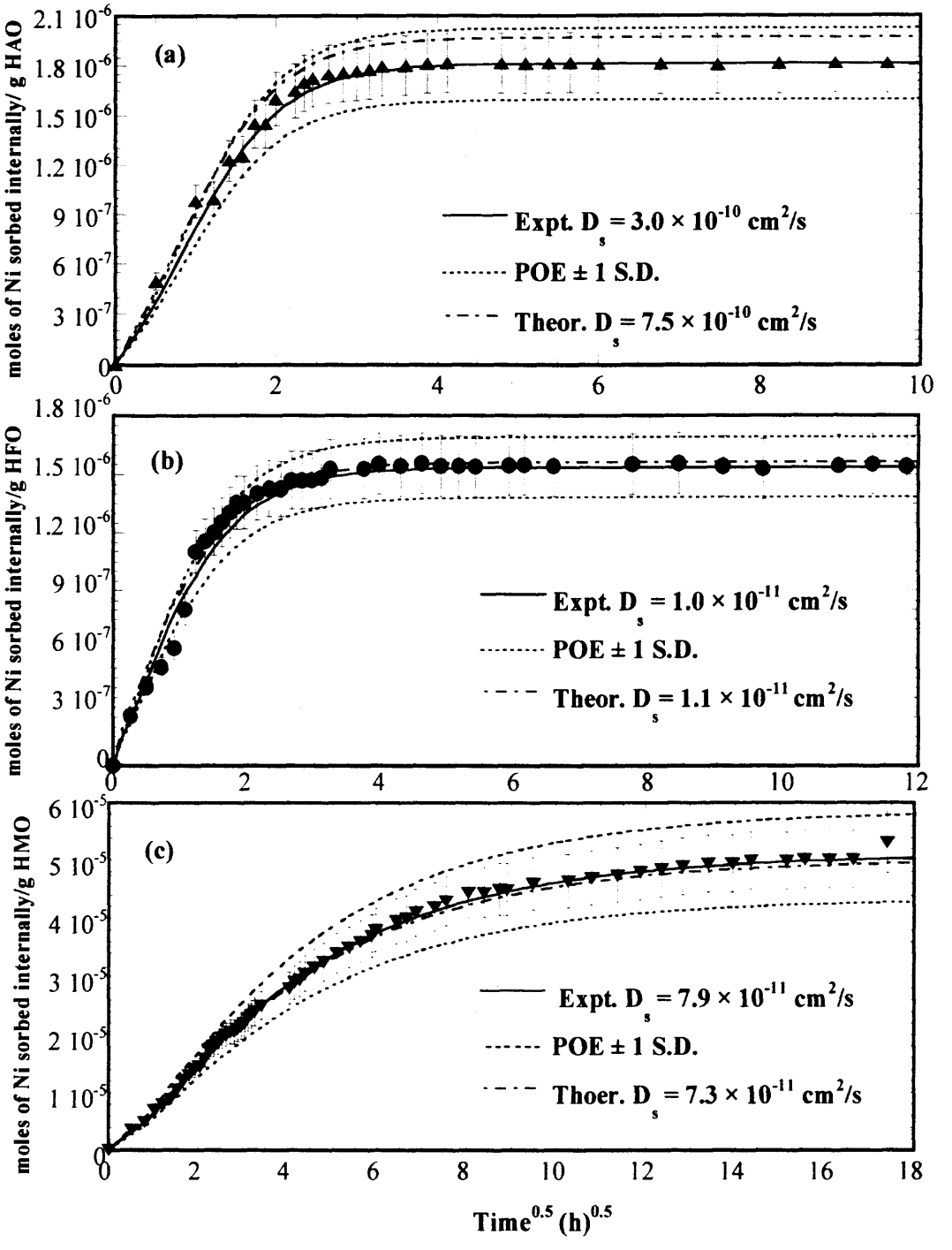

and the filtrates (Axe and Anderson, 1995, 1997). This procedure allows one to study the slow sorption process in a convenient time frame. The mass balance over spherically shaped particles includes the following assumptions: adsorption sites located along the micropore walls are no different from ones on the external surface, and because of trace metal concentrations, adsorbate-adsorbate interactions are insignificant resulting in a constant surface diffusivity. XAS studies (Axe et al., 1998, 2000) potentially support the former premise, where the average coordination environment for Sr^{2+} sorption was invariant as a function of time. Given initial and boundary conditions, integration of the analytical solution to the partial differential equation provides the amount of metal sorbed per particle at a given time (Equation 8) (Axe and Anderson, 1995, 1997; Crank, 1975). Summation of the amount of metal sorbed per particle times the number of the particles of that radius over the entire particle size distribution provides the theoretical value of metal sorbed at a given time (Axe and Anderson, 1995, 1997). In this analytical process, best-fit experimental diffusivities, the only fitting parameter, were obtained as described earlier by minimizing the variance between the fit and the experimental data (Axe and Anderson, 1995, 1997).

Experimental surface diffusivities ranged between 10^{-11} and 10^{-10} cm^2 s^{-1}. As demonstrated in earlier studies of metal sorption to these three oxides (Axe and Anderson, 1995, 1997), internal sorption contributed as much as 50% for HAO, 40% for HFO, and 90% for HMO. Activation energies used to estimate the theoretical diffusivities were calculated using the Polanyi relation ($E_A = \alpha \Delta H^o$) where for each oxide the Polanyi constant α has been defined for a group of metals from earlier work (Axe and Anderson, 1995, 1997). Because λ, the mean distance between the sites is known (Axe and

Anderson, 1997) the experimental activation energies can be compared to those predicted (Table 7 and Figure 27) and the theoretical diffusivity can be evaluated with Equation 9. These diffusivities illustrated in Figure 26 provide a good description (within the errors of the data and model) of the experimentally observed sorption. The agreement in activation energies illustrated in Figure 27 supports the hypothesis that the activation energy of a metal is comparable for all three hydrous oxides. Furthermore for a given oxide, metals of the same group of the Periodic Table form similar sorption complexes and hence exhibit an equivalent proportionality constant, α.

Based on site activation theory (Axe and Anderson, 1995, 1997; Kärger and Ruthven, 1992), where surface diffusivity is a function of the jump frequency – the product of the vibrational frequency and the Boltzmann factor. As discussed earlier, the vibrational frequency is a function of the force constant $k = d^2U/dx^2$, where U is the surface potential energy. Assuming a sinusoidal function describes the potential, the minima are the adsorption sites and the maxima are the barriers between sites. This energy barrier is simply the activation energy (Axe and Anderson, 1995, 1997; Kärger and Ruthven, 1992) and can also be expressed as a function of R_H and N as shown in Equation 15:

$$E_A = f\left(N \times \frac{Z^2}{R_H^2}\right) \tag{15}$$

Activation energies (Figure 28) are assessed for divalent metal contaminants applying the relation illustrated in Equation 15. Based on the agreement in experimental and predicted activation energies for Ca and Ni, potentially activation energies for other metals can be predicted given their hydrated structure.

Figure 27. Polanyi correlations predicting EA for (a) alkaline earth metals and (b) transition metals. $E_A = \alpha\ \Delta H°$, where the Polanyi constant α (slope) is equivalent for a group of metals.

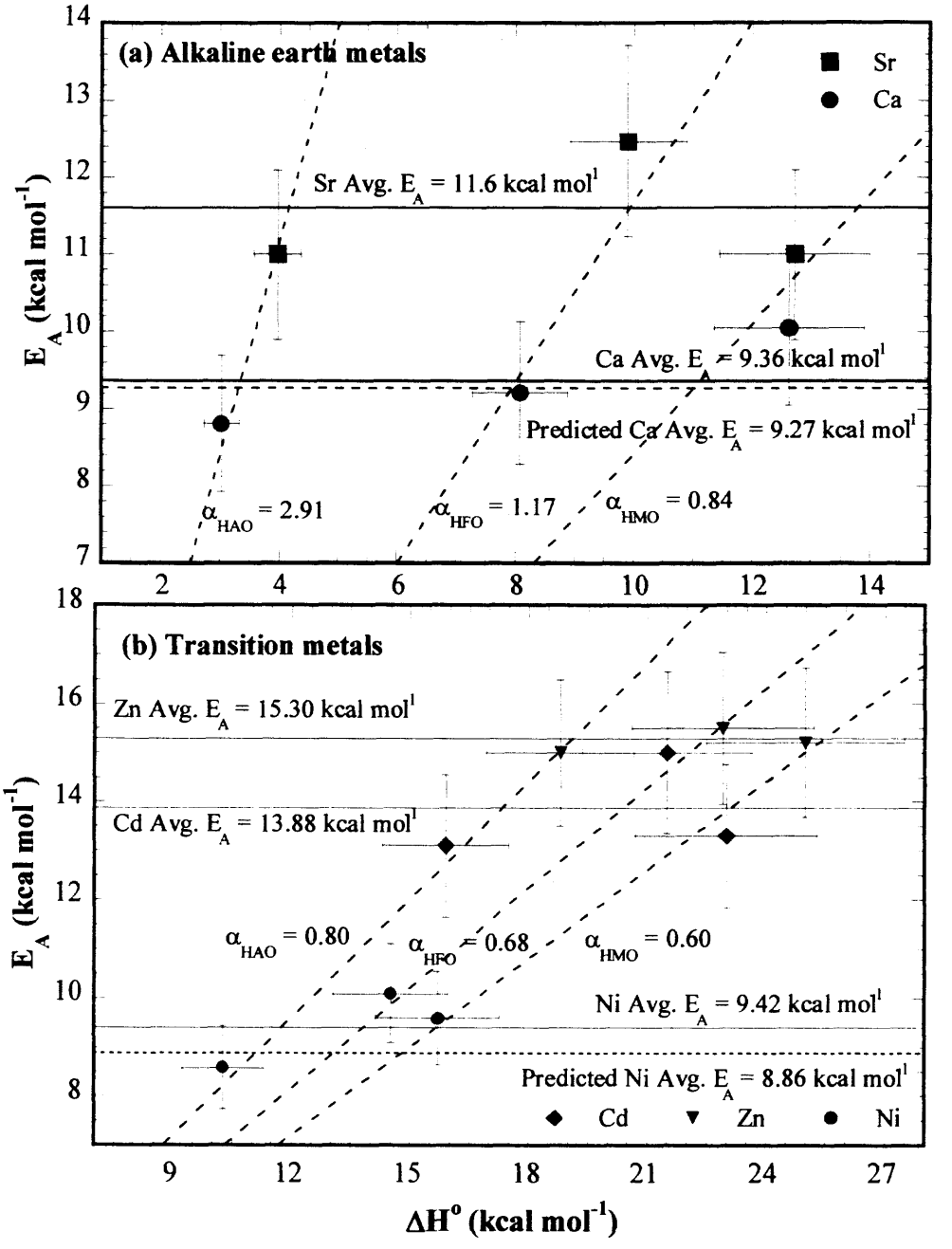

Overall, for a specific oxide, diffusivities decrease in the reverse order of the adsorption enthalpies. These trends suggest that a greater adsorption enthalpy is indicative of tighter bonding between the adsorbate and the adsorbent, and hence a greater barrier or activation energy and smaller diffusivity. For a given hydrous oxide, the diffusivity decreases in the order of Ni > Sr > Cd > Zn. A comparison of Cd and Cu diffusivities in Fe oxide-coated granular activated carbon (GAC) (Wang, 1995) with those in Mn oxide-coated GAC (Fan, 1996) also showed similar trends with respect to the metals and oxides.

5.4 Summary of Amorphous Oxides

Using the activation energy estimated for the divalent metal ion from correlations presented in Figures 15 and 22, theoretical surface diffusion coefficients have been predicted and are illustrated in Figure 29. This research demonstrates that thermodynamic and transport parameters can be predicted, potentially reducing the need for macroscopic analyses. Additionally, this type of research emphasizes the importance in accounting for slow sorption processes such as intraparticle diffusion to model contaminant mobility and bioavailability in aquatic environments.

Figure 28. Correlation between activation energy and the structural parameters (R_H is the hydrated radius (Å) and N is the hydration number of the hydrated metal ions). The correlation is based on the experimental activation energies of Sr, Cd, and Zn (with ± 2 S.D.).

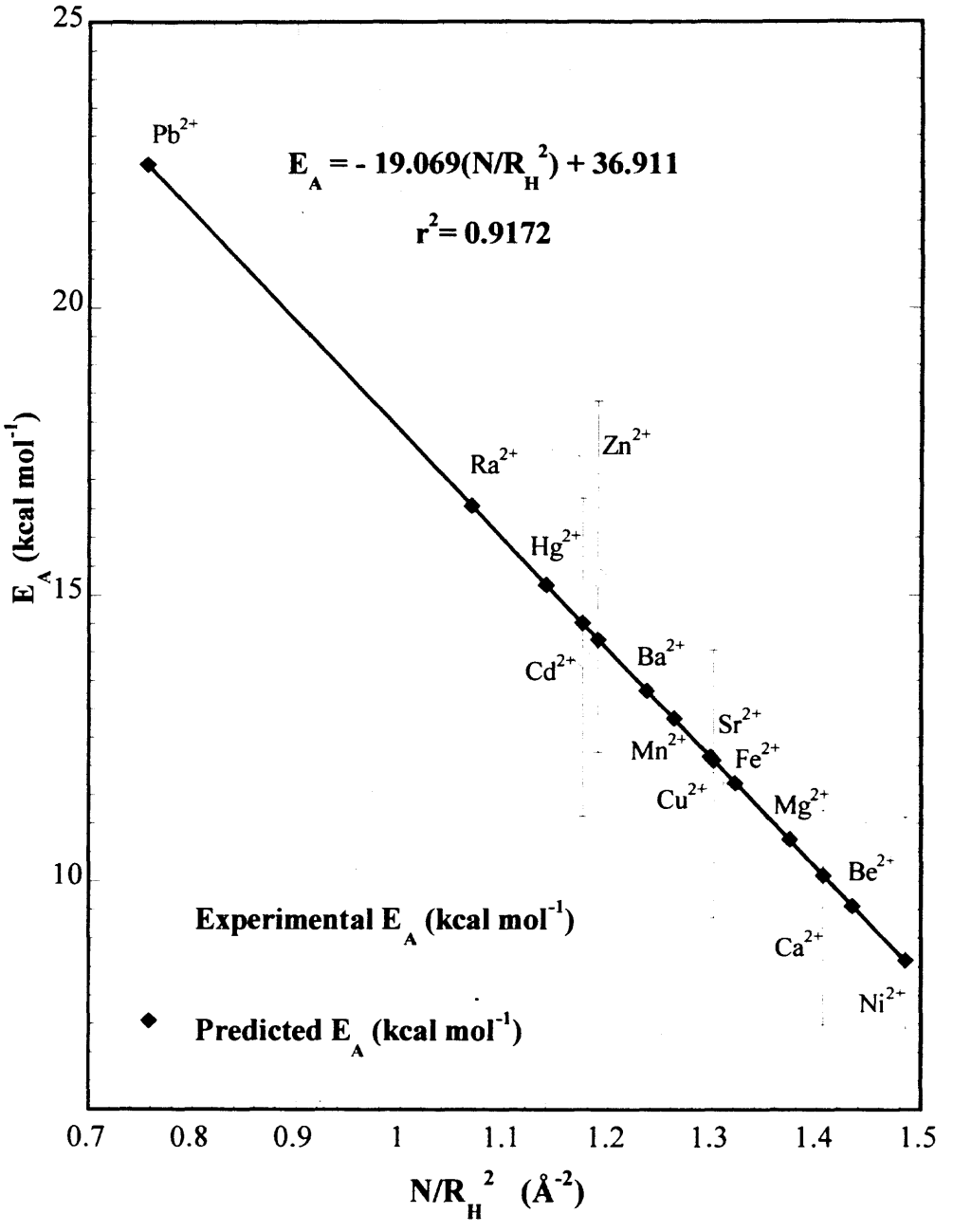

Figure 29. Theoretical surface diffusivities based on site activation theory. Solid symbols with error bars represent the theoretical D_s and open symbols represent experimental D_s (for Sr, Cd, Ni, and Zn).

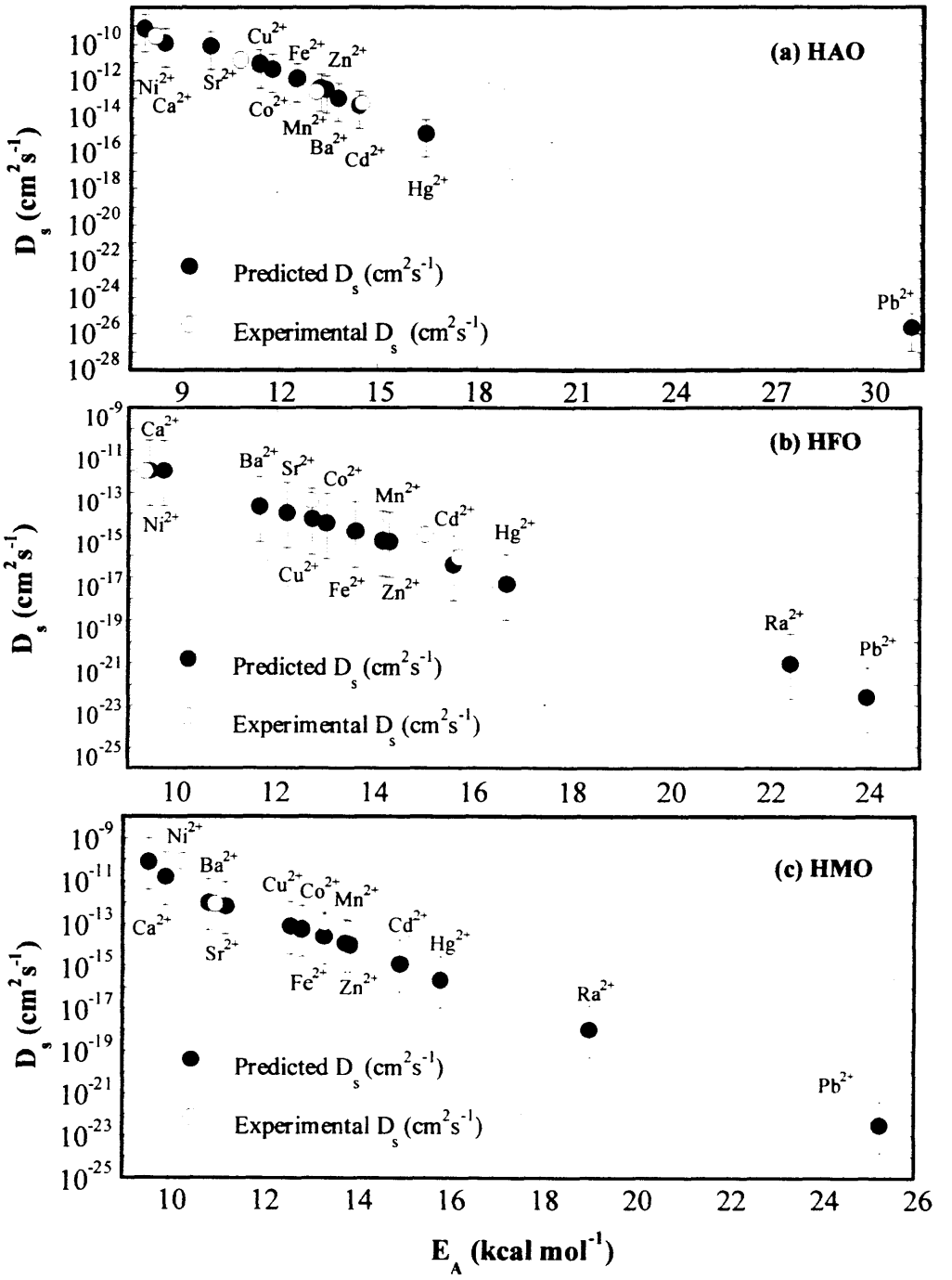

CHAPTER 6

ADSORPTION TO GOETHITE

Adsorption parameters of divalent metal ions to the amorphous oxides evaluated in the previous chapter may not apply to crystalline oxides such as goethite. Adsorbent properties and characteristics play a significant role in determining the nature of adsorption reaction. Site density of crystalline oxides is generally much smaller than that of amorphous oxides and hence there is a possibility of site saturation at much lower metal concentrations. This chapter discusses the metal adsorption to goethite studied for single adsorbate systems along with characterization of goethite. Next, based on the parameters of the single adsorbate systems, adsorption in binary systems is predicted and tested. This research provides parameters that are directly applicable for modeling the fate of environmentally important divalent metals in the aquatic environments that are laden in goethite.

6.1 Characterization of goethite

The ESEM images of goethite demonstrate that the crystals are needle shaped or acicular (Figure 30), which is in agreement with Schwertmann and Taylor (1989). Goethite crystals like HFO aggregate into a somewhat spherical shape. The aggregates were much larger than the individual crystals, and were also observed with an optical microscope. The resuspended (in a turbulent regime $Re > 3.0 \times 10^5$) freeze-dried goethite required at least 3 h for obtaining a stable size distribution. Results of the particle size analysis (Figure 31) reveal that the goethite particle size distributions are shifted to the left of that for the HFO to a smaller size range. As the pH increased, the particle size distribution

Figure 30. Results of (a and b) Environmental Scanning Electron Microscopy and (c) Optical Microscopy acicular goethite crystals as aggregated spherical particles.

(a)

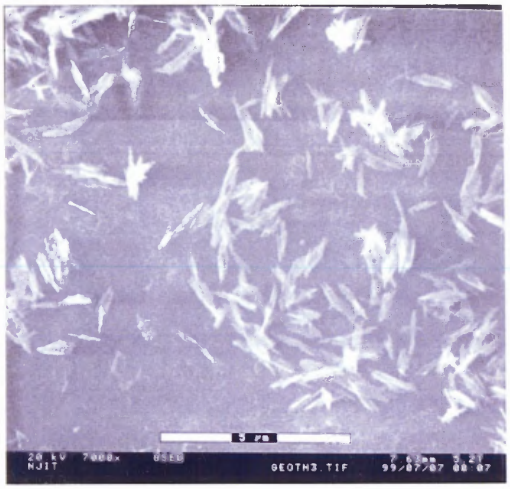

(b)

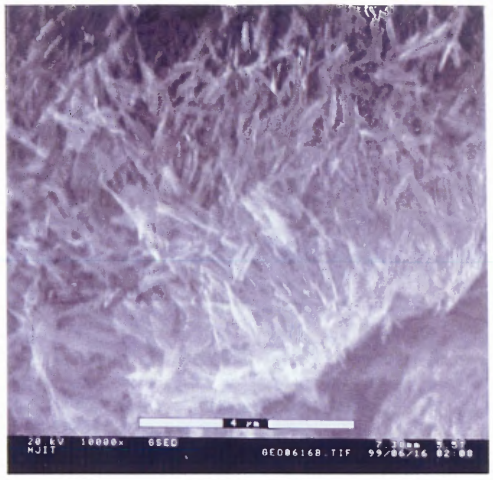

(c)

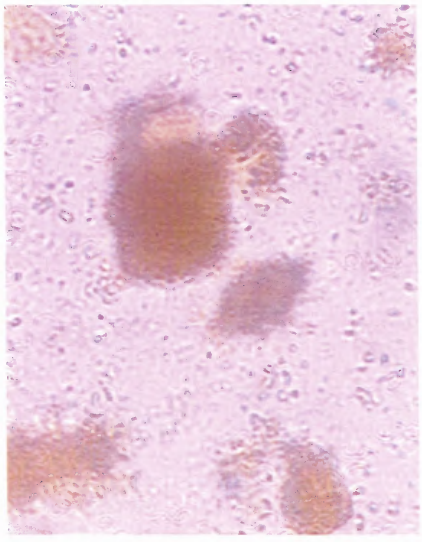

Figure 31. Comparison of particle size distributions of (a) HFO, (b) goethite at μ 10^{-3} and (c) goethite at μ 10^{-2} reveal goethite particles are smaller than HFO.

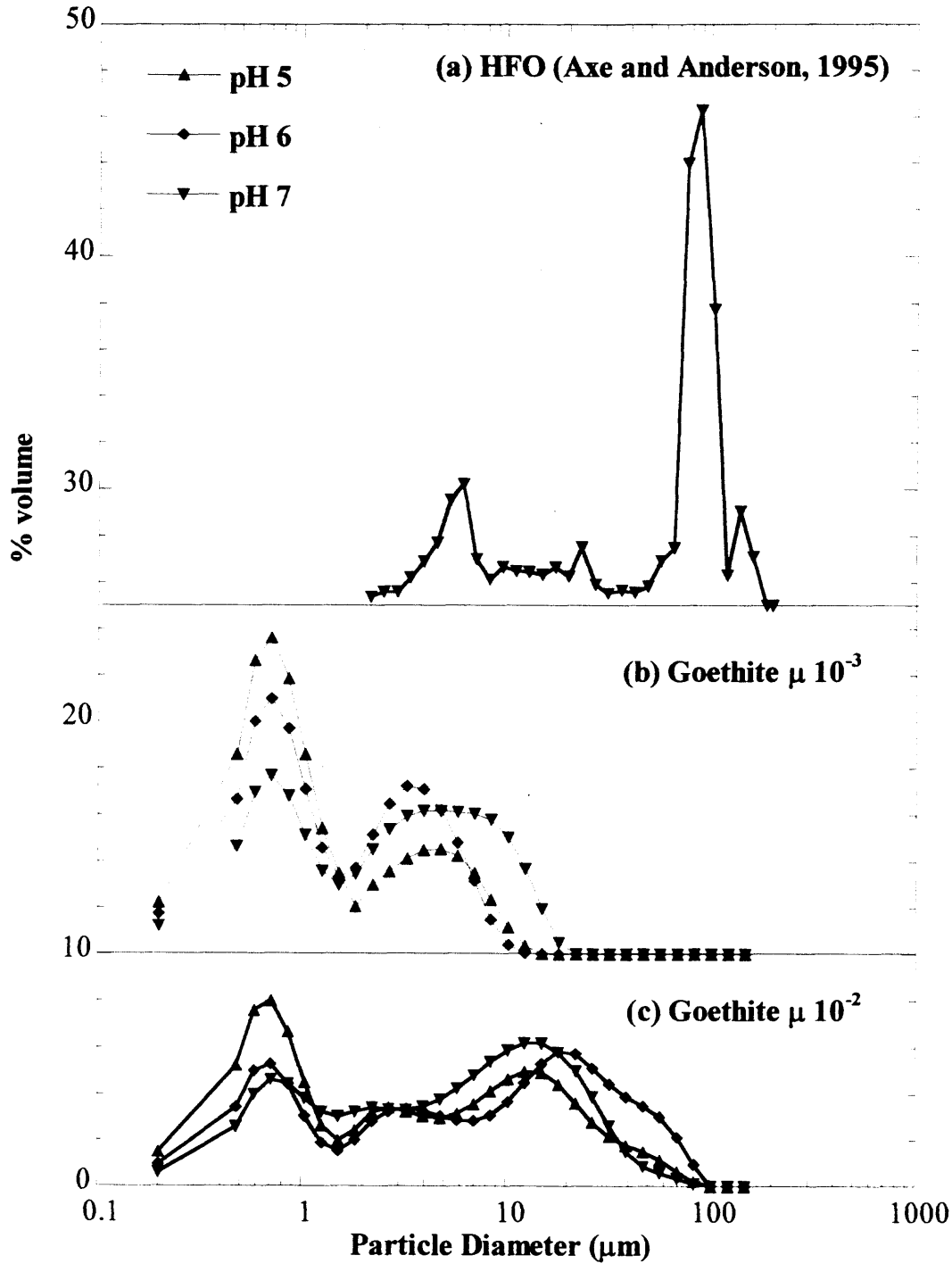

increased slightly; however, the effect of ionic strength was more significant as its increase from 10^{-3} to 10^{-2} resulted in overall larger particles. At the lower ionic strength of 10^{-3}, the largest aggregates were approximately 10 to 20 μm, whereas at 10^{-2} the particles ranged up to 100 μm. If microporosity is significant, intraparticle diffusion may be important.

Nitrogen adsorption (BET) and desorption were used for evaluating surface area and the pore size distribution. The goethite surface area was 27 $m^2\ g^{-1}$. Others (Atkinson, et al., 1967; Palmqvist et al., 1997; Weidler et al., 1998) have found the surface area of goethite ranges from 7.9 $m^2\ g^{-1}$ and 235 $m^2\ g^{-1}$. Using the nitrogen desorption, the pore size distribution ranges from 2 nm to 220 nm (Figure 32). Figure 32 also shows the pore size distribution using mercury porosimetry, where the pores range from 7 nm to 1 μm; the distribution indicates that both meso- and macro-pores exist, with the average size comprising macropores (Greg and Singh, 1982). Thus, the pores range from micro to macro-pores, with a bimodal distribution. The porosity of goethite however, is approximately only 0.3%. These results suggest that long-term sorption processes such as intraparticle diffusion may not be important in goethite systems; however, porosity and pore size like surface area are evaluated with freeze-dried particles that may not accurately represent the hydrated structure.

The surface charge distribution of HFO and goethite studied as a function of ionic strength are compared in Figure 33. The pH_{PZNPC} is 7.8 ± 0.4 for goethite, which is consistent with other work (Atkinson et al., 1967; Dzombak and Morel, 1990). The pH_{PZNPC} for goethite has been found to vary between 7.7 and 9 depending upon various factors like the method of determination, degree of hydration, and method of synthesis

Figure 32. Goethite pore size distributions as seen from (a) mercury porosimetry and (b) nitrogen desorption are bimodal distributions (IGT Report, 1999).

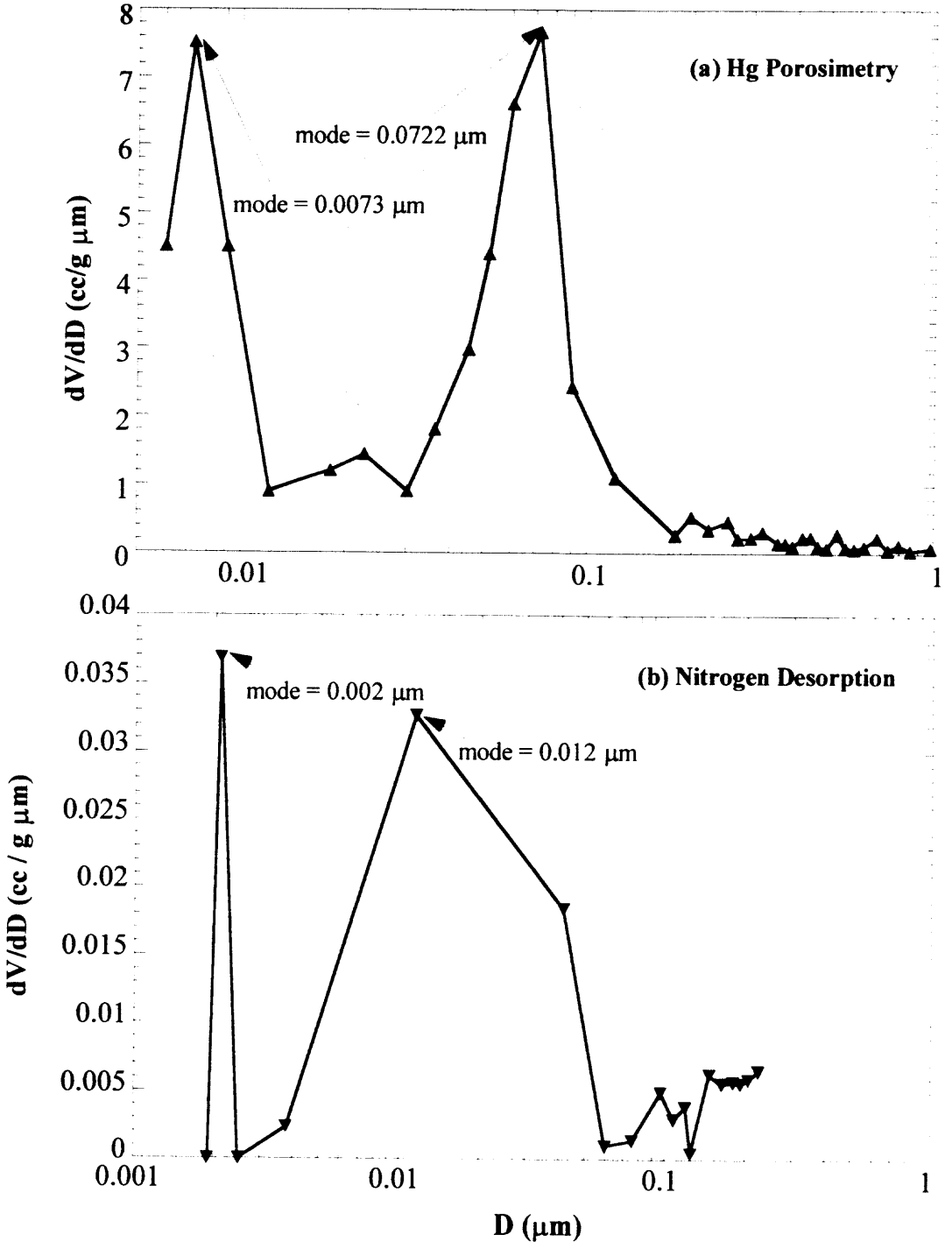

Figure 33. Acid-base potentiometric titrations conducted at 1 g L^{-1}, 25°C, and under closed systems conditions for (a) amorphous iron oxide, and (b) Electrophoretic mobility of goethite at 1 g L^{-1} and 25°C is shown in (c).

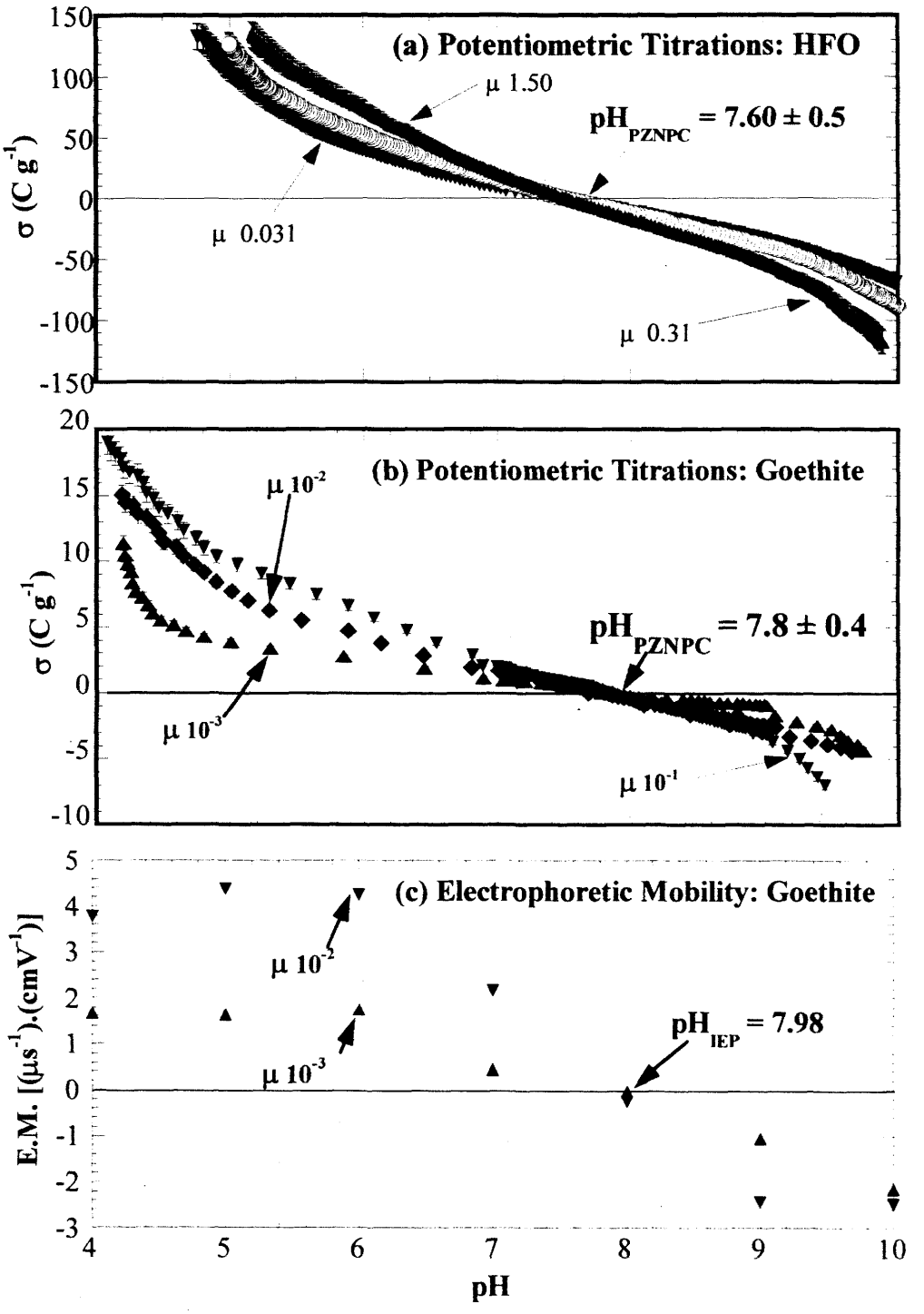

(Atkinson et al., 1967; Christopher, C. A., 1998; McBride, M. B., 1989). Interestingly, the surface charge of HFO is as much as 10 times that of goethite suggesting that HFO has a much greater surface area than goethite and therefore a greater adsorption capacity. Based on a compilation of HFO data on characteristics and sorption (Dzombak and Morel, 1990), surface areas have ranged from 159 to 720 $m^2\ g^{-1}$ with an estimate of 600 $m^2\ g^{-1}$ recommended for use. Electrophoretic mobility measured on goethite at ionic strengths of 10^{-3} and 10^{-2} resulted in a pH_{IEP} of 7.9 $\pm$ 0.1 (Figure 32); in this case, it is almost equivalent to the pH_{PZNPC} for goethite. The approximate agreement of the pH_{IEP} with the pH_{PZNPC} suggests the absence of adsorbed Na^+ or NO_3^- (Hesleitner et al., 1987).

6.2 Single Adsorbate Systems

Adsorption edges of Ni (Figure 34a), Zn (Figure 34b), and Ca (Figure 34c) were studied between pH 4 and 10 for ionic strengths 10^{-3} and 10^{-2}. The sharp and sigmoid edges for Zn and Ni are typical of transition metals (Balistrieri and Murray, 1982; Christophi and Axe, 2000; Okazaki et al., 1986). On the other hand, Ca adsorption edges are broad and consistent with those of other alkaline metals (Lützenkirchen, 1997; Axe and Anderson, 1995; Mishra and Tiwary, 1995). Ni, Zn, and Ca adsorption to goethite is independent of ionic strength, which is in agreement with the studies of other transition metals such as Cu (Christophi and Axe, 2000; Okazaki et al., 1986; Swallow et al., 1980), Pb (Christophi and Axe, 2000; Manceau et al., 1992; Okazaki et al., 1986; Hayes and Leckie, 1986), and Cd (Balistrieri and Murray, 1982; Christophi and Axe, 2000). In this earlier work, adsorption was attributed to inner sphere complexation.

Figure 34. Adsorption edges of (a) Ni, (b) Zn, and (c) Ca adsorption to 1 g L^{-1} goethite at 25°C.

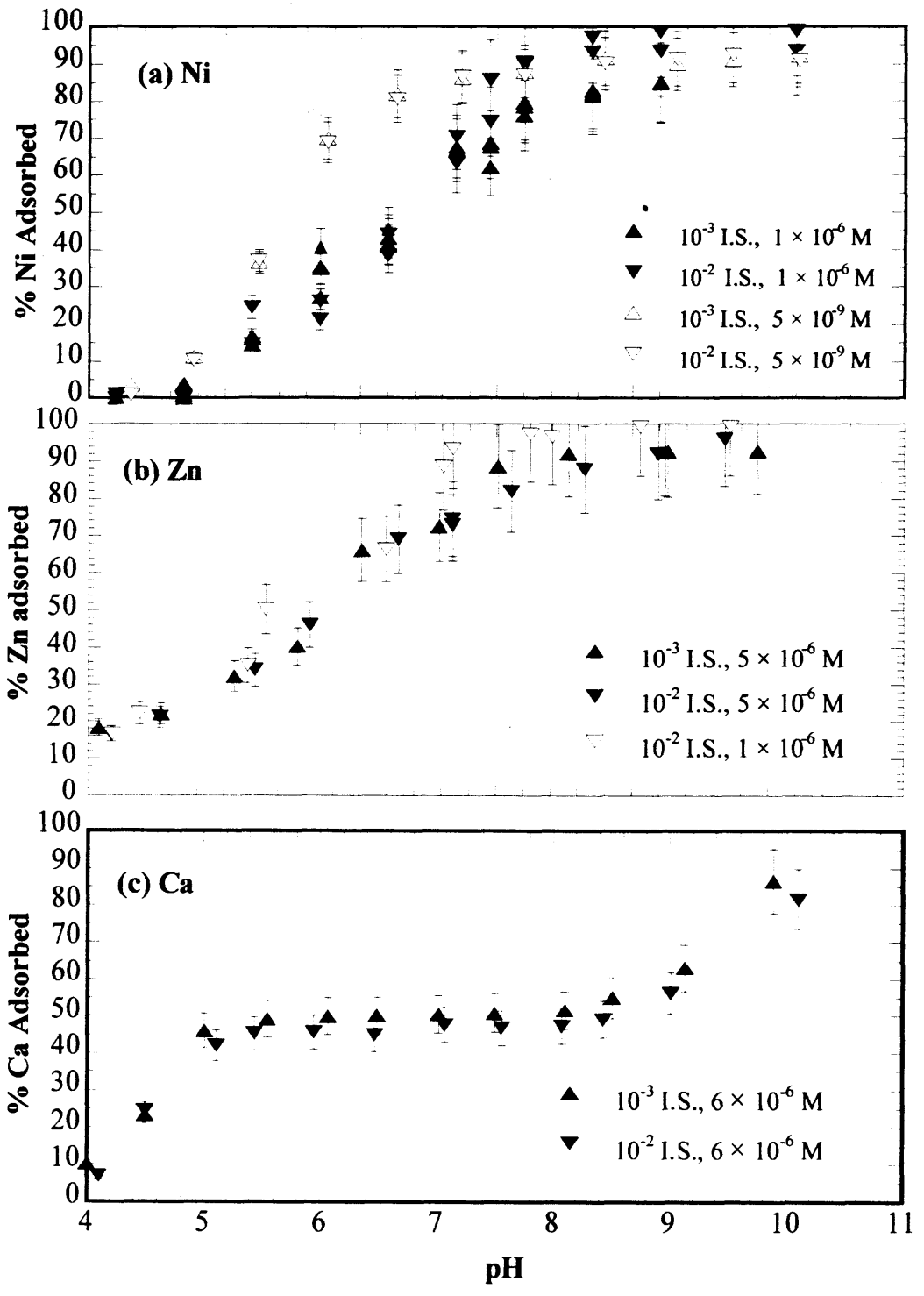

On the other hand, when Lützenkirchen (1997) observed a decrease in Ba adsorption to goethite with an increase in ionic strength, the reduction was credited to a decrease in the ion activity. Barrow et al. (1981) also observed a decrease in Ni adsorption with increasing ionic strength. This effect may be due to the appreciable silicon content in their goethite, which may not only affect the pH_{PZNPC} but also the surface characteristics. Interestingly, Balistrieri and Murray (1982) observed that Zn adsorption to goethite was equivalent whether in a 0.1 M $NaNO_3$ system or a 0.53 one. However Zn adsorption decreased in the seawater, which includes not only NaCl, but also Ca, Mg, K, and sulfate ions suggesting that other ions competed for the same sites.

A comparison of Ca, Ni, and Zn adsorption edges shows that their affinity for the goethite surface increases in the order of Zn > Ni > Ca, which is consistent with the reverse order of the inverse of the hydrated radius (R_H) multiplied by the number of waters of hydration (N) (Table 8). Rose and Bianchi-Mosquera (1993) also found that the adsorption of Zn was greater than that of Ni. On the other hand, Okazaki et al. (1986) reported the sequence of adsorption to goethite in the order of Cu > Zn > Mg, and attributed it to their electronegativity. McKenzie et al. (1980) observed the following trend Cu > Pb > Zn > Co > Ni > Mn, which with the exception of Co is in agreement with the order of the first hydrolysis constants of these cations. Overall, transition metals have a much greater affinity for the surface as compared to alkaline earth metals.

Isotherms were conducted to study Ni adsorption to goethite as a function of adsorbate concentration at 25°C for pH 5, 6, and 7 (Figure 35a-c). Goethite concentration was typically maintained 1 g L^{-1} for Ni concentrations in the range of 10^{-10} - 10^{-4} M; additionally in an effort to swamp all potential sites, studies were conducted using a 0.1 g

Table 8. Metal Ion Properties

Metal	Group	Eneg*	Polar.** (10^{-24} cm^3)	log K_{MOH}	R_{ionic} (Å)	$R_{covalent}$ (Å)	N	R_H (Å)	N/R_H ($Å^{-1}$)
Ca	IIA	1.00	25.00	1.22	1.26	1.74	9.0	2.53	3.56
Mg	IIA	1.31	10.60	2.56	1.03	1.30	6.0	2.09	2.87
Be	IIA	1.57	5.60	8.58	0.49	0.90	4.0	1.67	2.40
Sr	IIA	0.95	27.60	0.71	1.40	1.92	9.0	2.63	3.42
Ba	IIA	0.89	39.70	0.53	1.56	1.98	9.7	2.81	3.45
Ra	IIA	0.90	38.30	0.51	1.62	1.92	9.0	2.81	3.20
Pb	IVA	2.33	6.80	5.20	1.33	1.47	4.0	2.30	1.74
Co	VIII	1.88	7.50	3.18	0.79	1.26	6.0	2.09	2.87
Ni	VIII	1.91	6.80	4.14	0.83	1.21	6.3	2.06	3.06
Fe	VIII	1.83	8.40	4.50	0.75	1.25	6.0	2.13	2.82
Cu	IB	1.90	6.10	6.00	0.71	1.38	6.0	2.15	2.79
Zn	IIB	1.65	7.10	5.04	0.74	1.31	5.2	2.09	2.49
Cd	IIB	1.69	7.20	3.92	0.97	1.48	6.0	2.30	2.61
Hg	IIB	2.00	5.70	11.20	1.10	1.49	6.0	2.37	2.53
Mn	VIIB	1.55	9.40	3.41	0.97	1.39	6.0	2.18	2.75

All properties from CRC Handbook (Lide and Frederikse, 1998) with the exception of log K_{MOH} Stumm and Morgan (1998) and N and R_H Richens (1997).

* Eneg. = electronegativity

** Polar. = polarizability

Figure 35. Isotherms conducted at 25°C, and 1 g L^{-1} to goethite for Ni adsorption at (a) pH 5, (b) pH 6, and (c) pH 7 and for Zn at (d) pH 5, (e) pH 6, and (f) pH 7. Solid lines represent the model and dashed lines are the errors (± 2 S.D.).

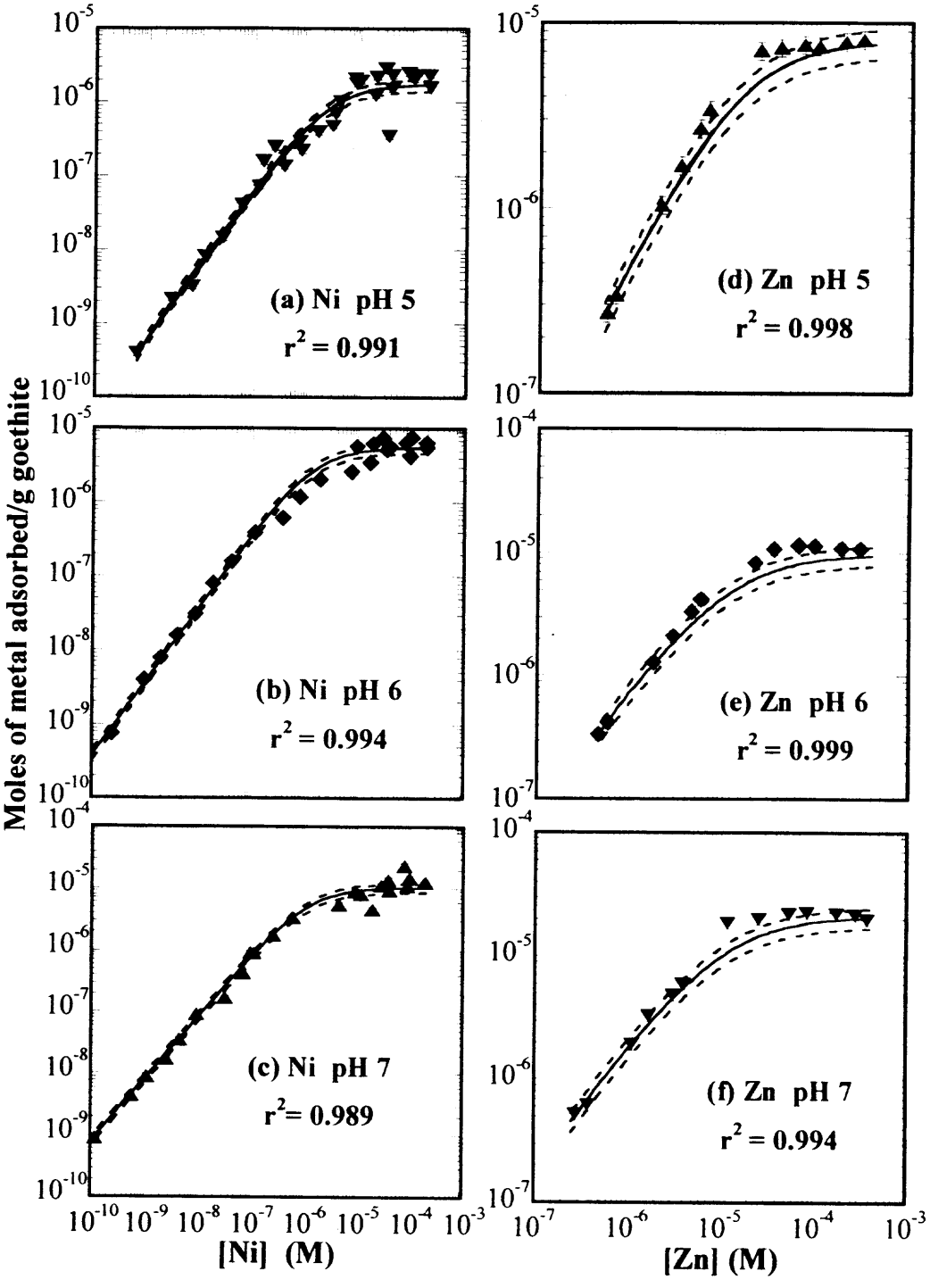

L^{-1} goethite suspension. In the lower concentration range (10^{-10} – 10^{-6} M Ni), isotherms reveal a linear relation between the metal in the bulk and adsorbed phases suggesting adsorption can be modeled with one average type of site. For higher concentrations the isotherm reaches an asymptote indicative of the saturation of adsorption sites. As seen in Figure 35a-c, site density is a function of the pH. Assuming monolayer adsorption, no adsorbate-adsorbate interactions, and a uniform driving force, the single-site Langmuir model is applied to the experimental data as shown in Equation 16 (Fogler, 1992):

$$\frac{1}{C} = \frac{1}{K C_t} \times \frac{1}{[S]} + \frac{1}{C_t} \tag{16}$$

where C is the moles of metal adsorbed g^{-1} goethite, K is the adsorption equilibrium constant, C_t is the site density in moles of metal g^{-1} goethite, and [S] is the molar concentration of metal ions in the bulk liquid phase at equilibrium. This model is based on Langmuir-Hinshelwood kinetics for a single-site surface reaction mechanism where in the maximum sorption density represents the site density or capacity (Dzombak and Morel, 1990; Fogler, 1992). In modeling, the intercept representing $(C_t)^{-1}$ was constrained to minimize the sum of the squares of the residuals; the model fits the data well (Figure 34a-c and Table 9). The site densities reported for Ni adsorption are consistent with that of Christophi and Axe (2000) where Cu, Pb, and Cd adsorption to goethite was studied (Table 10). Ni site densities for goethite are much smaller than those reported for Ni adsorption to HFO. Spadini et al. (1994) pointed out from their spectroscopic studies that HFO and goethite have similar local structure but goethite has much less of the high-energy edge sites per unit surface area and a smaller site density. Interestingly, the equilibrium constant (Table 9) is independent of pH given the errors, suggesting that the

Table 9. Summary of Isotherm Studies for Single-Adsorbate Systems

Metal	pH	r^2	K†	C_t†	Experimental C_t
			L $mole^{-1}$	Moles g^{-1} goethite	Moles g^{-1} goethite
Zn	5.0	0.998	6.78×10^4	*7.31×10^{-6}	7.88×10^{-6}
	6.0	0.999	6.76×10^4	*9.86×10^{-6}	1.12×10^{-5}
	7.0	0.994	6.79×10^4	*2.09×10^{-5}	2.22×10^{-5}
Ni	5.0	0.991	5.54×10^4	1.73×10^{-6}	2.30×10^{-6}
	6.0	0.994	6.81×10^4	5.5×10^{-6}	5.80×10^{-6}
	7.0	0.989	6.01×10^4	1.02×10^{-5}	1.25×10^{-5}
Ca	5.0	0.979	2.54×10^2	3.00×10^{-3}	2.01×10^{-3}
	6.0	0.948	2.55×10^2	3.30×10^{-3}	2.35×10^{-3}
	7.0	0.941	2.84×10^2	4.05×10^{-3}	3.01×10^{-3}

*Site densities selected for high affinity site capacity in competition studies.
Experimental errors for Zn and Ni studies are ± 9%, and for Ca it is ± 10%
† Parameters estimated using single-site Langmuir isotherm model

Table 10. Site Densities of Goethite Reported from the Literature

Reference	pH_{PZNPC}	S. A. ($m^2\ g^{-1}$)	Adsorbate	Studies	Model	K ($L\ mol^{-1}$)	C_t ($mol\ g^{-1}$)	at pH
Christophi and Axe (2000)	7.8	40.5	Cd	AE, AI	SSL	2.00×10^{6}	5.00×10^{-6}	6.00
			Cu	AE, AI	SSL	4.50×10^{6}	9.10×10^{-6}	6.00
			Pb	AE, AI	SSL	1.20×10^{7}	7.20×10^{-6}	6.00
Zachara et al. (2000)	NA	55.4	Fe	AE, AI	NA	NA	1.79×10^{-4}	6.50
			Co	AE, AI	NA	NA	4.85×10^{-5}	6.50
Angove et al. (1999)	8.2	49.6	Cd	AE, AI, T	SSL	2.80×10^{4}	2.68×10^{-5}	7.00
			Co	AE, AI, T	TSL (Type I site)	1.63×10^{5}	1.04×10^{-5}	7.00
					TSL (Type II site)	5.00×10^{3}	3.47×10^{-5}	7.00
Nowack and Sigg (1996)	7.4	21.0	NiEDTA	AE, AI	SCM	6.61×10^{5}	4.22×10^{-5}	3.45
			PbEDTA	AE, AI	SCM	1.82×10^{6}	3.54×10^{-5}	3.40
			ZnEDTA	AE, AI	SCM	5.50×10^{5}	1.78×10^{-5}	5.40
			Fe(III)EDTA	AE, AI	SCM	2.95×10^{6}	8.95×10^{-7}	3.30
Rodda et al. (1996)	8.1	55.0	Zn	AI, T	TSL (Type I site), FDM, BET	1.93×10^{5}	1.65×10^{-5}	6.50, 7.50
					TSL (Type II site)	2.8×10^{3}	1.60×10^{-4}	6.50, 7.50
			Pb	AI, T	TSL (Type I site), FDM, BET	1.85×10^{5}	7.76×10^{-6}	5.50
					TSL (Type II site)	4.40×10^{3}	5.50×10^{-5}	5.50
Johnson (1990)	9.1	76.0	Cd	AE, AI, T	SSL for pH <7.5	4.20×10^{3}	2.28×10^{-5}	6.5, 7.0
			Cd	AE, AI, T	TSL (Type I site) for pH 7.5	7.00×10^{5}	1.14×10^{-5}	7.50
					TSL (Type II site) for pH 7.5	3.60×10^{4}	3.88×10^{-5}	7.50
McKenzie (1980)	7.6	75.0	Cu	AE, AI	NA	NA	1.05×10^{-4}	5.50
			Pb	AE, AI	NA	NA	6.00×10^{-5}	5.50
			Zn	AE, AI	NA	NA	2.50×10^{-5}	5.50

AE = Adsorption edges, AI = Adsorption isotherms, BET = BET model, FDM = Farley, Dzombak, and Morel's surface precipitation model, NA = information not available, SCM = Surface complexation model, SSL = single-site Langmuir, T = temperature studies, TSL = two-site Langmuir

Ni adsorption mechanism is invariant between pH 5 and 7. Furthermore, this K is much greater than the ones reported for other hydrous iron oxides and even other adsorbents as seen in the previous chapter (Dzombak and Morel, 1990).

Isotherm studies of Zn adsorption to goethite were also conducted at 25°C for pH 5, 6, and 7. Similar to Ni, Zn adsorption isotherms (Figure 35d-f) demonstrate a linear relation between the metal in the bulk and adsorbed phases at lower concentrations ($< 5 \times 10^{-6}$ M Zn), while at higher concentrations site saturation is observed. Modeling with the single-site Langmuir isotherm revealed site densities (Table 9) ranging between 7.31×10^{-6} and 2.09×10^{-5} moles g^{-1} consistent with experimental results; these site densities are also a function of pH and are slightly greater than those for Ni. Rodda et al. (1996) estimated site densities of 10^{-5} and 10^{-4} moles Zn g^{-1} goethite using the one and two-site Langmuir models, respectively (Table 10). Recently Angove et al. (1999) also reported similar orders of site density for adsorption of Cd and Co to goethite at pH 7. On the other hand, Ankomah (1992) reported Zn adsorption site densities between pH 5.4 and 7.8, an order of magnitude greater than the ones observed in this research. However, Ankomah (1992) reported using goethite particles present as individual crystals that were almost an order of magnitude smaller in size than the aggregated ones used here.

The equilibrium constants for Zn adsorption at all pH values are equivalent given the errors, suggesting that Zn adsorption like Ni is independent of pH. Site densities and equilibrium constants have been found to increase with temperature indicating that adsorption of metals such as Cd, Co, Pb, and Zn to goethite is an endothermic process (Johnson, 1990; Rodda et al., 1993, 1996; Angove et al., 1999). Cd and Zn adsorption to HFO as well as other hydrous oxides is also an endothermic reaction. Because Ni and Zn

are from the same group in the Periodic Table and have similar affinities for goethite, a hypothesis of this research is that they form similar adsorption complexes competing for the same type of sites. For competition studies, the site densities selected for modeling are highlighted in Table 9.

On the other hand, for the alkaline earth metal calcium, site densities are at least 2-3 orders or magnitude greater than those of Ni and Zn (Figure 36a-c and Table 9). The equilibrium constant is also pH independent, but much smaller than those of Ni and Zn. The single-site Langmuir model provided a good fit for the data, suggesting that the range of adsorption sites on goethite can be described by one average type of site (a lower affinity one). Pivovarov (1998) applied a non-electrostatic model to describe Ali and Dzombak's (1996) data on Ca adsorption to goethite at 20°C and obtained a site density of 3.6×10^{-4} moles g^{-1}. Ca site densities presented in Table 8 are an order smaller than those reported for Sr adsorption to goethite (Christophi and Axe, 2000). On the hand, Vanìk and Jedináková (1986) reported the site densities for Ba adsorption to be 5.3×10^{-4} moles g^{-1} goethite. Given the observed site densities for Ca with a lower adsorption affinity as compared to Ni and Zn, it is hypothesized that Ca adsorbs to another set of sites, and therefore will not compete for the ones occupied by the transition metals. As seen in Table 10 the equilibrium constants for adsorption to goethite independent of pH and are much greater than those for HFO. The effect of temperature (Figure 37 and Table 11) further suggests that adsorption to HFO is due to physical forces while for goethite it is chemisorption. Given these enthalpies and the lack of ionic strength effects, interactions may be due to chemisorption (de Boer, 1967). Again, with each oxide, Zn demonstrates a stronger affinity for the surface than does Ni.

Figure 36. Isotherms of Ca adsorption to 1 g L^{-1} goethite at 25°C. Solid lines represent single-site Langmuir model along with associated errors of ± 2 S.D as shown with the dashed lines.

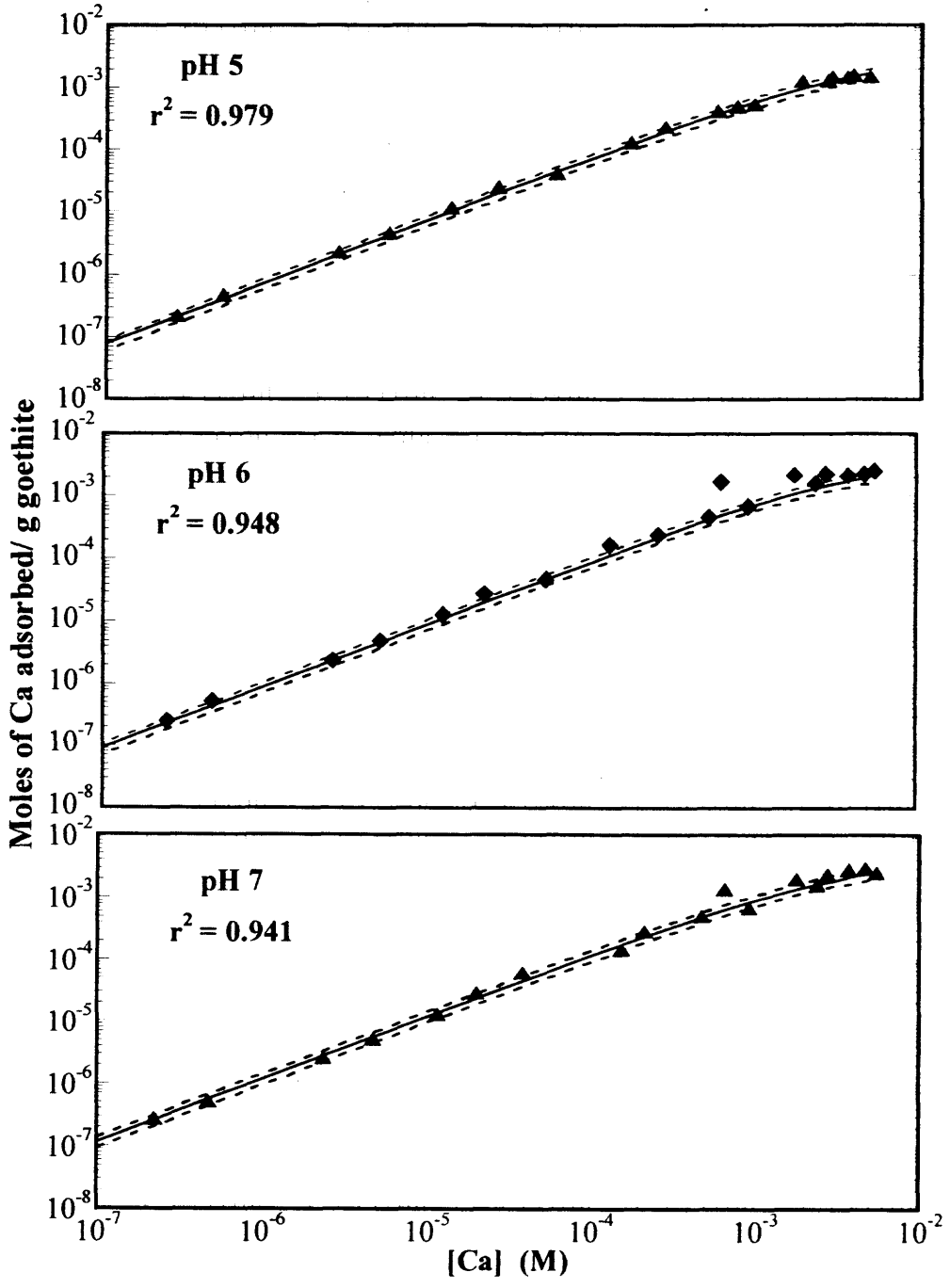

Table 11. Summary of Adsorption Parameters of Goethite and HFO

Metal	Adsorbent	pH	T	K	C_t (mole g^{-1})	ΔH^o (kcal mol^{-1})
Ni	HFO	6.0	25.0	1.11×10^3	3.70×10^{-3}	14.85 ± 1.49
			14.0	8.36×10^2		
			4.0	3.65×10^2		
	HFO	7.0	25.0	1.07×10^3	2.50×10^{-2}	
			14.0	6.68×10^2		
			4.0	2.56×10^2		
	Goethite	5.0	25.0	5.54×10^4	1.73×10^{-6}	
	Goethite	6.0	24.8	6.81×10^4	5.50 × 10-6	
	Goethite	7.0	24.8	6.01×10^4	1.02×10^{-5}	31.07 ± 3.11
			14.0	1.93×10^4	9.40×10^{-6}	
			3.9	1.15×10^3	7.50×10^{-6}	
Zn	HFO	6.0	25.0	3.89×10^3	3.7×10^{-3}	22.70 ± 2.27
			14.0	1.58×10^3		
			4.0	2.39×10^2		
	HFO	7.0	25.0	4.00×10^3	2.50×10^{-2}	
			14.0	8.12×10^2		
			4.0	1.47×10^2		
	HFO	8.0	25.0	3.41×10^3	3.30×10^{-2}	
			14.0	1.03×10^3		
			4.0	2.04×10^2		
	Goethite	5.0	24.7	6.78×10^4	7.31×10^{-6}	
	Goethite	6.0	24.8	6.76×10^4	9.86×10^{-6}	
	Goethite	7.0	24.6	6.79×10^4	2.09×10^{-5}	33.20 ± 3.32
			14.0	2.34×10^4	1.71×10^{-5}	
			4.1	1.17×10^3	1.21×10^{-5}	

Estimated parameters have an error of ± 10%

Activation energy can be calculated from the Polanyi relation: $E_A = \alpha \Delta H^o$ (*Ref.*)

Figure 37. van't Hoff plots for Ni and Zn adsorption to (a) goethite and (b) HFO.

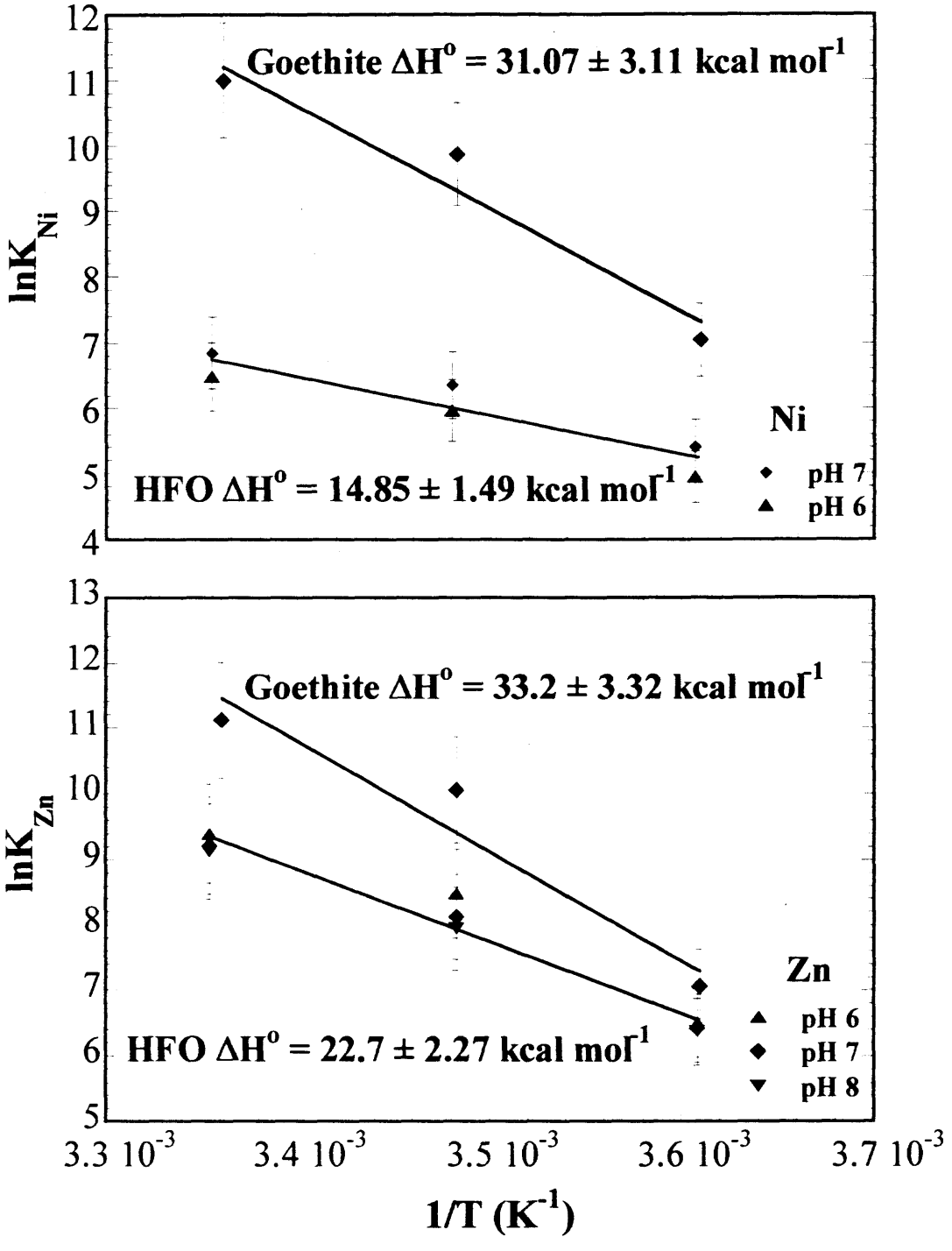

To assess whether intraparticle diffusion is significant in goethite systems, long-term sorption of Ni and Zn to goethite was studied at pH 7 applying CBC experiments (Figure 38). In these experiments, the metal concentration in the bulk aqueous phase was monitored and maintained constant by measuring the activity of the radioisotope in the suspension and filtrate (Ankomah, 1992; Christophi and Axe, 2000; Forbes et al., 1976; Grossl et al., 1997; Lützenkirchen, 1997). This procedure allows one to investigate the slow sorption process in a convenient time frame (Ankomah, 1992; Christophi and Axe, 2000; Forbes et al., 1976; Grossl et al., 1997; Lützenkirchen, 1997).

Although there is a slight increase in the amount of metal adsorbed as a function of time, the change falls within the analytical errors (± 1 S.D.) indicating that the 2 h contact time describes equilibrium. This long-term study demonstrates that microporosity is insignificant and therefore intraparticle (surface) diffusion does not contribute towards the total amount of metal adsorbed. On the other hand, in the previous chapter, for Ni and Zn sorption to HFO as much as 40% of the total sites are located internally.

6.3 Binary adsorbate systems

Results of reversibility studies revealed (Figure 39) that after two hours the amount of Ni adsorbed was equivalent to that for the single adsorbate isotherm. Upon adding Zn, Ni was displaced and the amount sorbed was predicted by the single-site Langmuir model

$$C_{Ni} = \frac{K_{Ni} C_{t,trans} [Ni]}{1 + K_{Ni}[Ni] + K_{Zn}[Zn]} \qquad (17)$$

Figure 38. Constant boundary condition studies at 25°C, IS 10^{-3}, pH 7, and 1 g L^{-1} goethite for (a) $[Ni]_{bulk} = 1.1 \times 10^{-6}$ M and (b) $[Zn]_{bulk} = 3.4 \times 10^{-7}$ M.

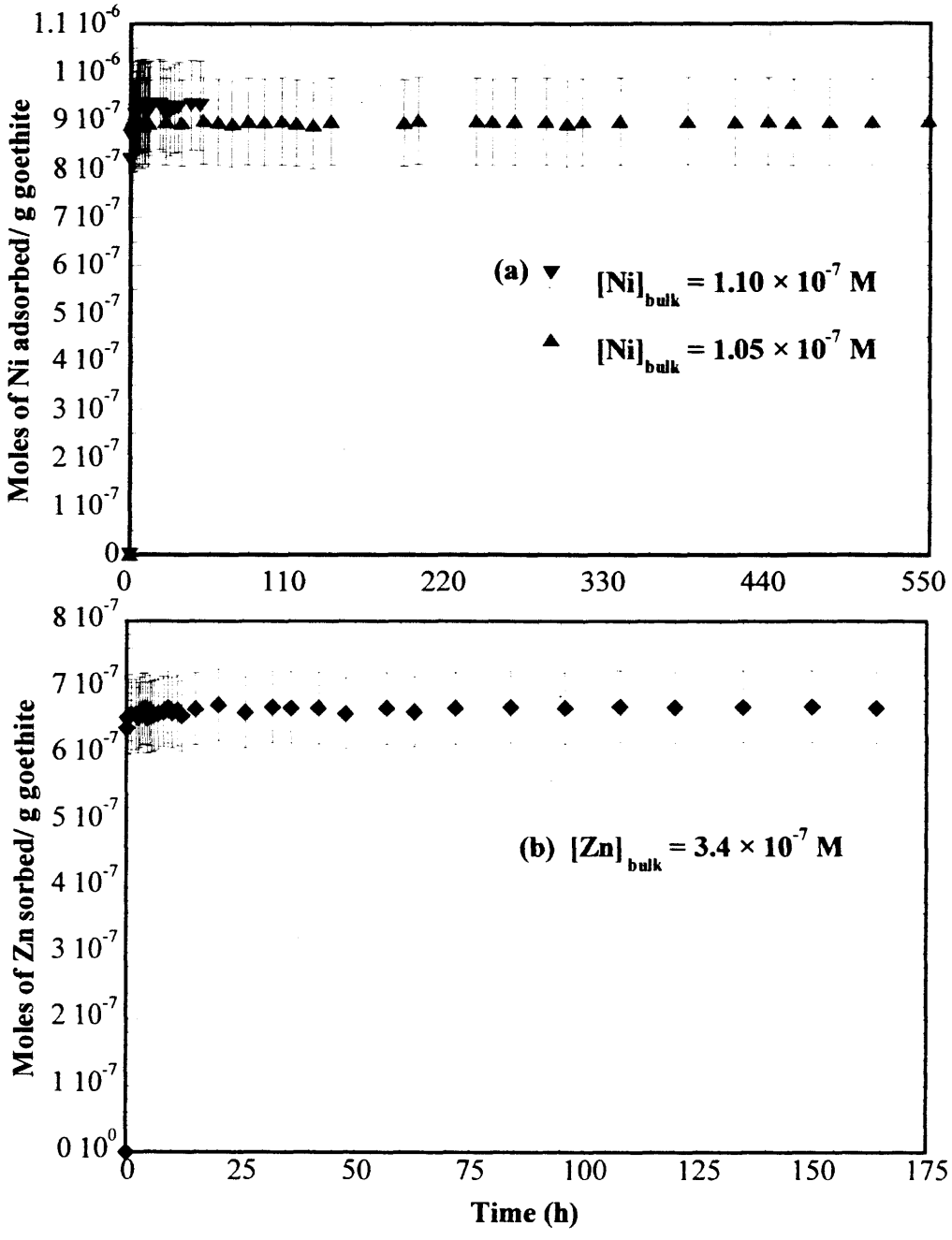

Figure 39. Competitive adsorption between Ni and Zn to 0.1 g L^{-1} goethite at pH 7, and 25°C, where one metal is added first at t = 0 h and then at t= 2h the system is titrated with other metal. Solid lines are single-site Langmuir adsorption model. Dashed lines are associated errors.

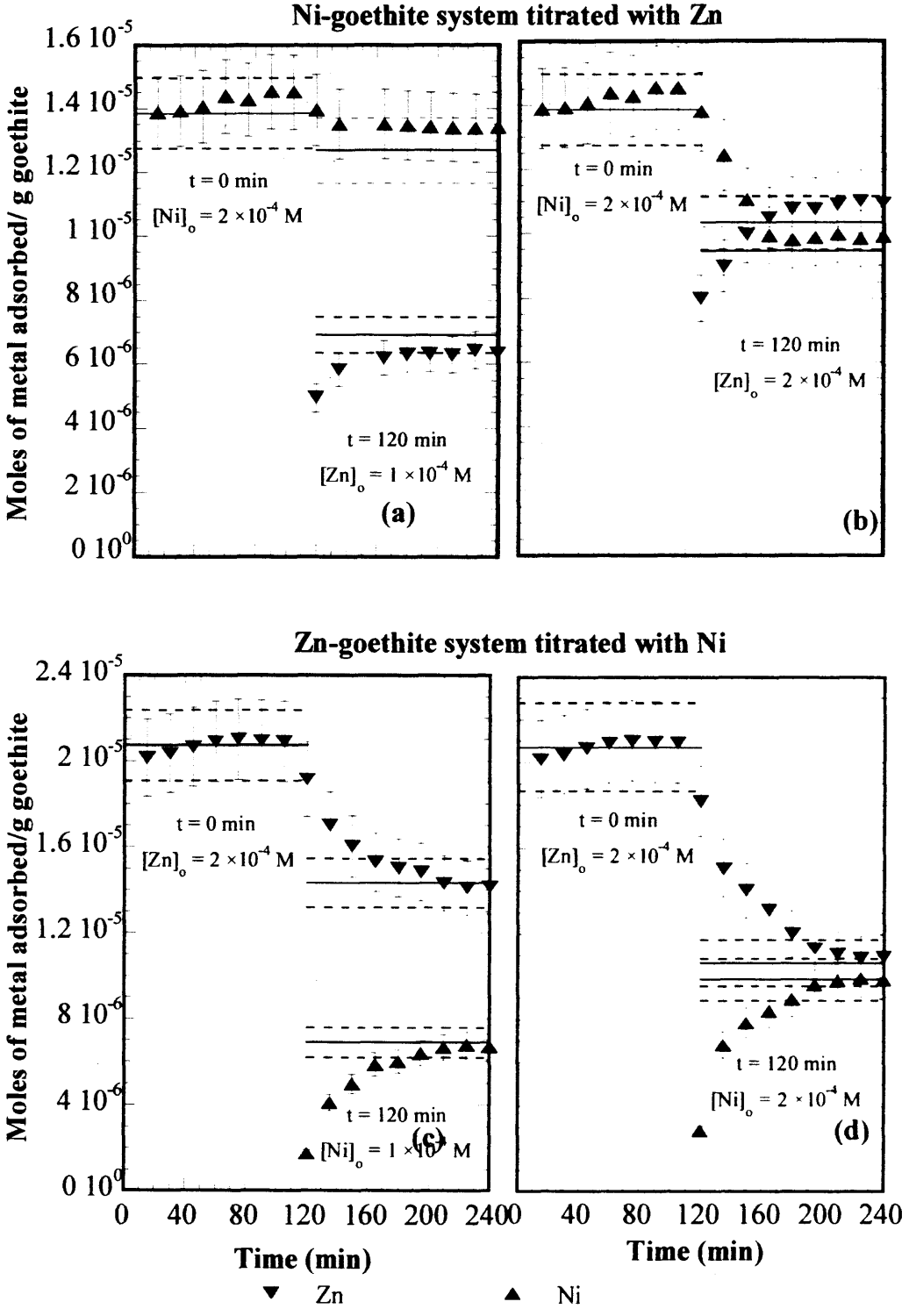

where $C_{t,trans}$ represents the site density for transition metals of which both metals compete. Likewise, in the other set of experiments, upon addition of Ni, Zn was displaced and again equilibrium was predicted by the single-site Langmuir model. These results demonstrate adsorption reversibility and that Ni and Zn as well as potentially other transition metals compete for the same type of sites on the goethite surface. Cowan et al. (1991) also observed that the adsorption of Ca and Cd to amorphous iron oxide was reversible; in their case, the large site density of amorphous iron oxides explains the absence of competition. Gunneriusson (1994) investigated the reversibility of Cd adsorption to goethite; he found that adsorption was nearly fully reversible where metal was released by lowering the pH.

Reversibility was observed over a wide range of metal concentrations and adsorption was well represented by single-site Langmuir model. Results of Ni–Zn competition studies for pH 5, 6, and 7 are presented in Figure 40. These studies show that at lower metal concentrations when sites are not limited, no competitive effects between Ni and Zn are expected or observed. However, competition is observed in the site saturation region. Furthermore, for each pH, in this site saturation region, the sum of the total sites occupied corresponds to the maximum number of sites found from the single adsorbate experiments and modeling. A comparison of the experimental data for these binary systems with the model for single adsorbate systems demonstrates the competitive effect, as the data cannot be represented by the single adsorbate isotherm parameters (Figure 41). On the other hand, assuming Ni and Zn adsorb to the same type of site, competition is well described by the model (Figure 40). Mesuere and Fish (1992) reported that in a binary system comprised of anions such as chromate and oxalate,

Figure 40. Competitive adsorption of Ni and Zn to 0.1 g L^{-1} goethite at 10^{-3} I.S. and 25°C. Solid lines represent predicted competitive Langmuir model. Dotted and dashed lines represent associated model errors (± 2 S.D.).

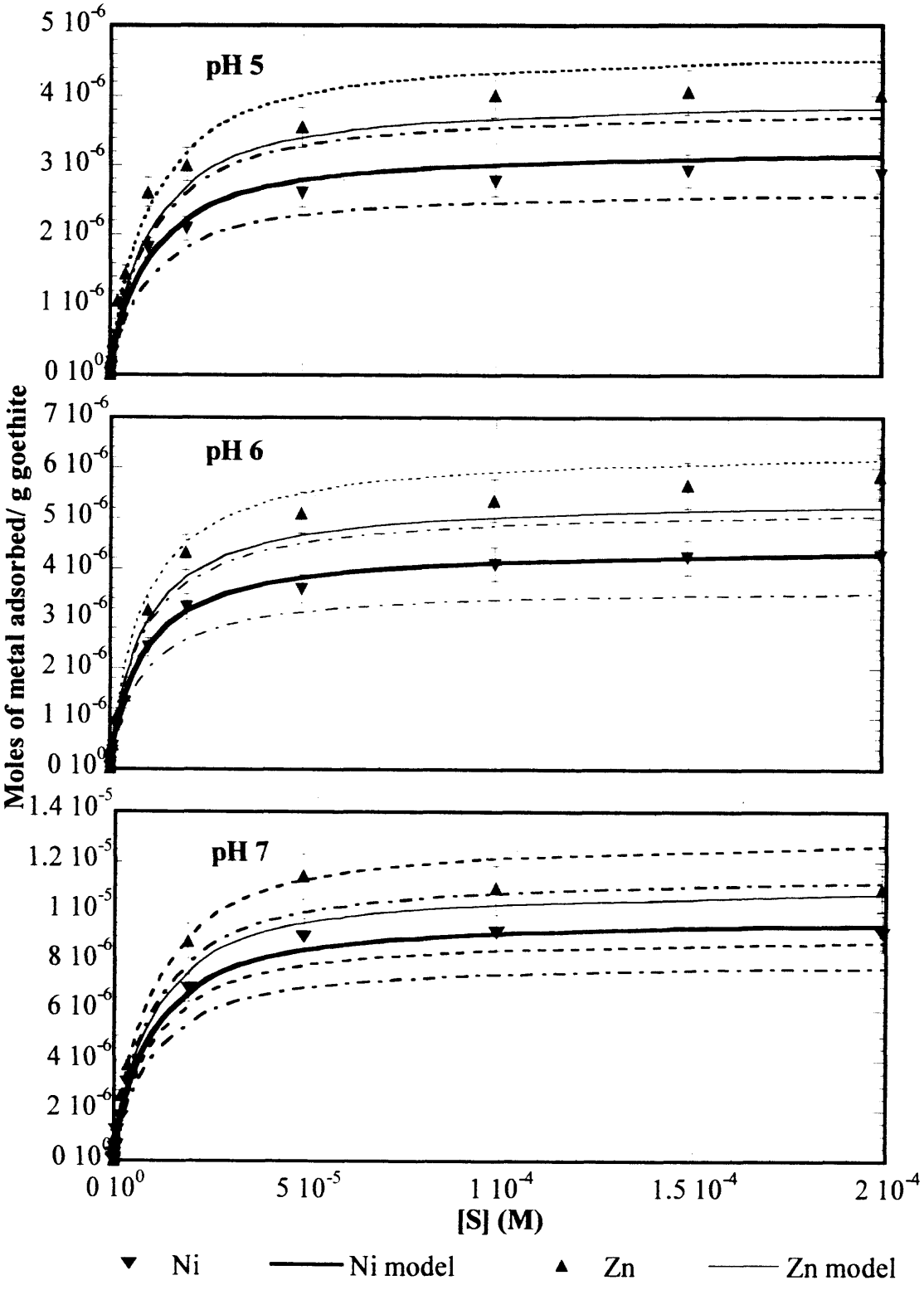

Figure 41. Competitive adsorption of Ni and Zn to 0.1 g L^{-1} goethite at 10^{-3} I.S. and 25°C. Solid lines represent Langmuir isotherms for single adsorbate systems and dotted and dashed lines represent associated model errors.

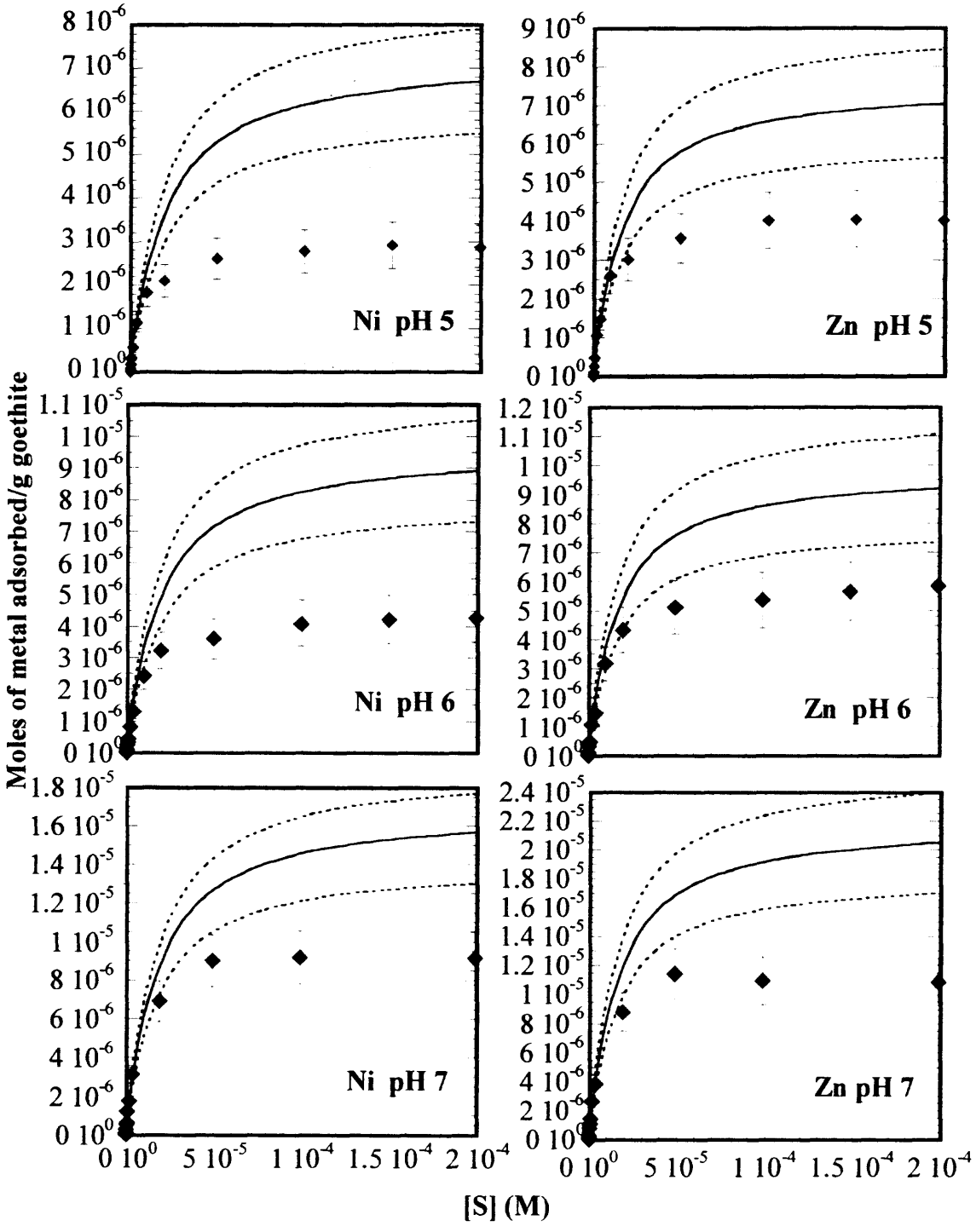

competitive effects were apparent only in the site saturation region. Their modeling results show that surface complexation models such as the diffuse double layer model (DDLM) and Triple Layer Model (TLM) provided very good fits for single-adsorbate systems but eluded the competition systems. Competitive effects were also observed among Cu and Pb adsorption to hematite between pH 4.5 and 6.3 (Christl and Kretzschmar, 1999). In the present work, both Ni and Zn adsorption can be adequately described by a single-site Langmuir model within the errors. These results confirm that Ni and Zn compete for the same type of adsorption site(s) on the goethite surface and hence must form similar adsorption complexes. Christophi and Axe (2000) found that the Cu-Cd and Pb-Cd competition studies with goethite were described very well with a single-site Langmuir model, concluding that these metals bind to the same types of sites. However, in Pb-Cu and Pb-Cu-Cd systems, they found that the single-site Langmuir model failed to describe Cu adsorption to goethite in the presence of Pb. Using an approach where Cu could bind to another set of sites not available to Pb or Cd with the difference in site density between Cu and Pb defining this capacity, Christophi and Axe (2000) were able to model the adsorption competition.

Balistrieri and Murray (1982) did not observe competition when working with metal concentrations of 3.0×10^{-6} M; given the goethite site density, this result is not surprising. Additionally the authors have estimated the site density from potentiometric titrations as 2.2×10^{-4} moles g^{-1} of oxide, which is greater than the site densities observed for transition metals. Palmqvist et al. (1999) studied binary competitive adsorption of Cu, Pb, and Zn to goethite at 25°C within the range $3.5 \leq pH \leq 8.5$ and with only two adsorbate concentrations ($\sim 4 \times 10^{-3}$ M and $\sim 10^{-6}$ M). They used the constant capacitance

model with the assumption that all three metals had the same site density (Palmqvist et al., 1999). However, at elevated concentrations like 10^{-3} M, these metals exceed their saturation in the higher pH region. From their surface complexation modeling (SCM) of Cu and Pb adsorption to hematite in single and binary systems, Christl and Kretzschmar (1999) found that site density was a key parameter in predicting competition. Further, using a 2-pK description of the hematite surface, they optimized the model by fitting site density (5 and 10 sites nm^{-2}) from competition experiments. Benjamin and Leckie (1981a, b) studied Cd adsorption to amorphous iron oxyhydroxide in the presence of Cu, Pb, or Zn and found little to no competition between the metals. They concluded that these metals bind to different types of sites; however amorphous iron oxides have been shown to exhibit large site densities as observed in Chapter 5 and in other work (Axe and Anderson, 1995).

Competition studies of Ca and Ni adsorption to goethite were conducted at 25°C and pH 5, 6, and 7 for three Ni:Ca molar ratios – 1:1, 1:10, and 1:100. Resulting Ni isotherms (Figure 42) show that for all molar ratios, competition between Ca and Ni was negligible. These experimental data follow the single system isotherm model for Ni given the errors. To test the hypothesis that Ca sorbs to another set of sites, a two site model was employed where Ca not only adsorbed to the sites based on Ni and Zn studies, but also to a set of lower affinity ones (with a much greater capacity) as defined in the following expression:

$$C_{Ca} = \frac{K_{Ca} C_{t,\,trans}[Ca]}{1 + K_{trans}[trans] + K_{Ca}[Ca]} + \frac{K_{Ca}(C_{t,\,Ca} - C_{t,\,trans})[Ca]}{1 + K_{trans}[trans] + K_{Ca}[Ca]} \qquad (18)$$

where $C_{t,Ca}$ and $C_{t,trans}$ are the site densities of calcium and the competing transition metal in moles g^{-1} goethite; K_{Ca} and K_{trans} are the respective equilibrium constants; and [Ca] and

Figure 42. Isotherms of Ni adsorption to 0.1 g L^{-1} goethite at 25°C in the presence of Ca. Solid lines are single-site Langmuir model for Ni and dashed lines are the associated errors (± 2 S.D.).

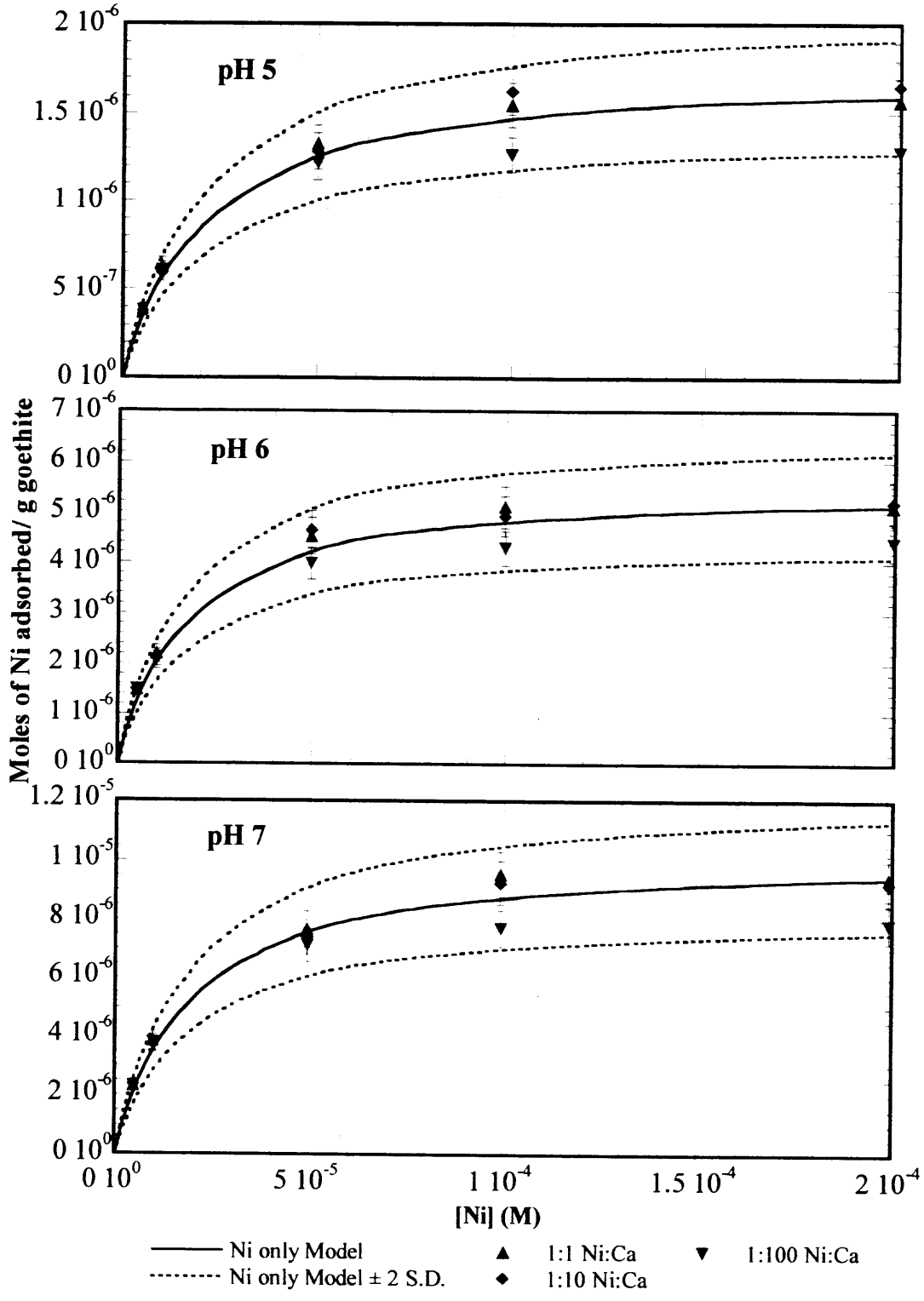

[trans] are their aqueous phase concentrations in moles L^{-1} at equilibrium. The results suggest that in Ni-Ca systems, only Ni ions adsorbs to the high affinity sites as sorption did not decrease, which would have been expected with 100× [Ca] additions. Therefore, Ca ions adsorb to only the lower affinity sites (Figure 43), which is modeled with the site densities found from the Ca isotherm studies.

Competition studies between Zn and Ca were also conducted in a similar fashion and are presented in Figures 44 and 45. These studies further demonstrate the lack of competition between Zn and Ca. Ankomah (1992) observed that for pH < 7, Zn adsorption to goethite decreased in the presence of Mg; however, at pH values greater than 7 Mg had no effect on Zn adsorption. Davis and Upadhyaya (1996) noted that Cd adsorption to goethite was not affected by the presence of Ca. Borah et al. (1989) found that Zn adsorption to kaolinite and goethite dominated soils was best described by the Langmuir isotherm. They also found that in Ca-saturated soils, the Langmuir model based on single adsorbate data accurately described Zn adsorption. Cowan et al. (1991) investigated Cd adsorption to amorphous iron oxide in the presence of alkaline earth metal ions (Ba^{2+}, Ca^{2+}, Mg^{2+}, and Sr^{2+}). The Cd concentration was approximately 10^{-6} M, while the alkaline earth metal concentrations were in the order of 10^{-3} M. They noted that Cd adsorption decreased only slightly in the presence of Ca. From their modeling, Cowan et al. found that both the TLM and the non-electrostatic model adequately represented the Ca-Cd competition at higher ionic strengths but not at lower ones.

In contrast, Balistrieri and Murray (1982) studied the influence of Mg^{2+} and SO_4^{2-} on the adsorption of Cd, Pb, Cu, and Ni to goethite. Sulfate adsorption was found to change the electrostatic conditions at the interface and enhance the metal adsorption.

Figure 43. Isotherms of Ca adsorption to 0.1 g L^{-1} goethite at 25°C and 10^{-3} I.S in the presence of Ni ion. The single-site Langmuir model (solid lines ± 2 S.D.) is based on C_t available to Ca only.

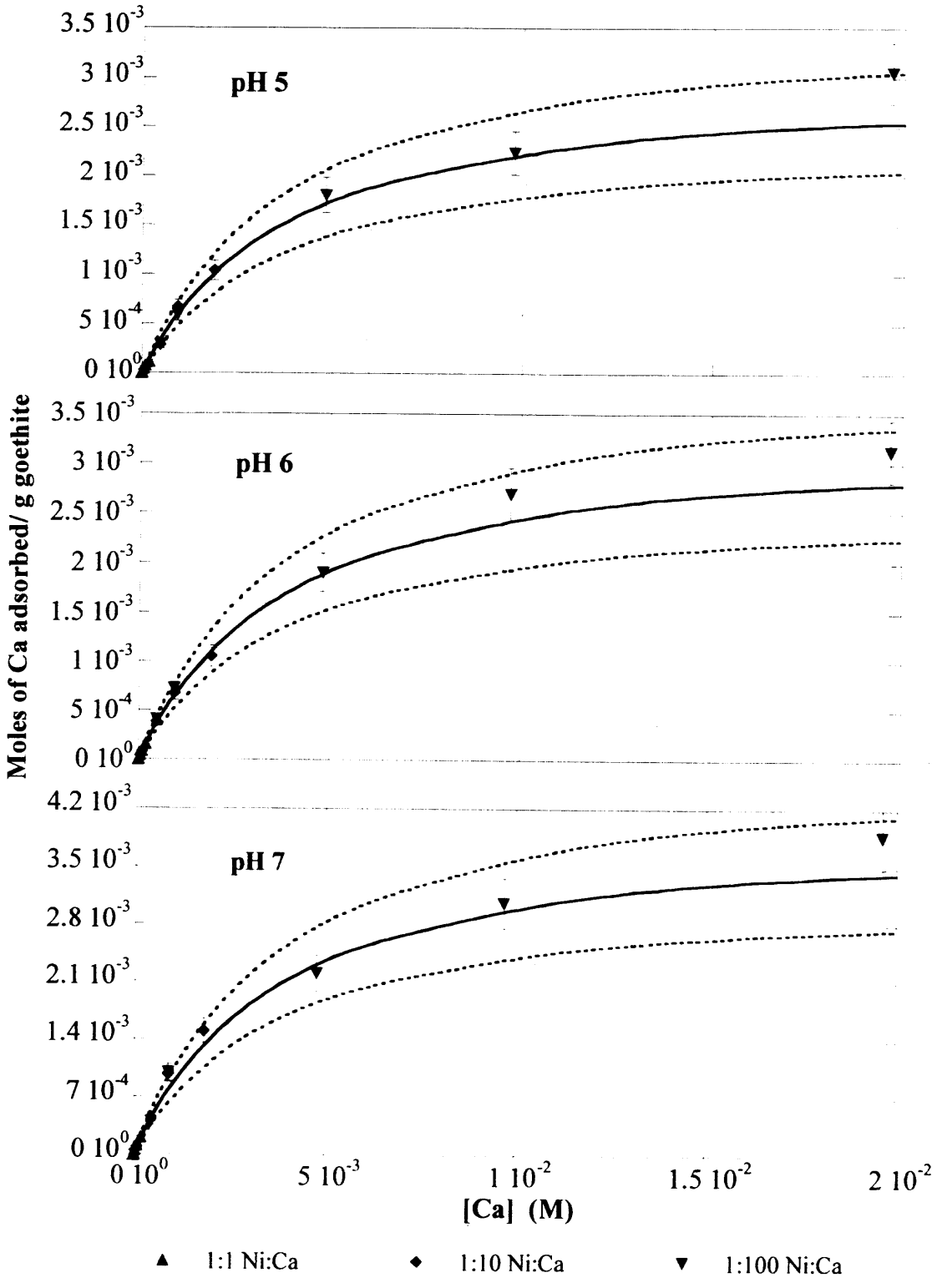

Figure 44. Isotherms of Zn adsorption to 0.1 g L^{-1} goethite at 25°C and 10^{-3} I.S. in the presence of Ca. Solid lines are single-site Langmuir model for Zn and dashed lines are the associated errors (± 2 S.D.).

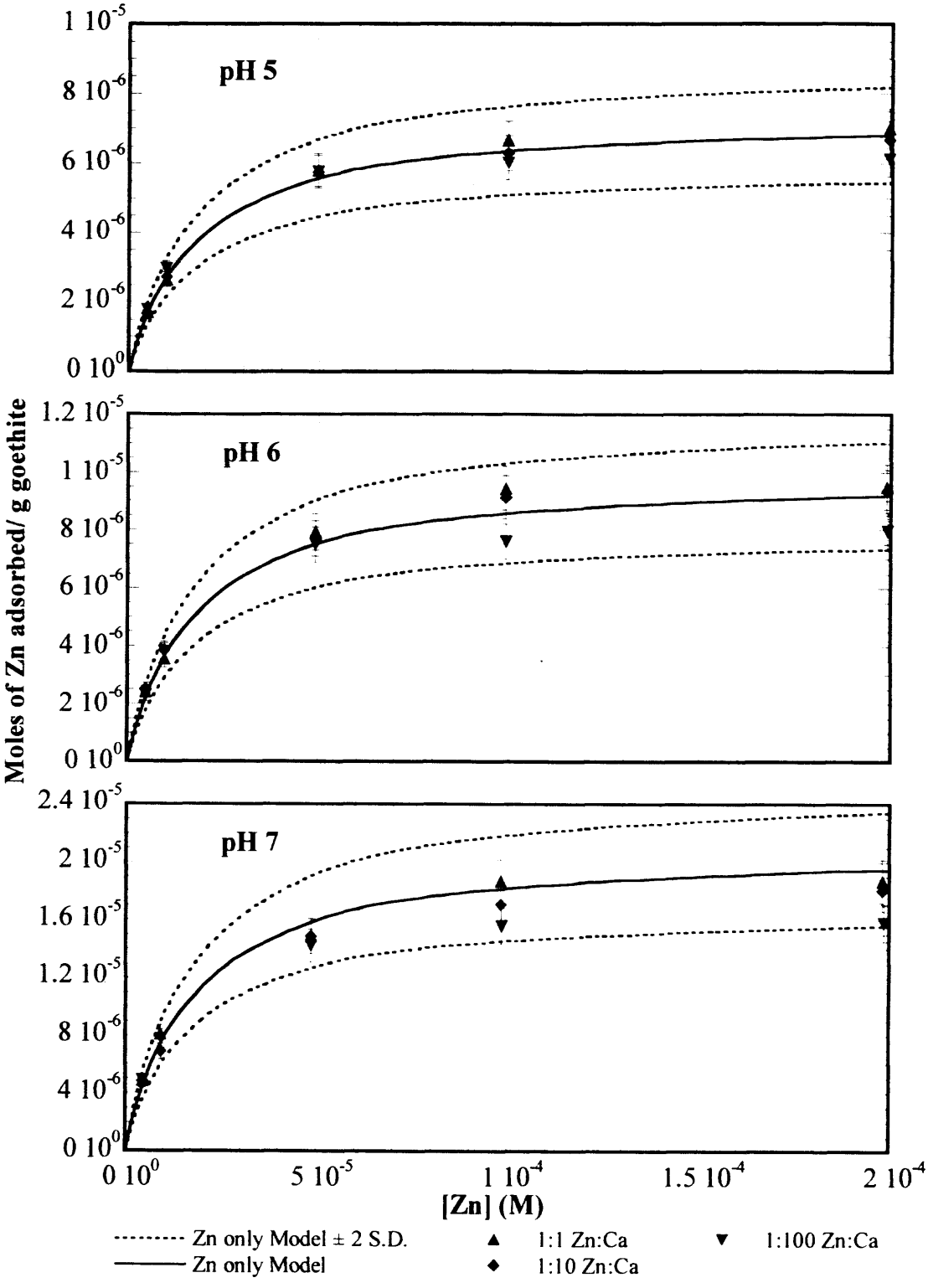

Figure 45. Isotherms of Ca adsorption to 0.1 g L^{-1} goethite at 25°C and 10^{-3} I.S. in the presence of Zn ion. The single-site Langmuir model (solid lines ± 2 S.D.) is based on C_t available to Ca only.

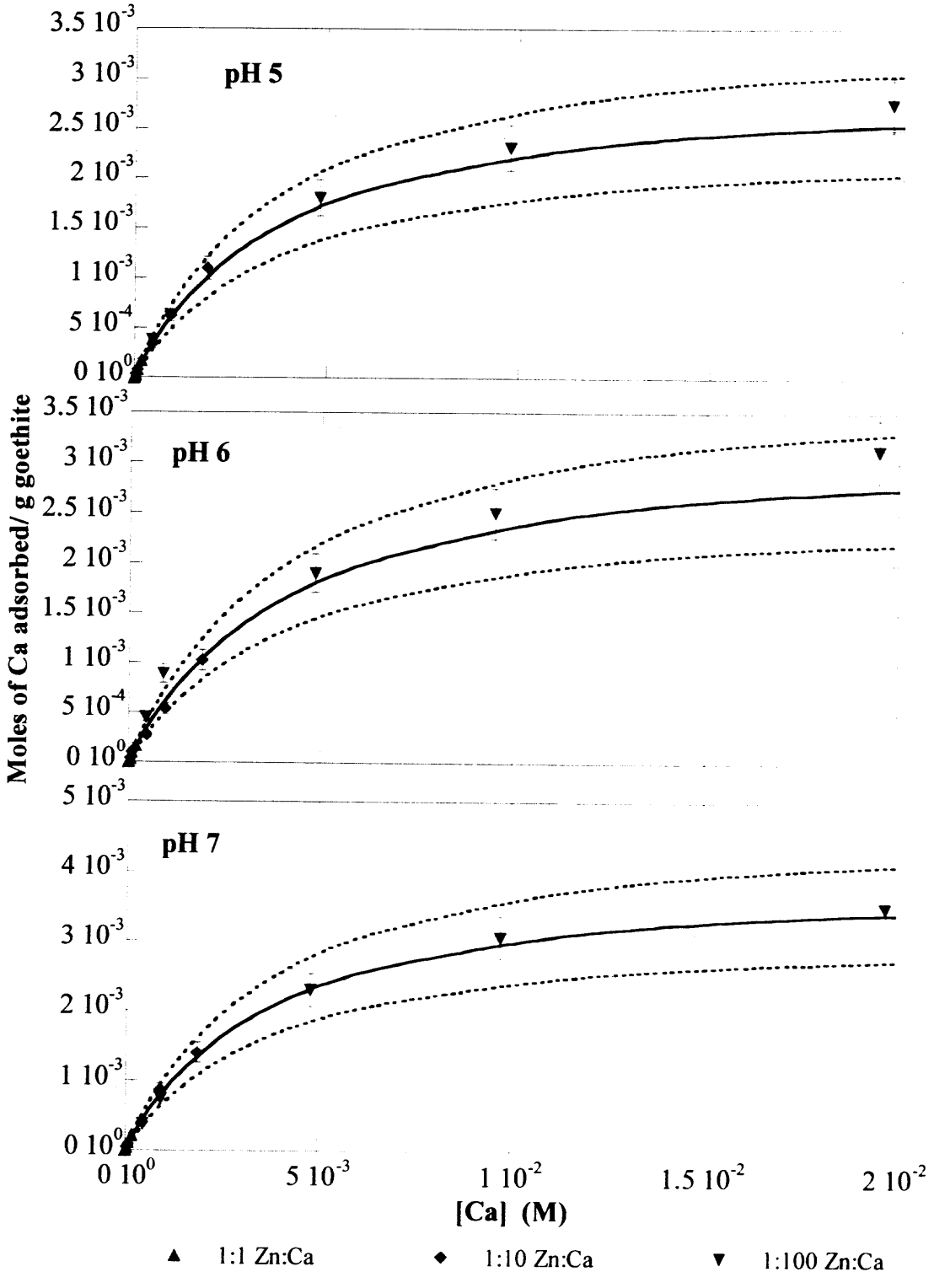

On the other hand, in the presence of 0.054 M Mg ions, adsorption of the heavy metals was suppressed. However, the investigators used adsorption edges and therefore did not evaluate site density as a function of pH. Ankomah (1992) found that Zn adsorption to goethite between pH 5.4 and 8.5 decreased in the presence of Mg by as much as 31% in terms of surface coverage. One reason for the differing results (from those reported here) may be due to the goethite used in the studies.

6.4 Summary of Goethite Studies

Adsorption of Ni, Zn, and Ca to goethite involves strong chemical forces. The adsorption affinity of these metals followed the order: Zn > Ni > Ca, where the transition metals bind to one type of site – a high affinity one. As such, these metals compete for adsorption sites on the goethite surface, which can be modeled and predicted by single-site Langmuir model. On the other hand, alkaline earth metals bind to a lower affinity site and therefore in binary systems they do not compete with the transition metals. Iron oxide minerals are prevalent in the subsurface as discrete particles and coatings. Although both amorphous and crystalline oxides exhibit microporosity, the relative contribution in goethite is not significant as potentially predicted from characterization studies on the freeze-dried particles. Also, because of the smaller particle size distribution, less time is required for the metal ions to adsorb and diffuse in a micropore system. Modeling of macroscopic experiments provides information on bulk equilibrium and kinetic processes, however, to determine the molecular mechanisms, XAS is needed. In the next chapter, results of XAS studies have been discussed to elucidate the sorption mechanisms of some of the systems studied in this chapter as well as in Chapter 5.

CHAPTER 7

XAS STUDIES

Macroscopic experiments provide information on bulk equilibrium and kinetic processes, however, to determine the molecular mechanisms, XAS is needed. XAS has proven to be a powerful tool in environmental research as it selectively probes the local coordination environment of a species over a wide range of concentrations. This structural information, including the identification of neighbors, their coordination numbers, and bond distances, provides contaminant sorption mechanisms under environmentally relevant conditions.

To complement the macroscopic studies, presented in Chapters 5 and 6, sorption to metal oxides were systematically studied using XAS analysis as a function of pH, adsorbate loading, method of contact (adsorption versus coprecipitation), and reaction time. One of the primary objectives was to identify and compare Zn sorption mechanisms to HFO and goethite. This objective aides in distinguishing different types of adsorption complexes such as inner- and outer-sphere ones, which are crucial in understanding contaminant mobility and bioavailability in subsurface systems. Another important objective was to discern sorption mechanisms of Ni and Zn with HMO. This objective supports the hypothesis that metals of a periodic group exhibit similar adsorption behavior with amorphous oxides. Additionally, XAS studies assist in demonstrating the slow sorption process of intraparticle diffusion.

7.1 Zinc Standards

The XAS spectra of zinc standards in Figure 46 show that for each standard the χ-amplitude decreased with increase in temperature as a result of the increase in contributions from thermal vibrations. Unlike other zinc standards, the spectra of aqueous zinc nitrate show only first shell contributions as would be expected. Figure 46 also includes chalcophanite, which was generated theoretically using FEFF7. Resultant Fourier transforms along with the fits for these standards are presented in Figure 47 and in Table 12 where their structural parameters generated from the fits are compared with those of their known structure (shown in parentheses). For aqueous zinc nitrate the first shell consists of 5.83 ± 0.4 O atoms at an average radial distance of 2.18 ± 0.04 Å; these parameters are indicative of the octahedral coordination of Zn by O in the aqueous solution. Recently, Trainor et al. (2000) reported 6.1 O atoms at 2.07 Å around Zn from XAFS studies with a 10 mM $Zn(NO_3)_2$ at pH 3.6; Numako and Nakai (1999) estimated the Zn-O distance in 0.1 M $Zn(NO_3)_2$ to be approximately 2.09 Å when they fixed the number of O atoms to 6. From XAFS studies with an aqueous ZnEDTA solution at pH 3, Schlegel et al. (1997) found two sets of O atoms contributing towards the first shell: 3.5 atoms at 2.01 Å and 3.2 atoms at 2.19 Å.

For ZnO and for $ZnO{\cdot}nH_2O$, the first shell was consistent with a tetragonal structure comprising of 3.3-4 O atoms (R = 1.96 Å) with a second shell of 11.7-14.3 Zn atoms (R = 3.21-3.22 Å), consistent with Trainor et al. (2000). Pandya et al. (1995) investigated the local structure of Zn^{2+} in concentrated aqueous hydroxide solutions.

Figure 46. Background subtracted, normalized, and averaged k^3-weighted XAS spectra of Zn standards studied at Zn K-edge in transmission mode as a function of temperature. $ZnMn_3O_7$ structure is generated from crystallographic data using FEFF7 [(Post and Appleman, 1988).

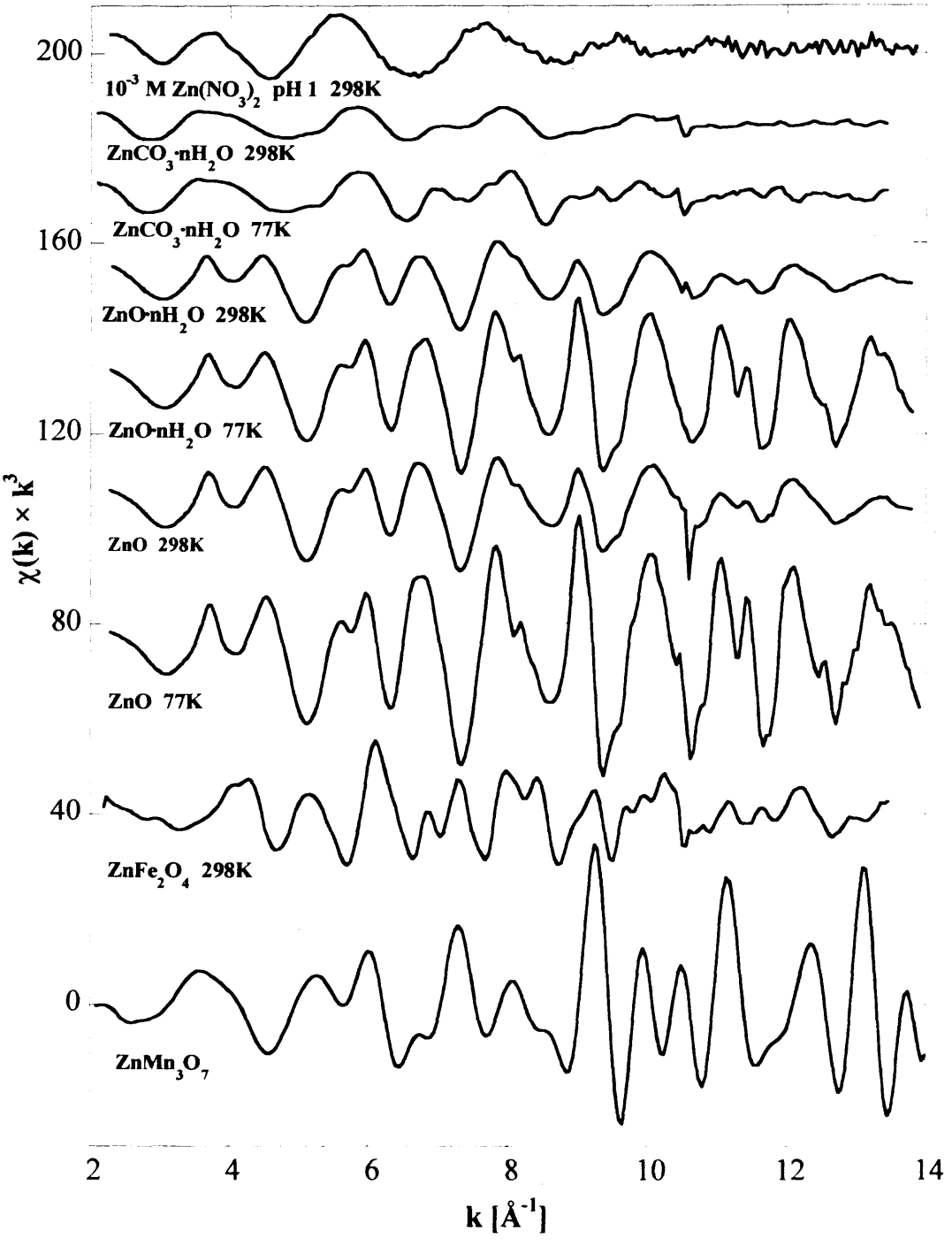

Figure 47. Fourier transforms (solid lines) of Zn standards studied at (a) 298 K and (b) 77 K, filtered over 2.65-13.65 $Å^{-1}$ (except $Zn(NO_3)_{2,aq}$ 2.3-9.2 $Å^{-1}$) and fitted (dashed lines) with $ZnMn_3O_7$ over 1.0-3.65 Å (except $ZnCO_3.nH_2O$ with hydrozincite over 0.6-3.8 Å and $Zn(NO_3)_{2,aq}$ with $ZnMn_3O_7$ over 0.5-2.20 Å).

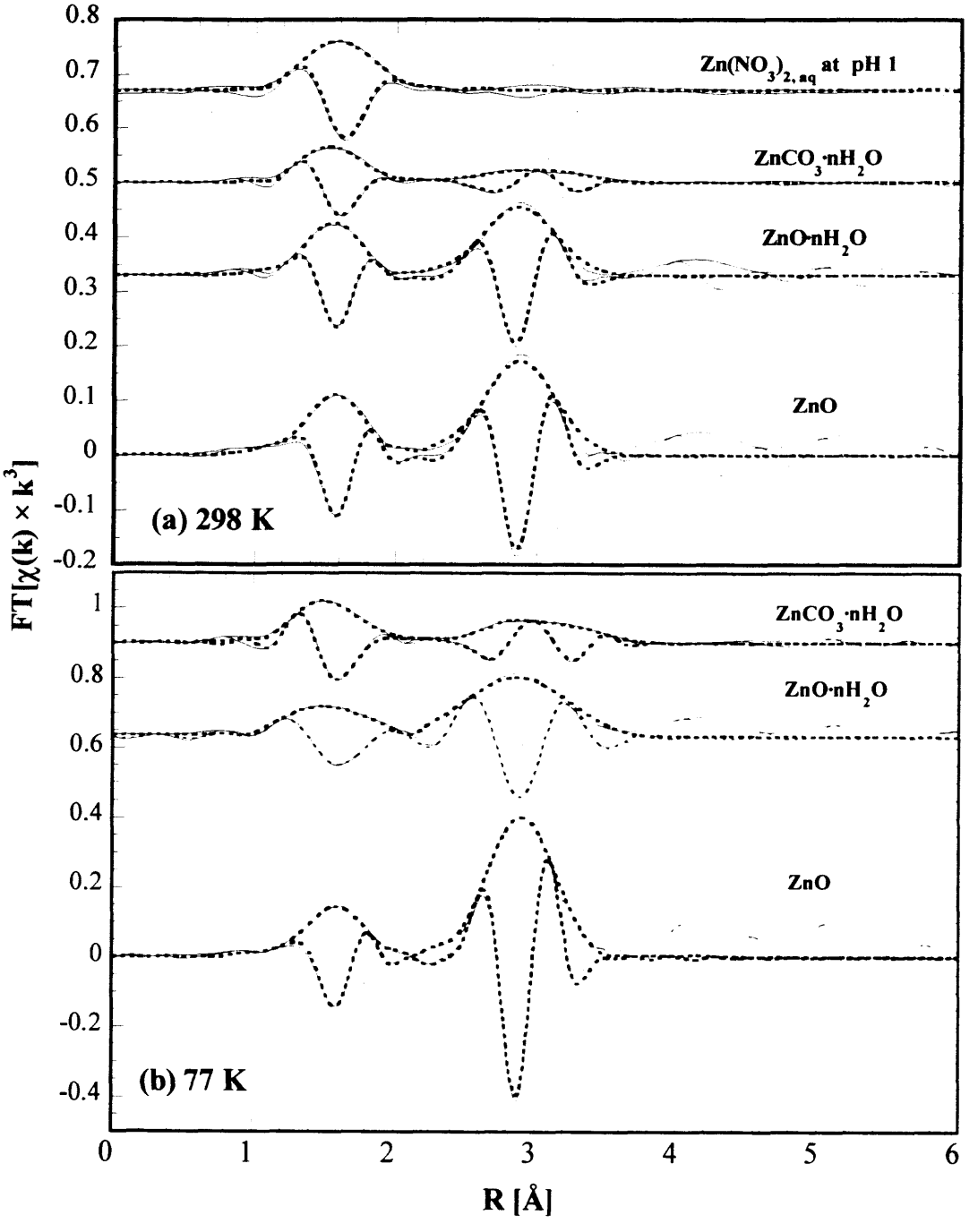

Table 12. Structural Parameters of Ni and Zn Standards

Standards	Element	N (atoms)	R (Å)	σ^2 (Å^2)	C3 (Å^3)	E_o shift (eV)
First Shell						
$Zn(NO_3)_{2,aq}$ 298 K	O	5.88 ± 0.69	$2.16 \pm 4.6 \times 10^{-2}$	$1.9 \times 10^{-3} \pm 7.2 \times 10^{-4}$	$5.00 \times 10^{-3} \pm 1.7 \times 10^{-5}$	3.62 ± 1.10
ZnO 77 K*	O	3.58 ± 0.30 (*4*)	$1.96 \pm 1.0 \times 10^{-3}$ (*1.97*)	$2.06 \times 10^{-3} \pm 2.0 \times 10^{-4}$	----------	1.23 ± 0.18
ZnO 298 K	O	3.27 ± 0.01	$1.96 \pm 6.4 \times 10^{-4}$	$2.63 \times 10^{-3} \pm 5.9 \times 10^{-5}$	----------	0.97 ± 0.06
$ZnO.nH_2O$ 77 K	O	3.51 ± 0.22	$1.98 \pm 6.8 \times 10^{-3}$	$3.57 \times 10^{-3} \pm 2.6 \times 10^{-4}$	----------	2.06 ± 0.31
$ZnO.nH_2O$ 298 K	O	4.06 ± 0.01	$2.00 \pm 2.6 \times 10^{-3}$	$4.09 \times 10^{-3} \pm 8.5 \times 10^{-5}$	$4.30 \times 10^{-4} \pm 4.7 \times 10^{-5}$	1.88 ± 0.13
$ZnCO_3.nH_2O$ 77 K	O	5.6 ± 0.35 (*6*)	$2.21 \pm 6.7 \times 10^{-2}$ (*2.11*)	$4.44 \times 10^{-3} \pm 4.2 \times 10^{-4}$	$3.87 \times 10^{-4} \pm 1.1 \times 10^{-5}$	4.93 ± 0.10
$ZnCO_3.xH_2O$ 298 K	O	5.19 ± 0.66	$2.12 \pm 6.2 \times 10^{-2}$	$6.64 \times 10^{-3} \pm 3.0 \times 10^{-4}$	$1.04 \times 10^{-3} \pm 8.0 \times 10^{-5}$	3.76 ± 0.35
$Ni(NO_3)_{2,aq}$ 298 K	O	6.08 ± 0.20	$2.07 \pm 2.0 \times 10^{-3}$	$4.88 \times 10^{-3} \pm 4.3 \times 10^{-4}$	$-6.46 \times 10^{-4} \pm 7.5 \times 10^{-4}$	3.40 ± 1.70
NiO 298 K	O	6.07 ± 0.32 (*6*)	$2.06 \pm 2.0 \times 10^{-3}$ (*2.08*)	$4.20 \times 10^{-3} \pm 2.8 \times 10^{-4}$	----------	3.11 ± 0.42
$NiCO_3.nH_2O$ 298 K	O	6.74 ± 0.48	$2.04 \pm 1.0 \times 10^{-3}$	$9.12 \times 10^{-3} \pm 3.9 \times 10^{-4}$	$-1.70 \times 10^{-3} \pm 7.1 \times 10^{-5}$	6.87 ± 1.72
Second Shell						% Res.
ZnO 77 K*	Zn	12.75 ± 1.48 (*12*)	$3.22 \pm 8.5 \times 10^{-4}$ (*3.21*)	$4.45 \times 10^{-3} \pm 1.4 \times 10^{-4}$	----------	7.16
ZnO 298 K	Zn	11.69 ± 0.14	$3.21 \pm 5.6 \times 10^{-4}$	$9.47 \times 10^{-3} \pm 1.0 \times 10^{-4}$	----------	10.25
$ZnO.nH_2O$ 77 K	Zn	14.27 ± 0.17	$3.22 \pm 2.9 \times 10^{-3}$	$7.64 \times 10^{-3} \pm 2.8 \times 10^{-4}$	----------	7.21
$ZnO.nH_2O$ 298 K	Zn	10.54 ± 0.09	$3.24 \pm 1.9 \times 10^{-3}$	$1.10 \times 10^{-2} \pm 7.5 \times 10^{-5}$	$2.75 \times 10^{-4} \pm 1.2 \times 10^{-5}$	8.35
$ZnCO_3.nH_2O$ 77 K	Zn	4.00 (*4*)	$3.14 \pm 7.9 \times 10^{-2}$ (*3.18*)	$1.05 \times 10^{-2} \pm 2.0 \times 10^{-3}$	$-1.73 \times 10^{-4} \pm 6.7 \times 10^{-5}$	11.01
	O	2.00 (*2*)	3.24 (*3.24*)	$3.04 \times 10^{-2} \pm 7.8 \times 10^{-4}$	0.00	
$ZnCO_3.nH_2O$ 298 K	Zn	4.00	$3.09 \pm 5.2 \times 10^{-2}$	$1.79 \times 10^{-2} \pm 5.9 \times 10^{-4}$	$-2.17 \times 10^{-4} \pm 4.9 \times 10^{-5}$	12.08
	O	2.00	3.24	$4.02 \times 10^{-2} \pm 1.4 \times 10^{-3}$	0.00	
NiO 298 K	Ni	11.31 ± 0.31 (*12*)	$2.93 \pm 1.0 \times 10^{-3}$ (*2.94*)	$4.22 \times 10^{-3} \pm 3.3 \times 10^{-4}$	----------	5.02
$NiCO_3.nH_2O$ 298 K	Ni	5.47 ± 0.0.15	$3.54 \pm 1.0 \times 10^{-3}$	$6.74 \times 10^{-3} \pm 9.9 \times 10^{-4}$	$6.33 \times 10^{-4} \pm 8.1 \times 10^{-5}$	7.63

Numbers in parentheses correspond to parameters determined from XRD. † Zn samples filtered over 2.64-13.65 Å^{-1} and fitted over 1.0-3.65 Å, except for aq. $Zn(NO_3)_2$ -- 2.3 - 9.2 Å^{-1} and fitted over 0.5-2.2 Å. ‡ Ni standards filtered over 2.40-9.2 Å^{-1}, except for NiO -- 2.40 – 13.33 Å^{-1}. NiO fitted over 0.41-3.20 Å, $NiCO_3$ fitted over 0.4-3.70 Å, and aq. $Ni(NO_3)_2$ fitted over 0.4-2.20Å.

Using single and multiple scattering, they determined that the Zn ions are in a tetrahedral configuration with a Zn-O bond distance of 1.96 Å, however, no satisfactory fits were obtained for the second shell. In the present research, the XAS spectra of $ZnCO_3 \cdot nH_2O$ were fitted with hydrozincite, where the second shell coordination numbers were fixed. The resultant first shell includes 5.2 to 5.6 O atoms at 2.12 Å, while the second shell showed good fits for four zinc atoms at 3.14 Å and two O atoms at 3.24 Å. No stable fits were obtained when carbon was included in the second shell; this may be due to the smaller single scattering contributions from carbon as compared to zinc and oxygen. Hesterberg et al. (1997) reported the first shell for $ZnCO_3$ (fitted with zincite) to consist of 6.2 O at 2.09 Å, while that of zinc carbonate hydroxide (also fitted with zincite) was comprised of 6.2 O atoms at 2.01 Å. For $ZnO \cdot nH_2O$ at 298 K and $ZnCO_3 \cdot nH_2O$ at all temperatures, stable fits were obtained only when the third cumulant (C_3) was included, which is indicative of moderate disorder in their structures. For all other standards, the fits were well described by a Gaussian distribution. Temperature studies revealed a decrease in the Debye-Waller factor (σ^2) with a decrease in temperature.

7.2 Zn-HFO Adsorption Samples

The XAS spectra for Zn-HFO adsorption systems studied as a function of pH, adsorbate loading, and scanning temperature appear to be similar to each other (Figure 48) as well as to that of the aqueous Zn^{2+}. These spectra exhibit a glitch at 10.2 $Å^{-1}$, which is due to the presence of a fracture in the Si(111) crystal at the X-11A beamline. The data are noisier in the higher k range due to the highly disordered structure from HFO. Except for

Figure 48. Background subtracted, normalized, and averaged k^3-weighted XAS spectra of Zn sorbed to 1 g L^{-1} HFO studied at Zn K-edge in fluorescence mode as a function of pH, adsorbate loading, and temperature compared with that of aq. $Zn(NO_3)_2$ collected in transmission mode.

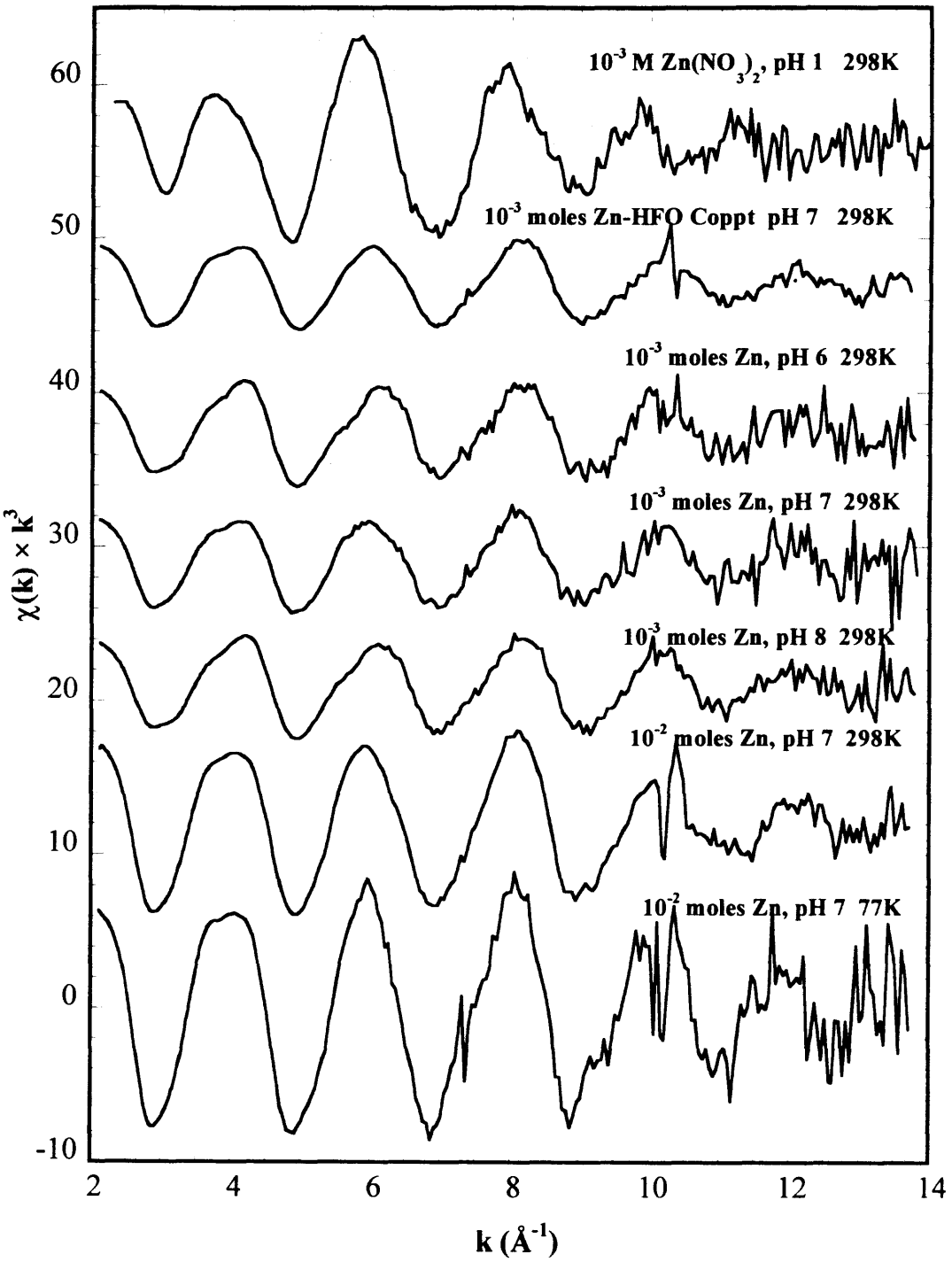

their magnitudes, these spectra resemble each other as a function of loading suggesting a similar adsorption reaction. Furthermore, adsorption does not appear to be a function of pH. Because these spectra are similar to aqueous Zn^{2+} spectra, it appears the only backscattering contribution is from the first shell of oxygen atoms. Fourier transforms of these spectra filtered over the k-range 2.3-9.2 $Å^{-1}$ show only one broad shell for all samples irrespective of adsorbate concentration, method of contact (Figure 48), and pH (Figure 49). Fitting this shell between 0.5 and 2.2 Å suggests the presence of 5.9-6.2 highly disordered oxygen atoms at an average radial distance of 2.18 Å. This distance is much shorter than those found for Sr, an alkaline earth metal, which was also found to be physically sorbed to HFO (Axe et al., 1998); this result explains the higher affinity of transition metals to HFO in comparison with that of alkaline earth metals (Axe and Anderson, 1997; see Chapter 5). Absence of a second shell rules out the formation of any well-ordered zinc precipitates or a Zn-Fe solid solution. The results demonstrate the adsorption mechanism is best represented as an outer-sphere complex. Temperature dependence (Table 13 and Figure 48) also confirms the physical type of adsorption due to a significant contribution by the thermal component of the Debye-Waller factor. Additionally, because these structural parameters (Table 13) did not vary with the adsorbate loading or pH, an earlier hypothesis that Zn sorbs to HFO through one average type of site is corroborated here as well as in the isotherm studies. The Zn-HFO coprecipitate was also found to exhibit a local structure consistent with the adsorption samples suggesting that Zn is only physically sorbed on the microporous surface of amorphous HFO. Interestingly, through macroscopic studies, Crawford et al. (1993) demonstrated that although the coprecipitation of metal ions like Zn and Ni with

Figure 49. Fourier transforms (solid lines) of Zn K-edge XAS spectra of Zn sorbed to 1 g L^{-1} HFO at pH 7, presented as a function of zinc concentration, method of contact, and temperature, each filtered over k-range 2.3-9.2 $Å^{-1}$ and fitted with chalcophanite (dashed lines) from 0.5 to 2.20 Å.

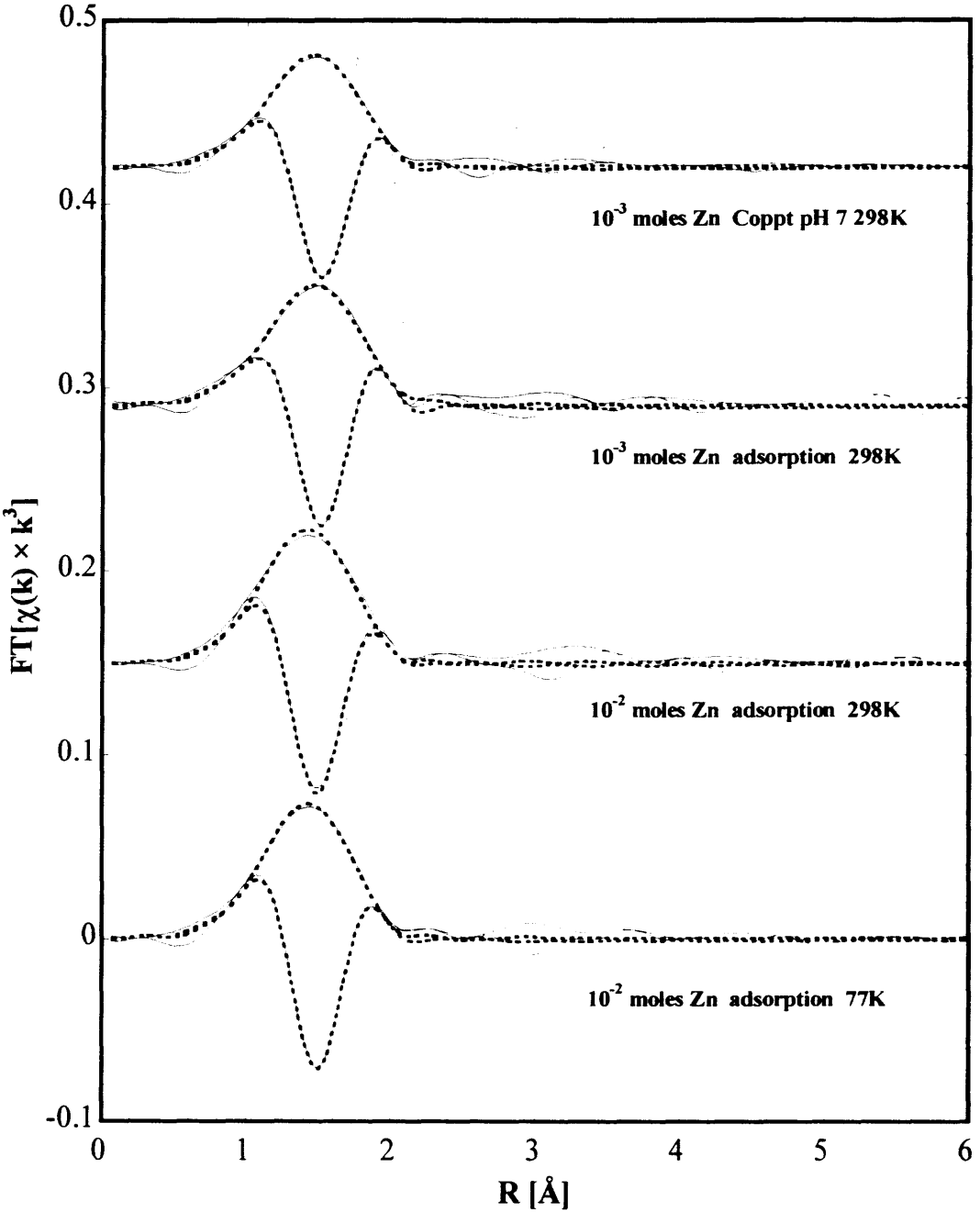

Figure 50. Fourier transforms (solid lines) of Zn K-edge XAS spectra of 10^{-3} moles of Zn sorbed to HFO (1 g L^{-1}) at 25°C, presented as a function of pH, each filtered over k-range 2.3-9.2 $Å^{-1}$ and fitted with chalcophanite (dashed lines) from 0.5 to 2.20.

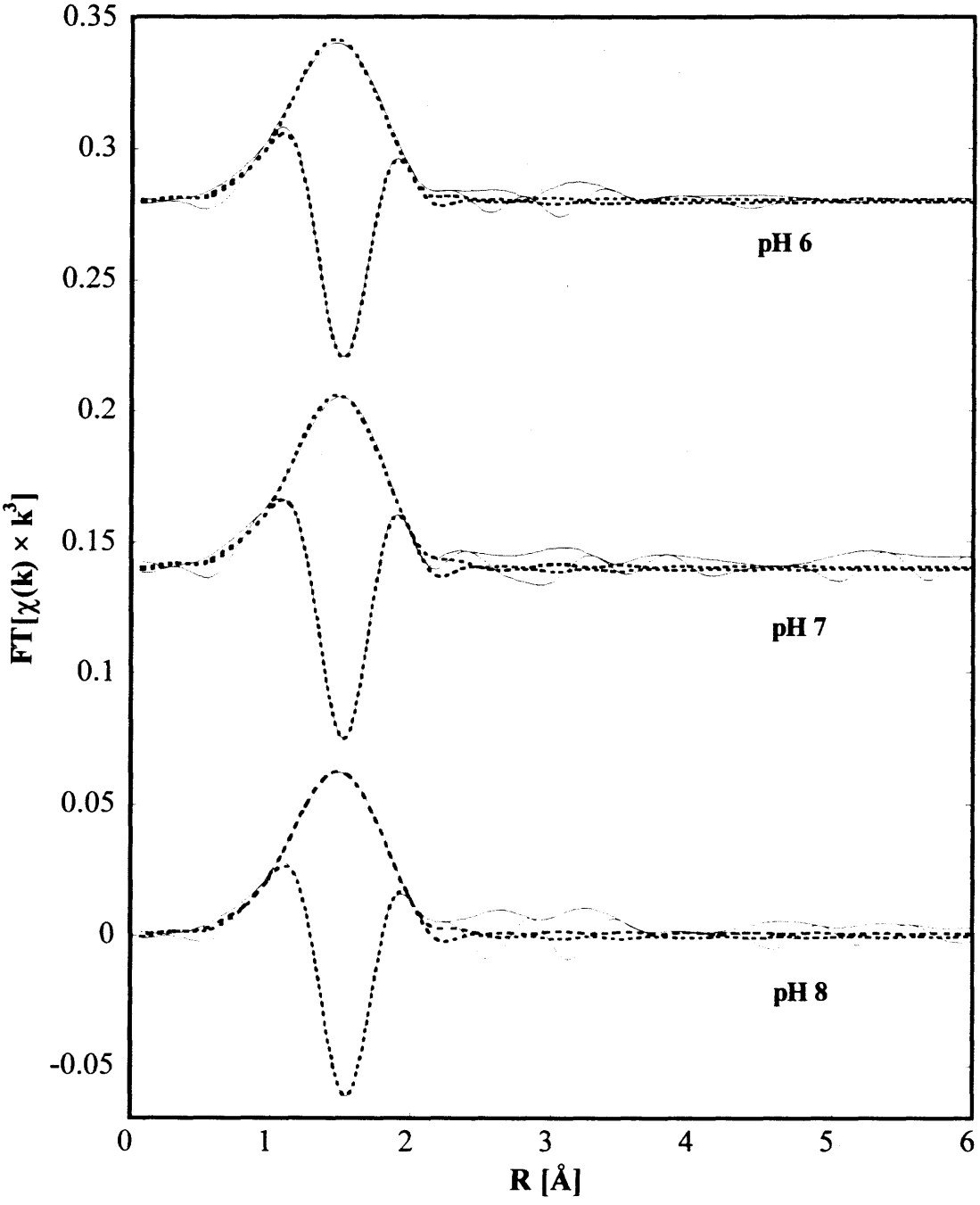

Table 13. XAS Parameters of Zn-HFO and Zn-Goethite Adsorption Samples Filtered from 2.3 to 9.2 $Å^{-1}$**.

Zn loadings (moles g^{-1})	Adsorbent	T (K)	N (atoms)	R (Å)	σ^2 ($Å^2$)	C3 ($Å^3$)	Eo shift (eV)	% Res
First shell: Oxygen								
10^{-2} pH 7	HFO	77	6.19 ± 0.28	2.18 ± 2.3 × 10^{-3}	8.83 × 10^{-3} ± 6.6 × 10^{-4}	-1.00 × 10^{-4} ± 3.4 × 10^{-4}	2.56 ± 0.86	4.09
10^{-2} pH 7	HFO	298	5.92 ± 0.24	2.19 ± 4.8 × 10^{-3}	9.11 × 10^{-3} ± 6.5 × 10^{-4}	-9.40 × 10^{-4} ± 4.0 × 10^{-4}	5.37 ± 1.69	5.21
10^{-3} pH 8	HFO	298	6.08 ± 0.26	2.18 ± 3.2 × 10^{-3}	8.10 × 10^{-3} ± 9.3 × 10^{-4}	-8.70 × 10^{-4} ± 2.9 × 10^{-4}	3.56 ± 0.31	5.51
10^{-3} pH 7	HFO	298	6.103 ± 0.53	2.18 ± 3.7 × 10^{-3}	9.99 × 10^{-3} ± 2.06 × 10^{-3}	-9.98 × 10^{-4} ± 3.3 × 10^{-4}	3.32 ± 0.98	4.63
10^{-3} pH 6	HFO	298	6.11 ± 0.51	2.18 ± 2.3 × 10^{-3}	9.66 × 10^{-3} ± 4.1 × 10^{-4}	-1.52 × 10^{-4} ± 1.9 × 10^{-4}	3.55 ± 0.97	7.52
*10^{-3} pH 7	HFO	298	6.21 ± 0.35	2.18 ± 4.2 × 10^{-3}	9.55 × 10^{-3} ± 7.6 × 10^{-4}	-4.99 × 10^{-4} ± 2.2 × 10^{-4}	3.50 ± 1.09	5.16
1.2 × 10^{-5} pH 6	Goethite	77	3.95 ± 0.53	1.97 ± 2.8 × 10^{-3}	9.39 × 10^{-3} ± 8.5 × 10^{-4}	-5.65 × 10^{-4} ± 1.1 × 10^{-4}	9.37 ± 0.70	8.78
2.0 × 10^{-5} pH 7	Goethite	77	3.94 ± 0.43	1.97 ± 2.1 × 10^{-3}	9.91 × 10^{-3} ± 3.6 × 10^{-4}	-2.54 × 10^{-4} ± 3.8 × 10^{-5}	9.10 ± 0.58	8.19
1.2 × 10^{-5} pH 6	Goethite	298	4.04 ± 0.36	1.97 ± 4.0 × 10^{-3}	9.50 × 10^{-3} ± 1.3 × 10^{-3}	-3.26 × 10^{-4} ± 4.5 × 10^{-4}	1.90 ± 0.90	9.86
2.0 × 10^{-5} pH 7	Goethite	298	4.09 ± 0.37	1.97 ± 5.1 × 10^{-3}	1.06 × 10^{-2} ± 9.9 × 10^{-4}	-6.60 × 10^{-5} ± 3.8 × 10^{-5}	2.16 ± 0.69	6.72
*Second shell**: Iron*								
1.2 × 10^{-5} pH 6	Goethite	77	2.84 ± 0.55	3.54 ± 3.1 × 10^{-3}	1.35 × 10^{-2} ± 1.5 × 10^{-4}	-3.35 × 10^{-4} ± 2.1 × 10^{-4}	9.37 ± 0.70	8.78
2.0 × 10^{-5} pH 7	Goethite	77	2.89 ± 0.14	3.54 ± 2.4 × 10^{-3}	1.01 × 10^{-2} ± 3.1 × 10^{-4}	-3.89 × 10^{-5} ± 2.6 × 10^{-5}	9.10 ± 0.58	8.19
1.2 × 10^{-5} pH 6	Goethite	298	1.74 ± 0.32	3.52 ± 4.8 × 10^{-3}	1.43 × 10^{-2} ± 2.6 × 10^{-3}	-4.81 × 10^{-4} ± 3.9 × 10^{-4}	1.90 ± 0.90	9.86
2.0 × 10^{-5} pH 7	Goethite	298	2.49 ± 0.29	3.51 ± 1.9 × 10^{-2}	1.08 × 10^{-2} ± 2.5 × 10^{-3}	-5.94 × 10^{-5} ± 3.6 × 10^{-5}	2.16 ± 0.69	6.72

Errors provided with the parameters are based on standard deviations.

Typically, the uncertainties in N are estimated to be 20% for the first shell and 30% for the second shell.

*Sample prepared by coprecipitating 10^{-3} moles of Zn with HFO (1 g L^{-1}) at pH 7 and aging for 4 h.

** For goethite adsorption samples, multiple shells were fitted over 0.5-4.2 Å and for all HFO samples were fitted over 0.5-2.2 Å.

amorphous iron oxide is more efficient than adsorption, the free energy changes of these two processes are comparable. Spadini et al. (1994) found from their XAFS studies that Cd sorption complexes with a "two-line ferrihydrite" type of hydrous ferric oxide are independent of pH and adsorbate loading as well. They observed approximately one Fe atom at 3.32 Å and 3.50 Å from the central Cd atom. Similarly, Scheinost et al. (2001) could fit one Fe atom at 3.3 Å from either Cu or Pb sorbed to two types of two-line ferrihydrite (freshly precipitated and resuspended freeze-dried oxide). They further observed that this local structure of sorbed Cu or Pb ion was invariant of time (up to 8 weeks), type of ferrihydrite, and presence of competing ions or fulvic acid.

7.3 Zn-Goethite Adsorption Samples

Zinc sorption to goethite was studied as a function of pH in the site saturation range as determined from macroscopic isotherm studies. The averaged XAS spectra are similar in phase suggesting that the zinc sorption mechanism does not change with pH (Figure 51). Interestingly, these spectra do not resemble those of aqueous $Zn(NO_3)_2$ or of Zn-HFO systems suggesting that the local structure of zinc changes upon sorption to goethite. These chi spectra appear to be a result of at least two backscattering envelopes: one probably from a lighter element such as O in the lower k-space, and an additional one from a heavier atom such as Fe or Zn in the higher k-space. Thermodynamic analyses from macroscopic experiments suggested that Zn adsorption to goethite is an endothermic chemical type of reaction resulting in the formation of inner-sphere complexes (see Chapter 5; Rodda et al., 1996). To further test the type of adsorption mechanism, the XAS spectra were fitted with a theoretical standard generated by

Figure 51. Background subtracted, normalized, and averaged k^3-weighted XAS spectra of Zn sorbed to goethite (1 g L^{-1}) studied in fluorescence mode using Ge solid state detector presented as function of pH and temperature.

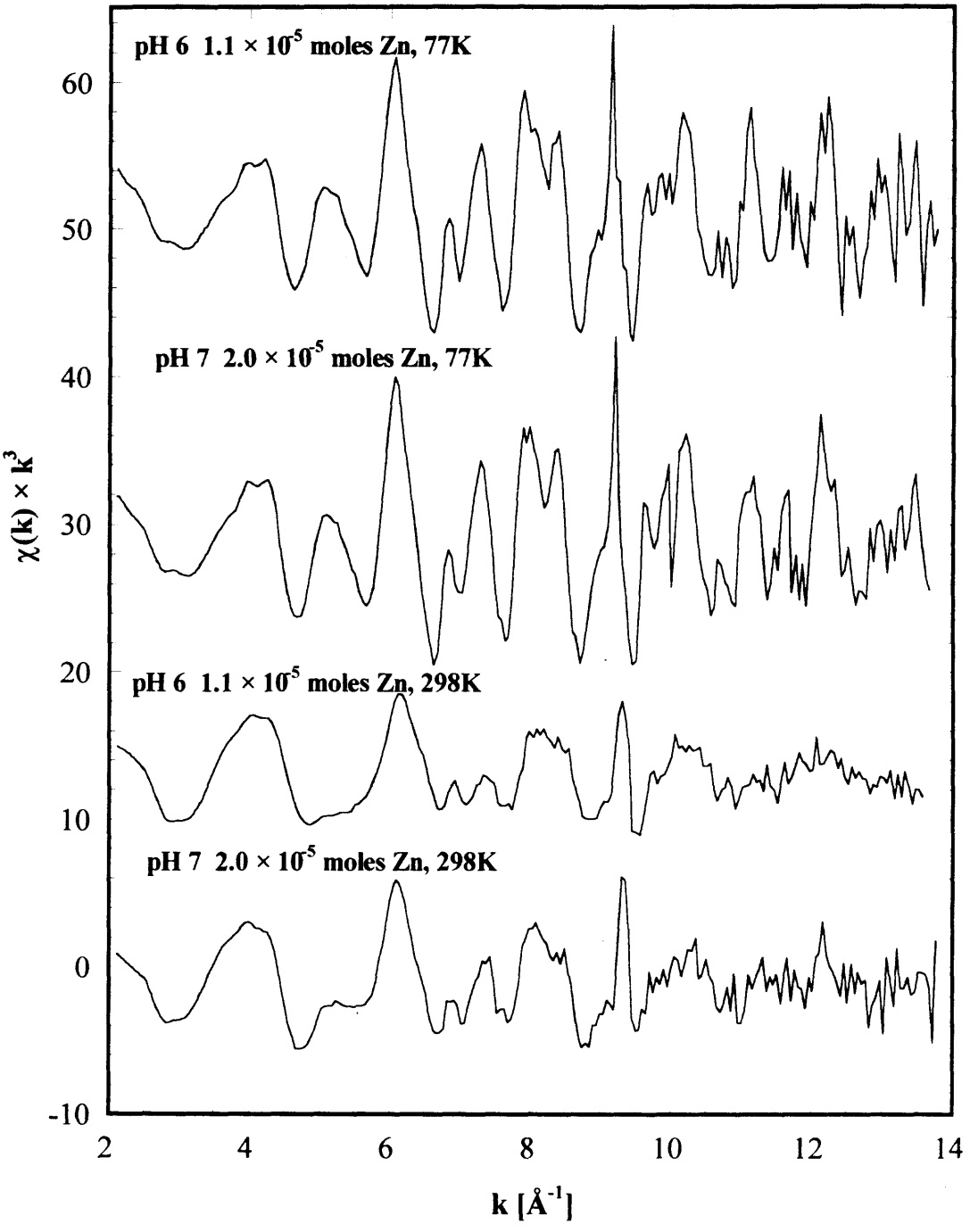

substituting Mn ions in chalcophanite with Fe ions as described in the XAS analyses section (Chapter 4). Accordingly, fitting of the Fourier transforms (Figure 52 and Table 13) shows that the first shell is disordered and consists of approximately four oxygen atoms at an average radial distance of 1.97 Å. These structural parameters suggest that Zn ions do not retain their octahedral hydration shell upon sorption to goethite. Waychunas et al. (1995) also found Zn^{2+} ions upon adsorption to ferrihydrite were converted from octahedral configuration to a tetrahedral one. Recently, Trainor et al. (2000) observed that at low sorption densities (< 1.1 μmol m^{-2}) Zn^{2+} sorbs to alumina as a mononuclear innersphere complex with tetragonal first shell coordination and an average Zn-O distance of 1.96 Å. Trainor et al. (2000) also observed two additional oxygen atoms in the first shell at the higher sorption densities; however, they argue that given the short Zn-O distances (2.01-2.04 Å) in the first shell, these additional oxygens may be from the alumina surface resulting in a distorted octahedra. In contrast, Zn sorbed to HFO (see section 7.2), to goethite (Schlegel et al., 1997), and to pyrophyllite (Ford and Sparks, 2000) appeared to retain its six-fold oxygen coordination.

In the Zn-goethite systems, the second shell was best fitted with 1.7 to 2.4 Fe ions at 2.49-2.51 Å (Table 13) suggesting that Zn ions are chemically sorbed to goethite forming an inner-sphere complex. These results are in agreement with the high adsorption enthalpies noted for Zn and Ni sorption to goethite (see Chapter 5). No fits were obtained with oxygen or zinc in the second shell. The structural parameters for Zn-goethite systems show very little temperature dependence (Table 13) suggesting greater static contributions as compared to thermal ones. This temperature effect is consistent with chemical bonding.

Figure 52. Fourier transforms (solid lines) of Zn-goethite adsorption sample XAS spectra fitted with (dashed lines) Fe substituted chalcophanite standard generated with FEFF7. The k-range for Fourier transforms is 2.3-9.2 $Å^{-1}$ while the R-window for multishell fitting is 0.5 4.20 Å.

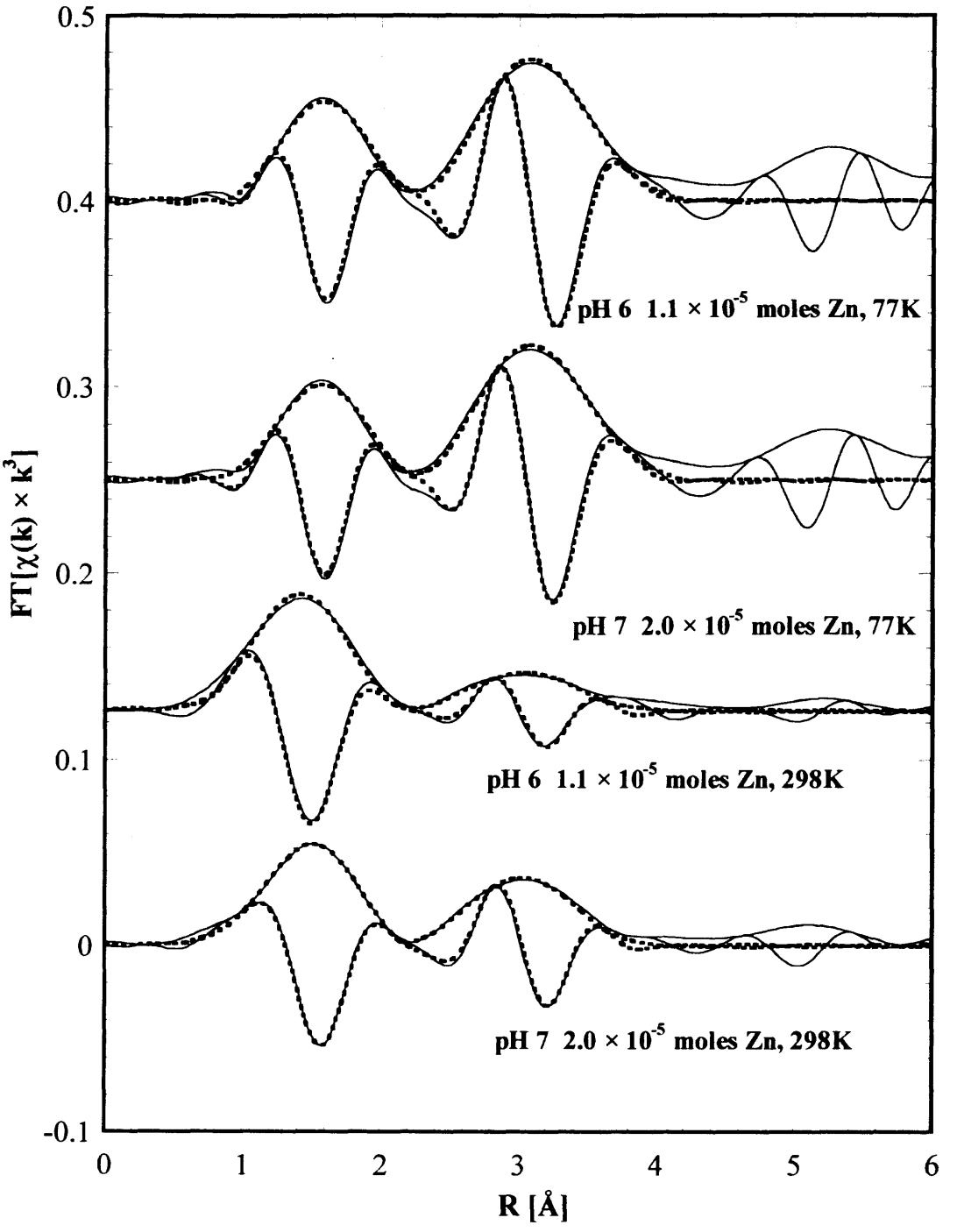

The Zn-Fe distances observed in this research, are comparable to many other systems studied (Table 14); for example Cd-Fe distances found for Cd adsorption to goethite are 3.26 and 3.48 Å, where the Fe coordination number at 3.48 Å is three times greater than at 3.26 Å (Spadini et al., 1994). Using γ-FeOOH to fit the second shell for Zn sorbed to goethite, Schlegel et al. (1997) estimated 0.9 Fe atoms at 3.00 Å and 1.2 Fe atoms at 3.20 Å. On the other hand, ZnEDTA, upon sorption to goethite, maintained its local structure similar to that in the aqueous phase (Schlegel et al., 1997). As discussed above, Scheinost et al. (2001) conducted kinetic studies for Cu and Pb sorption to two-line ferrihydrite in single and binary systems, where one Fe atom was observed in the second shell for either Cu or Pb. Mercury was also found to form an inner-sphere adsorption complex with goethite at pH 4.6, where its first shell contained approximately two oxygen atoms at 2.04 Å and the second shell consisted of approximately one Fe atom at 3.28 Å and 3.82 Å (25). From XAS studies of Pb sorption to goethite and hematite, Bargar et al. (1997, 1998) proposed that Pb ions formed mononuclear sorption complexes with Fe ions in the second shell at 3.27-3.31 Å for hematite and at 3.31-3.36 Å for goethite. However, no Pb atoms were observed in the second shell for Pb and Pb-chloro -adsorption complexes indicative of the absence of Pb precipitates. In chromate sorption to goethite, second shell contributions included two Fe atoms with one at 2.91 Å and the other at 3.29 Å, while in As(V)-goethite system, Fe atoms were observed at 2.85 Å, 3.24 Å, and 3.59 Å (Fendorf et al., 1997). For arsenite, a bidentate complex was found with Fe atoms located at 3.378 Å (Manning et al., 1998). On the other hand, O'Day et al. (1998) studied a zinc-iron oxyhydroxide coprecipitate,

Table 14. Other Relevant XAS Studies

References	Oxide	Metal	pH	First Shell (O)		Additional Shells		
				N	R (Å)	Element	N	R (Å)
Charlet and Manceau, 1992†	G	Cr^{3+}	4.0	*	*	Fe, Cr	1.1	3.01
						Fe, Cr	0.8	3.45
						Fe, Cr	1.2-1.9	3.95-3.99
	F	Cr^{3+}	4.0	*	*	Fe, Cr	2.1-3.0	3.00-3.05
						Fe, Cr	0.4-0.8	3.40-3.46
						Fe, Cr	1.5-2.2	3.95-4.03
Manceau and Charlet, 1994	G	SeO_4^{2-}	3.5	4.0	1.65	Fe	2.0	3.29
	F	SeO_4^{2-}	3.5	4.0	1.65	Se or Fe	0.4	2.76 or 2.80
						Fe	1.8	3.30
Spadini et al., 1994	G	Cd^{2+}	7.5	5.5-6.2	2.30	Fe	0.2-0.7	3.24-3.31
						Fe	0.6-1.2	3.46-3.51
	F	Cd^{2+}	6.7-9.5	4.0-5.0	2.27-2.31	Fe	0.7	3.32
						Fe	0.8	3.50
Bargar et al., 1997	G	Pb^{2+}	6.0-7.0	2.2-2.4	2.26-2.27	Fe	0.2-0.3	3.31-3.36
	H	Pb^{2+}	6.0-8.0	2.0-2.4	2.27-2.30	Fe	0.2-0.5	3.27-3.31
Fendorf et al., 1997	G	AsO_4^{3-}	6.0-9.0	3.7-3.9	1.66-1.67	Fe	0.6-1.3	2.84-2.85
						Fe	1.0-1.6	3.23-3.24
						Fe	0.4-1.1	3.59-3.60
	G	CrO_4^{2-}	5.0-6.0	3.9	1.68-1.69	Fe	0.4-1.0	2.91-3.29
							0.8-1.5	3.27-3.63
Schlegel et al., 1997	G	Zn^{2+}	7.0	6.0	2.10	Fe	0.9	3.00
							1.2	3.20
Bargar et al., 1998	G	Pb^{2+}	5.0-7.0	2.1-2.9	2.26-2.33	Fe	0.3-0.7	3.00-3.36
							0.3-1.1	3.86-3.93
Manning et al., 1998	G	AsO_4^{3-}	6.4-8.6	3.0-3.1	1.78-1.79	Fe	2.3-2.4	3.36-3.40
Weesner and Bleam	G	Pb^{2+}/ $H_2PO_4^-$	5.5	4.0	2.30	Fe	1.6	3.35
Collins et al., 1999	G	Hg^{2+}	4.6	2.0	2.04	Fe	1.0	3.28
Sahai et al., 2000	G	Sr^{2+}	6.4-8.6	8.2-9.7	2.58-2.61	**	**	**
			8.6-9.9	8.3-10.1	2.58-2.63	C	0.4-3.8	3.03-3.05
						Sr	1.5-3.3	4.13-4.90

G – goethite; F – two-line ferrihydrite; H – hematite.

† Fe and Cr equally contribute to the second shell and the corresponding R represents the averaged distance over both metals.

* Shells not reported.

** No shells observed.

where they fitted the first shell with two oxygens at 1.92 and 2.04 Å and the second shell with a mixture of 1.2 Zn at 3.54 Å and 0.7 Fe at 3.12 Å. Trainor et al. (2000) also observed that in low sorption density samples (< 1.3×10^{-4} moles Zn g^{-1}) second shell contributions were consistent with either Zn atoms or Zn as well as Al at an average distance of 3.10 Å. At higher sorption densities with alumina, a mixed Zn/Al second shell was observed at 3.05 Å where the coordination number increased with sorption density (Trainor et al., 2000). In another interesting study, Manceau et al. (2000) prepared Zn-goethite by aging Zn-ferrihydrite coprecipitate under alkaline conditions at 70°C for 93 days. The resultant oxide was found to have a first shell comprising two O subshells: N_1 = 1.1 at 1.87 Å and N_2 = 5.4 at 2.05 Å, while the second shell exhibited a wide distribution of Fe atoms with radial distances ranging from 3.0 to 3.48 Å.

Overall these results demonstrate that even though the local structures of HFO and goethite are similar, they form different sorption complexes with Zn. Hence they cannot represent each other in aquatic systems. To evaluate whether sorption to other amorphous oxides is consistent with HFO and to compare macroscopic observations with spectroscopic studies, Zn and Ni sorption to HMO has been investigated.

7.4 Zn-HMO Adsorption Samples

The average spectra for Zn sorbed to HMO presented (Figure 53) as a function of pH, adsorbate loading, temperature, and contact time reveal a glitch at 10.2 $Å^{-1}$like that observed in the other adsorption samples and standards. The backscattering envelopes of these spectra appear to be similar as a function of pH, adsorbate loading, and contact time

Figure 53. Background subtracted, normalized, and averaged k^3-weighted XAS spectra of Zn-HMO adsorption samples studied at Zn K-edge in fluorescence mode as a function of pH, adsorbate loading, temperature, and contact time.

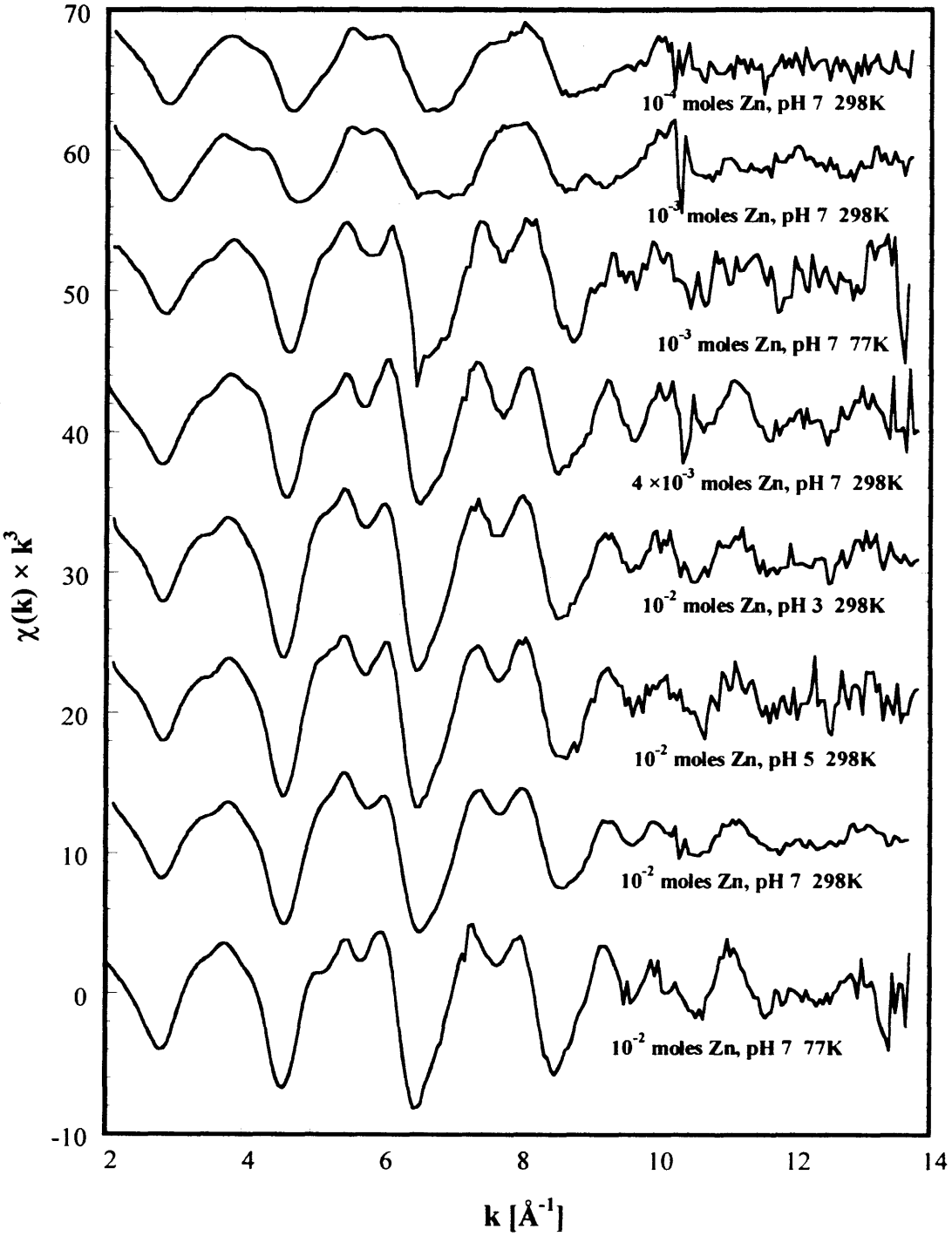

suggesting that the local coordination environment for zinc, and hence its adsorption mechanism with respect to HMO, is independent of these factors. In all of these samples, between 2.4 and 9.2 $Å^{-1}$ the spectra show similar envelopes indicative of a light atom such as O occupying the first shell. The amplitudes of the spectra increase with loading; also in higher k-space the background noise increases as the adsorbed zinc concentration decreases. The spectra from 77 K were found to have better signal-to-noise ratio and greater amplitude than those at 298 K.

The Fourier transformed data were fit using FEFF7 generated chalcophanite. The resulting first shell for all Zn-HMO adsorption samples revealed a broad distribution consisting of 6-7 O atoms at an average radial distance of 2.19 Å (Table 15 and Figures 54-56). Application of the third cumulant (C_3) to the fits indicates a disordered oxygen shell (Bunker, 1983). These parameters are in agreement with those of Zn^{2+} ions in aqueous solution (Table 12) as well as of Zn^{2+} sorbed to HFO suggesting that zinc is physically sorbed to HMO where it retains its waters of hydration upon sorption. Beyond the first shell, in the samples with higher zinc loadings and for samples with lower loadings studied at 77K, a second shell was also observed. This second shell is best fitted with 7-9 O atoms at 3.49-3.50 Å; these oxygens may be from functional groups on the hydrous oxide surface and/or from the hydrated oxide surface. No reasonable fits were obtained with Zn in the second shell suggesting the lack of precipitation or polynuclear complex formation. Similarly, no Zn-Mn pairing could be identified in the second shell further demonstrating that sorption is consistent with physical forces. An imprecision of ±20% is estimated with these coordination numbers for the first shell; this variance is expected to be greater for the second shell.

Table 15. XAS Fits for Zn-HMO Samples Filtered over 2.4-9.2 $Å^{-1}$.

Zn loadings (moles g^{-1})	T (K)	N (atoms)	R (Å)	σ^2 ($Å^2$)	C3 ($Å^3$)	Eo shift (eV)
First Shell: Oxygen						
10^{-2} pH 7	77	6.61 ± 0.43	2.19 ± 1.3 × 10^{-2}	1.76 × 10^{-3} ± 2.6 × 10^{-4}	3.40 × 10^{-4} ± 6.0 × 10^{-5}	4.13 ± 1.42
10^{-2} pH 7	298	7.02 ± 0.24	2.19 ± 2.3 × 10^{-3}	2.43 × 10^{-3} ± 1.1 × 10^{-4}	4.50 × 10^{-4} ± 1.3 × 10^{-5}	6.79 ± 0.61
10^{-2} pH 5	298	7.07 ± 0.43	2.19 ± 3.2 × 10^{-3}	2.65 × 10^{-3} ± 2.9 × 10^{-4}	4.25 × 10^{-4} ± 1.4 × 10^{-5}	6.24 ± 0.34
10^{-2} pH 3	298	7.04 ± 0.20	2.19 ± 3.3 × 10^{-3}	2.44 × 10^{-3} ± 2.4 × 10^{-4}	3.93 × 10^{-4} ± 7.1 × 10^{-5}	6.46 ± 0.38
4 ×10^{-3} pH 7	298	7.02 ± 0.39	2.19 ± 3.2 × 10^{-3}	3.53 × 10^{-3} ± 6.1 × 10^{-4}	3.39 × 10^{-4} ± 0.9 × 10^{-5}	6.81 ± 0.54
10^{-3} pH 7†	77	6.80 ± 0.19	2.19 ± 3.7 × 10^{-3}	2.79 × 10^{-3} ± 8.8 × 10^{-4}	-1.58 × 10^{-4} ± 3.0 × 10^{-5}	4.81 ± 1.37
10^{-3} pH 7*	298	6.41 ± 0.53	2.19 ± 6.6 × 10^{-3}	3.35 × 10^{-3} ± 5.5 × 10^{-4}	9.58 × 10^{-4} ± 1.9 × 10^{-4}	7.52 ± 1.10
10^{-4} pH 7*	298	6.41 ± 0.35	2.19 ± 6.2 × 10^{-3}	3.35 × 10^{-3} ± 4.5 × 10^{-4}	9.58 × 10^{-4} ± 1.31 × 10^{-4}	6.29 ± 0.89
*Second Shell: Oxygen***						% Res.
10^{-2} pH 7	77	8.09 ± 0.35	3.46 ± 2.3 × 10^{-2}	8.28 × 10^{-3} ± 7.2 × 10^{-4}	-1.10 × 10^{-3} ± 2.1 × 10^{-4}	6.89
10^{-2} pH 7	298	8.36 ± 0.49	3.50 ± 5.7 × 10^{-3}	9.88 × 10^{-3} ± 7.9 × 10^{-4}	-1.00 × 10^{-3} ± 1.9 × 10^{-4}	5.43
10^{-2} pH 5	298	8.10 ± 0.39	3.50 ± 1.3 × 10^{-2}	9.24 × 10^{-3} ± 5.9 × 10^{-4}	-7.79 × 10^{-4} ± 1.8 × 10^{-4}	7.61
10^{-2} pH 3	298	8.942 ± 0.92	3.50 ± 0.9 × 10^{-2}	9.60 × 10^{-3} ± 3.1 × 10^{-4}	-7.61 × 10^{-3} ± 1.7 × 10^{-4}	7.99
4 ×10^{-3} pH 7	298	8.01 ± 0.60	3.49 ± 2.2 × 10^{-2}	9.68 × 10^{-3} ± 3.0 × 10^{-4}	-1.00 × 10^{-3} ± 1.2 × 10^{-4}	7.76
10^{-3} pH 7	77	6.98 ± 0.40	3.50 ± 2.8 × 10^{-2}	1.29 × 10^{-2} ± 9.2 × 10^{-4}	-9.84 × 10^{-4} ± 2.1 × 10^{-4}	5.29

Errors provided with the parameters are based on standard deviations.
Typically the uncertainties in N are estimated to be 20% for the first shell and 30% for the second shell.
† Long-term sample analyzed after a contact time of 32 days.
* No second shell observed; these samples were fitted over 0.5-2.2 Å.
** Multiple shells fitted with 0.5-3.78 Å.

Figure 54. Fourier transforms (solid lines) of Zn K-edge XAS spectra of Zn-HMO adsorption samples at pH 7 and 298K, presented as a function of zinc concentration, each filtered over k-range 2.4-9.4 $Å^{-1}$ and fitted with chalcophanite (dashed lines) from 0.5 to 3.78 Å (except single shells were fitted between 0.5 and 2.2 Å).

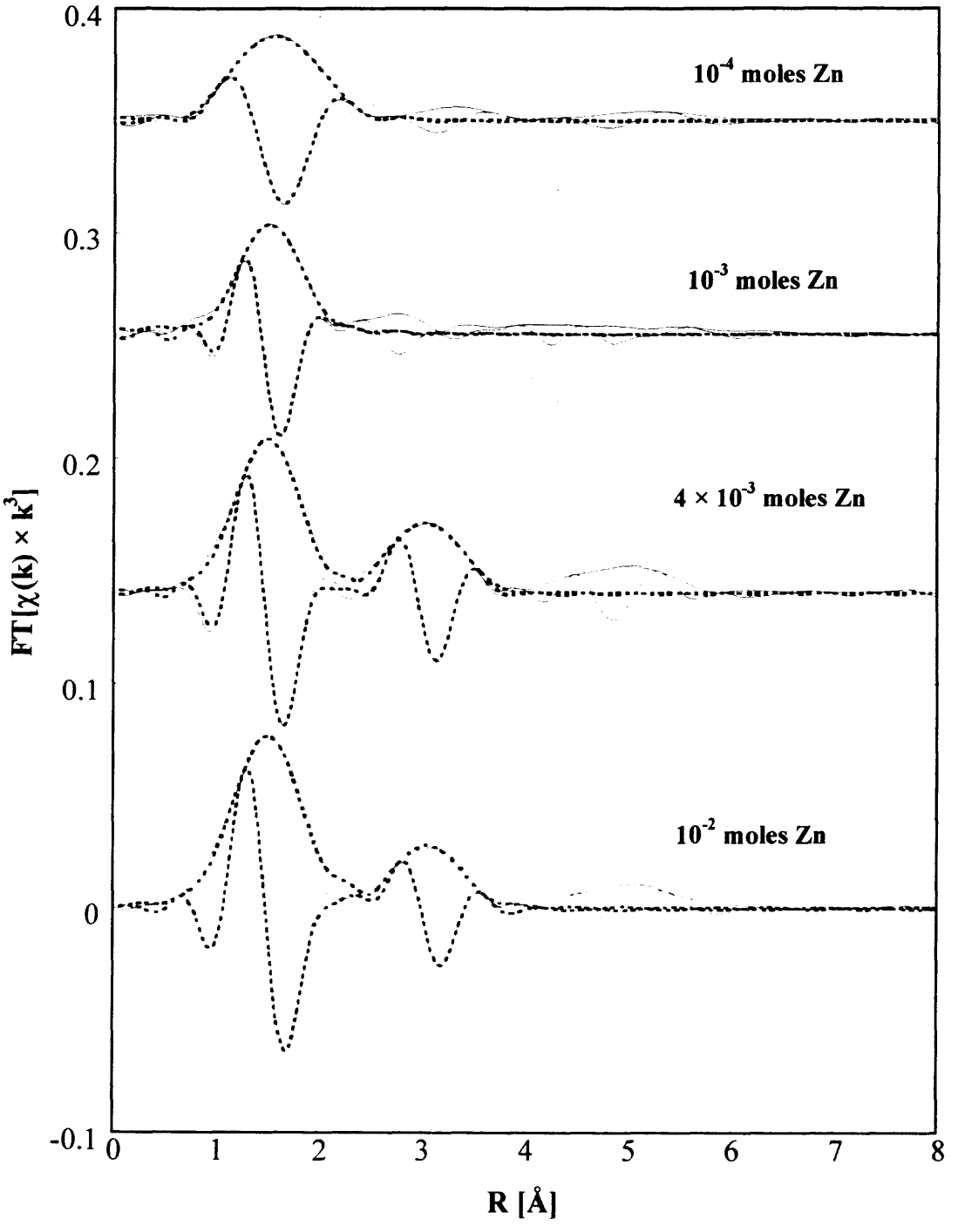

Figure 55. Fourier transforms (solid lines) of Zn K-edge XAS spectra of Zn-HMO adsorption samples at 298K, presented as a function of pH, each filtered over k-range 2.4-9.4 $Å^{-1}$ and fitted with chalcophanite (dashed lines) from 0.5 to 3.78 Å (except single shells were fitted between 0.5 and 2.2 Å).

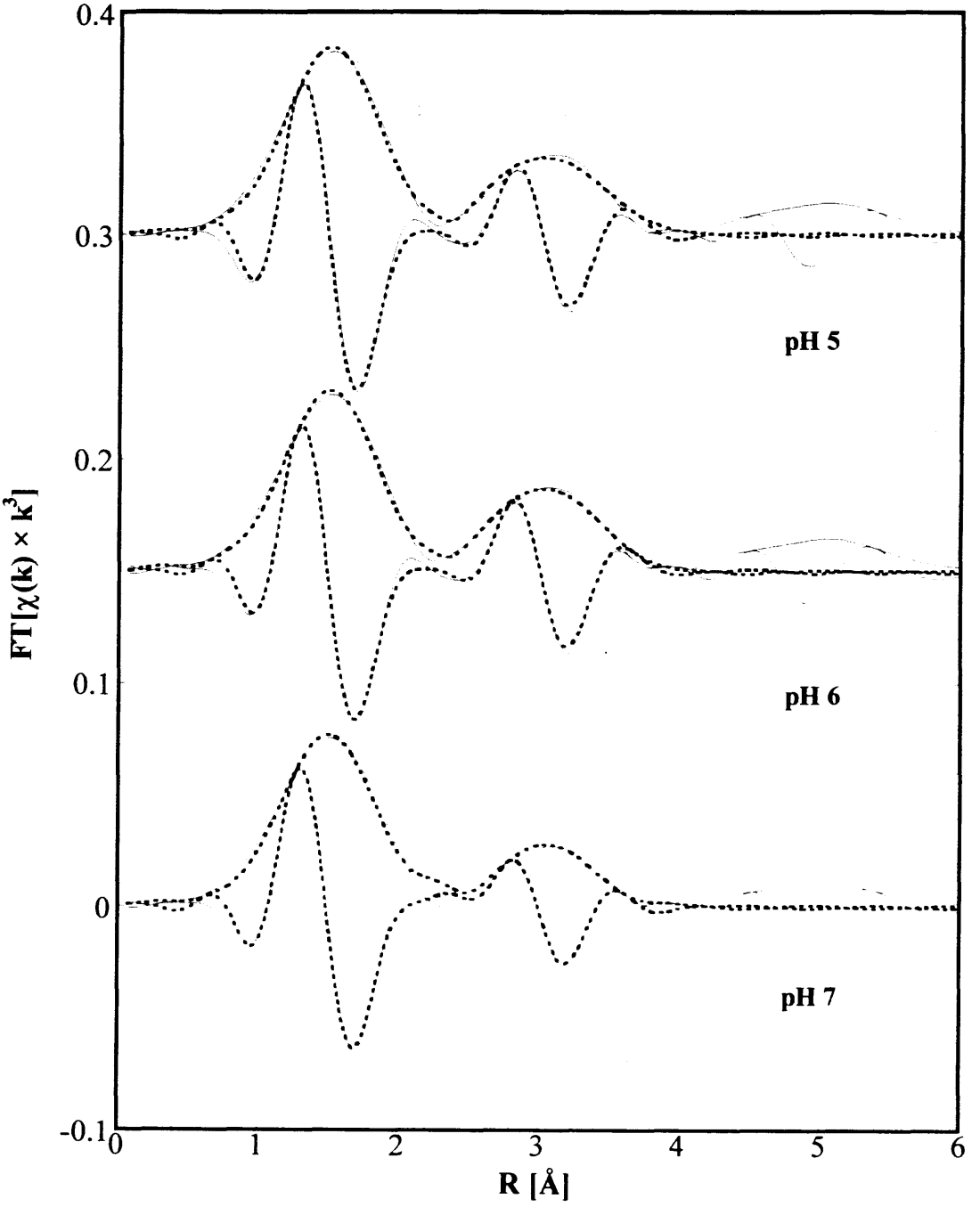

Figure 56. Fourier transforms (solid lines) of Zn K-edge XAS spectra of Zn-HMO adsorption samples at pH 7, presented as a function of temperature, each filtered over k-range 2.4-9.4 $Å^{-1}$ and fitted with chalcophanite (dashed lines) from 0.5 to 3.78 Å (except single shells were fitted between 0.5 and 2.2 Å).

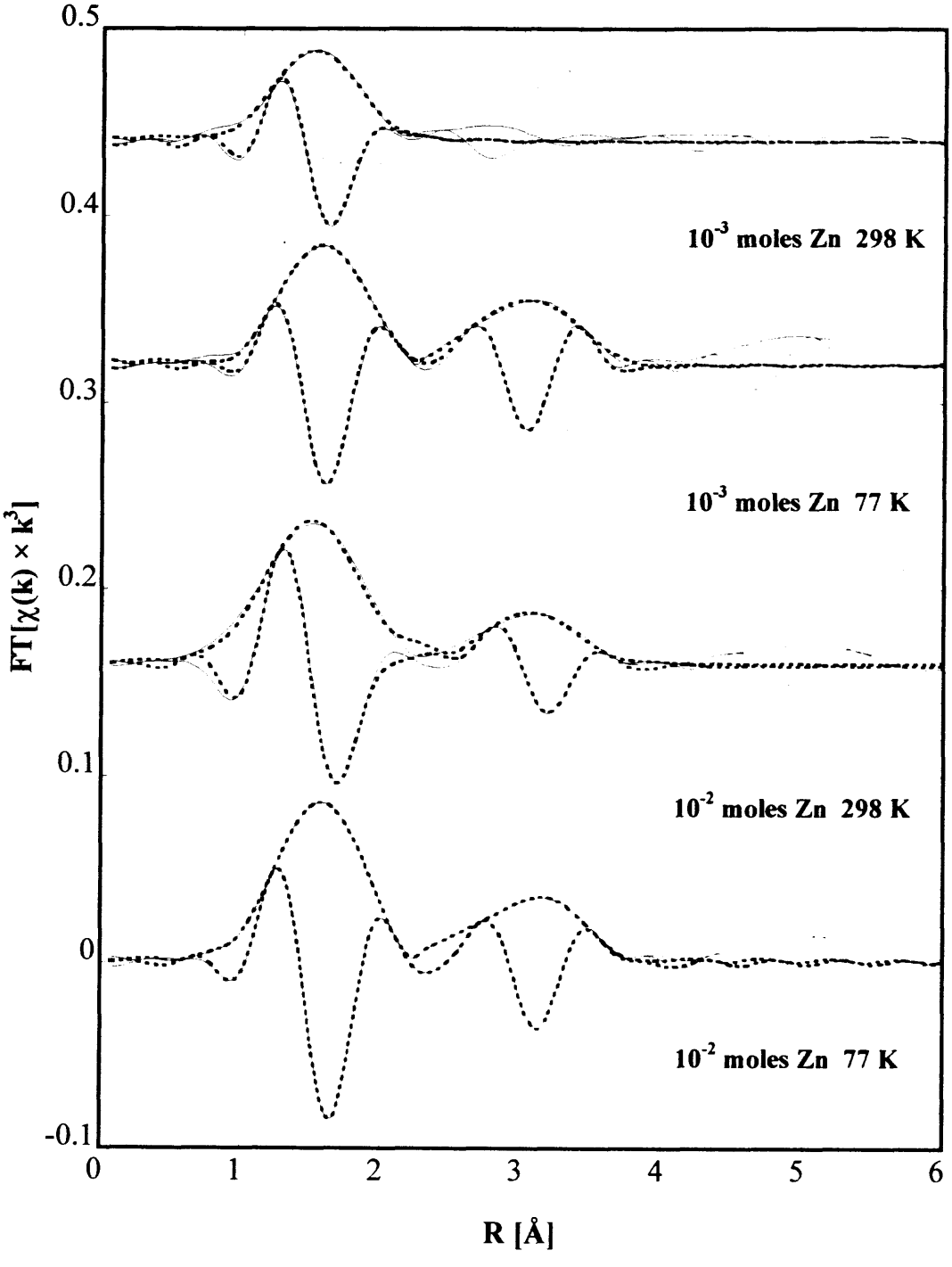

Temperature dependence (Table 15 and Figure 56) also confirms the physical type of adsorption due to a significant contribution by the thermal component of the Debye-Waller factor. Given the error, the local structure of adsorbed Zn ions is independent of adsorbate loading (Figure 54) and pH in the range of 3.0 to 7.0 (Figure 55), suggesting that the adsorption mechanism can be represented by one average type of site. This result is consistent with macroscopic studies (see Chapter 5). Interestingly, the long-term (32 days of reaction time) sample with an adsorbate loading of 4×10^{-3} moles of Zn g^{-1} HMO, as shown in Figure 54, was found to have a similar local structure to that of those with a 4 h contact time. Because the data represent a volume average where 30% of Zn is located internally, when Zn diffuses along the micropore walls of HMO, its sorption is similar to that of the 4 h contact time where the adsorption is restricted to the external surface. Axe and coworkers (1998, 2000) have demonstrated from their spectroscopic studies with Sr-HMO and Sr-HFO systems that the local structure of Mn in HMO and of Fe in HFO did not change in the presence or absence of Sr upto months.

One of the hypotheses from the macroscopic studies is that a group of metals from the Periodic table must form similar adsorption complexes. To test this hypothesis, the sorption mechanism of Ni to HMO is discussed in the next section; this work complements earlier macroscopic studies.

7.5 Nickel Standards

A comparison of the XAS spectra of all Ni standards (Figure 57) shows that except for aqueous nickel nitrate all other standards have second shell contributions. The XAS spectrum of Ni_6MnO_8 is generated from crystallographic data using FEFF7 (Porta et al.,

Figure 57. Background subtracted, normalized, and averaged k^3-weighted XAS spectra of Ni standards studied at 298 K and Ni K-edge in transmission mode. Ni_6MnO_8 structure is generated from crystallographic data using FEFF7 (Porta et al., 1991).

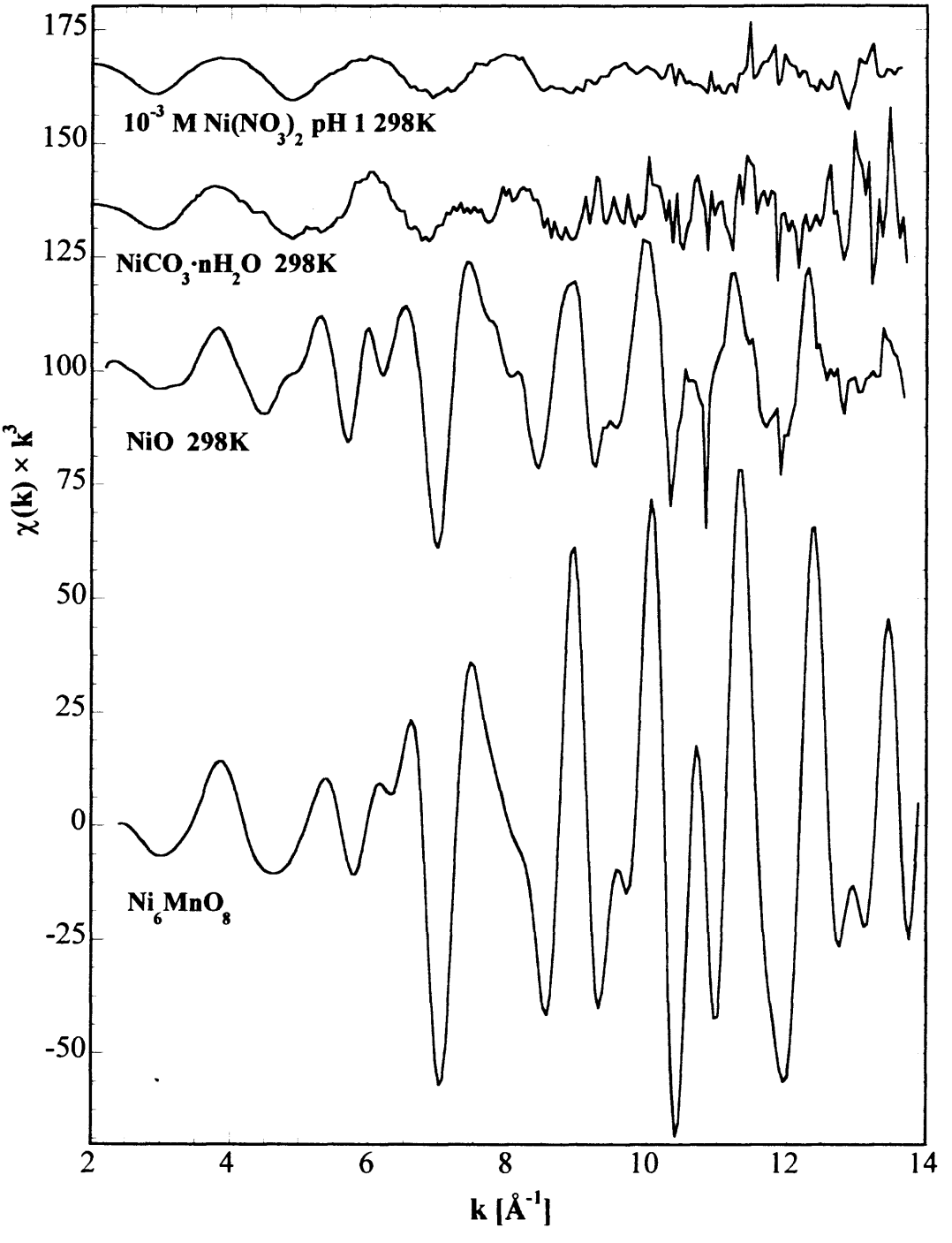

1991). Ni_6MnO_8 is isomorphous to Mg_6MnO_8 where octahedrally coordinated Ni^{2+} and Mn^{4+} are located in a cubic lattice with space group *Fm3m* (Porta et al., 1991). Accordingly, the first shell around Ni consists of two oxygen atoms at 2.077 Å and four oxygen atoms at 2.083 Å, with a second shell of four Mn atoms at 2.421 Å and eight Ni atoms at 2.937 Å (Porta et al., 1991). Resultant Fourier transforms of the other three standards presented in Figure 58 along with the fits (Table 15) show only one shell surrounding the Ni ion in aqueous nickel nitrate. This shell is comprised of 6.08 O atoms at 2.07 Å for the 10^{-3} M nickel nitrate solution at pH 1. Solution speciation shows Ni^{2+} as the dominant species for this sample (Allison et al., 1991). Consistently, Magini et al. (1988) reported the primary shell radius for Ni^{2+} to be 2.07 Å. This value is based on a compilation of various experiments including diffraction and scattering techniques, XAS, infrared and Raman spectroscopy, mass spectrometry, nuclear magnetic resonance spectroscopy, and various *ab initio* approaches.

The fits for the standards are shown in Table 12, and reveal that the local coordination environment is consistent with their known crystalline structure. Pandya et al. (1990) investigated the structure of α-$Ni(OH)_2$ and found 5.8 oxygen atoms in the first shell at 2.04 Å and approximately 5.7 Ni atoms in the second shell at an average radial distance of 3.07 Å. Scheidegger et al. (1998) presented a compilation of the structural parameters of β-$Ni(OH)_2$, $Ni(OH)_2$, and a coprecipitated phase containing Ni and Al (Ni:Al = 3:1) that was determined using XAFS, XRD, and neutron diffraction. They found that Ni^{2+} in these three standards has an octahedral first shell coordination with $R_{Ni\text{-}O}$ = 2.04-2.07 Å while the second shell in nickel hydroxides was composed of 5-6 Ni atoms at 3.09-3.13 Å. A second shell was also observed with

Figure 58. Fourier transforms (solid lines) of Ni standards studied at 298 K, each filtered over k-range 2.4-9.22 $Å^{-1}$ (except NiO – 2.4-13.3 $Å^{-1}$) and fitted with NiO (dashed lines) over 0.41-3.20 Å for NiO, 0.41-3.70 Å for $NiCO_3.nH_2O$, 0.41-2.20 Å for $Ni(NO_3)_{2,aq}$.

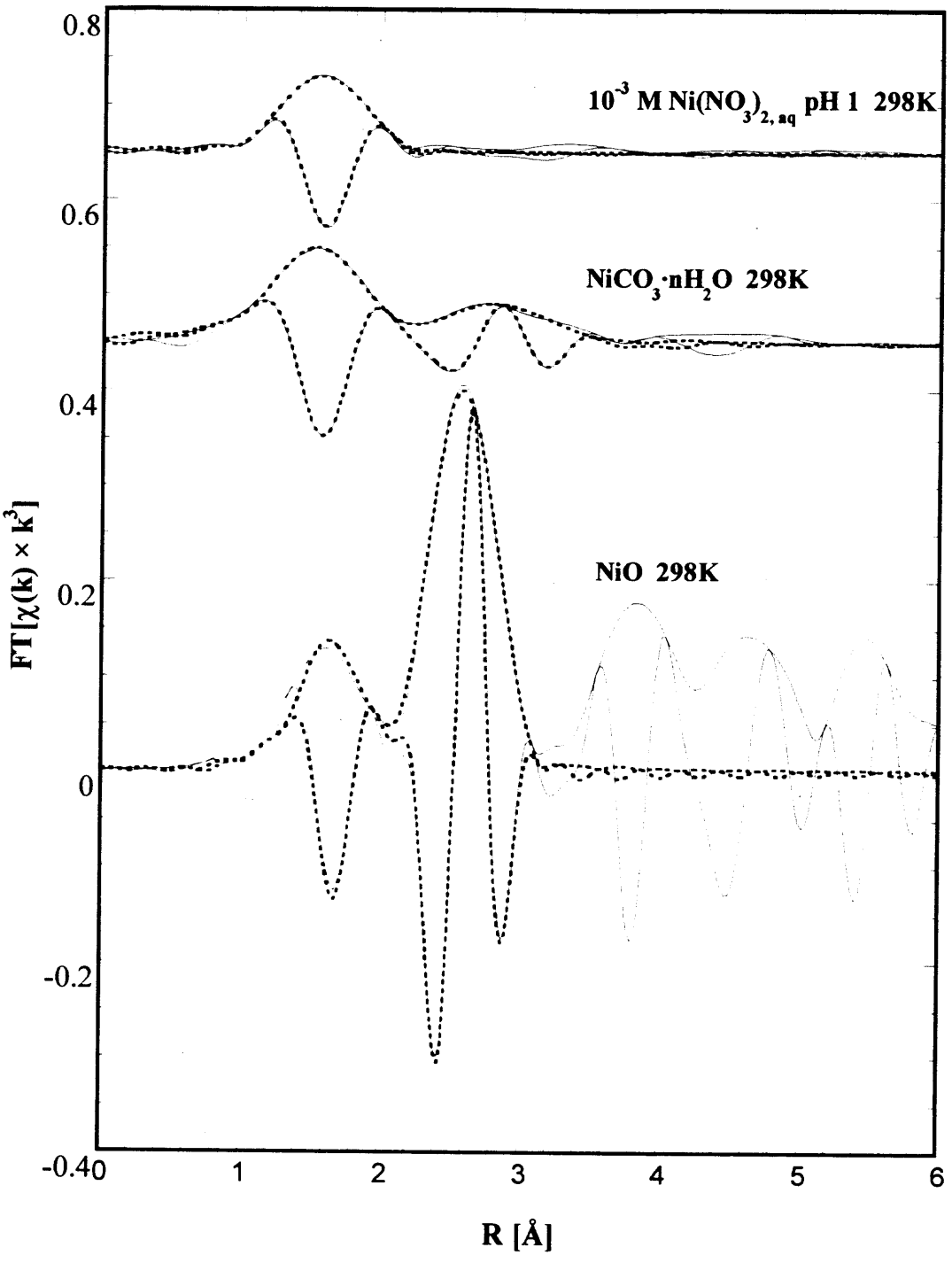

Ni-Al coprecipitate where it was comprised of 3.8-4.8 Ni atoms at 3.03-3.06 Å (Scheidegger et al., 1998). On the other hand, nickel carbonate hydrate was found to have 6.74 oxygens at an average radial distance of 2.04 Å and 5.47 Ni atoms at an average distance of 3.54 Å. These results are in agreement with the XRD findings of Pertlik (1985) who found six O atoms in the first shell located at 2.08 Å in $NiCO_3$, while the second shell consisted of six Ni atoms at an average radial distance of 3.62 Å.

7.6 Ni-HMO Adsorption Samples

The local structure of nickel sorbed to HMO was investigated with XAS as a function of pH, adsorbate concentration, and the reaction time. The spectra (Figure 60) of all the samples are similar suggesting that the adsorption mechanism is independent of these parameters. These spectra also reveal second shell contributions as well. The amplitude and the signal-to-noise ratio of these spectra improved with the adsorbate loading. Best fits the Fourier transforms of these samples revealed (Table 15 and Figures 61 and 62) 5.8-6.2 O in a disordered first shell at an average bond distance of 2.07 Å. The first shell parameters are similar to those of the aqueous Ni ion suggesting that the primary hydration shell of the Ni ion remains intact upon adsorption to HMO. Scheidegger et al. (1996) reported six oxygens at 2.02-2.04 Å around Ni sorbed to pyrophyllite at all sorption densities up to 2.99×10^{-4} mol g^{-1}. Roberts et al. (1999) observed a first shell coordination of 5.4-6.9 O atoms at 2.05-2.06 Å for Ni sorbed to a clay, and found this shell to be independent of pH and contact time. Present analyses also suggested that the second shell was best represented with 5.6-8.4 oxygens at 3.32-3.35 Å.

Figure 59. Background subtracted, normalized, and averaged k^3-weighted XAS spectra of Ni sorbed to HMO studied at 298 K and Ni K-edge in fluorescence mode as a function of pH, adsorbate loading, and contact time.

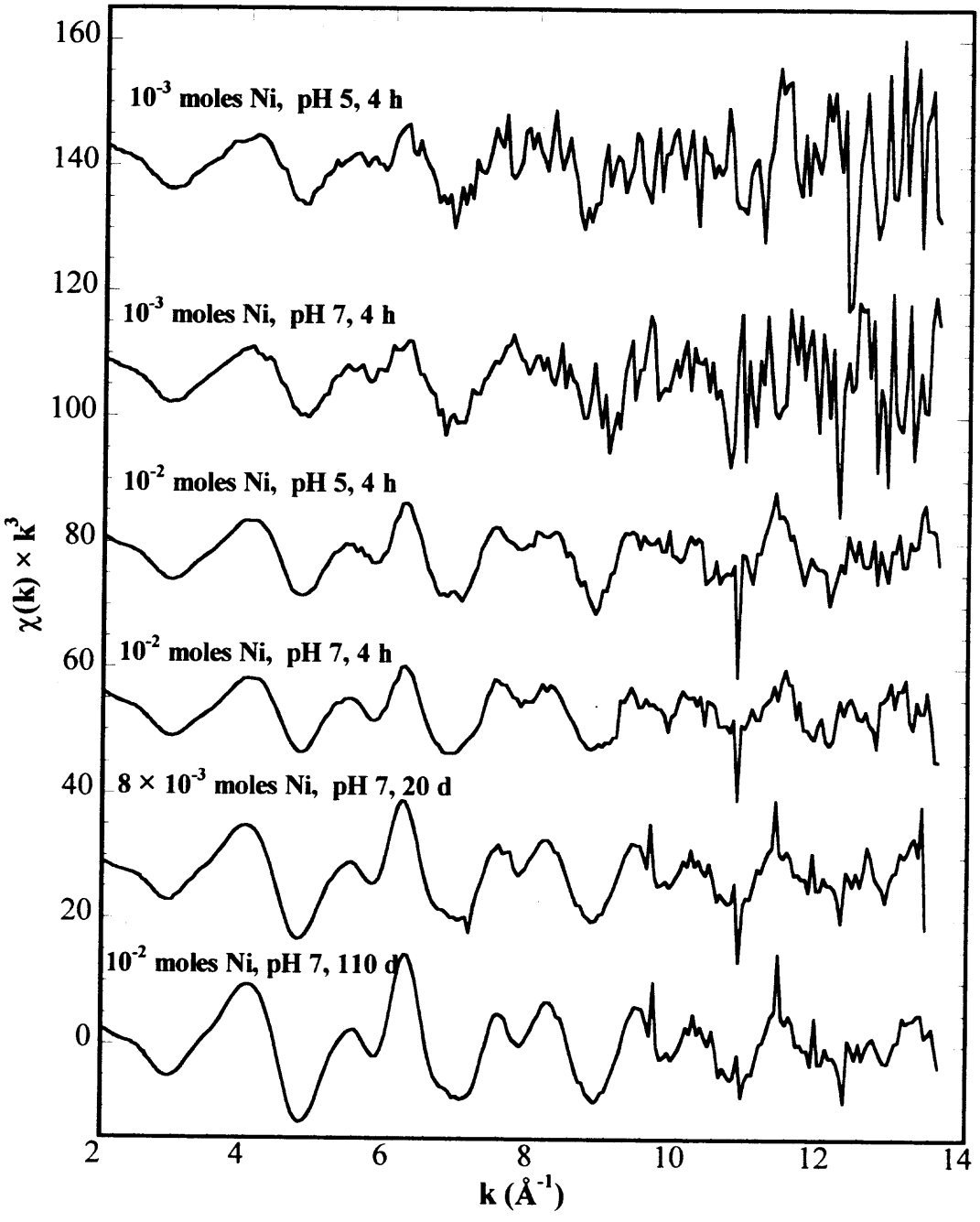

Table 16. Ni-HMO Samples Fitted with NiO Model

Ni loadings (moles g^{-1})	t_{rxn} (h)	N (atoms)	R (Å)	σ^2 ($Å^2$)	C3 ($Å^3$)	Eo shift (eV)
First Shell: Oxygen						
10^{-2} pH 7	4	5.95 ± 0.72	2.07 ± 3.0 × 10^{-2}	5.55 × 10^{-3} ± 2.2 × 10^{-4}	-6.49 × 10^{-4} ± 2.6 × 10^{-4}	5.71 ± 0.76
10^{-2} pH 5	4	6.14 ± 0.23	2.07 ± 1.0 × 10^{-3}	5.99 × 10^{-3} ± 8.0 × 10^{-4}	-4.40 × 10^{-4} ± 1.4 × 10^{-4}	2.18 ± 1.37
8.9 ×10^{-3} pH 7	2640	5.97 ± 0.47	2.07 ± 9.0 × 10^{-2}	5.76 × 10^{-3} ± 1.2 × 10^{-4}	-4.57 × 10^{-4} ± 5.5 × 10^{-4}	6.16 ± 0.85
8.8 ×10^{-3} pH 7	480	5.92 ± 0.83	2.07 ± 1.0 × 10^{-2}	4.00 × 10^{-3} ± 1.8 × 10^{-3}	-9.00 × 10^{-4} ± 5.2 × 10^{-4}	5.57 ± 0.92
10^{-3} pH 7	4	5.75 ± 0.30	2.07 ± 1.0 × 10^{-2}	5.80 × 10^{-3} ± 1.1 × 10^{-3}	-1.00 × 10^{-4} ± 6.2 × 10^{-4}	1.32 ± 1.3
10^{-3} pH 5	4	6.17 ± 0.41	2.07 ± 4.0 × 10^{-3}	7.47 × 10^{-3} ± 6.6 × 10^{-4}	-4.45 × 10^{-4} ± 1.01 × 10^{-3}	1.45 ± 1.3
Second Shell: Oxygen						% Res.
10^{-2} pH 7	4	5.71 ± 0.76	3.35 ± 5.0 × 10^{-2}	9.82 × 10^{-3} ± 3.7 × 10^{-4}	-8.79 × 10^{-3} ± 1.4 × 10^{-3}	8.84
10^{-2} pH 5	4	8.36 ± 0.49	3.35 ± 2.0 × 10^{-2}	9.70 × 10^{-3} ± 4.1 × 10^{-4}	-8.15 × 10^{-3} ± 1.7 × 10^{-3}	7.54
8.9 ×10^{-3} pH 7	2640	6.16 ± 0.85	3.34 ± 3.0 × 10^{-2}	9.00 × 10^{-3} ± 1.8 × 10^{-3}	-4.59 × 10^{-3} ± 1.0 × 10^{-3}	5.24
8.8 ×10^{-3} pH 7	480	5.57 ± 0.92	3.32 ± 9.0 × 10^{-2}	8.36 × 10^{-3} ± 2.3 × 10^{-3}	-5.40 × 10^{-3} ± 5.9 × 10^{-4}	5.01
10^{-3} pH 7	4	6.30 ± 0.94	3.34 ± 2.0 × 10^{-2}	9.90 × 10^{-3} ± 2.2 × 10^{-3}	-6.50 × 10^{-4} ± 5.1 × 10^{-4}	4.92
10^{-3} pH 5	4	6.21 ± 0.83	3.35 ± 1.0 × 10^{-2}	9.71 × 10^{-3} ± 4.2 × 10^{-4}	-2.83 × 10^{-4} ± 1.3 × 10^{-3}	9.04

Errors provided with the parameters are based on the standard deviations.
Typically the uncertainties in N are estimated to be 20% for the first shell and 30% for the second shell .
All samples were Fourier transformed from 2.45-9.21 Å-1 and fitted for multiple shells over 0.5-3.78 Å.

Figure 60. Fourier transforms (solid lines) of Ni K-edge XAS spectra of Ni sorbed to HMO (1 g L^{-1}) studied at 298 K presented as a function of pH and adsorbate concentration, each filtered over k-range 2.45-9.21 $Å^{-1}$ and fitted with Ni_6MnO_8 (dashed lines) over 0.41-4.00 Å.

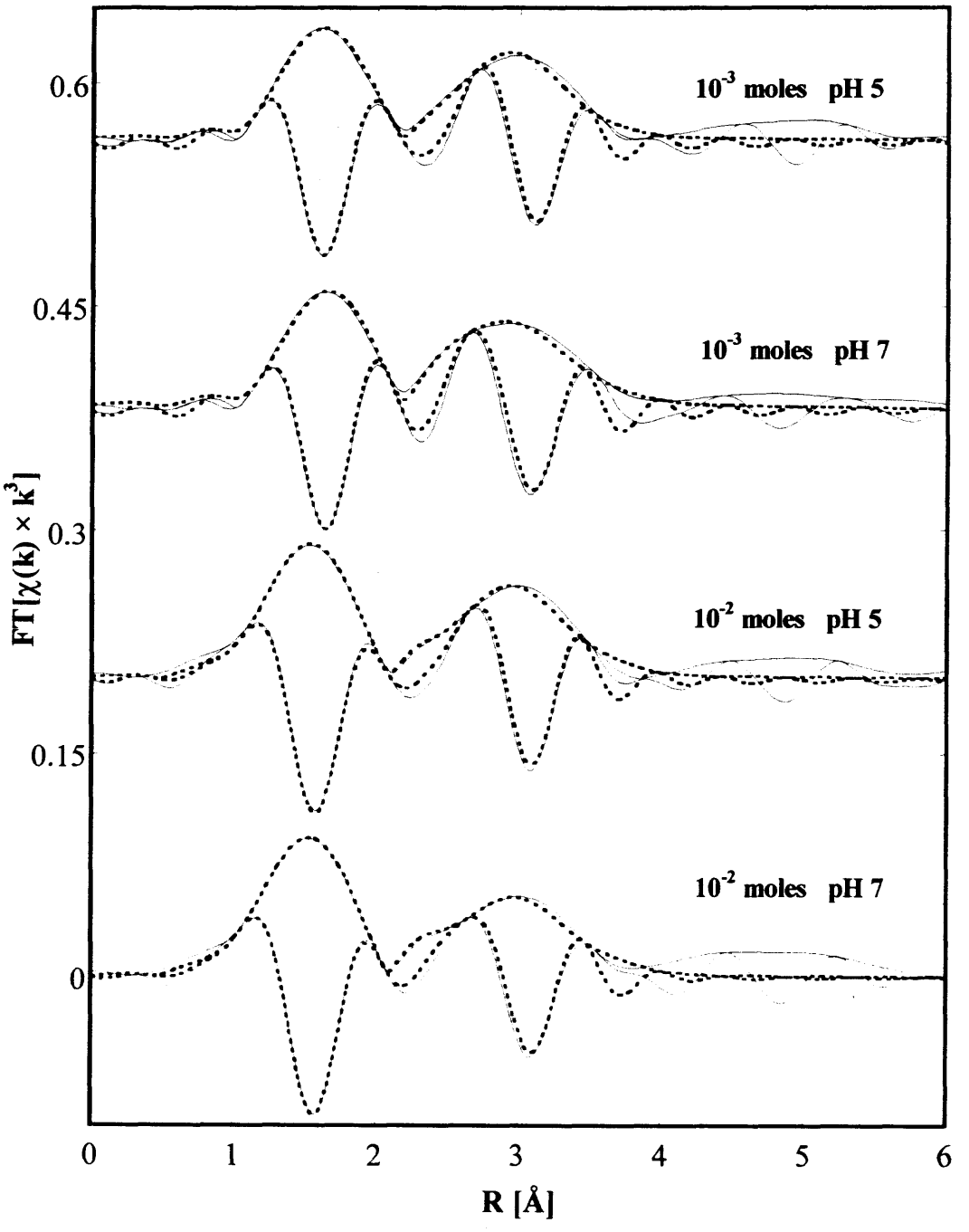

Figure 61. Fourier transforms (solid lines) of Ni K-edge XAS spectra of Ni sorbed to HMO (1 g L^{-1}) studied at pH 7 and 298 K, presented as a function of contact time, each filtered over k-range 2.45-9.21 $Å^{-1}$ and fitted with Ni_6MnO_8 (dashed lines) over 0.41-4.00 Å.

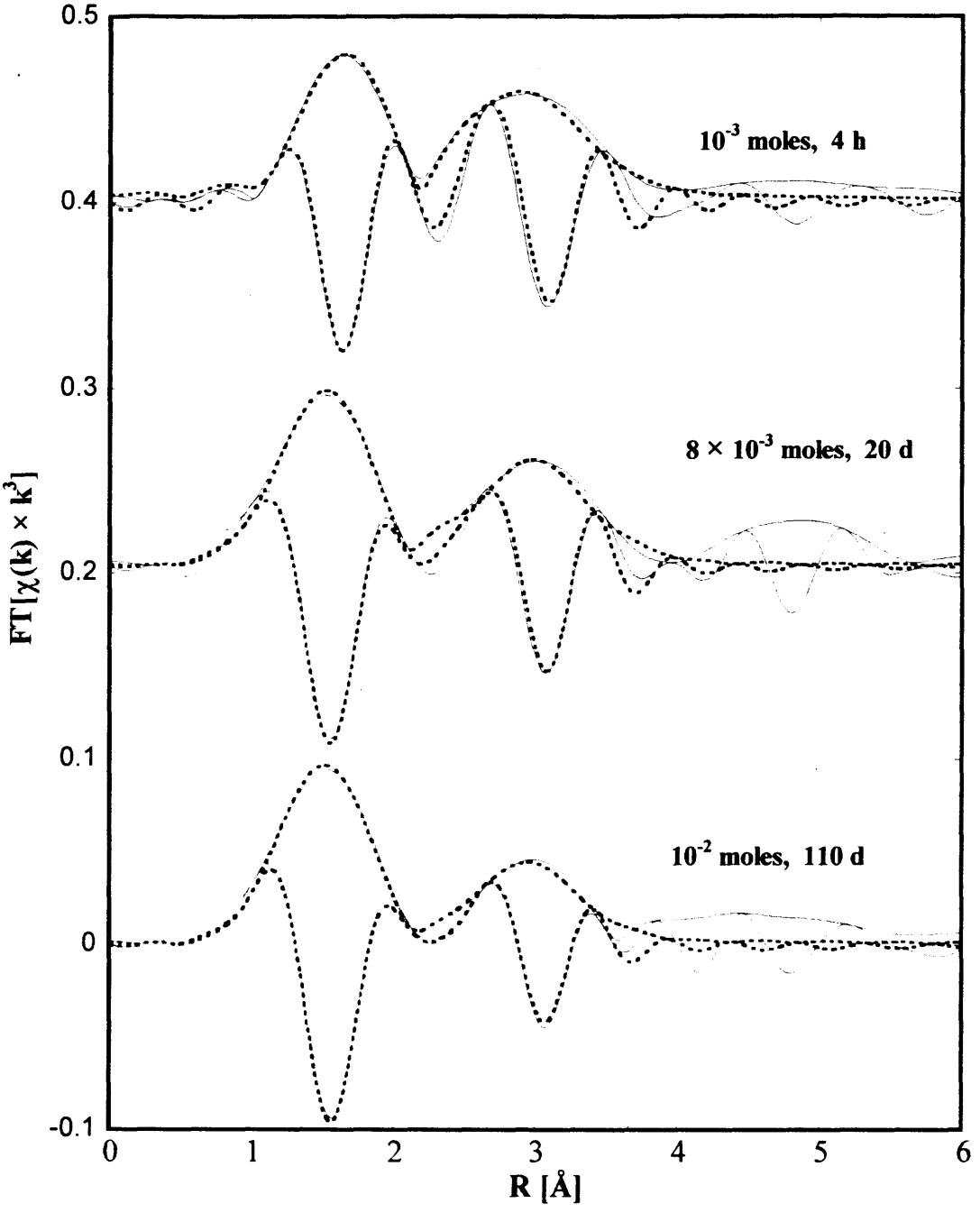

These oxygens are most likely contributing from the HMO surface. Surface precipitation of Ni is excluded since there was no evidence of Ni in the second shell. Similarly, second shell fits with Mn atoms revealed no plausible fits. Thus, Ni sorption to HMO can be best described as an outer sphere mechanism, which is independent of pH and adsorbate concentration. Figure 59 also presents the effect of reaction time on nickel adsorption to HMO. Fits (Table 15) show that the local structure of Ni did not change between 4 h and 110 days; thus eliminating the possibility of precipitation, polymerization, or coprecipitation. The continuous adsorption as a function of time is consistent with intraparticle surface diffusion. Therefore, these internal adsorption sites constituting as much as 98% of the total sorbed are no different from the external ones. This study supports macroscopic results (See Chapter 5). Other spectroscopic studies that support intraparticle diffusion as the rate limiting sorption mechanism in microporous oxides include: As(V) sorption to ferrihydrite (Waychunas et al et al., 1993); Cd and Se(IV) to alumina (Papelis, 1995); Sr sorption to HFO (Axe et al., 1998) and HMO (Axe et al., 2000); Pb sorption to aluminum oxide (Strawn et al.1998); and Cu and Pb sorption to ferrihydrite (Scheinost et al., 2000).

On the other hand, Sparks and coworkers (Scheidegger et al., 1996, 1998; Ford et al., 1999; Scheinost et al., 1999: Elzinga and Sparks, 1999) found from extensive kinetic studies of Ni sorption to clays including pyrophyllite, gibbsite, montmorillonite, talc, silica, and pyrophyllite-montmorillonite mixtures that Ni forms a coprecipitate phase with Al known as Ni-Al layered double hydroxide (LDH). In such precipitates, the second shell is generally a result of contributions from Ni at 3.05-3.06 Å and Al at 3.06-3.12 Å with Ni/Al coordination ratios ranging 1-3 depending upon the initial conditions.

The striking similarity in the local structures of Ni^{2+} and Zn^{2+} sorbed to HMO as a function of pH, adsorbate concentration, and reaction time confirms that a group of from the Periodic Table form similar adsorption complexes with HMO. A comparison of Sr sorption to HMO with Ni and Zn sorption to HMO also confirms the higher affinity of transition metals for adsorbents.

7.7 Summary of XAS Studies

The above spectroscopic work demonstrates that the divalent transition metal ions such as Ni and Zn are sorbed to amorphous manganese oxides such as HMO as fully hydrated ions and are attached to the oxide surface through physical forces. Absence of contributions from Mn atoms in the second shell suggests a highly disordered outer sphere type of adsorption mechanism that is independent of pH and adsorbate concentration. Additionally, there is no evidence for the formation of polynuclear complexes or any well-ordered precipitates of these adsorbates. Strong similarities in the local structures of Ni and Zn sorbed to HMO suggest that a group of metals from the Periodic Table exhibit similar adsorption behavior. Furthermore, the XAS analyses of the long-term samples support that sorption of these divalent metal ions is limited by intraparticle diffusion, where the sites located along the micropore walls are no different from those on the external surface. This research substantiates the need to include surface diffusion in estimating the bioavailability and mobility of the metal contaminants in soils and sediments.

Likewise based on the spectroscopic evidence, the Zn ion is physically sorbed to amorphous oxides such as HFO where it retains its hydration shell upon adsorption.

Absence of Zn contributions in the second shell rules out the possibility of formation of polynuclear complexes or any well-ordered zinc precipitates. Absence of contributions from Fe in the HFO systems suggests an outer sphere type of adsorption mechanism that is independent of pH and adsorbate concentration. Similarly, the local structure from the coprecipitate sample suggests that Zn is only physically sorbed in the micropores of amorphous HFO and does not appear to form any solid solution with ferric ions. On the other hand, zinc ions form strongly bonded mononuclear adsorption complexes with goethite where they do not retain their octahedral hydration shell. Overall, the results presented in this paper demonstrate that even though the local structure of HFO and goethite are found to have similarities (Spadini et al., 1994), they do not exhibit similar sorption properties. HFO is viewed as a mosaic of short octahedral chains resulting in larger sorption capacity than goethite. Most importantly, this research aids in selection of mechanistic models for describing the fate of zinc and nickel in soils and sediments that are rich in oxides.

CHAPTER 8

CONCLUSIONS AND FUTURE WORK

Hydrated oxides of Al, Fe, and Mn are prevalent in soils and sediments as discrete particles or as coatings. These microporous oxides have large surface areas and high affinity for metal ions, and hence they act as both a sink and a source for anthropogenically released metal contaminants. To understand their associated risks to the environment and to develop effective waste management programs, mechanistic models are needed to accurately predict their fate in soils and sediments.

To achieve this objective, sorption of Sr, Cd, Zn, Ni, and Ca to amorphous oxides were studied with short- and long-term experiments, as a function of pH, ionic strength, concentration, temperature, and reaction time. Results from these macroscopic experiments were complemented with the XAS studies. This chapter summarizes all the experimental and modeling results. Additionally, questions that would lead to more hypotheses and hence future research are also briefly proposed here.

Characterization studies showed that amorphous oxides of aluminum, iron, and manganese oxides have large surface areas and are microporous. As such, intraparticle diffusion is the rate limiting mechanism in the sorption process. On the other hand, even though crystalline oxides such as goethite are also microporous, their porosity is much smaller than that of amorphous oxides. As a result, metal sorption occurs on external (or macropore) surfaces. A comparison of potentiometric titrations of HFO and goethite shows that the surface charge density of HFO is as much as 10 times that of goethite suggesting that HFO has a much greater adsorption capacity. This difference in site capacity was demonstrated in isotherms, where the HFO density was over three orders of

magnitude greater than that for goethite. Furthermore, a correlation was developed relating site capacity (C_t) and surface charge density.

Macroscopic studies in combination with the XAS investigations suggest that the sorption of divalent metal ions to amorphous oxides is a two-step process: rapid adsorption to the external surface followed by slow intraparticle (surface) diffusion along the micropore walls. Adsorption is an endothermic physical reaction and can be represented by one average mechanism that is independent of pH and adsorbate concentration. Based on enthalpies, XAS, and the effect of ionic strength, the sorbed ions retain their primary hydration shell in forming an outer sphere adsorption complex. A second correlation was developed relating adsorption enthalpies ($\Delta H°$) and their structural parameters: the primary hydration number (N) and the hydrated radius (R_H).

On the other hand, metal ions chemically sorb to the goethite surface to form mononuclear inner sphere complexes. Although goethite may show a higher affinity for metal ions than HFO, their site capacity is much smaller than that of HFO. Macroscopic analyses disclosed two sets of adsorption sites on the goethite surface: a small set of high affinity sites available to transition metal ions and a large set of low affinity sites to which only alkaline earth metals such as Ca bind. This limited availability of high affinity sites induces competitive adsorption in a binary system of Ni and Zn, which was accurately described with the single-site Langmuir model. In contrast, no competition was observed in binary systems composed of one alkaline earth metal (Ca) and one transition metal (Ni or Zn). If Ni and Zn ions compete for the same type of sites, they may have similar local structures when sorbed to goethite. Therefore, the local structures of transition metals such as Ni and Zn sorbed to the goethite surface could be compared

with each other and with the local structure of an alkaline earth metal, Ca. Additionally to further demonstrate that sorption of Zn and Ni ions is not affected by the presence of Ca ions, the local structures of these metal ions could be studied with the help of XAS in the presence of Ca and compared to their local structures in single adsorbate systems.

The transient long-term studies demonstrated surface diffusion (the second step) as the rate-limiting mechanism where the internal surfaces accounted for as much as 90% of the total sites. XAS investigations of long-term (intraparticle diffusion) studies revealed that the local structure of metal ions sorbed to amorphous oxides do not change with time suggesting that the adsorption mechanism on the micropore walls is similar to the one on the external surface. Modeling results revealed surface diffusivities ranged from 10^{-16} to 10^{-10} cm^2 s^{-1}. Based on these surface diffusivities, sorption of metal ions to these microporous oxides may take a few days to few years to reach equilibrium. Based on the site activation theory, the surface diffusivities (D_s) can be estimated knowing the activation energy (E_A) and the site capacity (C_t). From Polanyi relation, this E_A is linearly related to $\Delta H°$ through a proportionality constant α. This E_A for a specific metal is comparable for HAO, HFO, and HMO. Likewise, one average value of α was found for a group of metals from the Periodic Table, suggesting similar sorption complexes. Strong similarities in the local structure of Ni and Zn ions sorbed to HMO fortify this hypothesis. Interestingly, no significant diffusion of metals ions was observed with goethite.

A combination of site density and thermodynamic studies suggests that site densities are a function of temperature. This phenomenon is already observed in this research for goethite (Table 11 Chapter 6). Hence the correlation developed here for predicting site density can be modified to include the effects of temperature. This

correlation would allow a transport model to account for effects of seasonal variations in aquatic systems. Correspondingly, it would also be interesting to validate diffusivities as a function of temperature. Soils and sediments are affected by naturally occurring organic compounds such as humic acids as well as anthropogenically released toxic compounds such as TCE, benzene, other aromatic and chlorinated compounds. In such systems, how is intraparticle diffusion effected, is competitive diffusion possible between the organics and the metal contaminants? Again, are all the sites located along the micropore walls of the amorphous oxides available? To answer these and questions, transient studies for metal contaminants sorbing to oxides must be conducted in the presence of environmentally important organic compounds. Similar to the divalent metal ions, is it possible to predict the adsorption of other multivalent metal ions such as uranium, cesium, chromium, arsenic, and selenium? Temperature studies may be useful in demonstrating the validity of the correlations developed in the current research for divalent ions.

Hydrous metal oxides occur in nature as either discrete particles and as coatings on other mineral surfaces. This research has established a baseline for understanding sorption mechanisms to the discrete oxide particles. As a result, the next step is to evaluate these oxides as coatings, where sorption can be studied macroscopically and spectroscopically. Also, it would be useful to test the correlations developed for the discrete particles in this research and assess whether they are applicable to the oxide coatings as well. Prior to sorption studies, it would be important to study the mineralogy and characteristics of these oxides in the presence of other minerals. It is equally important to assess their mineralogy in the presence of metal adsorbates, as a function of

pH, adsorbate loading, and time. Natural soils and sediments are generally a mixture of various oxides. In such systems is the total adsorption capacity a function of the site capacities of the individual oxides? Can the fate of metal ions be predicted in mixed oxide systems based on the single oxide studies?

Overall this research renders an insight into the mechanisms by which hydrated metal oxides control the partitioning and the bioavailability of metal contaminants. This study provides methods that can accurately predict important transport and thermodynamic parameters for describing the fate of metal pollutants in soils and sediments abundant in HAO, HFO, and HMO.

APPENDIX A

SOLUBILITY AND SPECIATION DIAGRAMS FOR CA, CD, NI, ZN, AND SR

Calcium speciation in 5×10^{-4} M $Ca(NO_3)_2$ aqueous solution at 298 K

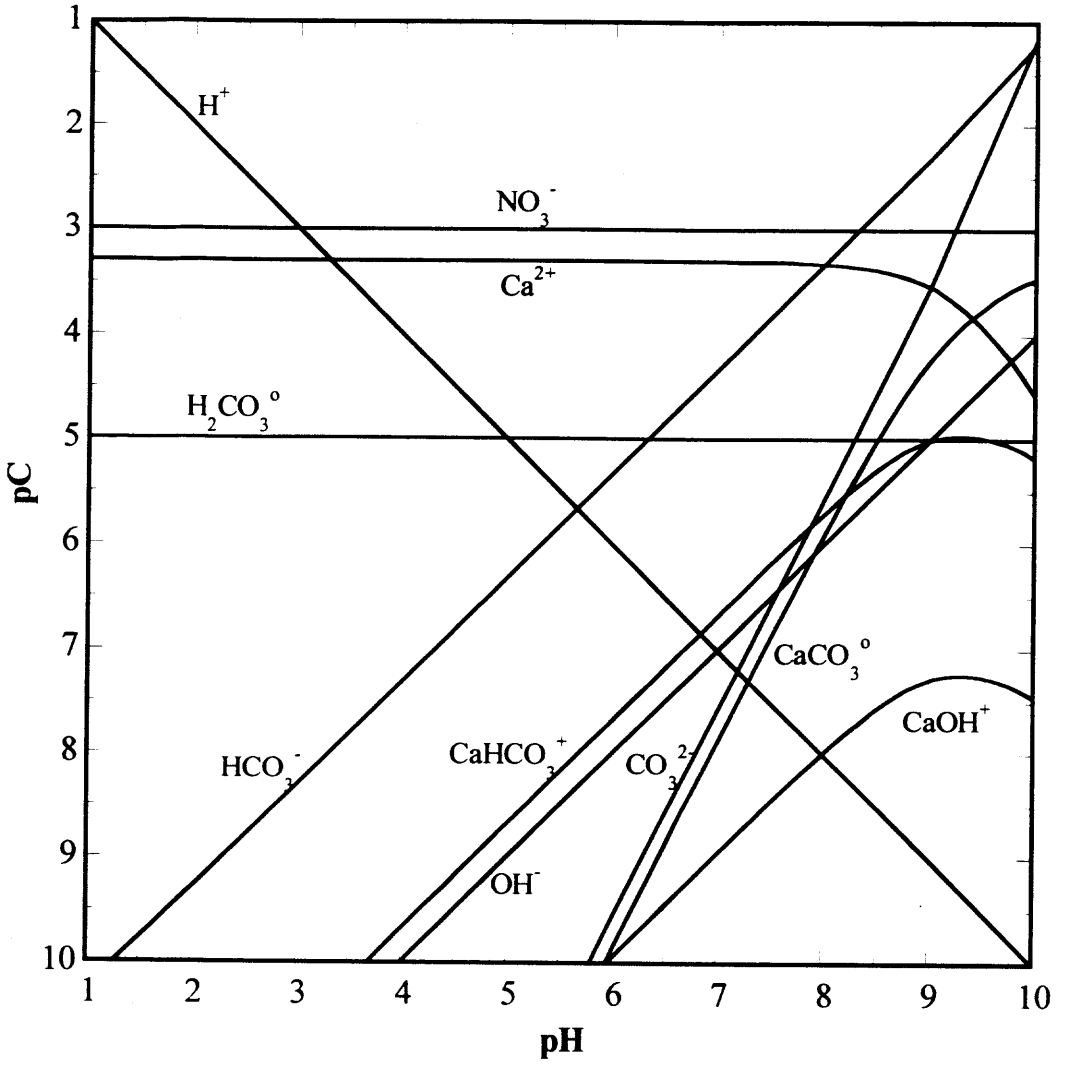

Calcium solubility diagram in open system conditions at 298 K

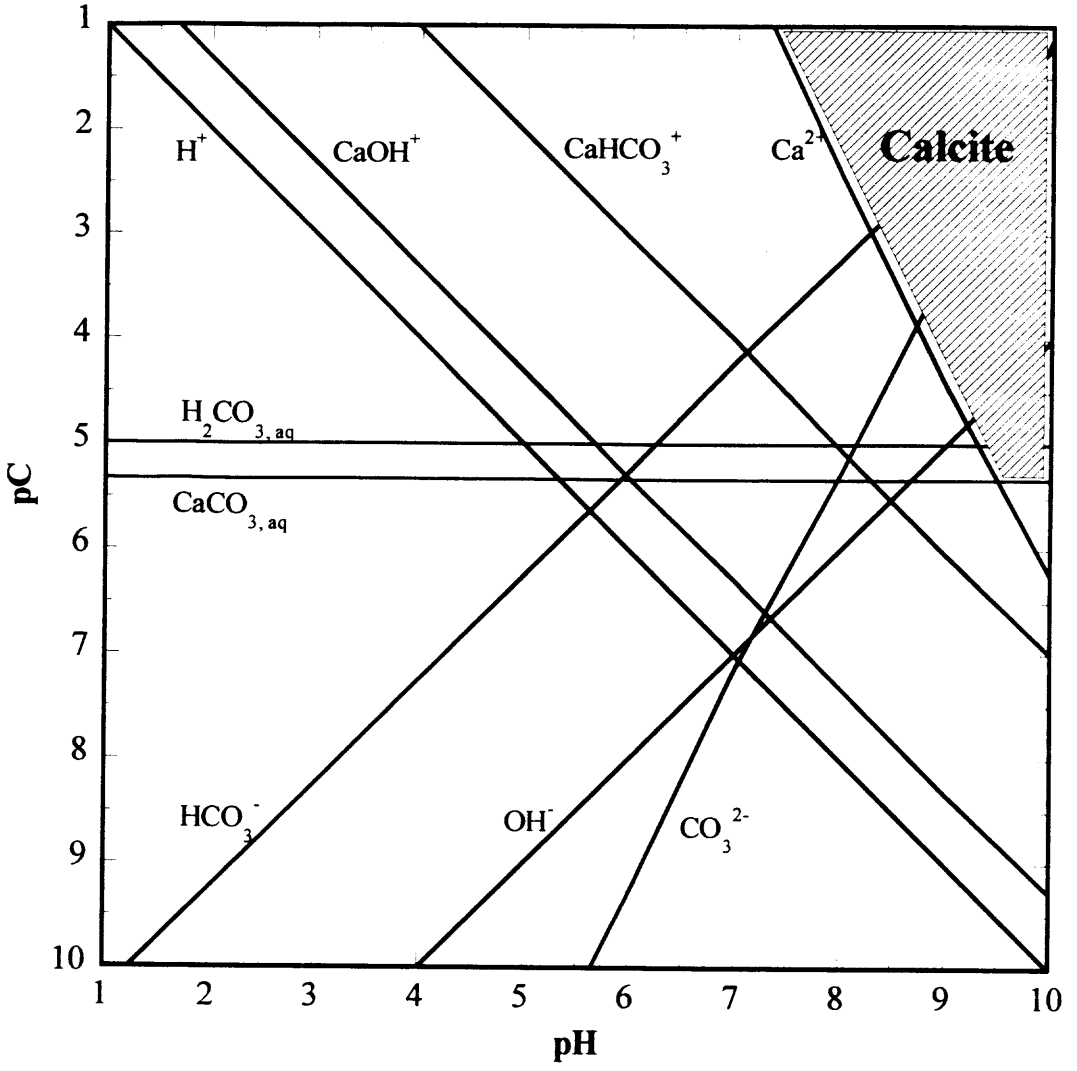

Cadmium speciation in 5×10^{-6} M $Cd(NO_3)_2$ aqueous solution at 298 K.

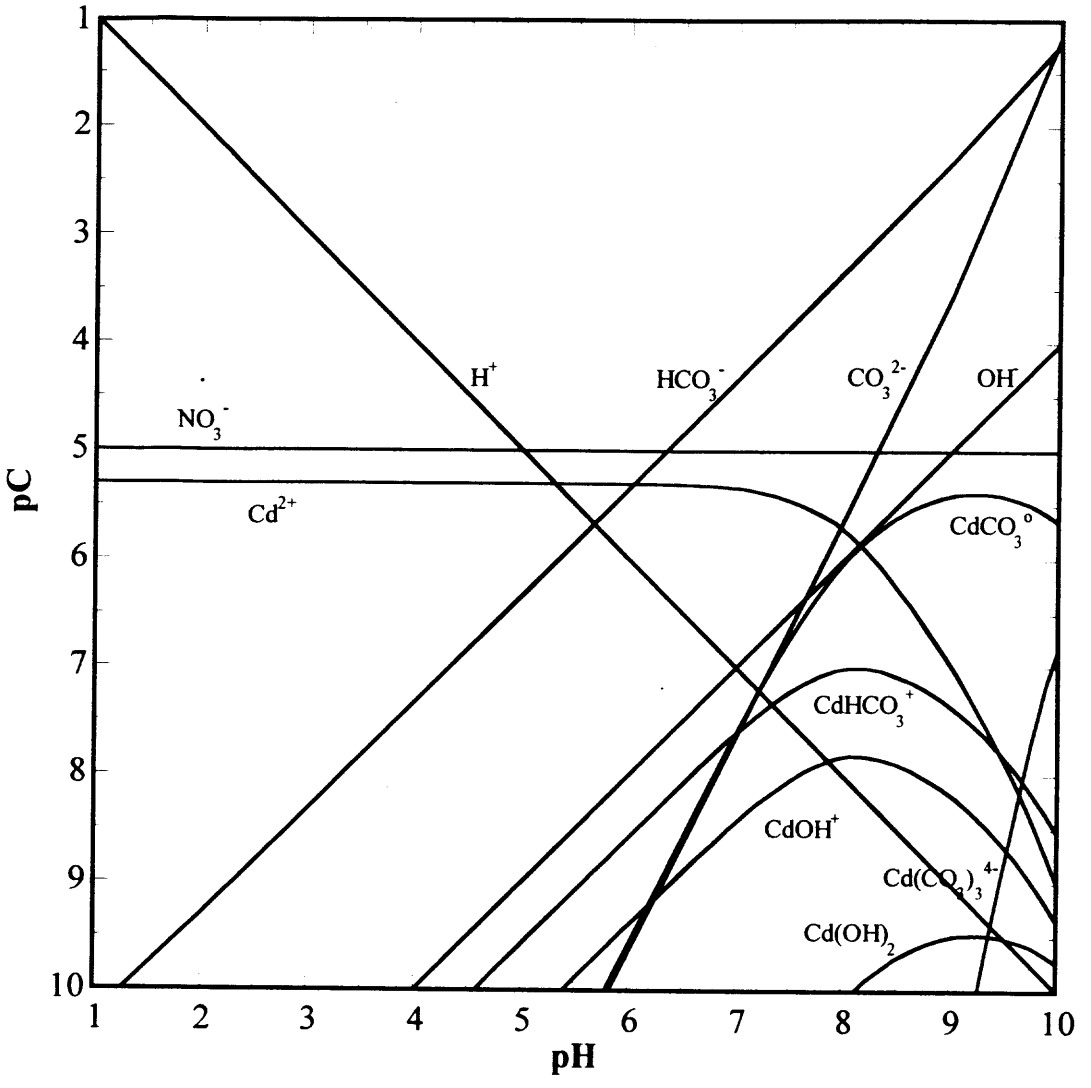

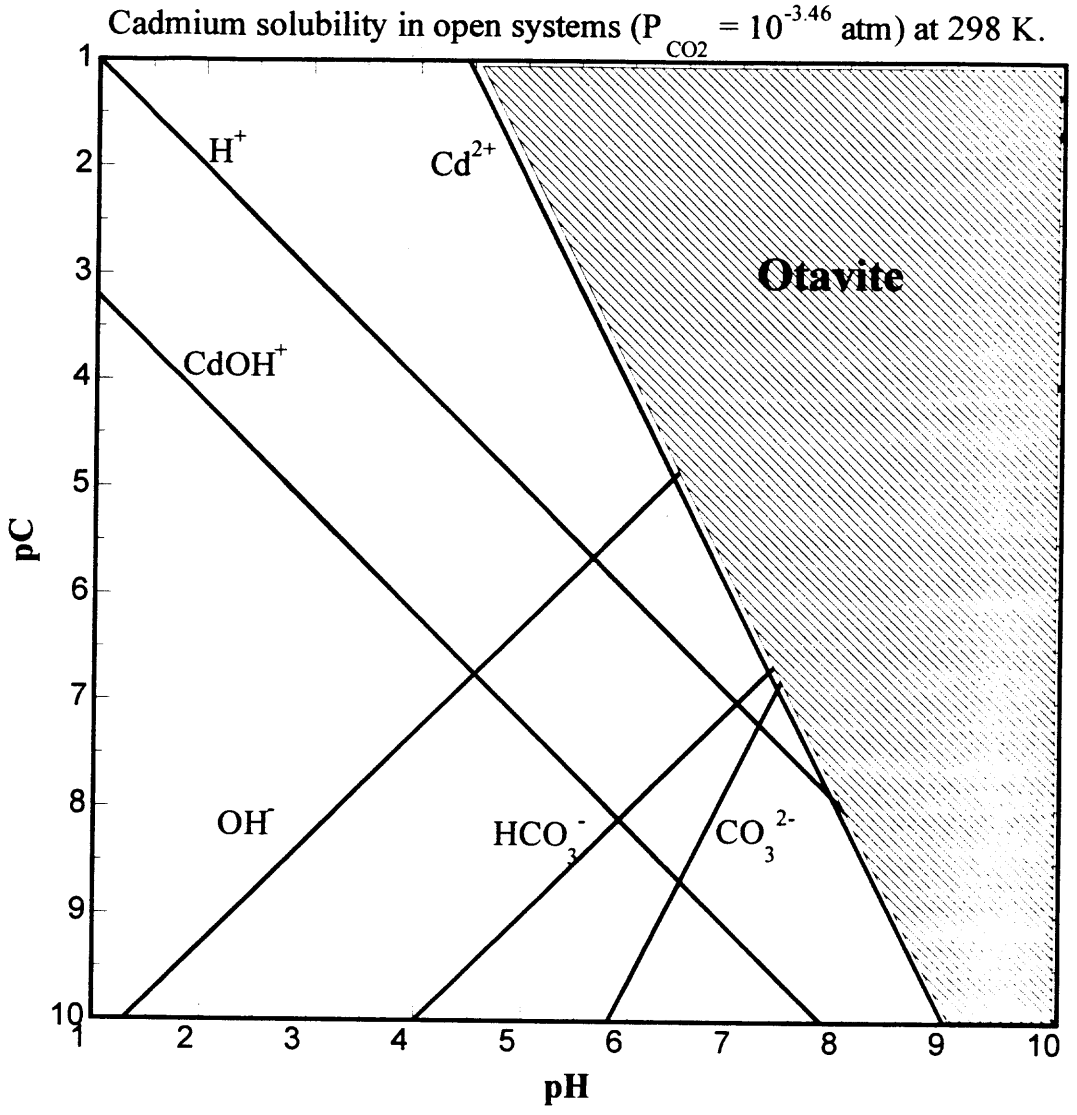
Cadmium solubility in open systems ($P_{CO2} = 10^{-3.46}$ atm) at 298 K.
pC
pH
1
2
3
4
5
6
7
8
9
10
H^+
Cd^{2+}
Otavite
$CdOH^+$
OH^-
HCO_3^-
CO_3^{2-}

Nickel speciation in 5×10^{-6} M $Ni(NO_3)_2$ aqueous solution at 298 K.

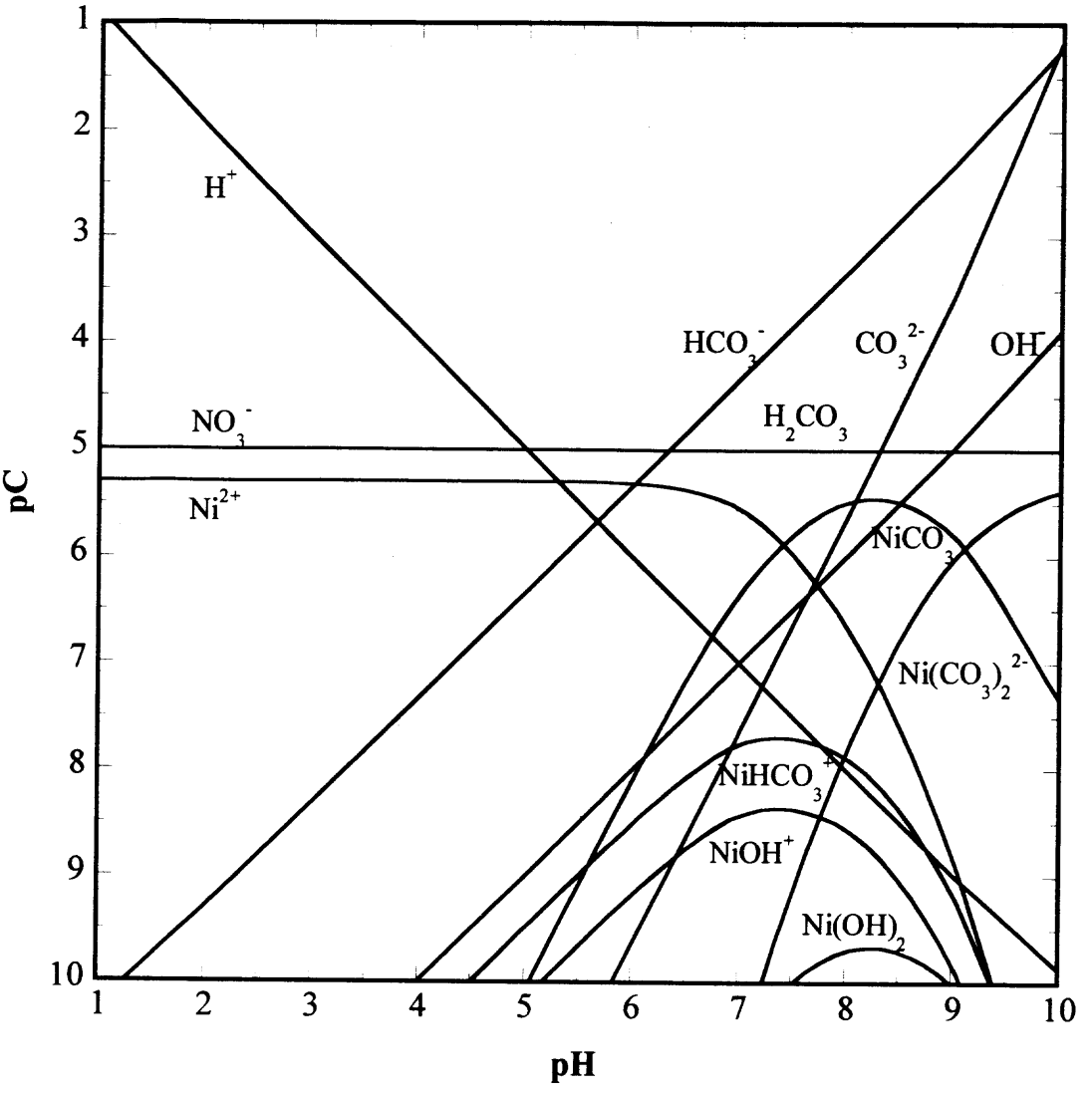

Ni solubility in open system ($P_{CO2} = 10^{-3.46}$ atm) at 298 K

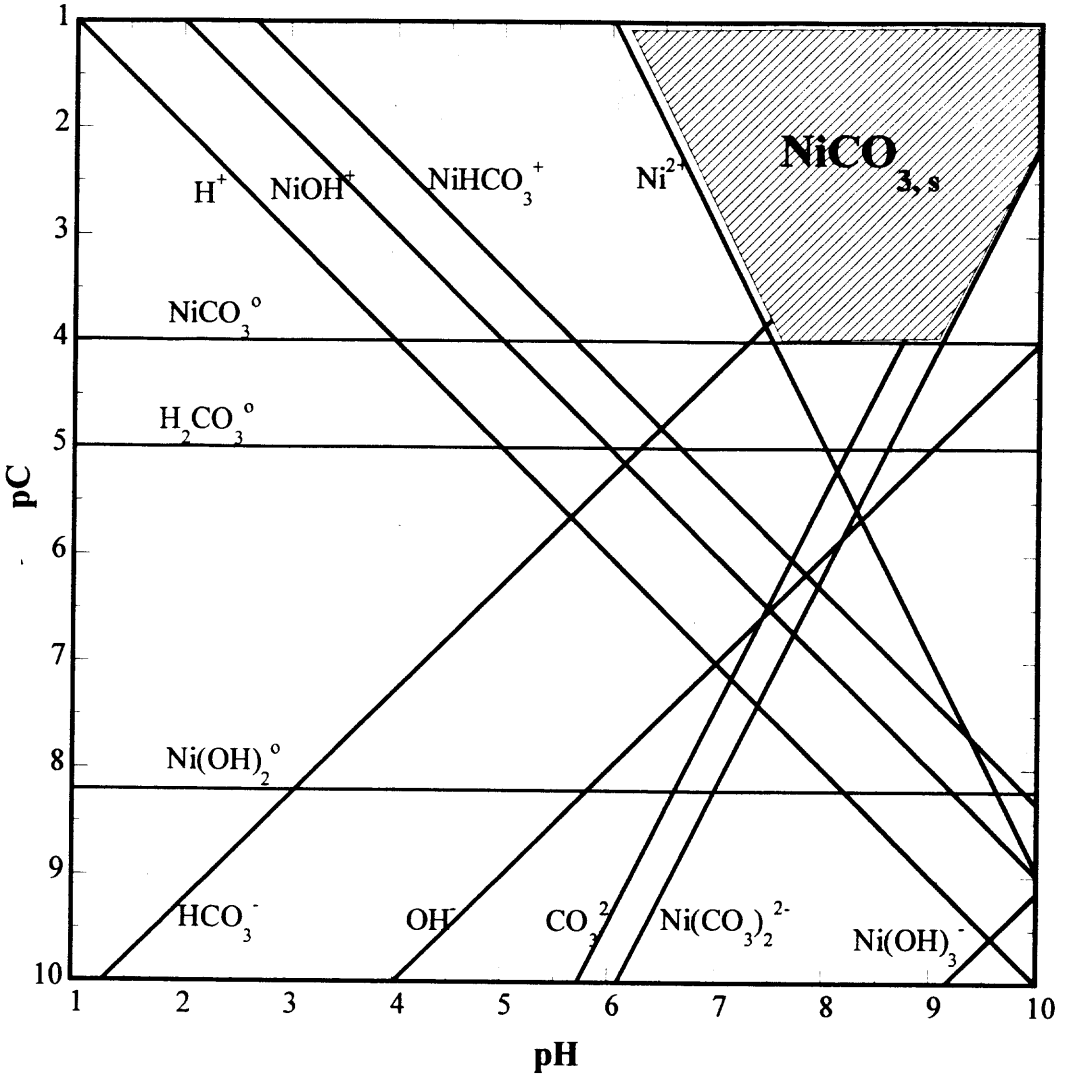

Strontium speciation in 5×10^{-4} M $Sr(NO_3)_2$ aqueous solution at 298 K.

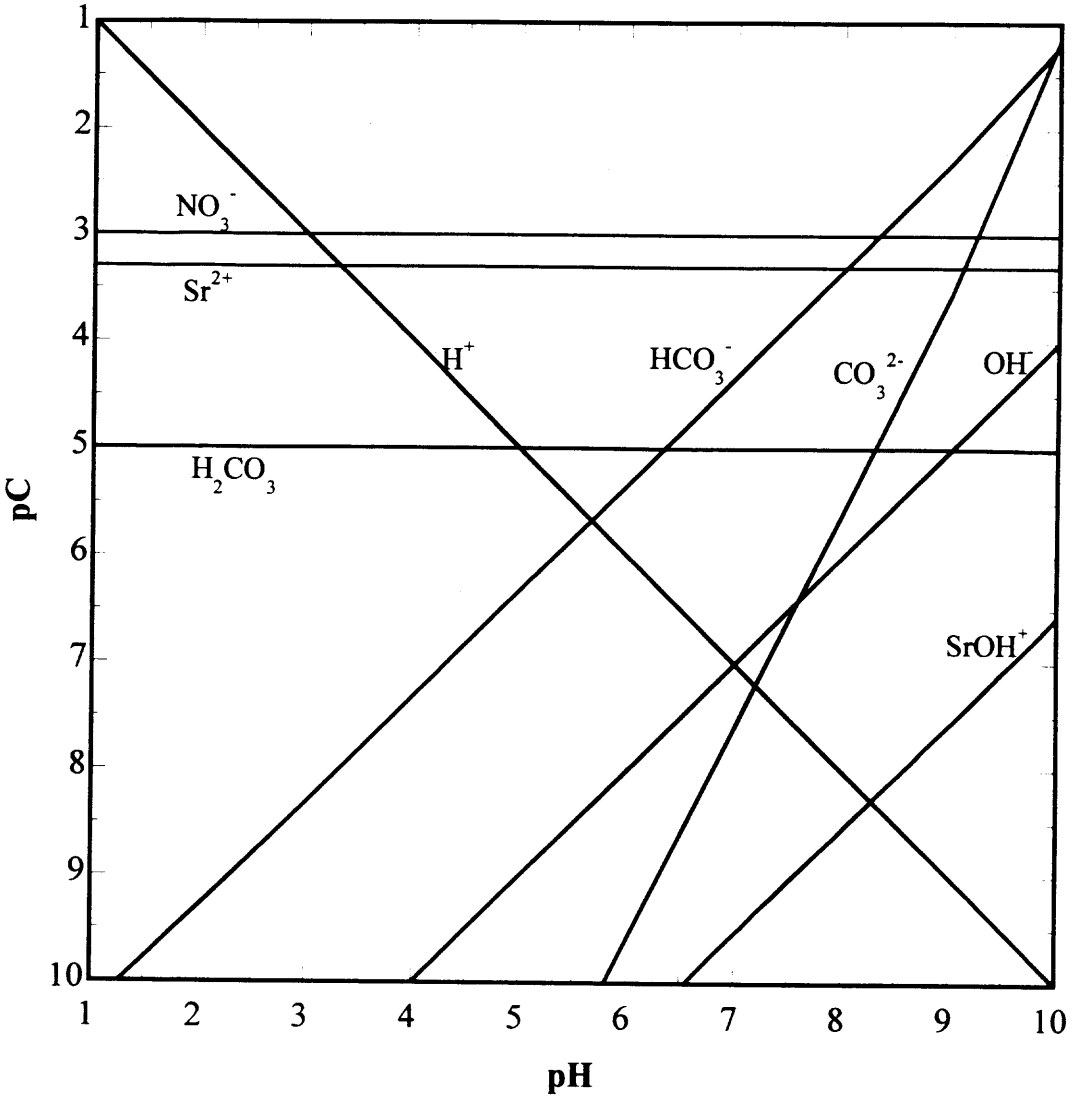

Strontium solubility in open system ($P_{CO2} = 10^{-3.46}$ atm) at 298 K.

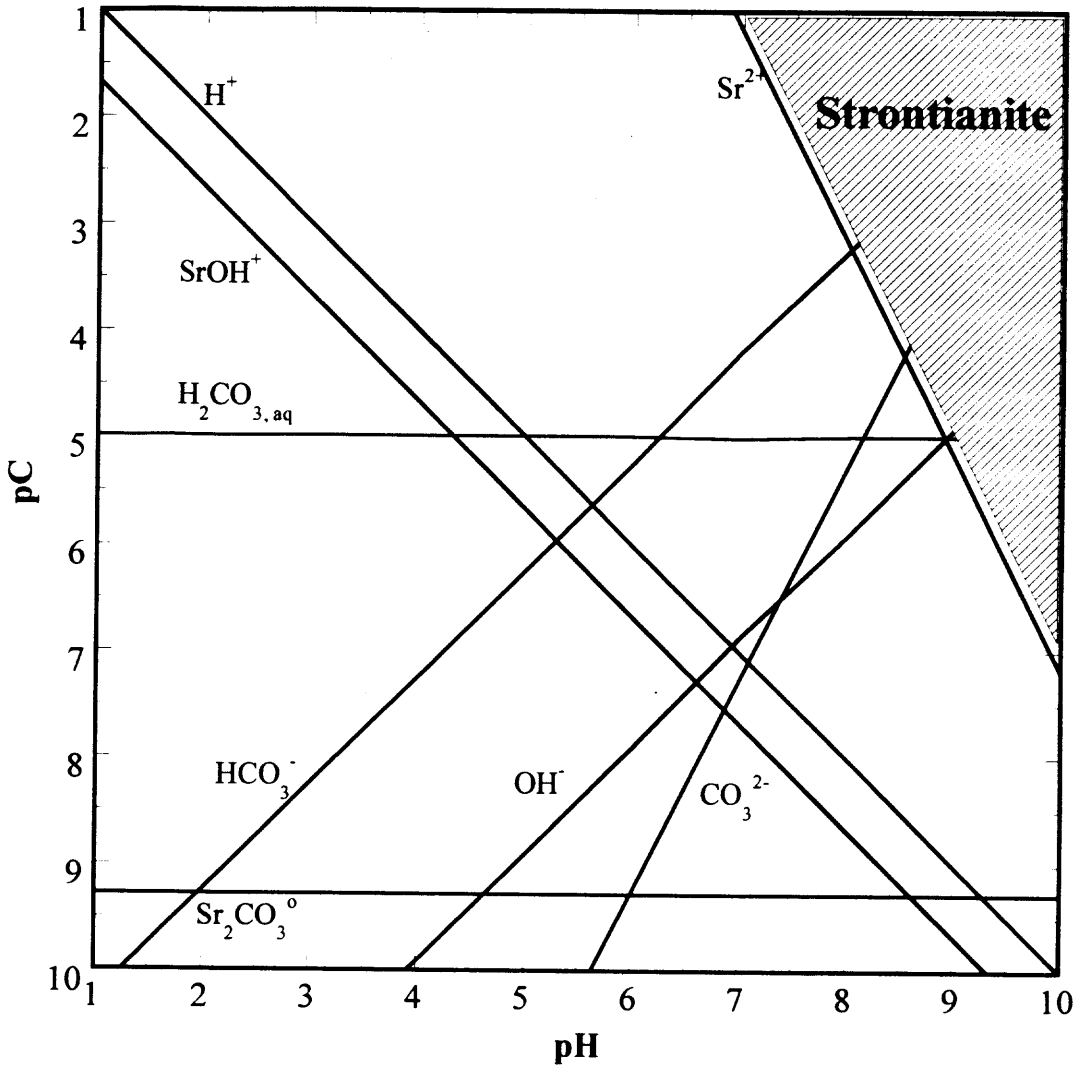

Zinc speciation in 5×10^{-7} m $Zn(NO_3)_2$ aqueous solution at 298 K.

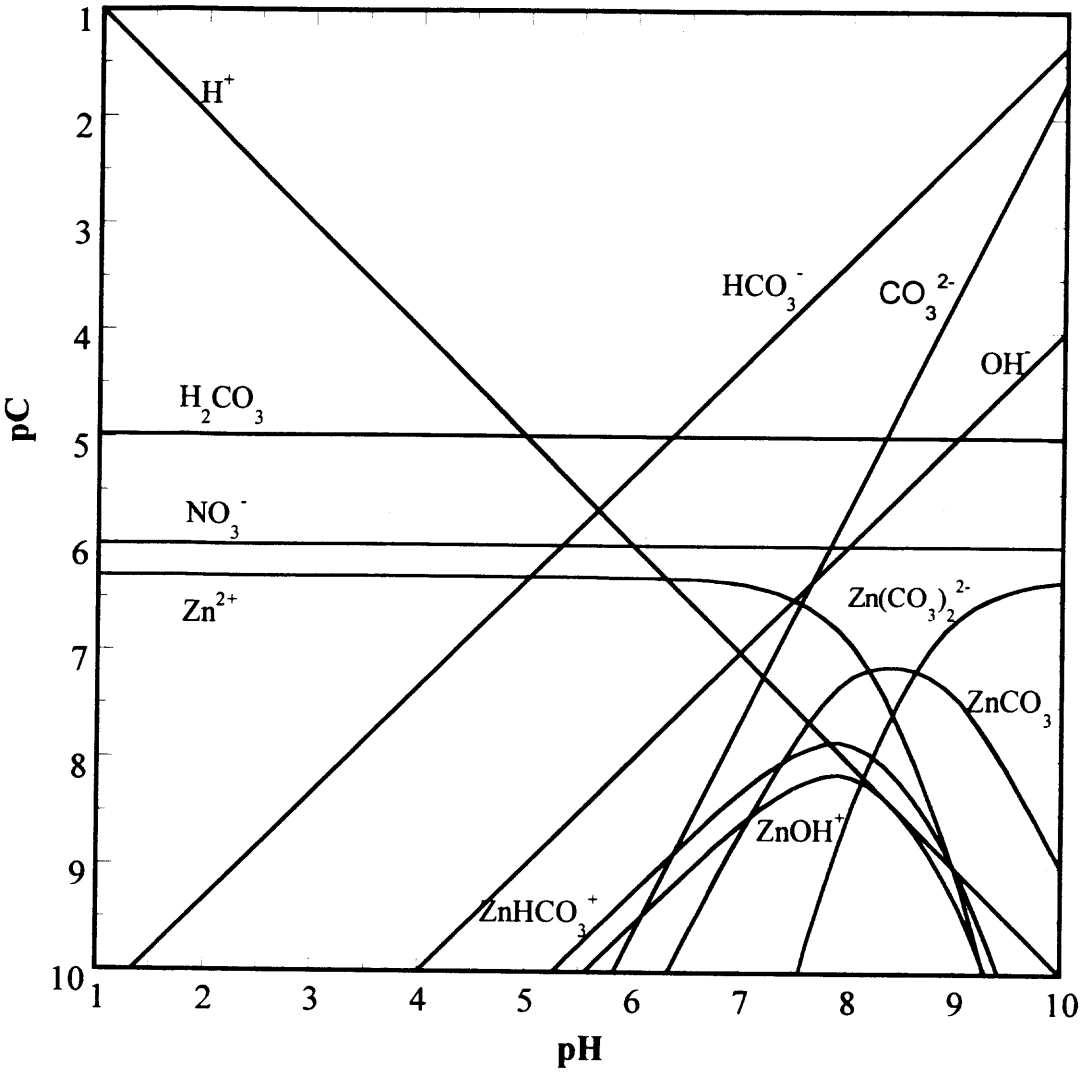

Zn solubility in open system ($P_{CO2} = 10^{-3.46}$ atm) at 298 K.

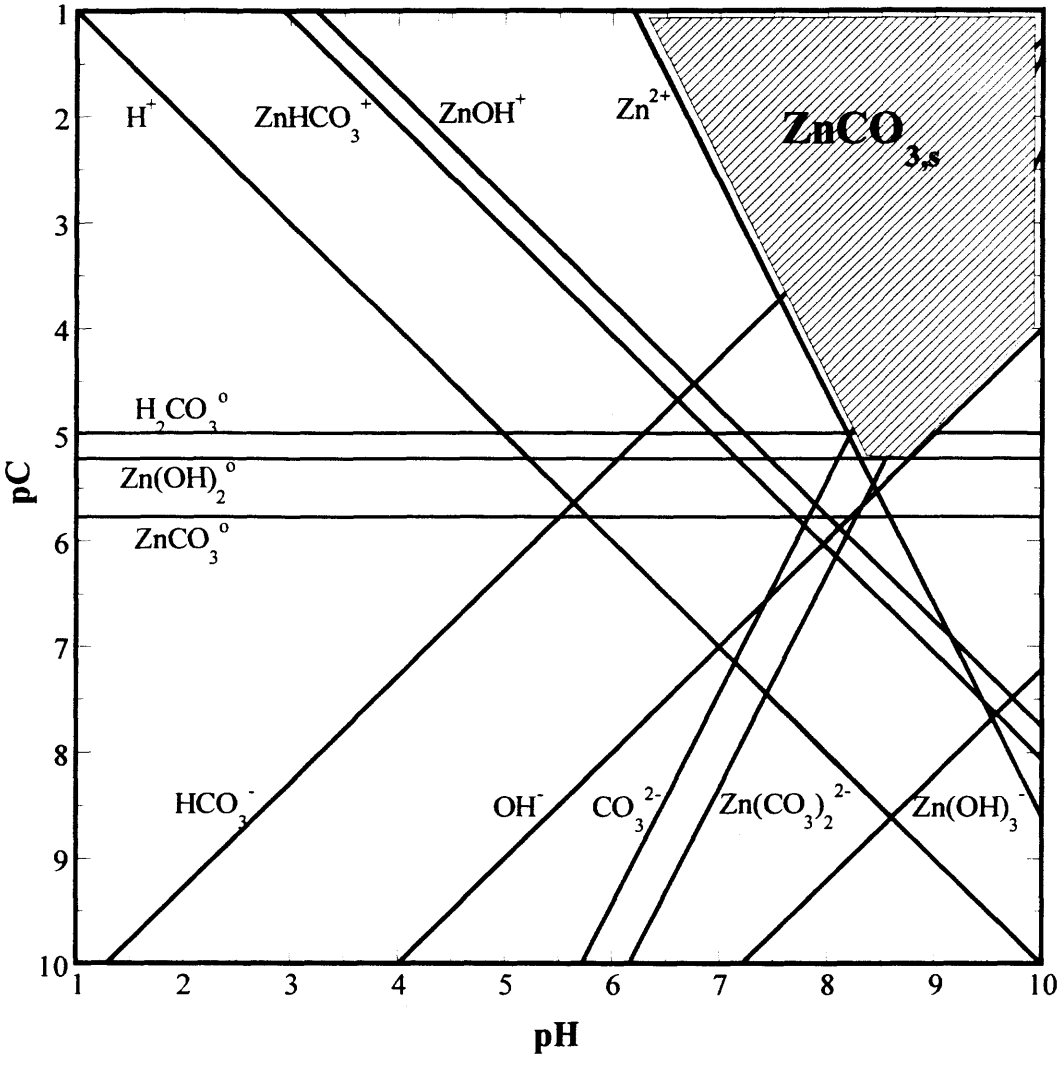

APPENDIX B

CHARACTERIZATION OF HYDRATED METAL OXIDES

Pore size distribution of freeze-dried goethite from N_2 desorption method (IGT Report, 1999)

Pore R (μm)	Cum. Pore Vol. (ml/g-μm)	dV/dR	Pore Dia. (μm)	Cum. Pore Vol. (ml/g-μm)	dV/dD
1.12E-01	1.63E-03	1.31E-02	2.24E-01	1.63E-03	6.54E-03
1.03E-01	1.51E-03	1.19E-02	2.05E-01	1.51E-03	5.93E-03
9.60E-02	1.43E-03	1.12E-02	1.92E-01	1.43E-03	5.60E-03
9.01E-02	1.36E-03	1.15E-02	1.80E-01	1.36E-03	5.73E-03
8.20E-02	1.27E-03	1.12E-02	1.64E-01	1.27E-03	5.62E-03
7.38E-02	1.18E-03	1.26E-02	1.48E-01	1.18E-03	6.29E-03
6.26E-02	1.04E-03	1.00E-03	1.25E-01	1.04E-03	5.00E-04
5.96E-02	1.03E-03	7.87E-03	1.19E-01	1.03E-03	3.94E-03
5.41E-02	9.90E-04	5.95E-03	1.08E-01	9.90E-04	2.98E-03
4.82E-02	9.55E-04	9.91E-03	9.63E-02	9.55E-04	4.96E-03
3.77E-02	8.51E-04	2.80E-03	7.54E-02	8.51E-04	1.40E-03
2.98E-02	8.29E-04	2.06E-03	5.96E-02	8.29E-04	1.03E-03
2.06E-02	8.10E-04	3.69E-02	4.12E-02	8.10E-04	1.84E-02
5.72E-03	2.61E-04	6.54E-02	1.14E-02	2.61E-04	3.27E-02
1.88E-03	1.00E-05	4.75E-03	3.76E-03	1.00E-05	2.38E-03
1.25E-03	7.00E-06	0.00E+00	2.50E-03	7.00E-06	0.00E+00
1.05E-03	7.00E-06	7.37E-02	2.10E-03	7.00E-06	3.68E-02
9.53E-04	0.00E+00	0.00E+00	1.91E-03	0.00E+00	0.00E+00

Pore size distribution of freeze-dried goethite from mercury porosimetry(IGT Report, 1999)

Pore Dia. (μm)	dV/dD
2.23E+02	0.00E+00
1.10E+02	0.00E+00
6.50E+01	2.00E-04
4.63E+01	4.00E-04
3.63E+01	1.10E-03
2.95E+01	8.00E-04
2.57E+01	2.90E-03
2.29E+01	0.00E+00
2.00E+01	2.80E-03
1.81E+01	2.80E-03
1.63E+01	0.00E+00
1.48E+01	5.40E-03
1.38E+01	5.40E-03
1.29E+01	3.10E-03
1.21E+01	1.31E-02
1.13E+01	6.50E-03
1.06E+01	4.20E-03
1.00E+01	1.42E-02
9.52E+00	1.06E-02
9.02E+00	5.50E-03
8.58E+00	1.86E-02
8.20E+00	1.42E-02
7.81E+00	2.11E-02
7.50E+00	1.77E-02
7.20E+00	9.10E-03

5.79E+00	1.36E-02
5.29E+00	2.17E-02
4.50E+00	2.44E-02
4.10E+00	2.69E-02
3.61E+00	2.80E-02
3.23E+00	2.84E-02
2.74E+00	3.37E-02
2.35E+00	3.50E-02
2.08E+00	3.04E-02
1.91E+00	6.25E-02
1.71E+00	2.76E-02
1.52E+00	5.86E-02
1.34E+00	4.54E-02
1.21E+00	4.07E-02
1.08E+00	6.67E-02
9.79E-01	7.76E-02
8.58E-01	4.52E-02
7.94E-01	1.28E-01
7.36E-01	4.70E-02
6.88E-01	2.30E-01
6.31E-01	9.48E-02
5.92E-01	6.97E-02
5.57E-01	7.89E-02
5.28E-01	2.80E-01
4.92E-01	7.61E-02
4.65E-01	1.03E-01
4.43E-01	2.40E-01
4.19E-01	2.32E-01
3.93E-01	1.04E-01
3.75E-01	1.53E-01
3.57E-01	1.54E-01
3.23E-01	3.18E-01
2.99E-01	2.28E-01
2.73E-01	2.16E-01
2.56E-01	4.71E-01
2.25E-01	3.53E-01
2.00E-01	5.39E-01
1.80E-01	2.70E-01
1.21E-01	1.12E+00
9.05E-02	2.44E+00
7.24E-02	7.67E+00
6.04E-02	6.61E+00
5.17E-02	4.39E+00
4.53E-02	2.98E+00
3.63E-02	1.82E+00
3.03E-02	9.07E-01
2.27E-02	1.44E+00
1.82E-02	1.21E+00
1.21E-02	9.02E-01
9.09E-03	4.51E+00
7.27E-03	7.51E+00

Pore size distributions of freeze-dried HAO N_2 desorption method (IGT Report, 1995)

HAO		
Pore Dia.	Cum. Pore Vol. (ml/g-μm)	dV/dD
962.03	31.01	0.07
653.94	30.98	0.20
495.14	30.95	0.30
398.81	30.92	0.24
311.18	30.90	0.79
229.27	30.84	1.25
180.45	30.78	1.74
149.45	30.72	2.89
127.62	30.66	3.25
111.31	30.61	3.69
94.22	30.54	8.90
77.02	30.39	14.50
64.94	30.21	25.00
56.15	30.00	39.39
49.40	29.73	55.55
43.97	29.43	89.24
39.58	29.04	501.70
35.71	27.09	1790.99
32.22	20.85	1377.14
29.19	16.67	1011.64
26.30	13.75	1475.66
23.70	9.92	1258.16
21.40	7.02	327.96

Particle size distributions of HAO, HFO (Axe and Anderson, 1995), and HMO

D (μm)	HMO pH 5	HMO pH 7	HAO pH 7	HAO pH 8	D (μm)	R (μm)	HFO pH 7
0.50	0.00	0.07	0.00	0.00	2.16	1.08	0.39
1.32	0.18	0.32	0.00	0.00	2.51	1.25	0.60
1.60	0.36	0.53	0.00	0.00	2.91	1.45	0.59
1.95	0.53	0.68	0.02	0.01	3.37	1.69	1.21
2.38	0.68	0.82	0.04	0.03	3.91	1.96	1.89
2.90	0.82	1.02	0.07	0.05	4.54	2.27	2.71
3.53	1.02	1.41	0.09	0.07	5.27	2.63	4.50
4.30	1.39	2.14	0.11	0.09	6.11	3.06	5.21
5.24	2.09	3.31	0.14	0.14	7.09	3.54	2.00
6.39	3.27	4.94	0.37	0.29	8.23	4.11	1.12
7.78	5.02	6.96	0.75	0.67	9.54	4.77	1.67
9.48	7.23	9.08	2.14	1.52	11.07	5.54	1.49
11.55	9.63	10.79	3.40	2.95	12.84	6.42	1.45
14.08	11.54	11.53	5.82	5.06	14.90	7.45	1.35
17.15	12.25	10.98	8.99	7.91	17.29	8.64	1.67
20.90	11.46	9.33	12.44	11.31	20.06	10.03	1.26
25.46	9.53	7.17	15.20	14.58	23.27	11.63	2.50
31.01	7.13	5.12	16.01	16.28	26.99	13.50	0.92
37.79	4.90	3.57	14.31	15.26	31.32	15.66	0.55
46.03	3.14	2.60	10.71	11.82	36.33	18.17	0.65
56.09	1.93	2.03	6.47	7.37	42.15	21.08	0.57
68.33	1.16	1.63	2.85	3.48	48.90	24.45	0.84
83.26	0.73	1.29	0.55	0.97	56.73	28.37	1.91
101.44	0.56	0.98	0.00	0.00	65.82	32.91	2.48
123.59	0.55	0.69			76.36	38.18	18.98
150.57	0.65	0.46			88.59	44.30	21.30
183.44	0.75	0.30			102.78	51.39	12.75
223.51	0.73	0.19			119.24	59.62	1.30
272.31	0.53	0.05			138.34	69.17	4.06
331.77	0.25	0.00			160.49	80.25	2.11
404.21	0.00	0.00			186.20	93.10	0.00
					200.00	100.00	0.00

Particle size distributions of goethite

	μ = 0.01				μ = 0.001		
R (μm)	pH 5	pH 6	pH 7	R (μm)	pH 5	pH 6	pH 7
0.20	1.50	0.97	0.60	0.20	2.24	1.75	1.21
0.48	5.22	3.42	2.57	0.48	8.59	6.66	4.64
0.59	7.58	4.98	3.98	0.59	12.64	10.00	6.97
0.71	7.99	5.27	4.59	0.71	13.61	10.97	7.67
0.86	6.65	4.42	4.42	0.86	11.85	9.69	6.83
1.04	4.49	3.04	3.81	1.04	8.60	7.10	5.14
1.26	2.67	1.90	3.22	1.26	5.43	4.60	3.60
1.52	1.98	1.54	3.02	1.52	3.48	3.34	2.97
1.84	2.42	2.02	3.21	1.84	2.07	3.72	3.46
2.23	3.20	2.81	3.41	2.23	2.99	5.15	4.52
2.70	3.39	3.24	3.35	2.70	3.60	6.49	5.39
3.27	3.25	3.36	3.32	3.27	4.15	7.23	5.96
3.95	3.05	3.26	3.45	3.95	4.49	7.11	6.19
4.79	2.97	3.04	3.75	4.79	4.55	6.22	6.20
5.79	3.15	2.85	4.23	5.79	4.26	4.84	6.15
7.01	3.56	2.82	4.80	7.01	3.51	3.15	6.07
8.48	4.11	3.08	5.38	8.48	2.37	1.49	5.80
10.27	4.64	3.65	5.87	10.27	1.18	0.42	5.06
12.43	4.96	4.47	6.17	12.43	0.36	0.06	3.70
15.05	4.91	5.30	6.17	15.05	0.04	0.00	1.96
18.21	4.42	5.81	5.77	18.21	0.00	0.00	0.49
22.04	3.61	5.72	4.98	22.04	0.00	0.00	0.00
26.68	2.78	5.13	3.89	26.68	0.00	0.00	0.00
32.29	2.16	4.43	2.63	32.29	0.00	0.00	0.00
39.08	1.78	3.89	1.52	39.08	0.00	0.00	0.00
47.30	1.51	3.49	0.86	47.30	0.00	0.00	0.00
57.25	1.14	3.01	0.57	57.25	0.00	0.00	0.00
69.30	0.66	2.13	0.35	69.30	0.00	0.00	0.00
83.87	0.23	0.96	0.12	83.87	0.00	0.00	0.00
101.52	0.00	0.00	0.00	101.52	0.00	0.00	0.00
122.87	0.00	0.00	0.00	122.87	0.00	0.00	0.00
148.72	0.00	0.00	0.00	148.72	0.00	0.00	0.00

Potentiometric titrations of HFO under closed system condition
For all three studies initial vol. of 0.1 N NaOH added = 13 ml

	Volume 0.1 N HNO_3 (ml)			Surface Charge density (C/g)		
pH	IS =0.031	IS = 0.31	IS = 1.50	IS =0.031	IS = 0.31	IS = 1.50
10.510	0.00			-94.209		
10.503	0.10			-93.743		
10.497	0.20			-93.200		
10.492	0.30			-92.582		
10.486	0.40			-92.028		
10.479	0.50			-91.535		
10.470	0.60			-91.167		
10.460	0.70			-90.850		
10.448	0.80			-90.643		
10.439	0.90			-90.234		
10.430	1.00			-89.813		
10.420	1.10			-89.439		
10.410	1.20			-89.052		
10.398	1.30			-88.763		
10.388	1.40			-88.347		
10.379	1.50			-87.866		
10.367	1.60			-87.530		
10.358	1.70			-87.026		
10.348	1.80			-86.562		
10.339	1.90			-86.038		
10.332	2.00			-85.410		
10.323	2.10			-84.870		
10.314	2.20			-84.322		
10.305	2.30			-83.765		
10.296	2.40			-83.199		
10.285	2.50			-82.712		
10.272	2.60			-82.295		
10.260	2.70			-81.822		
10.249	2.80			-81.296		
10.238	2.90			-80.760		
10.226	3.00			-80.250		
10.214	3.10			-79.727		
10.203	3.20			-79.157		
10.192	3.30			-78.578		
10.181	3.40			-77.988		
10.170	3.50			-77.390		
10.157	3.60			-76.846		
10.145	3.70			-76.258		
10.134	3.80			-75.630		
10.123	3.90			-74.994		

10.111	4.00	-74.378
10.098	4.10	-73.781
10.086	4.20	-73.145
10.073	4.30	-72.527
10.060	4.40	-71.899
10.046	4.50	-71.286
10.031	4.60	-70.685
10.017	4.70	-70.049
10.003	4.80	-69.402
9.991	4.90	-68.702
9.975	5.00	-68.079
9.960	5.10	-67.424
9.945	5.20	-66.758
9.931	5.30	-66.062
9.916	5.40	-65.377
9.899	5.50	-64.717
9.884	5.60	-64.012
9.868	5.70	-63.314
9.853	5.80	-62.591
9.839	5.90	-61.845
9.822	6.00	-61.135
9.801	6.10	-60.473
9.787	6.20	-59.702
9.766	6.30	-59.016
9.748	6.40	-58.279
9.736	6.50	-57.462
9.713	6.60	-56.768
9.693	6.70	-56.027
9.675	6.80	-55.256
9.655	6.90	-54.496
9.636	7.00	-53.718
9.607	7.10	-53.023
9.585	7.20	-52.251
9.565	7.30	-51.453
9.545	7.40	-50.647
9.525	7.50	-49.835
9.501	7.60	-49.044
9.476	7.70	-48.250
9.454	7.80	-47.428
9.430	7.90	-46.610
9.406	8.00	-45.785
9.382	8.10	-44.952
9.357	8.20	-44.118
9.331	8.30	-43.280

9.302	8.40	-42.449
9.279	8.50	-41.584
9.253	8.60	-40.726
9.227	8.70	-39.861
9.202	8.80	-38.988
9.168	8.90	-38.138
9.138	9.00	-37.268
9.107	9.10	-36.395
9.076	9.20	-35.515
9.046	9.30	-34.627
9.016	9.40	-33.734
8.983	9.50	-32.842
8.951	9.60	-31.943
8.921	9.70	-31.036
8.888	9.80	-30.130
8.852	9.90	-29.224
8.822	10.00	-28.305
8.787	10.10	-27.390
8.752	10.20	-26.471
8.716	10.30	-25.549
8.676	10.40	-24.629
8.639	10.50	-23.701
8.604	10.60	-22.769
8.564	10.70	-21.838
8.524	10.80	-20.905
8.474	10.90	-19.975
8.434	11.00	-19.035
8.392	11.10	-18.095
8.348	11.20	-17.153
8.304	11.30	-16.209
8.262	11.40	-15.262
8.220	11.50	-14.313
8.172	11.60	-13.365
8.133	11.70	-12.413
8.084	11.80	-11.462
8.032	11.90	-10.510
7.990	12.00	-9.555
7.945	12.10	-8.600
7.895	12.20	-7.644
7.843	12.30	-6.688
7.800	12.40	-5.730
7.750	12.50	-4.772
7.703	12.60	-3.813
7.640	12.70	-2.855

7.595	12.80	-1.894
7.535	12.90	-0.935
7.490	13.00	0.027
7.430	13.10	0.987
7.355	13.20	1.947
7.310	13.30	2.910
7.254	13.40	3.871
7.196	13.50	4.833
7.139	13.60	5.795
7.074	13.70	6.757
7.031	13.80	7.720
6.992	13.90	8.683
6.951	14.00	9.646
6.910	14.10	10.609
6.872	14.20	11.572
6.836	14.30	12.536
6.800	14.40	13.499
6.760	14.50	14.462
6.726	14.60	15.425
6.690	14.70	16.387
6.656	14.80	17.350
6.622	14.90	18.313
6.588	15.00	19.276
6.550	15.10	20.238
6.522	15.20	21.201
6.492	15.30	22.163
6.466	15.40	23.126
6.438	15.50	24.089
6.410	15.60	25.051
6.385	15.70	26.014
6.359	15.80	26.976
6.329	15.90	27.937
6.301	16.00	28.899
6.272	16.10	29.861
6.246	16.20	30.822
6.220	16.30	31.784
6.190	16.40	32.744
6.166	16.50	33.705
6.140	16.60	34.666
6.110	16.70	35.626
6.084	16.80	36.586
6.056	16.90	37.545
6.027	17.00	38.504
6.000	17.10	39.463

5.976	17.20	40.423
5.954	17.30	41.382
5.932	17.40	42.341
5.909	17.50	43.300
5.890	17.60	44.260
5.865	17.70	45.217
5.838	17.80	46.173
5.813	17.90	47.130
5.788	18.00	48.086
5.767	18.10	49.043
5.749	18.20	50.001
5.725	18.30	50.956
5.707	18.40	51.913
5.688	18.50	52.869
5.671	18.60	53.826
5.655	18.70	54.783
5.637	18.80	55.739
5.621	18.90	56.696
5.606	19.00	57.652
5.591	19.10	58.609
5.576	19.20	59.565
5.563	19.30	60.522
5.549	19.40	61.478
5.535	19.50	62.434
5.521	19.60	63.390
5.507	19.70	64.345
5.493	19.80	65.300
5.481	19.90	66.256
5.468	20.00	67.211
5.453	20.10	68.165
5.439	20.20	69.118
5.426	20.30	70.073
5.413	20.40	71.026
5.399	20.50	71.979
5.384	20.60	72.930
5.371	20.70	73.883
5.357	20.80	74.834
5.342	20.90	75.784
5.329	21.00	76.736
5.316	21.10	77.687
5.304	21.20	78.639
5.292	21.30	79.590
5.280	21.40	80.541
5.268	21.50	81.492

5.256	21.60	82.442
5.245	21.70	83.393
5.234	21.80	84.344
5.223	21.90	85.294
5.212	22.00	86.244
5.200	22.10	87.193
5.189	22.20	88.142
5.178	22.30	89.091
5.168	22.40	90.041
5.157	22.50	90.989
5.147	22.60	91.938
5.136	22.70	92.885
5.127	22.80	93.835
5.119	22.90	94.787
5.110	23.00	95.736
5.100	23.10	96.684
5.090	23.20	97.631
5.080	23.30	98.577
5.069	23.40	99.521
5.059	23.50	100.467
5.048	23.60	101.410
5.037	23.70	102.353
5.028	23.80	103.299
5.020	23.90	104.247
5.011	24.00	105.193
5.002	24.10	106.138
4.993	24.20	107.083
4.985	24.30	108.029
4.978	24.40	108.978
4.970	24.50	109.924
4.962	24.60	110.870
4.954	24.70	111.815
4.946	24.80	112.760
4.938	24.90	113.704
4.930	25.00	114.648
4.922	25.10	115.592
4.916	25.20	116.541
4.909	25.30	117.487
4.902	25.40	118.432
4.895	25.50	119.378
4.889	25.60	120.325
4.883	25.70	121.273
4.876	25.80	122.217
4.869	25.90	123.161

4.862	26.00		124.105
4.855	26.10		125.048
4.843	26.20		125.975
4.836	26.30		126.918
4.829	26.40		127.860
4.821	26.50		128.798
4.813	26.60		129.736
4.806	26.70		130.676
4.800	26.80		131.620
4.770	26.90		132.398
4.760	27.00		133.154
10.225		0.00	-109.233
10.220		0.10	-108.453
10.217		0.20	-107.599
10.213		0.30	-106.779
10.210		0.40	-105.923
10.204		0.50	-105.173
10.197		0.60	-104.455
10.190		0.70	-103.733
10.182		0.80	-103.041
10.174		0.90	-102.344
10.166		1.00	-101.642
10.157		1.10	-100.967
10.149		1.20	-100.255
10.140		1.30	-99.569
10.131		1.40	-98.877
10.121		1.50	-98.209
10.116		1.60	-97.390
10.108		1.70	-96.655
10.099		1.80	-95.944
10.091		1.90	-95.201
10.081		2.00	-94.507
10.072		2.10	-93.780
10.063		2.20	-93.049
10.054		2.30	-92.313
10.044		2.40	-91.597
10.035		2.50	-90.851
10.025		2.60	-90.124
10.014		2.70	-89.415
10.002		2.80	-88.722
9.993		2.90	-87.956
9.982		3.00	-87.228
9.972		3.10	-86.474
9.962		3.20	-85.715

9.951	3.30	-84.971
9.941	3.40	-84.203
9.930	3.50	-83.449
9.917	3.60	-82.726
9.904	3.70	-81.996
9.891	3.80	-81.259
9.879	3.90	-80.499
9.865	4.00	-79.766
9.852	4.10	-79.010
9.839	4.20	-78.247
9.824	4.30	-77.508
9.810	4.40	-76.748
9.800	4.50	-75.924
9.787	4.60	-75.139
9.773	4.70	-74.362
9.760	4.80	-73.566
9.745	4.90	-72.789
9.733	5.00	-71.971
9.717	5.10	-71.194
9.705	5.20	-70.367
9.692	5.30	-69.546
9.680	5.40	-68.711
9.667	5.50	-67.882
9.653	5.60	-67.059
9.640	5.70	-66.222
9.629	5.80	-65.363
9.616	5.90	-64.519
9.600	6.00	-63.698
9.584	6.10	-62.872
9.570	6.20	-62.025
9.556	6.30	-61.174
9.542	6.40	-60.319
9.526	6.50	-59.476
9.510	6.60	-58.628
9.490	6.70	-57.804
9.470	6.80	-56.973
9.451	6.90	-56.130
9.430	7.00	-55.294
9.411	7.10	-54.440
9.396	7.20	-53.560
9.378	7.30	-52.693
9.360	7.40	-51.821
9.340	7.50	-50.956
9.319	7.60	-50.091

9.299	7.70	-49.216
9.276	7.80	-48.351
9.253	7.90	-47.480
9.230	8.00	-46.604
9.206	8.10	-45.727
9.182	8.20	-44.846
9.161	8.30	-43.950
9.138	8.40	-43.057
9.110	8.50	-42.175
9.079	8.60	-41.296
9.048	8.70	-40.411
9.017	8.80	-39.520
8.985	8.90	-38.627
8.953	9.00	-37.728
8.921	9.10	-36.825
8.887	9.20	-35.921
8.854	9.30	-35.010
8.821	9.40	-34.096
8.789	9.50	-33.176
8.756	9.60	-32.255
8.723	9.70	-31.330
8.690	9.80	-30.403
8.656	9.90	-29.474
8.622	10.00	-28.542
8.589	10.10	-27.606
8.555	10.20	-26.670
8.523	10.30	-25.730
8.491	10.40	-24.788
8.459	10.50	-23.844
8.426	10.60	-22.899
8.385	10.70	-21.958
8.335	10.80	-21.018
8.306	10.90	-20.067
8.281	11.00	-19.113
8.248	11.10	-18.162
8.214	11.20	-17.210
8.180	11.30	-16.257
8.142	11.40	-15.304
8.104	11.50	-14.351
8.065	11.60	-13.397
8.029	11.70	-12.441
7.987	11.80	-11.486
7.945	11.90	-10.529
7.902	12.00	-9.573

7.859	12.10	-8.615
7.818	12.20	-7.657
7.778	12.30	-6.698
7.737	12.40	-5.738
7.699	12.50	-4.778
7.662	12.60	-3.817
7.622	12.70	-2.856
7.584	12.80	-1.895
7.548	12.90	-0.934
7.512	13.00	0.028
7.476	13.10	0.990
7.442	13.20	1.953
7.408	13.30	2.915
7.384	13.40	3.879
7.348	13.50	4.841
7.313	13.60	5.804
7.279	13.70	6.767
7.248	13.80	7.730
7.233	13.90	8.695
7.209	14.00	9.658
7.178	14.10	10.621
7.145	14.20	11.585
7.117	14.30	12.548
7.084	14.40	13.512
7.052	14.50	14.475
7.020	14.60	15.438
6.985	14.70	16.402
6.950	14.80	17.365
6.921	14.90	18.329
6.890	15.00	19.292
6.862	15.10	20.256
6.830	15.20	21.219
6.799	15.30	22.182
6.768	15.40	23.146
6.739	15.50	24.109
6.720	15.60	25.073
6.696	15.70	26.036
6.664	15.80	26.999
6.632	15.90	27.962
6.603	16.00	28.925
6.574	16.10	29.888
6.546	16.20	30.851
6.519	16.30	31.814
6.491	16.40	32.777

6.462	16.50	33.739
6.434	16.60	34.702
6.414	16.70	35.665
6.389	16.80	36.627
6.363	16.90	37.590
6.338	17.00	38.552
6.315	17.10	39.514
6.293	17.20	40.476
6.266	17.30	41.438
6.242	17.40	42.400
6.220	17.50	43.362
6.199	17.60	44.324
6.175	17.70	45.285
6.152	17.80	46.246
6.129	17.90	47.207
6.106	18.00	48.168
6.084	18.10	49.129
6.061	18.20	50.089
6.038	18.30	51.050
6.019	18.40	52.011
5.998	18.50	52.971
5.976	18.60	53.931
5.955	18.70	54.890
5.933	18.80	55.850
5.909	18.90	56.808
5.886	19.00	57.766
5.863	19.10	58.724
5.840	19.20	59.682
5.818	19.30	60.639
5.798	19.40	61.597
5.780	19.50	62.556
5.763	19.60	63.514
5.741	19.70	64.470
5.721	19.80	65.427
5.699	19.90	66.382
5.681	20.00	67.339
5.661	20.10	68.294
5.641	20.20	69.249
5.622	20.30	70.204
5.601	20.40	71.157
5.582	20.50	72.112
5.565	20.60	73.066
5.544	20.70	74.018
5.531	20.80	74.975

5.530	20.90	75.939
5.513	21.00	76.892
5.499	21.10	77.847
5.479	21.20	78.798
5.465	21.30	79.752
5.453	21.40	80.708
5.431	21.50	81.655
5.412	21.60	82.604
5.406	21.70	83.563
5.386	21.80	84.510
5.369	21.90	85.459
5.349	22.00	86.405
5.338	22.10	87.359
5.324	22.20	88.309
5.311	22.30	89.260
5.299	22.40	90.211
5.288	22.50	91.164
5.276	22.60	92.115
5.268	22.70	93.070
5.257	22.80	94.022
5.248	22.90	94.975
5.239	23.00	95.929
5.229	23.10	96.881
5.220	23.20	97.833
5.211	23.30	98.786
5.203	23.40	99.740
5.195	23.50	100.694
5.188	23.60	101.648
5.179	23.70	102.600
5.170	23.80	103.552
5.162	23.90	104.504
5.154	24.00	105.457
5.149	24.10	106.414
5.141	24.20	107.366
5.134	24.30	108.319
5.120	24.40	109.261
5.110	24.50	110.209
5.101	24.60	111.158
5.094	24.70	112.111
5.088	24.80	113.065
5.082	24.90	114.018
5.076	25.00	114.972
5.070	25.10	115.926
5.063	25.20	116.877

5.056	25.30	117.829	
5.050	25.40	118.782	
5.042	25.50	119.730	
5.036	25.60	120.683	
5.030	25.70	121.636	
5.023	25.80	122.586	
5.016	25.90	123.536	
5.011	26.00	124.490	
5.006	26.10	125.444	
5.001	26.20	126.398	
9.890	0.00		-117.941
9.882	0.10		-117.113
9.876	0.20		-116.249
9.870	0.30		-115.383
9.863	0.40		-114.533
9.855	0.50		-113.697
9.850	0.60		-112.811
9.843	0.70		-111.955
9.837	0.80		-111.083
9.830	0.90		-110.224
9.822	1.00		-109.378
9.812	1.10		-108.559
9.804	1.20		-107.708
9.797	1.30		-106.842
9.788	1.40		-106.001
9.780	1.50		-105.144
9.767	1.60		-104.351
9.759	1.70		-103.489
9.748	1.80		-102.662
9.739	1.90		-101.808
9.727	2.00		-100.988
9.715	2.10		-100.163
9.703	2.20		-99.335
9.691	2.30		-98.502
9.680	2.40		-97.656
9.667	2.50		-96.827
9.655	2.60		-95.985
9.642	2.70		-95.148
9.629	2.80		-94.308
9.618	2.90		-93.446
9.609	3.00		-92.563
9.600	3.10		-91.679
9.592	3.20		-90.784
9.583	3.30		-89.897

9.573	3.40	-89.016
9.563	3.50	-88.133
9.554	3.60	-87.241
9.546	3.70	-86.339
9.538	3.80	-85.436
9.529	3.90	-84.540
9.520	4.00	-83.642
9.511	4.10	-82.742
9.502	4.20	-81.842
9.494	4.30	-80.933
9.485	4.40	-80.030
9.475	4.50	-79.132
9.464	4.60	-78.239
9.454	4.70	-77.338
9.443	4.80	-76.442
9.431	4.90	-75.550
9.417	5.00	-74.668
9.403	5.10	-73.783
9.386	5.20	-72.912
9.370	5.30	-72.032
9.355	5.40	-71.144
9.339	5.50	-70.258
9.322	5.60	-69.374
9.305	5.70	-68.487
9.284	5.80	-67.614
9.265	5.90	-66.728
9.246	6.00	-65.840
9.228	6.10	-64.944
9.210	6.20	-64.045
9.191	6.30	-63.147
9.170	6.40	-62.253
9.152	6.50	-61.346
9.137	6.60	-60.428
9.123	6.70	-59.505
9.108	6.80	-58.584
9.091	6.90	-57.666
9.072	7.00	-56.752
9.054	7.10	-55.834
9.040	7.20	-54.903
9.018	7.30	-53.991
8.998	7.40	-53.071
8.978	7.50	-52.150
8.960	7.60	-51.222
8.939	7.70	-50.299

8.918	7.80	-49.373
8.898	7.90	-48.445
8.878	8.00	-47.514
8.854	8.10	-46.588
8.831	8.20	-45.659
8.805	8.30	-44.732
8.782	8.40	-43.799
8.757	8.50	-42.867
8.732	8.60	-41.933
8.708	8.70	-40.996
8.685	8.80	-40.057
8.661	8.90	-39.117
8.636	9.00	-38.177
8.609	9.10	-37.237
8.581	9.20	-36.297
8.554	9.30	-35.354
8.526	9.40	-34.411
8.499	9.50	-33.466
8.471	9.60	-32.520
8.442	9.70	-31.573
8.413	9.80	-30.626
8.384	9.90	-29.677
8.355	10.00	-28.727
8.323	10.10	-27.778
8.295	10.20	-26.826
8.267	10.30	-25.873
8.239	10.40	-24.919
8.211	10.50	-23.965
8.183	10.60	-23.010
8.155	10.70	-22.054
8.127	10.80	-21.098
8.099	10.90	-20.141
8.071	11.00	-19.184
8.043	11.10	-18.226
8.015	11.20	-17.268
7.987	11.30	-16.310
7.959	11.40	-15.351
7.931	11.50	-14.392
7.903	11.60	-13.432
7.875	11.70	-12.472
7.847	11.80	-11.512
7.819	11.90	-10.551
7.791	12.00	-9.590
7.763	12.10	-8.629

7.735	12.20	-7.668
7.707	12.30	-6.707
7.679	12.40	-5.745
7.651	12.50	-4.783
7.623	12.60	-3.821
7.596	12.70	-2.859
7.569	12.80	-1.897
7.542	12.90	-0.934
7.516	13.00	0.029
7.490	13.10	0.992
7.464	13.20	1.954
7.438	13.30	2.917
7.413	13.40	3.881
7.388	13.50	4.844
7.363	13.60	5.807
7.348	13.70	6.771
7.323	13.80	7.735
7.296	13.90	8.698
7.278	14.00	9.662
7.251	14.10	10.625
7.225	14.20	11.589
7.198	14.30	12.552
7.175	14.40	13.516
7.147	14.50	14.479
7.122	14.60	15.443
7.099	14.70	16.407
7.072	14.80	17.371
7.051	14.90	18.334
7.029	15.00	19.298
7.007	15.10	20.262
6.985	15.20	21.226
6.963	15.30	22.190
6.942	15.40	23.154
6.920	15.50	24.118
6.898	15.60	25.082
6.876	15.70	26.045
6.854	15.80	27.009
6.831	15.90	27.973
6.810	16.00	28.937
6.787	16.10	29.901
6.768	16.20	30.864
6.748	16.30	31.828
6.728	16.40	32.792
6.709	16.50	33.756

6.690	16.60	34.720
6.668	16.70	35.683
6.650	16.80	36.647
6.634	16.90	37.611
6.616	17.00	38.575
6.600	17.10	39.538
6.581	17.20	40.502
6.560	17.30	41.465
6.556	17.40	42.430
6.537	17.50	43.394
6.519	17.60	44.357
6.500	17.70	45.320
6.483	17.80	46.284
6.466	17.90	47.247
6.449	18.00	48.211
6.432	18.10	49.174
6.415	18.20	50.138
6.398	18.30	51.101
6.381	18.40	52.064
6.365	18.50	53.027
6.349	18.60	53.991
6.333	18.70	54.954
6.316	18.80	55.917
6.299	18.90	56.880
6.272	19.00	57.841
6.250	19.10	58.803
6.229	19.20	59.765
6.213	19.30	60.728
6.197	19.40	61.691
6.181	19.50	62.653
6.166	19.60	63.616
6.151	19.70	64.578
6.136	19.80	65.541
6.121	19.90	66.503
6.106	20.00	67.465
6.090	20.10	68.427
6.075	20.20	69.389
6.060	20.30	70.351
6.044	20.40	71.313
6.030	20.50	72.275
6.015	20.60	73.236
6.001	20.70	74.198
5.986	20.80	75.160
5.972	20.90	76.121

5.957	21.00	77.082
5.937	21.10	78.042
5.920	21.20	79.003
5.905	21.30	79.963
5.883	21.40	80.922
5.867	21.50	81.882
5.850	21.60	82.841
5.835	21.70	83.802
5.816	21.80	84.760
5.797	21.90	85.718
5.778	22.00	86.676
5.759	22.10	87.634
5.745	22.20	88.593
5.729	22.30	89.551
5.713	22.40	90.510
5.699	22.50	91.468
5.685	22.60	92.427
5.670	22.70	93.385
5.656	22.80	94.343
5.641	22.90	95.300
5.627	23.00	96.258
5.614	23.10	97.216
5.599	23.20	98.172
5.585	23.30	99.129
5.571	23.40	100.086
5.558	23.50	101.043
5.544	23.60	101.999
5.531	23.70	102.955
5.511	23.80	103.907
5.493	23.90	104.859
5.481	24.00	105.815
5.468	24.10	106.770
5.455	24.20	107.725
5.444	24.30	108.681
5.432	24.40	109.636
5.420	24.50	110.591
5.408	24.60	111.546
5.395	24.70	112.499
5.384	24.80	113.454
5.373	24.90	114.409
5.362	25.00	115.363
5.352	25.10	116.318
5.342	25.20	117.273
5.332	25.30	118.228

5.322	25.40	119.182
5.312	25.50	120.136
5.303	25.60	121.091
5.293	25.70	122.045
5.283	25.80	122.998
5.271	25.90	123.949
5.261	26.00	124.902
5.252	26.10	125.855
5.242	26.20	126.808
5.233	26.30	127.761
5.223	26.40	128.713
5.214	26.50	129.665
5.205	26.60	130.618
5.196	26.70	131.570
5.188	26.80	132.524
5.180	26.90	133.477
5.174	27.00	134.433

Potentiometric titrations of goethite under closed systems conditions
For all three studies initial vol. Of 0.1 N NaOH added = 1.0 ml

	Data as volume of acid added			Data as charge (C/g)		
pH	IS 0.001	IS 0.01	IS 0.1	IS 0.001	IS 0.01	IS 0.1
9.741	0			-4.33405		
9.696	0.1			-3.8923		
9.627	0.2			-3.6313		
9.571	0.3			-3.16095		
9.501	0.4			-2.73097		
9.394	0.5			-2.43395		
9.244	0.6			-2.16722		
9.08	0.7			-1.73463		
8.799	0.8			-1.32247		
8.387	0.9			-0.73003		
7.785	1			0.057228		
7.046	1.1			0.966898		
6.458	1.2			1.898861		
5.852	1.3			2.759574		
5.306	1.4			3.38266		
5.009	1.5			3.879288		
4.809	1.6			4.291342		
4.673	1.7			4.705383		
4.579	1.8			5.175172		
4.484	1.9			5.518052		
4.424	2			6.013899		
4.388	2.1			6.664622		
4.347	2.2			7.238521		
4.299	2.3			7.696217		
4.27	2.4			8.326367		
4.257	2.5			9.133769		

4.233	2.6			9.795269		
4.211	2.7			10.46693		
4.204	2.8			11.33534		
9.651		0			-4.37384	
9.573		0.1			-4.10922	
9.471		0.2			-3.89994	
9.347		0.3			-3.64398	
9.186		0.4			-3.34364	
8.98		0.5			-2.93808	
8.738		0.6			-2.36694	
8.448		0.7			-1.65936	
8.1		0.8			-0.84415	
7.681		0.9			0.044276	
7.15		1			0.971648	
6.811		1.1			1.921035	
6.445		1.2			2.862608	
6.132		1.3			3.789511	
5.889		1.4			4.700414	
5.538		1.5			5.509883	
5.299		1.6			6.269457	
5.137		1.7			7.015115	
5.017		1.8			7.755939	
4.898		1.9			8.428295	
4.811		2			9.122474	
4.728		2.1			9.773324	
4.655		2.2			10.40779	
4.599		2.3			11.07876	
4.504		2.4			11.44963	
4.466		2.5			12.13804	
4.426		2.6			12.78455	
4.378		2.7			13.32659	
4.308		2.8			13.58473	
4.275		2.9			14.17478	
4.218		3			14.42123	
4.191		3.1			15.01145	
9.445			0			-6.96035
9.391			0.1			-6.3098
9.32			0.2			-5.70299
9.262			0.3			-4.99016
9.172			0.4			-4.35546
9.057			0.5			-3.72416
8.913			0.6			-3.06982
8.774			0.7			-2.32131
8.538			0.8			-1.59697
8.06			0.9			-0.85491
7.824			1			0.06289
7.441			1.1			0.98799
7.065			1.2			1.932599
6.812			1.3			2.885933
6.546			1.4			3.835347
6.322			1.5			4.780307

6.08	1.6	5.710007
5.89	1.7	6.630402
5.65	1.8	7.503228
5.45	1.9	8.34158
5.24	2	9.093454
5.06	2.1	9.773112
4.898	2.2	10.358
4.806	2.3	11.03491
4.744	2.4	11.76831
4.655	2.5	12.33749
4.608	2.6	13.05828
4.533	2.7	13.57461
4.467	2.8	14.07533
4.428	2.9	14.73087
4.373	3	15.2095
4.35	3.1	15.95204
4.308	3.2	16.47928
4.246	3.3	16.71561
4.202	3.4	17.09659
4.182	3.5	17.77585
4.144	3.6	18.16048
4.108	3.7	18.52677
4.084	3.8	19.06412

Detailed potentiometric titrations of goethite under closed systems conditions

pH	IS 0.001	IS 0.01	IS 0.1	IS 0.001	IS 0.01	IS 0.1
9.016	0			-0.92873		
8.999	0.1			-0.87068		
8.962	0.2			-0.85282		
8.933	0.3			-0.81344		
8.886	0.4			-0.80179		
8.834	0.5			-0.78906		
8.794	0.6			-0.75052		
8.72	0.7			-0.74813		
8.664	0.8			-0.71293		
8.594	0.9			-0.68274		
8.551	1			-0.62199		
8.507	1.1			-0.5586		
8.449	1.2			-0.50092		
8.387	1.3			-0.44058		
8.269	1.4			-0.40018		
8.158	1.5			-0.34427		
8.057	1.6			-0.28653		
7.992	1.7			-0.19571		
7.922	1.8			-0.1135		
7.879	1.9			-0.02474		
7.802	2			0.059637		
7.741	2.1			0.147878		
7.712	2.2			0.240809		

7.669	2.3		0.332413
7.595	2.4		0.42146
7.52	2.5		0.51146
7.487	2.6		0.605378
7.403	2.7		0.695984
7.332	2.8		0.788111
7.204	2.9		0.877766
7.151	3		0.971695
7.063	3.1		1.064144
6.894	3.2		1.153063
9.086		0	-2.58685
9.06		0.1	-2.55872
9.034		0.2	-2.52661
9.001		0.3	-2.50648
8.985		0.4	-2.44498
8.947		0.5	-2.4266
8.914		0.6	-2.39261
8.895		0.7	-2.33001
8.862		0.8	-2.28897
8.839		0.9	-2.22871
8.811		1	-2.17382
8.799		1.1	-2.09435
8.768		1.2	-2.03972
8.732		1.3	-1.98824
8.704		1.4	-1.92427
8.684		1.5	-1.84976
8.643		1.6	-1.79528
8.607		1.7	-1.73255
8.586		1.8	-1.65451
8.541		1.9	-1.59466
8.509		2	-1.52201
8.482		2.1	-1.44432
8.439		2.2	-1.37547
8.411		2.3	-1.29556
8.387		2.4	-1.21246
8.344		2.5	-1.13819
8.301		2.6	-1.06183
8.275		2.7	-0.97659
8.228		2.8	-0.8988
8.18		2.9	-0.81945
8.124		3	-0.74072
8.085		3.1	-0.65533
8.044		3.2	-0.56949
8.02		3.3	-0.4788
7.99		3.4	-0.38912
7.945		3.5	-0.30203
7.899		3.6	-0.21421
7.857		3.7	-0.1249
7.833		3.8	-0.03222
7.804		3.9	0.059926
7.789		4	0.154272

7.751	4.1		0.245641
7.727	4.2		0.339105
7.703	4.3		0.43272
7.65	4.4		0.523363
7.6	4.5		0.614898
7.55	4.6		0.70691
7.5	4.7		0.79934
7.45	4.8		0.892135
7.35	4.9		0.98214
7.3	5		1.075751
7.213	5.1		1.167668
7.181	5.2		1.262582
7.144	5.3		1.357306
7.112	5.4		1.452307
7.089	5.5		1.547742
7.052	5.6		1.642561
7.014	5.7		1.737352
9.044		0	-3.1777
9.017		0.1	-3.14558
9.007		0.2	-3.07194
8.997		0.3	-2.99777
8.981		0.4	-2.93595
8.97		0.5	-2.86257
8.941		0.6	-2.82425
8.912		0.7	-2.78218
8.89		0.8	-2.72462
8.861		0.9	-2.67652
8.834		1	-2.62228
8.812		1.1	-2.55832
8.788		1.2	-2.49549
8.76		1.3	-2.43599
8.73		1.4	-2.37657
8.705		1.5	-2.30909
8.682		1.6	-2.23784
8.655		1.7	-2.16934
8.626		1.8	-2.10103
8.595		1.9	-2.03265
8.566		2	-1.96071
8.538		2.1	-1.88642
8.514		2.2	-1.80786
8.49		2.3	-1.72833
8.464		2.4	-1.64919
8.437		2.5	-1.56966
8.415		2.6	-1.48622
8.388		2.7	-1.40489
8.359		2.8	-1.32366
8.322		2.9	-1.24522
8.275		3	-1.16956
8.244		3.1	-1.08563
8.211		3.2	-1.00157
8.184		3.3	-0.91458

8.157	3.4	-0.82702
8.13	3.5	-0.73893
8.072	3.6	-0.65881
8.043	3.7	-0.56974
8.009	3.8	-0.48135
7.975	3.9	-0.39236
7.928	4	-0.30533
7.891	4.1	-0.21563
7.854	4.2	-0.12538
7.826	4.3	-0.03329
7.804	4.4	0.059926
7.778	4.5	0.152747
7.753	4.6	0.2459
7.727	4.7	0.339105
7.706	4.8	0.433071
7.685	4.9	0.527148
7.642	5	0.619021
7.6	5.1	0.711383
7.54	5.2	0.802552
7.48	5.3	0.894308
7.424	5.4	0.986828
7.389	5.5	1.081025
7.346	5.6	1.174873
7.312	5.7	1.269392
7.265	5.8	1.363309
7.204	5.9	1.456676
7.178	6	1.551892
7.144	6.1	1.646761
7.101	6.2	1.741258
7.071	6.3	1.836384
7.03	6.4	1.931034
7.002	6.5	2.026274
6.887	6.6	2.117592

Potentiometric titrations of HMO under closed system condition with 0.1 N HNO_3

Initial 0.1 N NaOH added	5 ml	8.1 ml	14 ml
pH	$\mu = 0.015$	$\mu = 0.15$	$\mu = 1.50$
0.92	122.5		
0.93	119.6		
0.94	116.9		
0.95	114.2		
0.96	111.5		
0.98	106.4		
0.99	103.8		
1.00	101.6		
1.05	90.6		
1.10	80.8		
1.16	70.5		
1.23	60.1		
1.30	51.2		
1.42	39.0		

1.55	29.1
1.77	17.8
2.35	5.2
2.55	3.4
3.21	1.1
5.26	0.4
8.45	0.3
10.34	0.0
0.95	120.2
0.96	117.2
0.97	114.2
1.00	106.6
1.03	99.4
1.10	85.0
1.13	79.3
1.19	69.2
1.20	67.7
1.22	64.7
1.23	63.3
1.24	61.8
1.25	60.4
1.26	59.1
1.27	57.7
1.28	56.4
1.29	55.1
1.30	53.7
1.31	52.4
1.32	51.2
1.33	50.0
1.34	48.8
1.35	47.7
1.37	45.6
1.38	44.5
1.40	42.6
1.42	40.7
1.43	39.6
1.45	37.8
1.47	36.1
1.49	34.5
1.51	32.9
1.53	31.5
1.56	29.4
1.58	28.0
1.61	26.2
1.64	24.5
1.67	22.8
1.71	20.8
1.76	18.6
1.82	16.3
1.88	14.2
1.96	11.9

2.06	9.6
2.33	5.4
2.51	3.7
3.23	1.1
5.34	0.5
9.10	0.3
9.89	0.2
10.17	0.0
11.07	0.0
10.87	0.9
10.61	1.8
10.21	2.5
9.54	3.1
8.35	3.7
6.90	4.2
5.95	4.7
4.86	5.2
3.61	5.9
2.95	7.3
2.63	9.0
2.44	10.8
2.32	12.5
2.22	14.2
2.14	15.9
2.07	17.7
2.00	19.7
1.95	21.4
1.90	23.3
1.86	25.0
1.82	26.8
1.78	28.8
1.75	30.5
1.71	32.7
1.69	34.1
1.66	36.0
1.63	38.1
1.61	39.7
1.59	41.4
1.56	43.7
1.54	45.5
1.52	51.4
1.50	53.3
1.49	54.5
1.47	56.6
1.45	58.6
1.52	38.4
1.55	35.8
1.61	31.6
1.70	26.4
1.85	20.0
0.99	108.2

1.20
1.36
1.46
1.62
1.95
2.03
2.17
2.41
3.00
5.44
9.96
10.85
9.75
8.68
7.07
5.90
4.69
3.55
2.96
2.65
2.30
2.19
2.10
2.02
1.96
1.90
1.85
1.81
1.77
1.73
1.70
1.67
1.64
1.61
1.58
1.56
1.54
1.52
1.50
1.48
1.46
1.45
0.97
0.99
1.02
1.04
1.06
1.09
1.12
1.15
1.18

68.5
48.6
39.1
27.9
14.7
12.7
10.0
7.1
4.1
3.0
2.8
2.1
0.0
0.6
1.1
1.6
2.1
2.8
4.2
5.8
9.1
11.0
13.0
15.1
17.0
19.1
21.2
23.0
25.0
27.2
29.0
30.9
33.0
35.1
37.4
39.1
40.9
42.7
44.7
46.7
48.7
50.0
107.2
102.4

100.0
95.6
91.4
85.4
79.8
74.8
70.0

1.22	64.1
1.25	60.0
1.30	53.8
1.34	49.3
1.39	44.2
1.45	38.8
1.51	34.2
1.58	29.5
1.66	24.9
1.76	20.3
1.89	15.8
2.04	11.9
2.27	8.1
2.76	4.3
4.15	2.6
6.56	2.4
9.63	2.3
10.92	1.4
7.68	0.0
5.84	0.5
4.43	1.0
3.34	2.0
2.77	3.7
2.47	5.9
2.28	8.2
2.14	10.7
2.03	13.3
1.94	16.0
1.87	18.5
1.81	21.0
1.75	23.8
1.70	26.4
1.65	29.4
1.61	32.0
1.58	34.3
1.54	37.3
1.51	39.9
1.48	42.6
1.46	44.7
1.43	47.6
1.41	49.9
1.39	52.2

Potentiometric titrations of HAO under closed system conditions with 0.1 N HNO_3

Initial 0.1 NaOH	20 ml	38.1 ml	44 ml
pH	$\mu = 0.061$	$\mu = 0.61$	$\mu = 1.20$
9.45	0.0		
9.34	2.1		
9.22	4.1		
9.08	6.2		
9	8.2		

8.85	10.2	
8.52	12.2	
8.31	14.3	
8.08	16.3	
7.86	18.3	
7.61	20.3	
7.39	22.3	
7.17	24.3	
6.97	26.3	
6.79	28.3	
6.62	30.3	
6.51	32.3	
6.42	34.3	
6.24	36.3	
6.1	38.3	
5.97	40.3	
5.82	42.3	
5.67	44.3	
5.5	46.2	
5.4	48.2	
5.32	50.2	
5.23	52.2	
5.16	54.2	
5.1	56.2	
5.04	58.2	
4.98	60.2	
4.94	62.2	
4.9	64.1	
4.89	66.1	
4.88	68.1	
9.43		0.0
9.39		2.0
9.34		4.0
9.26		6.1
9.19		8.1
9.13		10.1
9.07		12.2
8.98		14.2
8.96		16.2
8.86		18.2
8.77		20.2
8.67		22.2
8.54		24.2
8.41		26.2
8.27		28.2
8.1		30.3
7.92		32.3
7.72		34.3
7.54		36.3
7.34		38.3
7.13		40.3

6.97	42.3	
6.77	44.3	
6.62	46.3	
6.46	48.3	
6.29	50.3	
6.12	52.3	
5.94	54.2	
5.77	56.2	
5.61	58.2	
5.45	60.2	
5.3	62.2	
5.18	64.2	
5.07	66.2	
4.98	68.2	
4.91	70.1	
4.86	72.1	
4.8	74.1	
4.76	76.1	
4.72	78.1	
4.69	80.1	
4.66	82.0	
4.65	84.0	
9.41		0.0
9.38		2.0
9.33		4.0
9.29		6.1
9.21		8.1
9.16		10.1
9.11		12.1
9.06		14.1
8.98		16.2
8.95		18.2
8.88		20.2
8.81		22.2
8.73		24.2
8.63		26.2
8.53		28.2
8.42		30.2
8.3		32.2
8.16		34.2
8.02		36.2
7.86		38.2
7.7		40.2
7.52		42.2
7.39		44.2
7.22		46.2
7.05		48.2
6.91		50.2
6.75		52.2
6.59		54.2
6.44		56.2

6.29	58.2
6.13	60.2
5.98	62.2
5.82	64.2
5.66	66.2
5.51	68.2
5.36	70.2
5.23	72.2
5.12	74.2
5.03	76.2
4.96	78.1
4.9	80.1
4.85	82.1
4.8	84.1
4.77	86.1
4.73	88.1
4.72	90.1
4.71	92.0
4.7	94.0
4.7	96.0

APPENDIX C

SORPTION STUDIES WITH AMORPHOUS OXIDES

Strontium Studies with Amorphous Oxides

Strontium adsorption edges at 25°C

pH	μ = 0.06	μ = 0.60	pH	μ = 0.015	μ = 1.50
5.18	15.42		1.88	34.63	
6.07	45.86		2.52	38.51	
7.01	47.06		3.06	40.80	
7.01	46.93		3.55	43.71	
8.03	45.96		4.07	51.56	
8.07	46.99		4.53	64.37	
9.04	60.09		5.08	79.60	
10.01	96.20		5.57	87.09	
10.43	97.52		6.01	90.84	
4.99	8.59		6.58	91.88	
5.89	39.65		7.01	91.95	
6.97	44.34		2.00		22.84
6.97	44.12		2.54		29.51
8.04	45.36		3.06		31.65
8.06	46.19		3.49		34.14
8.88	51.32		4.01		38.19
9.98	96.16		4.51		45.58
10.51	98.85		5.05		60.02
5.15		8.22	5.53		68.69
5.23		10.58	6.04		77.21
6.01		34.10	6.47		80.54
6.08		36.16	7.01		81.49
7.02		40.85			
7.02		40.86			
7.05		43.12			
7.05		43.83			
8.09		41.85			
8.14		45.26			
9.02		44.58			
9.05		48.59			
9.07		49.95			
9.09		55.27			
10.04		68.92			
10.11		71.27			
10.44		75.26			

Strontium adsorption isotherms with HAO at pH 6 and multiple temperatures measured with liquid scintillating counter

T= 25°C			T = 14°C			T = 4°C	
Initial Sr (M)	[Sr] (M)	C (moles Sr/ g HAO)	Initial Sr (M)	[Sr] (M)	C (moles Sr/ g HAO)	[Sr] (M)	C (moles Sr/ g HAO)
1.00E-07	5.77E-08	4.23E-08	1.00E-07	5.95E-08	4.05E-08	6.41E-08	3.59E-08
5.00E-07	2.97E-07	2.03E-07	5.00E-07	2.86E-07	2.14E-07	3.11E-07	1.89E-07
1.00E-06	5.91E-07	4.09E-07	1.00E-06	6.02E-07	3.98E-07	6.40E-07	3.60E-07
5.00E-06	3.04E-06	1.96E-06	5.00E-06	2.98E-06	2.02E-06	3.22E-06	1.78E-06
1.00E-05	5.98E-06	4.02E-06	1.00E-05	5.94E-06	4.06E-06	6.21E-06	3.79E-06
5.00E-05	3.13E-05	1.87E-05	5.00E-05	2.93E-05	2.07E-05	3.19E-05	1.81E-05
1.00E-04	5.94E-05	4.06E-05	1.00E-04	6.21E-05	3.79E-05	6.54E-05	3.46E-05
2.00E-04	1.22E-04	7.84E-05	1.00E-04	6.21E-05	3.79E-05	6.22E-05	3.78E-05
1.00E-03	5.83E-04	4.17E-04	2.00E-04	1.22E-04	7.84E-05	1.36E-04	6.40E-05
1.00E-02	5.41E-03	4.59E-03	1.00E-03	5.83E-04	4.17E-04	7.60E-04	2.40E-04
4.00E-02	2.27E-02	1.73E-02	5.00E-03	2.92E-03	2.08E-03	3.12E-03	1.88E-03
			1.00E-02	6.06E-03	3.94E-03	6.40E-03	3.60E-03
			5.00E-02	3.00E-02	2.00E-02	2.52E-02	1.48E-02

Strontium adsorption isotherms with HAO at pH 7 and multiple temperatures measured with liquid scintillating counter

T= 25°C			T = 14°C			T = 4°C	
Initial Sr	[Sr] (M)	C (moles Sr/ g HAO)	Initial Sr	[Sr] (M)	C (moles Sr/ g HAO)	[Sr] (M)	C (moles Sr/ g HAO)
2.00E-02	1.04E-02	9.59E-03	1.00E-07	5.49E-08	4.51E-08	6.15E-08	3.85E-08
1.00E-02	4.68E-03	5.32E-03	5.00E-07	2.64E-07	2.36E-07	3.10E-07	1.90E-07
5.00E-03	2.34E-03	2.66E-03	1.00E-06	5.31E-07	4.69E-07	6.20E-07	3.80E-07
2.00E-03	1.02E-03	9.82E-04	5.00E-06	2.78E-06	2.22E-06	3.10E-06	1.90E-06
2.00E-03	9.98E-04	1.00E-03	1.00E-05	5.38E-06	4.62E-06	5.55E-06	4.45E-06
1.90E-03	8.95E-04	1.01E-03	5.00E-05	2.75E-05	2.25E-05	3.08E-05	1.92E-05
2.00E-04	8.57E-05	1.14E-04	1.00E-04	5.62E-05	4.38E-05	6.00E-05	4.00E-05
1.50E-04	8.40E-05	6.60E-05	1.00E-04	5.47E-05	4.53E-05	1.22E-04	7.77E-05
1.00E-04	4.81E-05	5.19E-05	2.00E-04	1.16E-04	8.38E-05	5.84E-04	4.16E-04
5.90E-05	3.00E-05	2.90E-05	5.00E-03	2.72E-03	2.29E-03	3.17E-03	1.83E-03
2.00E-05	9.80E-06	1.02E-05	1.00E-02	5.49E-03	4.52E-03	6.04E-03	3.96E-03
1.50E-05	8.43E-06	6.57E-06	5.00E-02	2.77E-02	2.23E-02	3.06E-02	1.94E-02
1.00E-05	4.52E-06	5.48E-06					
1.00E-05	4.48E-06	5.52E-06					
5.00E-06	3.16E-06	1.84E-06					
2.00E-06	8.09E-07	1.19E-06					
1.50E-06	6.95E-07	8.05E-07					
1.00E-06	6.02E-07	3.98E-07					
5.00E-07	2.87E-07	2.13E-07					
2.00E-07	1.18E-07	8.19E-08					
1.00E-07	5.78E-08	4.22E-08					
1.00E-07	5.81E-08	4.19E-08					

Strontium adsorption isotherms with HAO at pH 8 and multiple temperatures measured with liquid scintillating counter

	T= 25°C			T = 14°C		T = 4°C	
Initial Sr (M)	[Sr] (M)	C (moles Sr/ g HAO)	Initial Sr (M)	[Sr] (M)	C (moles Sr/ g HAO)	[Sr] (M)	C (moles Sr/ g HAO)
1.00E-07	5.02E-08	4.98E-08	1.00E-07	5.37E-08	4.63E-08	6.19E-08	3.81E-08
5.00E-07	2.64E-07	2.36E-07	5.00E-07	2.43E-07	2.57E-07	3.03E-07	1.97E-07
1.00E-06	5.22E-07	4.78E-07	1.00E-06	5.32E-07	4.68E-07	6.09E-07	3.91E-07
5.00E-06	2.79E-06	2.21E-06	5.00E-06	2.77E-06	2.23E-06	3.01E-06	1.99E-06
1.00E-05	3.27E-06	6.73E-06	1.00E-05	5.48E-06	4.52E-06	6.10E-06	3.90E-06
5.00E-05	2.57E-05	2.43E-05	5.00E-05	2.70E-05	2.30E-05	3.07E-05	1.93E-05
1.00E-04	5.59E-05	4.41E-05	1.00E-04	5.99E-05	4.01E-05	6.14E-05	3.86E-05
1.00E-03	5.10E-04	4.90E-04	1.00E-04	5.89E-05	4.11E-05	5.96E-05	4.04E-05
1.00E-02	5.40E-03	4.60E-03	2.00E-04	1.06E-04	9.36E-05	1.19E-04	8.12E-05
5.00E-02	2.43E-02	2.57E-02	5.00E-03	2.77E-03	2.23E-03	3.09E-03	1.91E-03
			1.00E-02	6.16E-03	3.84E-03	6.05E-03	3.95E-03
			4.00E-02	2.14E-02	1.86E-02	2.42E-02	1.58E-02

Strontium adsorption isotherms with HAO at pH 3.5 and multiple temperatures measured with liquid scintillating counter

	T= 4°C			T = 14°C		T = 25°C	
Initial Sr	[Sr] (M)	C (moles Sr/ g HMO)	Initial Sr	[Sr] (M)	C (moles Sr/ g HMO)	[Sr] (M)	C (moles Sr/ g HMO)
1.00E-07	8.67E-08	1.33E-07	1.00E-07	6.81E-08	3.19E-07	5.71E-08	4.29E-07
2.00E-07	1.73E-07	2.73E-07	2.00E-07	1.40E-07	6.00E-07	1.12E-07	8.83E-07
5.00E-07	4.33E-07	6.71E-07	5.00E-07	3.71E-07	1.29E-06	2.83E-07	2.17E-06
1.00E-06	8.71E-07	1.29E-06	1.00E-06	6.95E-07	3.05E-06	5.65E-07	4.35E-06
5.00E-06	4.30E-06	7.05E-06	5.00E-06	3.46E-06	1.54E-05	2.81E-06	2.19E-05
5.00E-06	4.31E-06	6.90E-06	5.00E-06	3.47E-06	1.53E-05	2.83E-06	2.17E-05
1.00E-05	8.61E-06	1.39E-05	1.00E-05	6.86E-06	3.14E-05	5.68E-06	4.32E-05
5.00E-05	3.86E-05	1.14E-04	5.00E-05	3.51E-05	1.49E-04	2.93E-05	2.07E-04
1.00E-04	8.59E-05	1.41E-04	1.00E-04	6.86E-05	3.14E-04	5.58E-05	4.42E-04
1.00E-03	8.64E-04	1.36E-03	1.00E-03	6.99E-04	3.01E-03	5.66E-04	4.34E-03
2.00E-03	1.73E-03	2.69E-03					

Strontium adsorption isotherms with HAO at pH 3.7 and multiple temperatures measured with liquid scintillating counter

	T= 4°C			T = 14°C			T = 25°C	
Initial Sr	[Sr] (M)	C (moles Sr/ g HAO)	Initial Sr	[Sr] (M)	C (moles Sr/ g HAO)	[Sr] (M)	C (moles Sr/ g HAO)
1.00E-07	3.17E-08	6.83E-07	1.00E-07	1.62E-08	8.38E-07	7.91E-09	9.21E-07
2.00E-07	6.20E-08	1.38E-06	2.00E-07	3.13E-08	1.69E-06	1.65E-08	1.84E-06
5.00E-07	1.59E-07	3.41E-06	5.00E-07	8.65E-08	4.13E-06	4.21E-08	4.58E-06
1.00E-06	3.10E-07	6.90E-06	1.00E-06	1.65E-07	8.35E-06	9.23E-08	9.08E-06
5.00E-06	1.68E-06	3.32E-05	5.00E-06	9.54E-07	4.05E-05	3.65E-07	4.64E-05
5.00E-06	1.58E-06	3.42E-05	5.00E-06	8.12E-07	4.19E-05	3.09E-07	4.69E-05
1.00E-05	3.04E-06	6.96E-05	1.00E-05	1.66E-06	8.34E-05	1.33E-06	8.67E-05
5.00E-05	1.62E-05	3.38E-04	5.00E-05	7.54E-06	4.25E-04	3.96E-06	4.60E-04
1.00E-04	3.10E-05	6.90E-04	1.00E-04	1.64E-05	8.36E-04	9.13E-06	9.09E-04
1.00E-03	3.13E-04	6.87E-03	1.00E-03	1.61E-04	8.39E-03	8.08E-05	9.19E-03
2.00E-03	6.12E-04	1.39E-02	2.00E-03	3.25E-04	1.67E-02	1.60E-04	1.84E-02

Site density studies for HAO at pH 7 using liquid scintillating counter

total cpm	final cpm	% Sorbed	Initial Sr	[Sr] (M)	C mol Sr / 0.1g
9103.22	7029.49	0.23	5.00E-02	3.86E-02	1.14E-02
9023.82	6992.96	0.23	5.00E-02	3.87E-02	1.13E-02
7803.34	5714.61	0.27	4.00E-02	2.93E-02	1.07E-02
5525.74	3662.30	0.34	3.00E-02	1.99E-02	1.01E-02
5716.75	3769.54	0.34	3.00E-02	1.98E-02	1.02E-02
4252.26	2387.79	0.44	2.00E-02	1.12E-02	8.77E-03
2923.66	1487.68	0.49	1.00E-02	5.09E-03	4.91E-03
2938.53	1474.70	0.50	1.00E-02	5.02E-03	4.98E-03

Site density studies for HAO at pH 8 using liquid scintillating counter

total cpm	final cpm	% Sorbed	Initial Sr	S mol/L	C mol/0.1g
9103.22	5774.47	0.37	5.00E-02	3.17E-02	1.83E-02
7175.49	4176.75	0.42	4.00E-02	2.33E-02	1.67E-02
5696.14	3138.53	0.45	3.00E-02	1.65E-02	1.35E-02
4179.86	2126.30	0.49	2.00E-02	1.02E-02	9.83E-03
2937.31	1409.05	0.52	1.00E-02	4.80E-03	5.20E-03

Site density – surface charge density correlation calculations

Oxide	pH	σ (C/ g)	Ct (moles Sr/ g HAO)	Ct (moles Sr/ g HAO)	lnCt	lnCt
HMO	3.50	-240.00	8.00E-03		-4.83	
HMO	5.00	-363.78	2.00E-02		-3.91	
HMO	7.00	-569.17	3.40E-02		-3.38	
HFO	7.00	63.11		2.50E-02		-3.69
HFO	6.00	207.96		1.10E-02		-4.51
HFO	5.00	399.51		5.70E-03		-5.17
HAO	8.00	86.37		2.00E-02		-3.91
HAO	7.00	179.49		1.20E-02		-4.42
HAO	6.00	270.20		1.00E-02		-4.61

Fortran Code for Estiamting Experimental Surface Diffusivity

```
PROGRAM CBCHMO
      IMPLICIT DOUBLE PRECISION (A-H,O-Z)
      IMPLICIT INTEGER (I-N)
C     THIS PROGRAM ESTIMATES SURFACE DIFFUSIVITY
      OPEN (3,FILE ='OPSR7M.DAT')
      OPEN (4,FILE ='VARS7M.DAT')
      OPEN (5,FILE ='ERRS7M.DAT')
      WRITE(*,*)'WHAT IS APPROX DS IN CM2/S?'
      READ (*,*)DS
      WRITE(*,*)'WHAT IS CBC IN MOLE/L?'
      READ (*,*)CBC
C     DEFINE PARAMETERS
      PI = 4*ATAN(1.)
C      RHO IS HMO DENSITY IN G/CC
      RHO = 1.75
C     E IS POROSITY OF HMO
      E = 0.35
      WRITE(*,*)'WHAT IS EXTERNAL KD IN L/G?'
      READ (*,*)EKDE
      EKD = 1000.0 * EKDE
      DK = E*EKD/(1-E)
      DO 50, M =1,100
      SUM1 = 0.0
      SUM2 = 0.0
      DS = DS
      OPEN (1, FILE = 'CBCSRM.DAT')
      DO 40 K =1,41
      OPEN (2, FILE = 'PSAHMO.DAT')
      READ (1,*) T, EM
C     T IS IN SECONDS, EM IS IN MOL/G
      TOTMASS = CBC
      DO 30  I=1,29
      READ (2,*) RP, PN
C     RP IS IN CM, PN IS NO OF PARTICLES
      DN = (DS)*(PI**2)*(RHO)*DK
      DD = (RP**2)*(RHO*DK+E)
      D = DN/DD
      SM = 4.0*PI*(RP**3)/3.0
      DO 20 N =1,100
      SF =8.0*((RP**3.0)/(PI*(N**2)))*EXP(-D*(N**2)*T)
      SM = (SM-SF)
20    CONTINUE
      SUBM = SM*PN*CBC*RHO
      TOTMAS=TOTMAS + SUBM
30    CONTINUE
      TOTMAS = TOTMAS +CBC
C     TO ACCOUNT FOR VARIANCE
      DIFF = ABS(TOTMAS-EM)
      PERCENT = (DIFF/EM)*100.0
      DIFF2 = DIFF**2
      SUM1 =SUM1 +DIFF
      SUM2= SUM2 +DIFF2
      PERSUM =PERCENT + PERSUM
```

Fortran Code for Estimating Experimental Surface Diffusivity (Contd.)

```
      WRITE (3,*) T, TOTMAS, EM
40    CONTINUE
      VAR = ((SUM2-((SUM1)**2)/30.0))/29.0
      AVEER = PERSUM/29.0
      WRITE(4,*) T, VAR
      WRITE (5,*) T, AVEER
      DS = DS * 0.1
50    CONTINUE
      END
```

CBC of Sr sorbed to 0.1 g/L HMO at pH 7 and 25°C

Time (d)	Total CPM	Final CPM	Sr ml	Add Sr	Total Sr M	CBC Sr	Sr/g HMO
0.000	0	0	0.0	0.00	0.00E+00	0.00E+00	0.00E+00
0.0003	1993.05	238.02	2.0	0.00	1.00E-05	1.19E-06	8.81E-05
0.001	1995.36	217.1	2.0	0.00	1.00E-05	1.09E-06	8.91E-05
0.003	1995.56	199.05	2.0	0.00	1.00E-05	9.97E-07	9.00E-05
0.010	2038.31	214.05	2.0	0.00	1.00E-05	1.05E-06	8.95E-05
0.021	1938.39	178.04	2.0	0.00	1.00E-05	9.18E-07	9.08E-05
0.042	2037.09	176.34	2.0	0.00	1.00E-05	8.66E-07	9.13E-05
0.083	1995.53	171.12	2.0	0.00	1.00E-05	8.58E-07	9.14E-05
0.167	2001.37	172.45	2.0	0.00	9.98E-06	8.60E-07	9.12E-05
1.000	1924.05	180.01	2.0	0.00	9.96E-06	9.32E-07	9.03E-05
2.000	1951.24	153.33	2.0	0.01	9.96E-06	7.83E-07	9.18E-05
2.000	1946.02	110.1	2.0	0.05	1.00E-05	5.67E-07	9.45E-05
3.000	2061.35	175.49	2.1	0.00	1.03E-05	8.76E-07	9.42E-05
5.000	2051.05	100.01	2.1	0.20	1.03E-05	5.02E-07	9.79E-05
5.007	2209.06	168.45	2.3	0.00	1.13E-05	8.61E-07	1.04E-04
6.000	2209.06	90.01	2.3	1.00	1.13E-05	4.60E-07	1.08E-04
6.007	2309.18	173.06	3.3	0.00	1.63E-05	1.22E-06	1.51E-04
7.000	2335.49	119.08	3.3	0.50	1.63E-05	8.31E-07	1.55E-04
7.007	2705.06	170.21	3.8	0.00	1.88E-05	1.18E-06	1.76E-04
8.000	2646.2	91	3.8	0.50	1.88E-05	6.46E-07	1.81E-04
8.007	3009.56	170.01	4.3	0.00	2.13E-05	1.20E-06	2.01E-04
10.007	3028.07	64.07	4.3	1.00	2.13E-05	4.51E-07	2.08E-04
10.014	3839.07	166.42	5.3	0.00	2.63E-05	1.14E-06	2.52E-04
13.014	3880.01	31.01	5.3	1.00	2.63E-05	2.10E-07	2.61E-04
13.021	4850.68	166.22	6.3	0.00	3.13E-05	1.07E-06	3.02E-04
16.021	4916.65	38.13	6.3	1.00	3.13E-05	2.43E-07	3.10E-04
16.028	5782.54	168.44	7.3	0.00	3.63E-05	1.06E-06	3.52E-04
18.028	5766.37	40.28	7.3	1.00	3.63E-05	2.54E-07	3.60E-04
18.035	6770.29	167.14	8.3	0.00	4.13E-05	1.02E-06	4.03E-04
20.035	6768.35	39.49	8.3	1.00	4.13E-05	2.41E-07	4.11E-04
20.042	7775.02	169.33	9.3	0.00	4.63E-05	1.01E-06	4.53E-04
23.042	7775.53	34.11	9.3	0.50	4.63E-05	2.03E-07	4.61E-04
23.049	8412.36	171.58	9.8	0.00	4.88E-05	9.95E-07	4.78E-04
26.049	8403.22	53.92	9.8	0.50	4.88E-05	3.13E-07	4.85E-04
26.056	8815.74	179.17	10.3	0.00	5.13E-05	1.04E-06	5.03E-04
29.056	8799.78	43.17	10.3	0.50	5.13E-05	2.52E-07	5.10E-04
29.063	9414.24	168.74	10.8	0.00	5.38E-05	9.64E-07	5.28E-04
32.063	9445.26	37.88	10.8	0.50	5.38E-05	2.16E-07	5.36E-04
32.069	9968.19	170.33	11.3	0.00	5.63E-05	9.62E-07	5.53E-04
35.069	10012.41	40.15	11.3	0.50	5.63E-05	2.26E-07	5.61E-04
35.076	10563.19	179.99	11.8	0.00	5.88E-05	1.00E-06	5.78E-04
38.076	10549.08	39.79	11.8	0.50	5.88E-05	2.22E-07	5.86E-04
38.083	11187.35	170.55	12.3	0.00	6.13E-05	9.34E-07	6.04E-04
41.083	11179.84	46.01	12.3	0.50	6.13E-05	2.52E-07	6.10E-04
41.090	11656.18	191.32	12.8	0.00	6.38E-05	1.05E-06	6.27E-04
44.090	11634.21	45.37	12.8	0.50	6.38E-05	2.49E-07	6.35E-04
44.097	12207.5	188.37	13.3	0.00	6.63E-05	1.02E-06	6.53E-04

CBC of Sr sorbed to 0.1 g/L HMO at pH 7 and 25°C (contd.)

Time (d)	Total CPM	Final CPM	Sr ml	Add Sr	Total Sr M	CBC Sr	Sr/g HMO
47.097	12196.64	43.17	13.3	0.50	6.63E-05	2.35E-07	6.61E-04
47.104	12400.04	180.61	13.8	0.00	6.88E-05	1.00E-06	6.78E-04
50.104	12372.15	44.04	13.8	0.50	6.88E-05	2.45E-07	6.85E-04
50.111	12685.2	184.15	14.3	0.00	7.13E-05	1.03E-06	7.03E-04
53.111	12678.12	36.01	14.3	0.50	7.13E-05	2.02E-07	7.11E-04
53.118	12945.59	181.37	14.8	0.00	7.38E-05	1.03E-06	7.28E-04
56.118	13316.25	43.27	14.8	0.50	7.38E-05	2.40E-07	7.36E-04
56.125	13895.24	188.34	15.3	0.00	7.63E-05	1.03E-06	7.53E-04
59.125	13882.16	38.24	15.3	0.50	7.63E-05	2.10E-07	7.61E-04
59.132	14315.3	175.44	15.8	0.00	7.88E-05	9.66E-07	7.78E-04

CBC of Sr sorbed to 1 g/L HAO at pH 7 and 25°C with $[Sr]_{bulk} = 2.6 \times 10^{-5}$ M maintained constant

Time (h)	Time (d)	Moles Sr / g HAO
0.00	0.000	1.12E-05
0.03	0.001	2.01E-05
0.07	0.003	2.19E-05
0.08	0.003	2.25E-05
0.17	0.007	2.36E-05
0.25	0.010	2.47E-05
0.33	0.014	2.48E-05
0.50	0.02	2.52E-05
0.53	0.02	2.52E-05
0.75	0.03	2.56E-05
0.78	0.03	2.56E-05
1.00	0.04	2.57E-05
1.25	0.05	2.55E-05
1.75	0.07	2.51E-05
2.00	0.08	2.52E-05
2.25	0.09	2.54E-05
2.50	0.10	2.54E-05
4.00	0.17	2.52E-05
28.00	1.17	2.54E-05
52.00	2.17	2.55E-05
76.00	3.17	2.54E-05
100.00	4.17	2.56E-05
148.00	6.17	2.62E-05
148.17	6.17	2.65E-05
220.17	9.17	2.89E-05
220.33	9.18	2.90E-05
292.18	12.17	3.13E-05
292.34	12.18	3.16E-05
388.34	16.18	3.48E-05
388.51	16.19	3.54E-05
460.51	19.19	3.81E-05
460.66	19.19	3.81E-05
556.66	23.19	3.97E-05

CBC of Sr sorbed to 1 g/L HAO at pH 7 and 25°C with $[Sr]_{bulk} = 2.6 \times 10^{-5}$ M maintained constant (Contd.)

Time (h)	Time (d)	Moles Sr / g HAO
556.82	23.20	3.97E-05
676.99	28.21	4.13E-05
772.99	32.21	4.22E-05
773.16	32.22	4.23E-05
869.16	36.22	4.34E-05
869.33	36.22	4.36E-05
965.33	40.22	4.44E-05
965.50	40.23	4.46E-05
1061.50	44.23	4.52E-05
1061.66	44.24	4.53E-05
1157.66	48.24	4.55E-05
1157.83	48.24	4.58E-05
1253.66	52.24	4.60E-05
1253.83	52.24	4.62E-05
1349.83	56.24	4.66E-05
1350.00	56.25	4.67E-05
1446.00	60.25	4.67E-05
1542.00	64.25	4.66E-05
1662.00	69.25	4.66E-05
1758.00	73.25	4.65E-05
1854.00	77.25	4.66E-05
1950.00	81.25	4.66E-05
2046.00	85.25	4.66E-05
2118.00	88.25	4.66E-05

CBC of Sr sorbed to 1 g/L HAO at pH 8 and 25°C with $[Sr]_{bulk} = 2.6 \times 10^{-5}$ M maintained constant

Time (h)	Time (d)	Moles of Sr/ g HAO
0.00	0.000	1.31E-05
0.03	0.001	2.44E-05
0.07	0.003	2.68E-05
0.10	0.004	3.10E-05
0.17	0.007	3.11E-05
0.25	0.010	3.12E-05
0.33	0.014	3.12E-05
0.50	0.02	3.14E-05
0.75	0.03	3.15E-05
1.00	0.04	3.16E-05
1.50	0.06	3.14E-05
2.50	0.10	3.16E-05
3.00	0.13	3.22E-05
4.00	0.17	3.23E-05
5.00	0.21	3.24E-05
24.00	1.00	3.24E-05
48.00	2.00	3.31E-05

CBC of Sr sorbed to 1 g/L HAO at pH 8 and 25°C with $[Sr]_{bulk} = 2.6 \times 10^{-5}$ M maintained constant (Contd.)

Time (h)	Time (d)	Moles of Sr/ g HAO
72.00	3.00	3.38E-05
72.17	3.01	3.36E-05
168.00	7.00	3.51E-05
168.17	7.01	3.53E-05
216.17	9.01	3.87E-05
216.33	9.01	3.89E-05
576.17	24.01	4.44E-05
576.34	24.01	4.45E-05
648.34	27.01	4.58E-05
648.50	27.02	4.58E-05
744.50	31.02	4.78E-05
744.67	31.03	4.79E-05
936.50	39.02	4.95E-05
936.67	39.03	4.95E-05
1128.67	47.03	5.14E-05
1128.84	47.04	5.16E-05
1224.84	51.04	5.34E-05
1225.01	51.04	5.36E-05
1321.01	55.04	5.51E-05
1321.18	55.05	5.51E-05
1465.18	61.05	5.57E-05
1465.34	61.06	5.55E-05
1561.34	65.06	5.62E-05
1561.49	65.06	5.64E-05
1657.49	69.06	5.65E-05
1729.49	72.06	5.64E-05
1825.51	76.06	5.66E-05
1969.51	82.06	5.64E-05
2065.49	86.06	5.65E-05
2161.49	90.06	5.66E-05
2233.51	93.06	5.66E-05

Cadmium Studies with Amorphous Oxides

Cadmium adsorption edges at 25°C

HAO			HMO		
pH	μ = 0.060	μ =1.20	pH	μ = 0.015	μ =0.15
5.50	76.18		2.50	96.61	
6.00	90.25		3.00	97.44	
6.50	94.71		4.00	97.71	
7.00	96.22		5.00	97.89	
7.50	97.13		6.00	97.83	
7.60	97.22		7.00	97.76	
8.00	97.84		7.00	98.09	
9.00	97.95		8.00	98.24	
9.50	98.33		2.50		87.88
5.00	71.92		3.00		92.20
6.20	89.55		4.00		96.76
6.70	93.92		5.00		96.61
7.20	96.33		6.00		96.71
7.20	96.11		7.00		97.22
7.70	96.81		7.00		98.09
8.10	97.72		8.00		98.24
8.50	97.52				
8.80	97.58				
9.30	97.74				
10.00	97.94				
5.06		41.63			
5.52		44.94			
6.02		54.24			
6.50		76.27			
7.00		91.45			
7.00		91.19			
7.56		93.30			
8.07		94.25			
8.51		95.11			
9.00		95.21			
9.54		95.24			

Cadmium adsorption isotherms with HAO at pH 6 and multiple temperatures measured with liquid scintillating counter

		T= 25°C		T = 14°C		T = 4°C	
Initial Cd (M)	[Cd] (M)	C (moles Cd/ g HAO)	Initial Cd (M)	[Cd] (M)	C (moles Cd/ g HAO)	[Cd] (M)	C (moles Cd/ g HAO)
1.00E-06	7.90E-08	9.21E-07	1.00E-06	1.60E-07	8.40E-07	4.62E-07	5.38E-07
1.00E-06	8.81E-08	9.12E-07	8.00E-07	1.27E-07	6.73E-07	3.55E-07	4.45E-07
8.00E-07	7.20E-08	7.28E-07	5.00E-07	8.15E-08	4.19E-07	2.22E-07	2.78E-07
8.00E-07	7.16E-08	7.28E-07	3.00E-07	4.82E-08	2.52E-07	1.38E-07	1.62E-07
5.00E-07	4.50E-08	4.55E-07	1.00E-07	1.63E-08	8.37E-08	4.75E-08	5.25E-08
3.00E-07	2.80E-08	2.72E-07	8.00E-08	1.29E-08	6.71E-08	3.65E-08	4.35E-08
1.00E-07	1.19E-08	8.81E-08	5.00E-08	8.08E-09	4.19E-08	2.27E-08	2.73E-08
8.00E-08	6.69E-09	7.33E-08	5.00E-08	8.00E-09	4.20E-08	2.26E-08	2.74E-08
5.00E-08	4.32E-09	4.57E-08	3.00E-08	4.82E-09	2.52E-08	1.34E-08	1.66E-08
5.00E-08	4.30E-09	4.57E-08	1.00E-08	1.59E-09	8.41E-09	4.52E-09	5.48E-09
3.00E-08	2.49E-09	2.75E-08	8.00E-09	1.29E-09	6.71E-09	3.60E-09	4.40E-09
1.00E-08	9.19E-10	9.08E-09	8.00E-09	1.28E-09	6.72E-09	3.62E-09	4.38E-09
8.00E-09	7.21E-10	7.28E-09	5.00E-09	8.20E-10	4.18E-09	2.29E-09	2.71E-09
8.00E-09	7.38E-10	7.26E-09	3.00E-09	4.82E-10	2.52E-09	1.46E-09	1.54E-09
5.00E-09	4.76E-10	4.52E-09	1.00E-09	1.60E-10	8.40E-10	4.44E-10	5.56E-10
3.00E-09	2.57E-10	2.74E-09					
1.00E-09	1.10E-10	8.90E-10					

Cadmium adsorption isotherms with HAO at pH 7 and multiple temperatures measured with liquid scintillating counter

		T= 25°C		T = 11°C		T = 4°C	
Initial Cd (M)	[Cd] (M)	C (moles Cd/ g HAO)	Initial Cd (M)	[Cd] (M)	C (moles Cd/ g HAO)	[Cd] (M)	C (moles Cd/ g HAO)
1.00E-06	3.57E-08	9.64E-07	1.00E-06	5.79E-08	9.42E-07	2.54E-07	7.46E-07
8.00E-07	2.91E-08	7.71E-07	8.00E-07	4.35E-08	7.57E-07	1.95E-07	6.05E-07
5.00E-07	1.70E-08	4.83E-07	5.00E-07	2.73E-08	4.73E-07	1.27E-07	3.73E-07
3.00E-07	1.10E-08	2.89E-07	3.00E-07	1.68E-08	2.83E-07	7.98E-08	2.20E-07
1.00E-07	5.50E-09	9.45E-08	1.00E-07	5.60E-09	9.44E-08	2.48E-08	7.52E-08
8.00E-08	2.98E-09	7.70E-08	8.00E-08	4.43E-09	7.56E-08	2.05E-08	5.95E-08
5.00E-08	1.84E-09	4.82E-08	5.00E-08	2.79E-09	4.72E-08	1.19E-08	3.81E-08
5.00E-08	1.80E-09	4.82E-08	5.00E-08	2.78E-09	4.72E-08	1.25E-08	3.75E-08
3.00E-08	1.04E-09	2.90E-08	3.00E-08	1.69E-09	2.83E-08	7.64E-09	2.24E-08
1.00E-08	3.89E-10	9.61E-09	1.00E-08	5.66E-10	9.43E-09	2.49E-09	7.51E-09
8.00E-09	2.88E-10	7.71E-09	8.00E-09	4.49E-10	7.55E-09	2.00E-09	6.00E-09
8.00E-09	2.96E-10	7.70E-09	8.00E-09	4.44E-10	7.56E-09	2.01E-09	5.99E-09
5.00E-09	1.84E-10	4.82E-09	5.00E-09	2.81E-10	4.72E-09	1.23E-09	3.77E-09
3.00E-09	1.08E-10	2.89E-09	3.00E-09	1.66E-10	2.83E-09	7.60E-10	2.24E-09
1.00E-09	3.98E-11	9.60E-10	1.00E-09	5.61E-11	9.44E-10	2.45E-10	7.55E-10

Cadmium adsorption isotherms with HAO at pH 8 and multiple temperatures measured with liquid scintillating counter

	T= 25°C			T = 11°C			T = 4°C	
Initial Cd (M)	[Cd] (M)	C (moles Cd/ g HAO)	Initial Cd (M)	[Cd] (M)	C (moles Cd/ g HAO)		[Cd] (M)	C (moles Cd/ g HAO)
1.00E-06	9.73E-07	2.67E-08	1.00E-06	5.26E-08	9.47E-07		1.82E-07	8.18E-07
1.00E-06	9.74E-07	2.62E-08	8.00E-07	4.18E-08	7.58E-07		1.45E-07	6.55E-07
8.00E-07	7.79E-07	2.12E-08	5.00E-07	2.72E-08	4.73E-07		9.41E-08	4.06E-07
8.00E-07	7.79E-07	2.15E-08	3.00E-07	1.53E-08	2.85E-07		5.66E-08	2.43E-07
5.00E-07	4.87E-07	1.29E-08	1.00E-07	5.05E-09	9.50E-08		1.77E-08	8.23E-08
3.00E-07	2.92E-07	7.98E-09	8.00E-08	4.26E-09	7.57E-08		1.51E-08	6.49E-08
1.00E-07	9.70E-08	3.03E-09	5.00E-08	2.59E-09	4.74E-08		9.35E-09	4.06E-08
8.00E-08	7.79E-08	2.08E-09	5.00E-08	2.54E-09	4.75E-08		9.14E-09	4.09E-08
5.00E-08	4.87E-08	1.33E-09	3.00E-08	1.58E-09	2.84E-08		5.30E-09	2.47E-08
5.00E-08	4.87E-08	1.34E-09	1.00E-08	5.18E-10	9.48E-09		1.87E-09	8.13E-09
3.00E-08	2.92E-08	8.15E-10	8.00E-09	4.19E-10	7.58E-09		1.44E-09	6.56E-09
1.00E-08	9.73E-09	2.70E-10	8.00E-09	4.17E-10	7.58E-09		1.46E-09	6.54E-09
8.00E-09	7.79E-09	2.12E-10	5.00E-09	2.65E-10	4.73E-09		9.24E-10	4.08E-09
8.00E-09	7.78E-09	2.16E-10	3.00E-09	1.55E-10	2.85E-09		5.36E-10	2.46E-09
5.00E-09	4.87E-09	1.34E-10	1.00E-09	5.27E-11	9.47E-10		1.82E-10	8.18E-10
3.00E-09	2.92E-09	8.10E-11						
1.00E-09	9.73E-10	2.68E-11						

Cadmium adsorption isotherms with HMO at pH 7 and multiple temperatures measured with liquid scintillating counter

	T= 25°C			T = 14°C		T = 4°C	
Initial Cd (M)	[Cd] (M)	Moles Cd/g HMO	Cd] (M)	Moles Cd/g HMO		Cd] (M)	Moles Cd/g HMO
2.00E-10	4.12E-12	1.96E-09	1.77E-11	1.82E-09		5.83E-11	1.42E-09
5.00E-10	1.66E-11	4.83E-09	4.23E-11	4.58E-09		1.34E-10	3.66E-09
1.00E-09	1.99E-11	9.80E-09	1.12E-10	8.88E-09		2.81E-10	7.19E-09
5.00E-09	9.87E-11	4.90E-08	4.32E-10	4.57E-08		1.36E-09	3.64E-08
1.00E-08	4.39E-10	9.56E-08	8.24E-10	9.18E-08		2.66E-09	7.34E-08
5.00E-08	1.25E-09	4.88E-07	3.97E-09	4.60E-07		1.20E-08	3.80E-07
1.00E-07	2.10E-09	9.79E-07	9.18E-09	9.08E-07		2.87E-08	7.13E-07
5.00E-07	8.63E-09	4.91E-06	8.31E-08	4.17E-06		1.49E-07	3.51E-06
1.00E-06	2.43E-08	9.76E-06	8.50E-08	9.15E-06		2.89E-07	7.11E-06
4.00E-06	8.58E-08	3.91E-05	3.44E-07	3.66E-05		1.14E-06	2.86E-05
8.00E-06	1.71E-07	7.83E-05	6.72E-07	7.33E-05		2.35E-06	5.65E-05

Cadmium adsorption isotherms with HMO at pH 3.5 and multiple temperatures measured with liquid scintillating counter

		T= 25°C		T = 14°C		T = 4°C
Initial Cd (M)	[Cd] (M)	Moles Cd/g HMO	Cd] (M)	Moles Cd/g HMO	Cd] (M)	Moles Cd/g HMO
2.00E-10	2.92E-11	1.71E-09	7.27E-11	1.27E-09	1.46E-10	5.35E-10
5.00E-10	7.07E-11	4.29E-09	1.82E-10	3.18E-09	3.74E-10	1.26E-09
1.00E-09	2.01E-10	7.99E-09	3.61E-10	6.39E-09	7.45E-10	2.55E-09
5.00E-09	7.02E-10	4.30E-08	1.89E-09	3.11E-08	3.82E-09	1.18E-08
1.00E-08	1.24E-09	8.76E-08	4.29E-09	5.71E-08	7.27E-09	2.73E-08
5.00E-08	6.98E-09	4.30E-07	1.58E-08	3.42E-07	3.73E-08	1.27E-07
1.00E-07	1.42E-08	8.58E-07	3.68E-08	6.32E-07	7.27E-08	2.73E-07
5.00E-07	6.78E-08	4.32E-06	1.80E-07	3.20E-06	3.83E-07	1.17E-06
1.00E-06	1.35E-07	8.65E-06	3.74E-07	6.26E-06	7.37E-07	2.63E-06
4.00E-06	5.54E-07	3.45E-05	1.47E-06	2.53E-05	3.02E-06	9.85E-06
8.00E-06	1.06E-06	6.94E-05	2.92E-06	5.08E-05	5.95E-06	2.05E-05

CBC of Cd sorbed to 0.1 g/L HMO at pH 7 and 25°C

Time (d)	Total CPM	Final CPM	Cd ml	Add Cd	Total Cd M	CBC Cd	Cd/g HMO
0.000	0.00	0	0.0	0.0	0.00E+00	0.00E+00	0
0.000	2766.11	73.02	7.0	0.0	7.00E-08	1.85E-09	6.8152E-07
0.001	2766.11	70.56	7.0	0.0	7.00E-08	1.79E-09	6.8214E-07
0.003	2766.11	68.23	7.0	0.0	7.00E-08	1.73E-09	6.8273E-07
0.01	2766.11	64.25	7.0	0.0	7.00E-08	1.63E-09	6.8374E-07
0.02	2766.11	61.04	7.0	0.0	7.00E-08	1.54E-09	6.8455E-07
0.04	2766.11	62.37	7.0	0.0	7.00E-08	1.58E-09	6.8422E-07
0.08	2766.11	61.79	7.0	0.0	7.00E-08	1.56E-09	6.8436E-07
0.17	2766.11	62.5	7.0	0.0	7.00E-08	1.58E-09	6.8418E-07
0.35	2766.11	58.33	7.0	0.0	7.00E-08	1.48E-09	6.8524E-07
1.00	2766.11	57.44	7.0	0.1	7.00E-08	1.45E-09	6.8546E-07
1.01	3034.26	62.04	7.1	0.0	7.10E-08	1.45E-09	6.9548E-07
2.01	3078.04	10.53	7.1	1.5	7.10E-08	2.43E-10	7.0757E-07
2.01	4000.65	68.66	8.6	0.0	8.64E-08	1.48E-09	8.4875E-07
3.01	4008.74	40.31	8.6	1.5	8.64E-08	8.68E-10	8.5489E-07
3.02	4859.22	72.04	10.1	0.0	1.01E-07	1.50E-09	9.9854E-07
4.02	4913.18	47.05	10.1	2.0	1.01E-07	9.71E-10	1.0039E-06
4.03	5466.05	73.21	12.1	0.0	1.21E-07	1.63E-09	1.1973E-06
5.03	5454.07	43.45	12.1	2.0	1.21E-07	9.67E-10	1.2039E-06
5.03	6035.66	66.89	14.1	0.0	1.41E-07	1.57E-09	1.3979E-06
6.03	6738.15	41.26	14.1	2.0	1.41E-07	8.66E-10	1.4049E-06
6.04	7313.14	69.25	16.1	0.0	1.61E-07	1.53E-09	1.5983E-06
7.04	7257.68	40.11	16.1	1.5	1.61E-07	8.92E-10	1.6047E-06
7.05	7646.35	70.37	17.6	0.0	1.76E-07	1.62E-09	1.7473E-06
8.05	7332.16	33.14	17.6	0.5	1.76E-07	7.97E-10	1.7556E-06
8.06	7757.65	80.23	18.1	0.0	1.81E-07	1.88E-09	1.7948E-06
9.05	7741.14	28.16	18.1	0.6	1.81E-07	6.60E-10	1.807E-06
9.06	8103.26	71.22	18.7	0.0	1.87E-07	1.65E-09	1.8571E-06
10.05	8120.56	34.22	18.7	0.5	1.87E-07	7.90E-10	1.8657E-06
10.06	8427.61	74.16	19.2	0.0	1.92E-07	1.69E-09	1.9066E-06
11.05	8333.33	24.97	19.2	1.0	1.92E-07	5.76E-10	1.9159E-06
11.06	8717.09	70.25	20.2	0.0	2.02E-07	1.63E-09	2.0054E-06
12.05	8700.69	28.05	20.2	1.0	2.02E-07	6.51E-10	2.0138E-06
12.06	8974.26	68.42	21.2	0.0	2.12E-07	1.62E-09	2.1042E-06
14.05	8744.16	16.13	21.2	1.0	2.12E-07	3.91E-10	2.1153E-06
14.06	9104.22	66.17	22.2	0.0	2.22E-07	1.61E-09	2.2031E-06
16.05	9380.37	17.14	22.2	1.0	2.22E-07	4.05E-10	2.214E-06
16.06	9799.61	65.42	23.2	0.0	2.32E-07	1.55E-09	2.3026E-06
18.05	9883.26	22.8	23.2	1.0	2.32E-07	5.35E-10	2.3122E-06
18.06	10024.07	68.17	24.2	0.0	2.42E-07	1.64E-09	2.4011E-06
21.06	9891.45	17.05	24.2	1.0	2.42E-07	4.17E-10	2.4134E-06
21.06	10014.69	68.32	25.2	0.0	2.52E-07	1.72E-09	2.5004E-06
24.06	10037.99	11.14	25.2	1.0	2.52E-07	2.79E-10	2.5148E-06
24.07	10430.47	66.25	26.2	0.0	2.62E-07	1.66E-09	2.601E-06
28.07	10683.15	10.84	26.2	1.0	2.62E-07	2.65E-10	2.6133E-06
28.08	11005.49	64.23	27.2	0.0	2.72E-07	1.59E-09	2.7001E-06
32.08	10744.53	10.09	27.2	2.5	2.72E-07	2.55E-10	2.7126E-06
32.08	11179.50	59.06	29.7	0.0	2.97E-07	1.57E-09	2.9494E-06

CBC of Cd sorbed to 0.1 g/L HMO at pH 7 and 25°C (contd.)

Time (d)	Total CPM	Final CPM	Cd ml	Add Cd	Total Cd M	CBC Cd	Cd/g HMO
35.08	11791.35	10.36	29.7	1.5	2.97E-07	2.61E-10	2.9625E-06
35.09	11954.54	61.45	31.2	0.0	3.12E-07	1.60E-09	3.0991E-06
39.09	12007.16	16.27	31.1	2.0	3.11E-07	4.22E-10	3.1099E-06
39.10	12141.75	68.34	33.1	0.0	3.31E-07	1.87E-09	3.2954E-06
42.10	12088.01	14.22	33.1	1.0	3.31E-07	3.89E-10	3.3065E-06
42.10	12370.24	67.23	34.1	0.0	3.41E-07	1.85E-09	3.3919E-06
45.10	12370.20	15.06	34.1	1.0	3.41E-07	4.15E-10	3.4063E-06
45.11	12715.40	67.54	35.1	0.0	3.51E-07	1.86E-09	3.4918E-06
48.11	12646.19	10.41	35.1	1.0	3.51E-07	2.89E-10	3.5076E-06
48.12	12900.33	64.25	36.1	0.0	3.61E-07	1.80E-09	3.5925E-06
51.12	12832.72	10.53	36.1	1.0	3.61E-07	2.96E-10	3.6075E-06
51.13	12991.03	64.93	37.1	0.0	3.71E-07	1.85E-09	3.6919E-06
55.13	13037.06	12.1	37.1	0.5	3.71E-07	3.44E-10	3.707E-06
55.13	13149.09	63.56	37.6	0.0	3.76E-07	1.82E-09	3.7423E-06
58.13	13144.35	15.38	37.6	0.5	3.76E-07	4.40E-10	3.756E-06
58.14	13200.00	60.53	38.1	0.0	3.81E-07	1.75E-09	3.793E-06
61.14	13184.51	15.41	38.1	0.2	3.81E-07	4.45E-10	3.806E-06
61.15	13285.26	60.41	38.3	0.0	3.83E-07	1.74E-09	3.813E-06

CBC of Cd sorbed to 1 g/L HAO at pH 7 and 25°C with $[Cd]_{bulk} = 1 \times 10^{-8}$ M maintained constant

Time (h)	Time (d)	Moles of Cd/ g HAO
0.000	0.0000	4.855E-07
0.017	0.0007	5.361E-07
0.083	0.0035	5.385E-07
0.167	0.0069	5.414E-07
0.167	0.0069	5.409E-07
0.250	0.0104	5.419E-07
0.333	0.0139	5.418E-07
0.500	0.0208	5.417E-07
0.667	0.0278	5.415E-07
0.750	0.0313	5.418E-07
0.833	0.0347	5.417E-07
1.000	0.0417	5.419E-07
1.500	0.0625	5.415E-07
2.000	0.0833	5.419E-07
3.000	0.1250	5.413E-07
4.000	0.1667	5.419E-07
24.000	1.0000	5.418E-07
48.000	2.0000	5.417E-07
72.000	3.0000	5.418E-07
120.000	5.0000	5.418E-07
144.000	6.0000	5.418E-07
168.000	7.0000	5.419E-07
192.000	8.0000	5.420E-07
216.000	9.0000	5.432E-07
216.166	9.0069	5.767E-07

CBC of Cd sorbed to 1 g/L HAO at pH 7 and 25°C with $[Cd]_{bulk} = 1 \times 10^{-8}$ M maintained constant (Contd.)

Time (h)	Time (d)	Moles of Cd/ g HAO
288.168	12.0070	5.781E-07
288.336	12.0140	6.067E-07
336.336	14.0140	6.079E-07
336.504	14.0210	6.370E-07
408.504	17.0210	6.378E-07
408.672	17.0280	6.570E-07
480.672	20.0280	6.575E-07
480.840	20.0350	6.769E-07
528.840	22.0350	6.773E-07
529.008	22.0420	6.966E-07
577.008	24.0420	6.973E-07
577.176	24.0490	7.163E-07
649.176	27.0490	7.171E-07
721.176	30.0490	7.364E-07
769.176	32.0490	7.374E-07
769.344	32.0560	7.492E-07
817.344	34.0560	7.577E-07
817.488	34.0620	7.768E-07
913.488	38.0620	7.777E-07
913.656	38.0690	7.965E-07
961.656	40.0690	7.976E-07
961.824	40.0760	8.168E-07
1009.824	42.0760	8.175E-07
1009.992	42.0830	8.317E-07
1057.992	44.0830	8.324E-07
1058.160	44.0900	8.413E-07
1106.160	46.0900	8.425E-07
1106.328	46.0970	8.567E-07
1154.328	48.0970	8.575E-07
1154.496	48.1040	8.719E-07
1202.496	50.1040	8.723E-07
1202.928	50.1220	8.818E-07
1250.928	52.1220	8.823E-07
1251.336	52.1390	8.917E-07
1299.336	54.1390	8.923E-07
1300.008	54.1670	9.018E-07
1372.008	57.1670	9.023E-07
1372.656	57.1940	9.117E-07
1468.656	61.1940	9.125E-07
1469.328	61.2220	9.218E-07
1565.328	65.2220	9.223E-07
1566.000	65.2500	9.318E-07
1662.000	69.2500	9.324E-07
1662.672	69.2780	9.419E-07
1758.672	73.2780	9.424E-07
1759.344	73.3060	9.518E-07

CBC of Cd sorbed to 1 g/L HAO at pH 7 and 25°C with $[Cd]_{bulk} = 1 \times 10^{-8}$ M maintained constant (Contd.)

Time (h)	Time (d)	Moles of Cd/ g HAO
1831.344	76.3060	9.523E-07
1831.992	76.3330	9.569E-07
1927.992	80.3330	9.574E-07
1928.664	80.3610	9.620E-07
1976.664	82.3610	9.626E-07
1977.336	82.3890	9.672E-07
2073.336	86.3890	9.675E-07
2074.008	86.4170	9.720E-07
2170.008	90.4170	9.725E-07
2170.656	90.4440	9.769E-07
2218.656	92.4440	9.770E-07
2219.328	92.4720	9.770E-07
2339.328	97.4720	9.772E-07
2340.000	97.5000	9.817E-07
2436.000	101.5000	9.820E-07
2436.720	101.5300	9.827E-07
2532.720	105.5300	9.830E-07
2533.440	105.5600	9.840E-07

Zinc Studies with Amorphous Oxides

Zinc adsorption edges at 25°C

HAO			HFO			HMO		
pH	m = 0.060	m =1.50	pH	m = 0.031	m =1.50	pH	m = 0.015	m =1.50
5.02	64.87		4.43	36.47		2.15	68.92	
5.52	81.89		5.01	66.65		2.54	81.56	
6.04	91.74		5.47	85.18		2.99	89.92	
6.53	92.47		6.06	93.46		3.47	92.49	
7.04	97.28		6.56	94.53		4.05	95.20	
7.57	97.46		7.02	98.36		4.51	97.88	
8.07	98.02		7.53	98.91		5.04	98.31	
8.54	98.88		8.04	99.09		5.51	98.48	
9.00	99.15		8.51	99.51		6.10	98.74	
9.49	99.15		9.06	99.63		7.06	98.85	
9.91	99.20		9.57	99.66		2.08		59.29
5.05		13.62	10.00	99.65		2.51		66.57
5.51		38.51	4.43		13.28	3.02		74.45
6.06		55.68	5.09		28.18	3.51		82.88
6.52		85.24	5.44		53.06	4.00		90.79
7.06		87.80	6.00		65.08	4.49		93.51
7.56		89.29	6.52		80.66	5.01		94.28
8.04		93.39	7.04		89.31	5.55		95.00
8.51		90.65	7.51		90.05	6.03		95.02
9.05		91.24	8.01		92.11	7.03		95.23
9.53		91.36	8.51		92.41			
10.01		91.33	9.02		92.61			
			9.47		93.83			
			9.98		93.84			

Zinc adsorption isotherms with HAO at pH 6 and multiple temperatures measured with liquid scintillating counter

	T= 25°C		T = 14°C		T = 4°C	
Initial Zn (M)	[Zn] (M)	Moles Zn/g HAO	[Zn] (M)	Moles Zn/g HAO	[Zn] (M)	Moles Zn/g HAO
1.00E-05	8.09E-07	9.19E-06	1.71E-06	8.29E-06	4.92E-06	5.08E-06
8.00E-06	6.80E-07	7.32E-06	1.40E-06	6.60E-06	3.93E-06	4.07E-06
8.00E-06	6.86E-07	7.31E-06	1.39E-06	6.61E-06	3.87E-06	4.13E-06
5.00E-06	4.08E-07	4.60E-06	8.78E-07	4.12E-06	2.32E-06	2.68E-06
3.00E-06	2.29E-07	2.77E-06	5.06E-07	2.49E-06	1.57E-06	1.43E-06
1.00E-06	8.85E-08	9.11E-07	1.90E-07	8.10E-07	4.77E-07	5.23E-07
5.00E-07	4.74E-08	4.52E-07	8.86E-08	4.11E-07	2.13E-07	2.86E-07
3.00E-07	2.63E-08	2.74E-07	4.93E-08	2.51E-07	1.47E-07	1.53E-07
1.00E-07	8.74E-09	9.13E-08	1.78E-08	8.22E-08	4.81E-08	5.19E-08
1.00E-07	4.83E-09	9.52E-08	1.74E-08	8.26E-08	5.09E-08	4.91E-08
8.00E-08	8.37E-09	7.17E-08	1.50E-08	6.51E-08	4.06E-08	3.94E-08
5.00E-08	3.98E-09	4.61E-08	9.05E-09	4.10E-08	2.41E-08	2.60E-08
3.00E-08	2.43E-09	2.75E-08	4.86E-09	2.51E-08	1.39E-08	1.61E-08
1.00E-08	8.06E-10	9.19E-09	1.90E-09	8.10E-09	5.50E-09	4.50E-09
8.00E-09	7.37E-10	7.27E-09	1.40E-09	6.60E-09	3.80E-09	4.20E-09

Zinc adsorption isotherms with HAO at pH 7 and multiple temperatures measured with liquid scintillating counter

		T= 25°C		T = 14°C		T = 4°C
Initial Zn (M)	[Zn] (M)	Moles Zn/g HAO	[Zn] (M)	Moles Zn/g HAO	[Zn] (M)	Moles Zn/g HAO
1.00E-05	3.15E-07	9.68E-06	7.17E-07	9.28E-06	2.64E-06	7.36E-06
8.00E-06	2.65E-07	7.73E-06	5.86E-07	7.41E-06	2.21E-06	5.79E-06
8.00E-06	2.66E-07	7.73E-06	5.62E-07	7.44E-06	2.23E-06	5.77E-06
5.00E-06	1.67E-07	4.84E-06	4.30E-07	4.57E-06	1.24E-06	3.77E-06
3.00E-06	1.15E-07	2.88E-06	2.01E-07	2.80E-06	6.32E-07	2.37E-06
1.00E-06	2.73E-08	9.73E-07	7.45E-08	9.25E-07	2.69E-07	7.31E-07
5.00E-07	1.99E-08	4.80E-07	2.67E-08	4.73E-07	1.35E-07	3.65E-07
3.00E-07	7.47E-09	2.93E-07	2.15E-08	2.79E-07	8.71E-08	2.13E-07
1.00E-07	3.31E-09	9.67E-08	7.33E-09	9.27E-08	2.87E-08	7.14E-08
1.00E-07	3.72E-09	9.63E-08	7.75E-09	9.23E-08	3.34E-08	6.67E-08
8.00E-08	2.63E-09	7.74E-08	5.46E-09	7.46E-08	1.84E-08	6.16E-08
5.00E-08	1.60E-09	4.84E-08	4.32E-09	4.57E-08	1.51E-08	3.49E-08
3.00E-08	1.44E-09	2.85E-08	1.93E-09	2.80E-08	7.68E-09	2.23E-08
1.00E-08	6.49E-10	9.35E-09	7.68E-10	9.23E-09	2.89E-09	7.11E-09
8.00E-09	1.36E-10	7.87E-09	5.67E-10	7.44E-09	1.74E-09	6.26E-09
5.00E-09	1.94E-10	4.81E-09	1.74E-10	4.83E-09	1.47E-09	3.53E-09
3.00E-09	1.07E-10	2.89E-09	2.40E-10	2.76E-09	8.41E-10	2.16E-09
1.00E-09	3.37E-11	9.66E-10	8.24E-11	9.17E-10	2.78E-10	7.21E-10

Zinc adsorption isotherms with HAO at pH 8 and multiple temperatures measured with liquid scintillating counter

		T= 25°C		T = 14°C		T = 4°C
Initial Zn (M)	[Zn] (M)	Moles Zn/g HAO	[Zn] (M)	Moles Zn/g HAO	[Zn] (M)	Moles Zn/g HAO
1.00E-05	1.79E-07	9.82E-06	4.87E-07	9.51E-05	1.61E-06	8.39E-06
8.00E-06	1.26E-07	7.87E-06	3.85E-07	7.61E-05	1.32E-06	6.68E-06
8.00E-06	1.32E-07	7.87E-06	3.97E-07	7.60E-05	1.26E-06	6.74E-06
5.00E-06	9.79E-08	4.90E-06	2.47E-07	4.76E-05	7.15E-07	4.29E-06
3.00E-06	4.20E-08	2.96E-06	1.50E-07	2.85E-05	6.02E-07	2.40E-06
1.00E-06	2.29E-08	9.77E-07	8.91E-08	9.11E-06	1.64E-07	8.36E-07
5.00E-07	9.00E-09	4.91E-07	2.11E-08	4.79E-06	6.57E-08	4.34E-07
3.00E-07	5.31E-09	2.95E-07	1.42E-08	2.86E-06	4.53E-08	2.55E-07
1.00E-07	1.71E-09	9.83E-08	4.38E-09	9.57E-07	1.46E-08	8.55E-08
1.00E-07	1.62E-09	9.84E-08	4.50E-09	9.55E-07	1.51E-08	8.49E-08
8.00E-08	1.14E-09	7.89E-08	4.21E-09	7.58E-07	1.27E-08	6.73E-08
5.00E-08	7.05E-10	4.93E-08	2.86E-09	4.72E-07	7.58E-09	4.25E-08
3.00E-08	5.40E-10	2.94E-08	2.41E-09	2.76E-07	4.60E-09	2.54E-08
1.00E-08	1.71E-10	9.83E-09	5.01E-10	9.50E-08	1.12E-09	8.88E-09
8.00E-09	1.33E-10	7.87E-09	4.01E-10	7.60E-08	1.24E-09	6.76E-09
5.00E-09	9.13E-11	4.91E-09	2.38E-10	4.76E-08	6.76E-10	4.33E-09
3.00E-09	3.32E-11	2.97E-09	1.89E-10	2.81E-08	4.60E-10	2.54E-09
1.00E-09	1.56E-11	9.84E-10	8.01E-11	9.20E-09	1.42E-10	8.58E-10

Zinc adsorption isotherms with HFO at pH 6 and multiple temperatures measured with liquid scintillating counter

	T= 25°C		T = 14°C		T = 4°C	
Initial Zn (M)	[Zn] (M)	Moles Zn/g HFO	[Zn] (M)	Moles Zn/g HFO	[Zn] (M)	Moles Zn/g HFO
1.00E-05	6.52E-07	9.35E-06	1.43E-06	8.57E-06	5.23E-06	4.76E-06
8.00E-06	5.43E-07	7.46E-06	1.17E-06	6.83E-06	4.27E-06	3.73E-06
8.00E-06	5.01E-07	7.50E-06	1.18E-06	6.82E-06	4.37E-06	3.63E-06
5.00E-06	3.36E-07	4.67E-06	7.67E-07	4.24E-06	2.69E-06	2.31E-06
3.00E-06	1.70E-07	2.83E-06	4.53E-07	2.55E-06	1.63E-06	1.36E-06
1.00E-06	5.69E-08	9.43E-07	1.51E-07	8.49E-07	5.36E-07	4.64E-07
5.00E-07	2.90E-08	4.71E-07	7.60E-08	4.24E-07	2.79E-07	2.21E-07
3.00E-07	2.39E-08	2.76E-07	5.17E-08	2.49E-07	1.65E-07	1.35E-07
1.00E-07	7.32E-09	9.27E-08	1.57E-08	8.43E-08	5.42E-08	4.58E-08
1.00E-07	3.17E-09	9.68E-08	1.55E-08	8.45E-08	5.50E-08	4.50E-08
8.00E-08	6.55E-09	7.35E-08	1.52E-08	6.48E-08	4.23E-08	3.77E-08
5.00E-08	2.86E-09	4.72E-08	7.14E-09	4.29E-08	2.70E-08	2.30E-08
3.00E-08	1.61E-09	2.84E-08	5.31E-09	2.47E-08	1.59E-08	1.41E-08
1.00E-08	4.18E-10	9.58E-09	1.71E-09	8.29E-09	4.56E-09	5.44E-09
8.00E-09	6.20E-10	7.38E-09	1.26E-09	6.74E-09	4.39E-09	3.61E-09
5.00E-09			7.82E-10	4.22E-09	2.77E-09	2.23E-09
3.00E-09			5.00E-10	2.50E-09	1.54E-09	1.46E-09
1.00E-09			1.80E-10	8.20E-10	5.58E-10	4.42E-10

Zinc adsorption isotherms with HFO at pH 7 and multiple temperatures measured with liquid scintillating counter

	T= 25°C		T = 14°C		T = 4°C	
Initial Zn (M)	[Zn] (M)	Moles Zn/g HFO	[Zn] (M)	Moles Zn/g HFO	[Zn] (M)	Moles Zn/g HFO
1.00E-05			4.41E-07	9.56E-06	2.09E-06	7.91E-06
8.00E-06	1.18E-07	7.88E-06	4.08E-07	7.59E-06	1.74E-06	6.26E-06
8.00E-06	1.24E-07	7.88E-06	3.94E-07	7.61E-06	1.73E-06	6.27E-06
5.00E-06	1.04E-07	4.90E-06	1.74E-07	4.83E-06	1.09E-06	3.91E-06
3.00E-06	5.31E-08	2.95E-06	1.56E-07	2.84E-06	6.46E-07	2.35E-06
1.00E-06	1.87E-08	9.81E-07	5.02E-08	9.50E-07	1.73E-07	8.27E-07
5.00E-07	9.11E-09	4.91E-07	2.50E-08	4.75E-07	1.06E-07	3.93E-07
3.00E-07	4.40E-09	2.96E-07	1.60E-08	2.84E-07	7.64E-08	2.24E-07
1.00E-07	1.30E-09	9.87E-08	5.05E-09	9.50E-08	2.26E-08	7.75E-08
1.00E-07	1.37E-09	9.86E-08	4.92E-09	9.51E-08	2.30E-08	7.70E-08
8.00E-08	1.48E-09	7.86E-08	4.42E-09	7.56E-08	1.97E-08	6.03E-08
5.00E-08	9.89E-10	4.90E-08	2.05E-09	4.80E-08	9.97E-09	4.01E-08
3.00E-08	5.87E-10	2.94E-08	1.44E-09	2.85E-08	6.72E-09	2.33E-08
1.00E-08	2.30E-10	9.77E-09	5.00E-10	9.50E-09	2.18E-09	7.82E-09
8.00E-09	1.24E-10	7.88E-09	2.86E-10	7.72E-09	1.72E-09	6.29E-09
5.00E-09	1.10E-10	4.89E-09	2.26E-10	4.78E-09	1.06E-09	3.94E-09
3.00E-09	4.96E-11	2.95E-09	1.71E-10	2.83E-09	7.00E-10	2.30E-09
1.00E-09	2.42E-11	9.76E-10	5.06E-11	9.49E-10	2.28E-10	7.72E-10

Zinc adsorption isotherms with HFO at pH 8 and multiple temperatures measured with liquid scintillating counter

	T= 25°C		T = 14°C		T = 4°C	
Initial Zn (M)	[Zn] (M)	Moles Zn/g HFO	[Zn] (M)	Moles Zn/g HFO	[Zn] (M)	Moles Zn/g HFO
1.00E-05	9.14E-08	9.91E-06	2.70E-07	9.73E-06	1.31E-06	8.68E-06
8.00E-06	7.11E-08	7.93E-06	2.53E-07	7.75E-06	9.82E-07	7.02E-06
8.00E-06	6.96E-08	7.93E-06	2.28E-07	7.77E-06	9.95E-07	7.01E-06
5.00E-06	4.91E-08	4.95E-06	1.30E-07	4.87E-06	6.19E-07	4.38E-06
3.00E-06	2.94E-08	2.97E-06	6.51E-08	2.93E-06	3.09E-07	2.69E-06
1.00E-06	9.17E-09	9.91E-07	2.72E-08	9.73E-07	1.17E-07	8.83E-07
5.00E-07	5.26E-09	4.95E-07	1.59E-08	4.84E-07	5.35E-08	4.46E-07
3.00E-07	2.94E-09	2.97E-07	1.00E-08	2.90E-07	4.09E-08	2.59E-07
1.00E-07	6.39E-10	9.94E-08	1.77E-09	9.83E-08	1.08E-08	8.93E-08
1.00E-07	4.74E-10	9.95E-08	1.87E-09	9.81E-08	1.10E-08	8.90E-08
8.00E-08	6.86E-10	7.94E-08	1.74E-09	7.83E-08	9.66E-09	7.04E-08
5.00E-08	4.76E-10	4.96E-08	1.47E-09	4.86E-08	5.71E-09	4.43E-08
3.00E-08	3.53E-10	2.96E-08	9.65E-10	2.90E-08	4.24E-09	2.57E-08
1.00E-08	6.48E-11	9.94E-09	3.67E-10	9.63E-09	1.10E-09	8.90E-09
8.00E-09	8.87E-11	7.91E-09	1.96E-10	7.81E-09	1.04E-09	6.96E-09
5.00E-09	4.81E-11	4.95E-09	1.34E-10	4.87E-09	6.15E-10	4.39E-09
3.00E-09	2.51E-11	2.97E-09	8.94E-11	2.91E-09	5.53E-10	2.45E-09
1.00E-09	8.81E-12	9.91E-10	3.18E-11	9.68E-10	1.23E-10	8.77E-10

Zinc adsorption isotherms with HMO at pH 7 and multiple temperatures measured with liquid scintillating counter

	T= 25°C		T = 14°C		T = 4°C	
Initial Zn (M)	[Zn] (M)	C molesZn/ g HMO	[Zn] (M)	C molesZn/ g HMO	[Zn] (M)	C molesZn/ g HMO
1.00E-05	1.07E-07	9.89E-05	4.87E-07	9.51E-05	2.24E-06	7.76E-05
8.00E-06	1.12E-07	7.89E-05	3.85E-07	7.61E-05	1.77E-06	6.23E-05
8.00E-06	1.00E-07	7.90E-05	3.97E-07	7.60E-05	1.82E-06	6.18E-05
5.00E-06	6.64E-08	4.93E-05	2.47E-07	4.76E-05	1.13E-06	3.87E-05
3.00E-06	2.99E-08	2.97E-05	1.50E-07	2.85E-05	6.89E-07	2.31E-05
1.00E-06	1.69E-08	9.83E-06	8.91E-08	9.11E-06	4.10E-07	5.90E-06
5.00E-07	4.68E-09	4.95E-06	2.11E-08	4.79E-06	9.73E-08	4.03E-06
3.00E-07	4.49E-09	2.96E-06	1.42E-08	2.86E-06	6.52E-08	2.35E-06
1.00E-07	1.41E-09	9.86E-07	4.38E-09	9.57E-07	2.02E-08	7.99E-07
1.00E-07	1.31E-09	9.87E-07	4.50E-09	9.55E-07	2.07E-08	7.93E-07
8.00E-08	1.10E-09	7.89E-07	4.21E-09	7.58E-07	1.94E-08	6.07E-07
5.00E-08	6.25E-10	4.94E-07	2.86E-09	4.72E-07	1.31E-08	3.69E-07
3.00E-08	4.25E-10	2.96E-07	2.41E-09	2.76E-07	1.11E-08	1.89E-07
1.00E-08	1.52E-10	9.85E-08	5.01E-10	9.50E-08	2.30E-09	7.70E-08
8.00E-09	1.01E-10	7.90E-08	4.01E-10	7.60E-08	1.84E-09	6.16E-08
5.00E-09	4.88E-11	4.95E-08	2.38E-10	4.76E-08	1.09E-09	3.91E-08
3.00E-09	3.87E-11	2.96E-08	1.89E-10	2.81E-08	8.71E-10	2.13E-08
1.00E-09	1.17E-11	9.88E-09	8.01E-11	9.20E-09	2.29E-10	7.71E-09

Zinc adsorption isotherms with HMO at pH 5 and multiple temperatures measured with liquid scintillating counter

	T= 25°C		T = 14°C		T = 4°C	
Initial Zn (M)	[Zn] (M)	C molesZn/ g HMO	[Zn] (M)	C molesZn/ g HMO	[Zn] (M)	C molesZn/ g HMO
1.00E-05	2.05E-07	9.80E-06	1.08E-06	8.92E-05	3.56E-06	6.43E-05
8.00E-06	1.60E-07	7.84E-06	9.07E-07	7.09E-05	2.92E-06	5.08E-05
8.00E-06	1.68E-07	7.83E-06	9.41E-07	7.06E-05	2.99E-06	5.01E-05
5.00E-06	9.88E-08	4.90E-06	6.10E-07	4.39E-05	1.36E-06	3.64E-05
3.00E-06	6.78E-08	2.93E-06	4.47E-07	2.55E-05	8.98E-07	2.10E-05
1.00E-06	1.99E-08	9.80E-07	1.02E-07	8.98E-06	6.08E-07	3.92E-06
5.00E-07	1.03E-08	4.90E-07	5.82E-08	4.42E-06	1.72E-07	3.28E-06
3.00E-07	5.51E-09	2.94E-07	3.84E-08	2.62E-06	1.10E-07	1.91E-06
1.00E-07	2.12E-09	9.79E-08	1.27E-08	8.74E-07	4.25E-08	5.76E-07
1.00E-07	1.77E-09	9.82E-08	1.29E-08	8.71E-07	3.87E-08	6.13E-07
8.00E-08	1.84E-09	7.82E-08	1.00E-08	7.00E-07	2.89E-08	5.11E-07
5.00E-08	1.20E-09	4.88E-08	4.17E-09	4.59E-07	2.26E-08	2.74E-07
3.00E-08	5.89E-10	2.94E-08	3.32E-09	2.67E-07	2.12E-08	8.73E-08
1.00E-08	2.02E-10	9.80E-09	1.14E-09	8.86E-08	3.53E-09	6.47E-08
8.00E-09	9.52E-11	7.90E-09	9.19E-10	7.08E-08	2.73E-09	5.27E-08
5.00E-09	8.70E-11	4.91E-09	5.80E-10	4.42E-08	1.83E-09	3.17E-08
3.00E-09	4.02E-11	2.96E-09	3.39E-10	2.66E-08	1.47E-09	1.53E-08
1.00E-09	2.40E-11	9.76E-10	1.09E-10	8.91E-09	2.62E-10	7.38E-09
5.00E-10	1.28E-11	4.87E-10				

Zinc adsorption isotherms with HMO at pH 3.5 and multiple temperatures measured with liquid scintillating counter

	T= 25°C		T = 14°C		T = 4°C	
Initial Zn (M)	[Zn] (M)	C molesZn/ g HMO	[Zn] (M)	C molesZn/ g HMO	[Zn] (M)	C molesZn/ g HMO
1.00E-05	7.73E-07	9.23E-05	3.00E-06	7.00E-05	6.47E-06	3.53E-05
8.00E-06	5.39E-07	7.46E-05	2.47E-06	5.53E-05	5.41E-06	2.58E-05
8.00E-06	5.67E-07	7.43E-05	2.36E-06	5.64E-05	5.40E-06	2.60E-05
5.00E-06	3.20E-07	4.68E-05	1.43E-06	3.58E-05	3.08E-06	1.92E-05
3.00E-06	2.35E-07	2.77E-05	6.29E-07	2.37E-05	1.73E-06	1.27E-05
1.00E-06	7.43E-08	9.26E-06	3.77E-07	6.23E-06	6.13E-07	3.87E-06
5.00E-07	2.17E-08	4.78E-06	1.47E-07	3.53E-06	3.25E-07	1.74E-06
3.00E-07	1.68E-08	2.83E-06	8.45E-08	2.16E-06	1.92E-07	1.09E-06
1.00E-07	9.27E-09	9.07E-07	3.00E-08	7.01E-07	5.86E-08	4.14E-07
1.00E-07	8.77E-09	9.12E-07	2.93E-08	7.07E-07	6.68E-08	3.32E-07
8.00E-08	9.01E-09	7.10E-07	2.16E-08	5.84E-07	5.46E-08	2.54E-07
5.00E-08	3.70E-09	4.63E-07	1.30E-08	3.70E-07	3.41E-08	1.59E-07
3.00E-08	1.98E-09	2.80E-07	1.10E-08	1.90E-07	2.30E-08	7.01E-08
1.00E-08	8.17E-10	9.18E-08	3.01E-09	6.99E-08	6.71E-09	3.29E-08
8.00E-09	6.78E-10	7.32E-08	2.35E-09	5.65E-08	5.01E-09	2.99E-08
5.00E-09	4.55E-10	4.55E-08	1.58E-09	3.42E-08	3.61E-09	1.39E-08
3.00E-09	1.84E-10	2.82E-08	7.89E-10	2.21E-08	2.89E-09	1.06E-09
1.00E-09	9.03E-11	9.10E-09	3.06E-10	6.94E-09	8.07E-10	1.93E-09

CBC of Zn sorbed to HAO at pH 7 and 25°C

Time s	Total CPM	Final CPM	Zn ml	Add Zn	Total Zn M	CBC Zn	Zn/g HAO
0	0	0	0.000	0.00	0.00E+00	0.00E+00	0.00E+00
30	2400.26	150	4.100	0.00	4.10E-08	2.56E-09	3.84E-08
60	2400.26	97	4.100	0.00	4.10E-08	1.66E-09	3.93E-08
300	2400.26	78.6	4.100	0.00	4.10E-08	1.34E-09	3.97E-08
900	2400.26	86.22	4.100	0.00	4.10E-08	1.47E-09	3.95E-08
1800	2400.26	81.43	4.100	0.00	4.10E-08	1.39E-09	3.96E-08
3600	2400.26	82.35	4.100	0.00	4.10E-08	1.41E-09	3.96E-08
7200	2400.26	80.42	4.100	0.00	4.10E-08	1.37E-09	3.96E-08
14400	2400.26	79.09	4.100	0.00	4.10E-08	1.35E-09	3.96E-08
86400	2589.48	10.34	4.100	0.60	4.10E-08	1.64E-10	4.08E-08
87000	3250.09	91.77	4.700	0.00	4.70E-08	1.33E-09	4.57E-08
172800	3264.16	27.95	4.697	0.50	4.70E-08	4.02E-10	4.66E-08
173400	3638.21	95.26	5.197	0.00	5.20E-08	1.36E-09	5.06E-08
259200	3638.21	43.25	5.197	0.40	5.20E-08	6.18E-10	5.14E-08
259800	4105.23	100.01	5.597	0.00	5.60E-08	1.36E-09	5.46E-08
345600	4135.69	47.02	5.597	0.20	5.60E-08	6.36E-10	5.53E-08
346200	4623.07	101.44	5.797	0.00	5.80E-08	1.27E-09	5.67E-08
432000	4584.31	32.09	5.797	0.10	5.80E-08	4.06E-10	5.76E-08
432600	4788.5	97.44	5.897	0.00	5.90E-08	1.20E-09	5.78E-08
518400	4760.33	52.15	5.897	0.10	5.90E-08	6.46E-10	5.83E-08
519000	4952.12	94.03	5.997	0.00	6.00E-08	1.14E-09	5.88E-08
604800	4907.36	26.04	5.997	0.00	6.00E-08	3.18E-10	5.97E-08
605400	5217.61	96.11	5.997	0.00	6.00E-08	1.10E-09	5.89E-08
691200	5220.16	21.41	5.997	0.10	6.00E-08	2.46E-10	5.97E-08
691800	5608.14	96.42	6.097	0.00	6.10E-08	1.05E-09	5.99E-08
777600	5574.42	20.64	6.097	0.00	6.10E-08	2.26E-10	6.07E-08
778200	6000.14	99.03	6.097	0.00	6.10E-08	1.01E-09	6.00E-08
864000	6012.79	23.25	6.097	0.10	6.10E-08	2.36E-10	6.07E-08
864600	6254.37	102.76	6.197	0.00	6.20E-08	1.02E-09	6.10E-08
950400	6303.28	20.26	6.197	0.10	6.20E-08	1.99E-10	6.18E-08
951000	6581.24	104.84	6.297	0.00	6.30E-08	1.00E-09	6.20E-08
1036800	6560.19	21.54	6.297	0.10	6.30E-08	2.07E-10	6.28E-08
1037400	6797.25	104.92	6.397	0.00	6.40E-08	9.87E-10	6.30E-08
1123200	6791.42	21.89	6.397	0.08	6.40E-08	2.06E-10	6.38E-08
1123800	6935.01	105.62	6.477	0.00	6.48E-08	9.86E-10	6.38E-08
1209600	6941.31	18.44	6.477	0.05	6.48E-08	1.72E-10	6.46E-08
1210200	7188.09	104.27	6.527	0.00	6.53E-08	9.47E-10	6.43E-08
1296000	7091.64	20.24	6.527	0.05	6.53E-08	1.86E-10	6.51E-08
1296600	7240.65	101.32	6.577	0.00	6.58E-08	9.20E-10	6.49E-08
1382400	7227.16	22.49	6.577	0.05	6.58E-08	2.05E-10	6.56E-08
1383000	7404	103.75	6.627	0.00	6.63E-08	9.29E-10	6.53E-08
1468800	7379.31	20.61	6.627	0.05	6.63E-08	1.85E-10	6.61E-08
1469400	7461.22	100.29	6.677	0.00	6.68E-08	8.98E-10	6.59E-08
1555200	7426.48	21.37	6.677	0.05	6.68E-08	1.92E-10	6.66E-08
1555800	7608.79	101.18	6.727	0.00	6.73E-08	8.95E-10	6.64E-08
1900800	7502.13	11.01	6.727	0.15	6.73E-08	9.87E-11	6.72E-08
1901400	7914.45	99.26	6.877	0.00	6.88E-08	8.63E-10	6.79E-08
1987200	7922.06	14.55	6.877	0.05	6.88E-08	1.26E-10	6.86E-08

CBC of Zn sorbed to HAO at pH 7 and 25°C (contd.)

Time s	Total CPM	Final CPM	Zn ml	Add Zn	Total Zn M	CBC Zn	Zn/g HAO
1987800	8202.06	100.02	6.927	0.00	6.93E-08	8.45E-10	6.84E-08
2073600	8241.26	8.05	6.927	0.05	6.93E-08	6.77E-11	6.92E-08
2074200	8522.35	100.13	6.977	0.00	6.98E-08	8.20E-10	6.90E-08
2160000	8600.09	12.85	6.977	0.05	6.98E-08	1.04E-10	6.97E-08
2160600	8874.32	98.52	7.027	0.00	7.03E-08	7.80E-10	6.95E-08
2246400	8891.02	20.16	7.027	0.05	7.03E-08	1.59E-10	7.01E-08
2247000	9063.14	101.33	7.077	0.00	7.08E-08	7.91E-10	7.00E-08
2419200	9071	28.2	7.077	0.05	7.08E-08	2.20E-10	7.06E-08
2419800	9122.02	100.64	7.127	0.00	7.13E-08	7.86E-10	7.05E-08
2592000	9200.34	15.83	7.127	0.05	7.13E-08	1.23E-10	7.12E-08
2592600	9500.31	101.37	7.177	0.00	7.18E-08	7.66E-10	7.10E-08
2764800	9606.36	11.04	7.177	0.05	7.18E-08	8.25E-11	7.17E-08
2765400	9887.17	100.77	7.227	0.00	7.23E-08	7.37E-10	7.15E-08
2851200	9757.11	26.55	7.227	0.05	7.23E-08	1.97E-10	7.21E-08
2851800	9834.26	105.89	7.277	0.00	7.28E-08	7.84E-10	7.20E-08
3024000	9604.15	16.6	7.277	0.05	7.28E-08	1.26E-10	7.26E-08
3024600	9830.09	101.33	7.327	0.00	7.33E-08	7.55E-10	7.25E-08
3283200	9771.49	21.07	7.327	0.05	7.33E-08	1.58E-10	7.31E-08
3283800	9894.27	97.09	7.377	0.00	7.38E-08	7.24E-10	7.30E-08
3542400	9825.25	20.25	7.377	0.05	7.38E-08	1.52E-10	7.36E-08
3543000	10041.07	98.16	7.427	0.00	7.43E-08	7.26E-10	7.35E-08
3715200	10124.38	3.7	7.427	0.05	7.43E-08	2.71E-11	7.42E-08
3715800	10889.34	85.21	7.477	0.00	7.48E-08	5.85E-10	7.42E-08
3974400	10802.63	16.91	7.477	0.05	7.48E-08	1.17E-10	7.47E-08
3975000	11263.57	98.25	7.527	0.00	7.53E-08	6.57E-10	7.46E-08
4147200	11310.04	78.09	7.527	0.05	7.53E-08	5.20E-10	7.48E-08
4147800	11349.5	102.67	7.577	0.00	7.58E-08	6.85E-10	7.51E-08
4406400	11275.17	36.12	7.577	0.05	7.58E-08	2.43E-10	7.55E-08
4407000	11421.01	101.39	7.627	0.00	7.63E-08	6.77E-10	7.56E-08
4579200	11388.14	21.09	7.627	0.05	7.63E-08	1.41E-10	7.61E-08
4579800	11508.45	103.16	7.677	0.00	7.68E-08	6.88E-10	7.61E-08
4752000	11526.2	80.19	7.677	0.05	7.68E-08	5.34E-10	7.62E-08
4752600	11642	112.59	7.727	0.00	7.73E-08	7.47E-10	7.65E-08
4838400	11599.61	107.42	7.727	0.00	7.73E-08	7.16E-10	7.66E-08
4839000	11734.1	80.5	7.727	0.00	7.73E-08	5.30E-10	7.67E-08

CBC of Zn sorbed to HFO at pH 7 and 25°C

Time s	Total CPM	Final CPM	Zn ml	Add Zn	Total Zn M	CBC Zn	Zn/g HFO
0	0	0	0.00	0.000	0.00E+00	0.00E+00	0.00E+00
30	2961.01	160.52	9.00	0.000	9.00E-07	4.88E-08	8.51E-07
60	2961.01	122.22	9.00	0.000	9.00E-07	3.71E-08	8.63E-07
300	2961.01	80.48	9.00	0.000	9.00E-07	2.45E-08	8.76E-07
900	2961.01	61.59	9.00	0.000	9.00E-07	1.87E-08	8.81E-07
1800	2961.01	53.02	9.00	0.000	9.00E-07	1.61E-08	8.84E-07
3600	2961.01	50.11	9.00	0.000	9.00E-07	1.52E-08	8.85E-07
7200	2961.01	51.65	9.00	0.000	9.00E-07	1.57E-08	8.84E-07
14400	2961.01	50.32	9.00	0.000	9.00E-07	1.53E-08	8.85E-07
30000	2961.01	52.38	9.00	0.000	9.00E-07	1.59E-08	8.84E-07
86400	2961.01	32.18	9.00	0.050	9.00E-07	9.78E-09	8.90E-07
87000	3188.71	54.04	9.05	0.000	9.05E-07	1.53E-08	8.90E-07
172800	3168.04	34.29	9.05	0.000	9.05E-07	9.80E-09	8.95E-07
173400	3416.16	64.22	9.05	0.000	9.05E-07	1.70E-08	8.88E-07
259800	3383.22	54.07	9.05	0.000	9.05E-07	1.45E-08	8.91E-07
346200	3375.12	50.19	9.05	0.000	9.05E-07	1.35E-08	8.92E-07
432600	3395.43	50.12	9.05	0.050	9.05E-07	1.34E-08	8.92E-07
433200	3528.04	64.33	9.10	0.000	9.10E-07	1.66E-08	8.93E-07
519600	3508.04	31.66	9.10	0.000	9.10E-07	8.21E-09	9.02E-07
520200	3731.11	64.26	9.10	0.000	9.10E-07	1.57E-08	8.94E-07
606000	3706.15	56.07	9.10	0.000	9.10E-07	1.38E-08	8.96E-07
692400	3719.09	44.25	9.10	0.050	9.10E-07	1.08E-08	8.99E-07
693000	3990.99	68.09	9.15	0.000	9.15E-07	1.56E-08	8.99E-07
778800	3997.13	63.71	9.15	0.000	9.15E-07	1.46E-08	9.00E-07
865200	3984.75	53.08	9.15	0.060	9.15E-07	1.22E-08	9.03E-07
865800	4102.97	68.34	9.21	0.000	9.21E-07	1.53E-08	9.06E-07
951600	4087.56	44.91	9.21	0.050	9.21E-07	1.01E-08	9.11E-07
952200	4351.16	72.03	9.26	0.000	9.26E-07	1.53E-08	9.11E-07
1038000	4319.48	64.49	9.26	0.000	9.26E-07	1.38E-08	9.12E-07
1124400	4350.84	50.67	9.26	0.030	9.26E-07	1.08E-08	9.15E-07
1038600	4577.11	76.12	9.29	0.000	9.29E-07	1.54E-08	9.14E-07
1210800	4558.23	71.29	9.29	0.000	9.29E-07	1.45E-08	9.14E-07
1297200	4500.87	56.02	9.29	0.030	9.29E-07	1.16E-08	9.17E-07
1297800	4722.36	79.92	9.32	0.000	9.32E-07	1.58E-08	9.16E-07
1470600	4688.05	60.37	9.32	0.030	9.32E-07	1.20E-08	9.20E-07
1471200	4641.29	82.5	9.35	0.000	9.35E-07	1.66E-08	9.18E-07
1730400	4617.02	63.25	9.35	0.020	9.35E-07	1.28E-08	9.22E-07
1731000	4823.44	104.83	9.37	0.000	9.37E-07	2.04E-08	9.17E-07
1990200	4750.36	81.34	9.37	0.000	9.37E-07	1.60E-08	9.21E-07
1990800	4750.36	81.34	9.37	0.000	9.37E-07	1.60E-08	9.21E-07
2336400	4693.43	59.32	9.37	0.020	9.37E-07	1.18E-08	9.25E-07
2337000	4737.57	75.49	9.39	0.000	9.39E-07	1.50E-08	9.24E-07
2596200	4701.09	76.77	9.39	0.010	9.39E-07	1.53E-08	9.24E-07
2596800	4701.09	76.77	9.40	0.000	9.40E-07	1.54E-08	9.25E-07
2856000	4652.34	67.24	9.40	0.000	9.40E-07	1.36E-08	9.26E-07
2856600	4684.15	72.34	9.40	0.000	9.40E-07	1.45E-08	9.25E-07
3115800	4600.32	66.49	9.40	0.010	9.40E-07	1.36E-08	9.26E-07
3116400	4652.78	74.26	9.41	0.000	9.41E-07	1.50E-08	9.26E-07

CBC of Zn sorbed to HFO at pH 7 and 25°C (contd.)

Time s	Total CPM	Final CPM	Zn ml	Add Zn	Total Zn M	CBC Zn	Zn/g HFO
3462600	4666.27	76.48	9.42	0.000	9.42E-07	1.54E-08	9.27E-07
3721800	4610.5	74.22	9.42	0.000	9.42E-07	1.52E-08	9.27E-07
3722400	4585.34	84.5	9.42	0.000	9.42E-07	1.74E-08	9.25E-07
3981600	4613.48	72.48	9.42	0.000	9.42E-07	1.48E-08	9.27E-07
3982200	4613.48	72.48	9.42	0.000	9.42E-07	1.48E-08	9.27E-07
4241400	4568.79	68.35	9.42	0.010	9.42E-07	1.41E-08	9.28E-07
4242000	4622.04	74.19	9.43	0.000	9.43E-07	1.51E-08	9.28E-07
4501200	4609.17	68.83	9.43	0.010	9.43E-07	1.41E-08	9.29E-07
4501800	4649.17	70.83	9.44	0.000	9.44E-07	1.44E-08	9.30E-07
4761000	4633.58	69.8	9.44	0.000	9.44E-07	1.42E-08	9.30E-07
4761600	4643.58	72.38	9.44	0.000	9.44E-07	1.47E-08	9.29E-07
5193600	4620.45	69.02	9.44	0.000	9.44E-07	1.41E-08	9.30E-07

CBC of Zn sorbed to 0.1 g/L HMO at pH 7 and 25°C

Time s	Total CPM	Final CPM	Zn ml	Add Zn	Total Zn M	CBC Zn	Zn/g HMO
0	0	0	0.0	0.0	0.00E+00	0.00E+00	0.00E+00
30	6620.11	60	12.5	0.0	1.25E-07	1.13E-09	1.24E-06
60	6624.17	73	12.5	0.0	1.25E-07	1.38E-09	1.24E-06
300	6704.15	71	12.5	0.0	1.25E-07	1.32E-09	1.24E-06
900	6683.55	74	12.5	0.0	1.25E-07	1.38E-09	1.24E-06
1800	6686.15	84	12.5	0.0	1.25E-07	1.57E-09	1.23E-06
3600	6749.56	84	12.5	0.0	1.25E-07	1.56E-09	1.24E-06
7200	6749.56	85	12.5	0.0	1.25E-07	1.57E-09	1.23E-06
14400	6642.01	80	12.5	0.0	1.25E-07	1.51E-09	1.24E-06
30000	6671.25	83	12.5	0.0	1.25E-07	1.56E-09	1.24E-06
86400	6618.02	41	12.5	0.1	1.25E-07	7.75E-10	1.24E-06
87000	7195.12	92	12.6	0.0	1.26E-07	1.61E-09	1.24E-06
172800	7228.04	49	12.6	0.1	1.26E-07	8.53E-10	1.25E-06
259200	7436.16	91.22	12.7	0.1	1.27E-07	1.55E-09	1.25E-06
259800	7783.22	104	12.8	0.0	1.28E-07	1.70E-09	1.26E-06
346200	7165.12	47	12.7	0.1	1.27E-07	8.35E-10	1.27E-06
346800	7765.43	91	12.8	0.0	1.28E-07	1.50E-09	1.27E-06
433200	7728.04	63	12.8	0.1	1.28E-07	1.04E-09	1.27E-06
433800	8200.61	113.45	12.9	0.0	1.29E-07	1.79E-09	1.27E-06
606600	8376.04	99	12.9	0.0	1.29E-07	1.53E-09	1.28E-06
607200	8383.02	101.26	12.9	0.0	1.29E-07	1.56E-09	1.28E-06
780000	8241.2	46.04	12.9	0.1	1.29E-07	7.21E-10	1.28E-06
780600	8856.17	110.17	13.0	0.0	1.30E-07	1.62E-09	1.28E-06
953400	8773.43	56.49	13.0	0.1	1.30E-07	8.37E-10	1.29E-06
954000	8801.05	106.44	13.1	0.0	1.31E-07	1.58E-09	1.29E-06
1213200	8757.65	49.64	13.1	0.1	1.31E-07	7.41E-10	1.30E-06
1213800	8799.21	100.03	13.2	0.0	1.32E-07	1.50E-09	1.30E-06
1386600	8843.01	25.1	13.2	0.2	1.32E-07	3.74E-10	1.31E-06
1387200	9423.16	112.16	13.3	0.0	1.33E-07	1.59E-09	1.32E-06
1560000	9305.5	46.12	13.3	0.1	1.33E-07	6.60E-10	1.33E-06
1560600	9305.5	110.48	13.4	0.0	1.34E-07	1.59E-09	1.33E-06
1819800	9262.15	58.52	13.4	0.1	1.34E-07	8.48E-10	1.33E-06
1820400	9633.71	115.92	13.5	0.0	1.35E-07	1.63E-09	1.34E-06
1993200	9633.71	57.89	13.5	0.1	1.35E-07	8.12E-10	1.34E-06
1993800	9527.04	108.42	13.6	0.0	1.36E-07	1.55E-09	1.35E-06
2166600	9433	68.44	13.6	0.1	1.36E-07	9.88E-10	1.35E-06
2167200	9854.37	119.01	13.7	0.0	1.37E-07	1.66E-09	1.36E-06
2340000	9731.03	83.66	13.7	0.1	1.37E-07	1.18E-09	1.36E-06
2340600	10041.22	119.62	13.8	0.0	1.38E-07	1.64E-09	1.36E-06
2772600	9435.02	31.43	13.8	0.1	1.38E-07	4.60E-10	1.38E-06
2773200	9786.17	112.05	13.9	0.0	1.39E-07	1.59E-09	1.38E-06
3032400	9470.15	68.32	13.9	0.1	1.39E-07	1.00E-09	1.38E-06
3033000	9770.15	110.1	14.0	0.0	1.40E-07	1.57E-09	1.38E-06
3292200	9791.26	71.03	14.0	0.1	1.40E-07	1.01E-09	1.39E-06
3292800	10089.63	118.04	14.1	0.0	1.41E-07	1.65E-09	1.39E-06
3552000	10113.56	77.23	14.1	0.0	1.41E-07	1.07E-09	1.40E-06
3552600	10113.56	111.4	14.1	0.0	1.41E-07	1.55E-09	1.40E-06

CBC of Zn sorbed to 0.1 g/L HMO at pH 7 and 25°C (contd.)

Time s	Total CPM	Final CPM	Zn ml	Add Zn	Total Zn M	CBC Zn	Zn/g HMO
3811800	10092.17	89.66	14.1	0.1	1.41E-07	1.25E-09	1.40E-06
3812400	11546.12	117.36	14.2	0.0	1.42E-07	1.44E-09	1.41E-06
3985200	11703.59	101.22	14.2	0.0	1.42E-07	1.23E-09	1.41E-06
3985800	11683.47	116.89	14.2	0.0	1.42E-07	1.42E-09	1.41E-06
4245000	10439.25	68.34	14.2	0.1	1.42E-07	9.32E-10	1.41E-06
4245600	11733.28	131.54	14.3	0.0	1.43E-07	1.61E-09	1.42E-06
4418400	11502	91.66	14.3	0.1	1.43E-07	1.14E-09	1.42E-06
4419000	12032.4	134.55	14.4	0.0	1.44E-07	1.61E-09	1.43E-06
4591800	11760.79	90	14.4	0.1	1.44E-07	1.10E-09	1.43E-06
4592400	12487.02	141.05	14.5	0.0	1.45E-07	1.64E-09	1.44E-06
4851600	11331.16	117.23	14.5	0.0	1.45E-07	1.50E-09	1.44E-06
4852200	12006.34	123.05	14.5	0.0	1.45E-07	1.49E-09	1.44E-06

Calcium Studies with Amorphous Oxides

HAO			HFO			HMO		
pH	$\mu = 0.060$	$\mu = 1.50$	pH	$\mu = 0.031$	$\mu = 1.50$	pH	$\mu = 0.015$	$\mu = 1.50$
5.02	23.00		4.49	36.50		2.02	40.00	
5.49	25.25		5.00	36.85		2.50	42.50	
6.06	31.25		5.50	38.50		3.02	47.50	
6.55	38.50		6.02	45.25		3.51	53.00	
7.00	45.50		6.50	47.25		4.00	59.50	
7.00	47.75		6.98	52.00		4.51	70.00	
7.50	54.50		6.98	53.25		5.00	76.50	
8.00	60.50		7.58	61.00		5.51	90.00	
8.56	63.25		8.04	68.75		6.02	97.50	
9.01	70.25		8.62	72.25		7.00	98.25	
9.46	72.75		9.00	78.95		8.00	98.75	
10.01	73.25		9.51	81.48		2.02		35.00
4.87		14.25	9.99	86.10		2.50		37.50
5.50		17.00	4.51		31.00	3.02		40.00
6.00		22.00	5.00		32.38	3.51		44.00
6.48		27.75	5.50		34.75	4.00		50.00
7.00		38.50	6.02		37.40	4.51		61.50
7.50		43.50	6.50		41.25	5.00		70.00
8.01		51.00	7.01		46.25	5.51		76.50
8.52		56.50	7.01		46.25	6.02		85.00
9.04		66.25	7.58		49.50	7.00		90.00
9.99		71.50	8.04		59.50	8.00		94.00
			8.62		64.75			
			9.00		75.80			
			9.51		76.83			
			9.99		82.38			

Calcium adsorption isotherms with HAO at pH 7 and multiple temperatures

	T = 25°C		T = 14.1°C		T = 3.8°C	
Initial Ca (M)	C (M)	S (moles Ca/g)	C (M)	C (moles Ca/g)	S (M)	C (moles Ca/g)
5.00E-04	2.66E-04	2.34E-04	2.93E-04	2.07E-04	3.10E-04	1.90E-04
2.50E-04	1.33E-04	1.17E-04	1.47E-04	1.03E-04	1.57E-04	9.30E-05
1.00E-04	5.37E-05	4.63E-05	5.85E-05	4.15E-05	6.30E-05	3.70E-05
5.00E-05	2.75E-05	2.25E-05	2.91E-05	2.09E-05	3.13E-05	1.88E-05
2.50E-05	1.35E-05	1.15E-05	1.45E-05	1.05E-05	1.55E-05	9.55E-06
2.50E-05	1.31E-05	1.19E-05	1.49E-05	1.01E-05	1.57E-05	9.30E-06
1.00E-05	5.70E-06	4.30E-06	5.83E-06	4.18E-06	6.35E-06	3.65E-06
5.00E-06	2.53E-06	2.48E-06	2.95E-06	2.05E-06	3.15E-06	1.85E-06
2.50E-06	1.33E-06	1.17E-06	1.46E-06	1.04E-06	1.58E-06	9.25E-07
1.00E-06	4.95E-07	5.05E-07	5.88E-07	4.13E-07	6.25E-07	3.75E-07
5.00E-07	2.63E-07	2.38E-07	2.90E-07	2.10E-07	3.13E-07	1.88E-07

Calcium adsorption isotherms with HFO at pH 7 and multiple temperatures

	T = 25°C		T = 14.1°C		T = 3.8°C	
Initial Ca (M)	[S] (M)	C(moles Ca/g)	[S] (M)	C(moles Ca/g)	[S] (M)	C(moles Ca/g)
5.00E-04	2.53E-04	2.47E-04	3.08E-04	1.93E-04	3.73E-04	1.27E-04
2.50E-04	1.25E-04	1.25E-04	1.55E-04	9.55E-05	1.84E-04	6.60E-05
1.00E-04	5.06E-05	4.94E-05	6.20E-05	3.80E-05	7.40E-05	2.60E-05
5.00E-05	2.53E-05	2.47E-05	3.05E-05	1.95E-05	3.75E-05	1.25E-05
2.50E-05	1.30E-05	1.20E-05	1.54E-05	9.60E-06	1.90E-05	6.00E-06
1.00E-05	5.05E-06	4.95E-06	6.13E-06	3.88E-06	7.50E-06	2.50E-06
5.00E-06	2.50E-06	2.50E-06	3.15E-06	1.85E-06	3.70E-06	1.30E-06
2.50E-06	1.24E-06	1.26E-06	1.56E-06	9.38E-07	1.86E-06	6.38E-07
1.00E-06	5.13E-07	4.88E-07	6.00E-07	4.00E-07	7.45E-07	2.55E-07
5.00E-07	2.50E-07	2.50E-07	3.15E-07	1.85E-07	3.63E-07	1.38E-07

Calcium adsorption isotherms with HMO at pH 7 and multiple temperatures

	T = 24.5°C		T = 13.7°C		T = 4°C	
Initial Ca (M)	S (M)	C (moles Ca/g)	S (M)	C (moles Ca/g)	S (M)	C (moles Ca/g)
5.00E-04	4.57E-05	4.54E-03	8.80E-05	4.12E-03	1.62E-04	3.38E-03
2.50E-04	2.28E-05	2.27E-03	4.39E-05	2.06E-03	8.60E-05	1.64E-03
1.00E-04	9.20E-06	9.08E-04	1.70E-05	8.30E-04	3.24E-05	6.76E-04
5.00E-05	4.50E-06	4.55E-04	8.60E-06	4.14E-04	1.67E-05	3.33E-04
2.50E-05	2.28E-06	2.27E-04	4.25E-06	2.08E-04	8.40E-06	1.66E-04
1.00E-05	9.13E-07	9.09E-05	1.80E-06	8.20E-05	3.20E-06	6.80E-05
5.00E-06	4.63E-07	4.54E-05	8.63E-07	4.14E-05	1.80E-06	3.20E-05
2.50E-06	2.50E-07	2.25E-05	4.25E-07	2.08E-05	7.75E-07	1.73E-05
1.00E-06	9.00E-08	9.10E-06	1.75E-07	8.25E-06	3.25E-07	6.75E-06
5.00E-07	4.00E-08	4.60E-06	8.25E-08	4.18E-06	1.75E-07	3.25E-06

Nickel Studies with Amorphous Oxides

Nickel adsorption edges at 25°C

HAO			HFO			HMO		
pH	μ = 0.060	μ =1.50	pH	μ = 0.031	μ =1.50	pH	μ = 0.015	μ =1.50
5.00	39.94		5.00	27.40		2.00	43.24	
5.50	46.50		5.50	30.28		2.50	48.78	
6.00	68.21		6.00	48.43		3.00	63.17	
6.50	77.24		6.50	79.19		3.50	78.99	
7.00	90.54		7.00	89.31		4.00	90.34	
7.50	96.81		7.50	96.03		4.50	92.89	
8.00	96.54		8.00	96.74		5.00	95.38	
8.50	97.82		8.50	96.70		5.50	96.27	
9.00	98.06		9.00	96.85		6.00	97.57	
9.50	98.13		9.50	96.93		7.00	97.67	
5.00		9.99	5.00		49.66	8.00	97.69	
5.50		18.13	5.50		57.09	2.00		36.12
6.00		30.88	6.00		81.04	2.50		41.82
6.50		50.72	6.50		94.37	3.00		54.51
7.00		60.50	7.00		96.06	3.50		67.33
7.50		82.33	7.50		97.36	4.00		79.53
8.00		90.62	8.00		97.90	4.50		88.22
8.50		91.53	8.50		97.84	5.00		91.07
9.00		92.42	9.00		97.95	5.50		93.29
9.50		93.23	9.50		97.82	6.00		95.59
						7.00		95.77
						8.00		96.44

Nickel adsorption isotherms with HAO at pH 7 and multiple temperatures analyzed with liquid scintillating counter

		T = 25°C	T = 14.1°C		T = 3.8°C	
Initial Conc.	[Ni]aq M	moles Ni Adsorbed / g HAO	[Ni]aq M	moles Ni Adsorbed / g HAO	[Ni]aq M	moles Ni Adsorbed / g HAO
1.00E-04	9.51E-06	9.05E-05	1.87E-05	8.13E-05	2.09E-05	7.91E-05
5.00E-05	4.69E-06	4.53E-05	7.72E-06	4.23E-05	1.32E-05	3.68E-05
1.00E-05	1.03E-06	8.97E-06	1.80E-06	8.20E-06	2.24E-06	7.76E-06
5.00E-06	4.76E-07	4.52E-06	7.38E-07	4.26E-06	1.01E-06	3.99E-06
1.00E-06	9.26E-08	9.07E-07	1.54E-07	8.46E-07	2.13E-07	7.87E-07
5.00E-07	4.85E-08	4.52E-07	7.82E-08	4.22E-07	1.07E-07	3.93E-07
1.00E-07	9.63E-09	9.04E-08	1.60E-08	8.40E-08	2.05E-08	7.95E-08
5.00E-08	3.74E-09	4.63E-08	5.80E-09	4.42E-08	1.05E-08	3.95E-08
1.00E-08	1.12E-09	8.88E-09	1.58E-09	8.42E-09	1.88E-09	8.12E-09
5.00E-09	4.59E-10	4.54E-09	7.74E-10	4.23E-09	9.59E-10	4.04E-09
1.00E-09	9.76E-11	9.02E-10	1.55E-10	8.45E-10	2.22E-10	7.78E-10
5.00E-10	4.72E-11	4.53E-10	7.82E-11	4.22E-10	1.04E-10	3.96E-10

Nickel adsorption isotherms with HAO at pH 6 and multiple temperatures analyzed with liquid scintillating counter

		T = 25°C	T = 14.1°C		T = 3.8°C	
Initial Conc.	[Ni]aq M	moles Ni Adsorbed / g HAO	[Ni]aq M	moles Ni Adsorbed / g HAO	[Ni]aq M	moles Ni Adsorbed / g HAO
1.00E-04	3.08E-05	6.92E-05	4.26E-05	5.74E-05	5.53E-05	4.47E-05
5.00E-05	1.56E-05	3.44E-05	1.75E-05	3.25E-05	2.73E-05	2.27E-05
1.00E-05	4.08E-06	5.92E-06	4.25E-06	5.75E-06	6.41E-06	3.59E-06
5.00E-06	1.53E-06	3.47E-06	2.18E-06	2.82E-06	2.74E-06	2.26E-06
1.00E-06	3.29E-07	6.71E-07	3.67E-07	6.33E-07	5.70E-07	4.30E-07
5.00E-07	9.24E-08	4.08E-07	2.13E-07	2.87E-07	2.73E-07	2.27E-07
1.00E-07	3.18E-08	6.82E-08	5.69E-08	4.31E-08	5.44E-08	4.56E-08
5.00E-08	1.66E-08	3.34E-08	2.00E-08	3.00E-08	2.73E-08	2.27E-08
1.00E-08	3.20E-09	6.80E-09	4.17E-09	5.83E-09	4.37E-09	5.63E-09
5.00E-09	1.61E-09	3.39E-09	2.16E-09	2.84E-09	2.80E-09	2.20E-09
1.00E-09	3.21E-10	6.79E-10	4.64E-10	5.36E-10	5.17E-10	4.83E-10
5.00E-10	1.61E-10	3.39E-10	2.12E-10	2.88E-10	2.76E-10	2.24E-10

Nickel adsorption isotherms with HFO at pH 7 and multiple temperatures analyzed with liquid scintillating counter

		T = 25°C	T = 14.1°C		T = 3.8°C	
Initial Conc.	[Ni]aq M	moles Ni Adsorbed / g HFO	[Ni]aq M	moles Ni Adsorbed / g HFO	[Ni]aq M	moles Ni Adsorbed / g HFO
1.00E-04	3.52E-06	9.65E-05	5.60E-06	9.44E-05	1.32E-05	8.68E-05
5.00E-05	1.86E-06	4.81E-05	2.86E-06	4.71E-05	6.89E-06	4.31E-05
1.00E-05	5.02E-07	9.50E-06	1.01E-06	8.99E-06	1.25E-06	8.75E-06
5.00E-06	2.35E-07	4.77E-06	3.10E-07	4.69E-06	6.79E-07	4.32E-06
1.00E-06	3.39E-08	9.66E-07	5.86E-08	9.41E-07	1.36E-07	8.64E-07
5.00E-07	1.95E-08	4.80E-07	1.92E-08	4.81E-07	6.70E-08	4.33E-07
1.00E-07	4.86E-09	9.51E-08	5.20E-09	9.48E-08	2.12E-08	7.88E-08
5.00E-08	2.66E-09	4.73E-08	3.53E-09	4.65E-08	6.73E-09	4.33E-08
1.00E-08	2.49E-10	9.75E-09	5.56E-10	9.44E-09	1.31E-09	8.69E-09
5.00E-09	1.78E-10	4.82E-09	3.29E-10	4.67E-09	5.44E-10	4.46E-09
1.00E-09	5.38E-11	9.46E-10	6.12E-11	9.39E-10	1.30E-10	8.70E-10
5.00E-10	2.37E-11	4.76E-10	3.06E-11	4.69E-10	6.89E-11	4.31E-10

Nickel adsorption isotherms with HFO at pH 6 and multiple temperatures analyzed with liquid scintillating counter

		T = 25°C	T = 14.1°C		T = 3.8°C	
Initial Conc.	[Ni]aq M	moles Ni Adsorbed / g HFO	[Ni]aq M	moles Ni Adsorbed / g HMO	[Ni]aq M	moles Ni Adsorbed / g HFO
1.00E-04	2.14E-05	7.86E-05	2.24E-05	7.76E-05	4.29E-05	5.71E-05
5.00E-05	9.21E-06	4.08E-05	1.50E-05	3.50E-05	2.02E-05	2.98E-05
1.00E-05	1.62E-06	8.38E-06	2.07E-06	7.93E-06	4.48E-06	5.52E-06
5.00E-06	9.87E-07	4.01E-06	1.07E-06	3.93E-06	2.67E-06	2.33E-06
1.00E-06	1.55E-07	8.45E-07	2.19E-07	7.81E-07	4.24E-07	5.76E-07
5.00E-07	1.67E-07	3.33E-07	1.16E-07	3.84E-07	1.37E-07	3.63E-07
1.00E-07	1.99E-08	8.01E-08	3.07E-08	6.93E-08	4.23E-08	5.77E-08
5.00E-08	7.55E-09	4.25E-08	1.11E-08	3.89E-08	2.21E-08	2.79E-08
1.00E-08	2.42E-09	7.58E-09	2.26E-09	7.74E-09	4.61E-09	5.39E-09
5.00E-09	1.37E-09	3.63E-09	9.02E-10	4.10E-09	2.11E-09	2.89E-09
1.00E-09	1.78E-10	8.22E-10	2.58E-10	7.42E-10	4.25E-10	5.75E-10
5.00E-10	8.89E-11	4.11E-10	8.27E-11	4.17E-10	2.45E-10	2.55E-10

Nickel adsorption isotherms with HMO at pH 7 and multiple temperatures analyzed with liquid scintillating counter

		T = 25°C	T = 14.1°C		T = 3.8°C	
Initial Conc.	[Ni]aq M	moles Ni Adsorbed / g HMO	[Ni]aq M	moles Ni Adsorbed / g HMO	[Ni]aq M	moles Ni Adsorbed / g HMO
1.00E-04	2.19E-06	9.78E-04	5.99E-06	9.40E-04	9.52E-06	9.05E-04
5.00E-05	1.30E-06	4.87E-04	2.53E-06	4.75E-04	4.53E-06	4.55E-04
1.00E-05	3.14E-07	9.69E-05	6.23E-07	9.38E-05	9.40E-07	9.06E-05
5.00E-06	1.90E-07	4.81E-05	3.52E-07	4.65E-05	4.47E-07	4.55E-05
1.00E-06	2.22E-08	9.78E-06	6.24E-08	9.38E-06	9.76E-08	9.02E-06
5.00E-07	1.18E-08	4.88E-06	2.12E-08	4.79E-06	4.70E-08	4.53E-06
1.00E-07	2.84E-09	9.72E-07	6.11E-09	9.39E-07	9.88E-09	9.01E-07
5.00E-08	1.11E-09	4.89E-07	3.10E-09	4.69E-07	4.83E-09	4.52E-07
1.00E-08	1.72E-10	9.83E-08	5.09E-10	9.49E-08	9.26E-10	9.07E-08
5.00E-09	1.16E-10	4.88E-08	2.93E-10	4.71E-08	4.86E-10	4.51E-08
1.00E-09	1.84E-11	9.82E-09	5.90E-11	9.41E-09	9.52E-11	9.05E-09
5.00E-10	1.91E-11	4.81E-09	2.36E-11	4.76E-09	4.58E-11	4.54E-09

Nickel adsorption isotherms with HMO at pH 5 and multiple temperatures analyzed with liquid scintillating counter

		T = 25°C	T = 14.1°C		T = 3.8°C	
Initial Conc.	[Ni]aq M	moles Ni Adsorbed / g HFO	[Ni]aq M	moles Ni Adsorbed / g HFO	[Ni]aq M	moles Ni Adsorbed / g HFO
1.00E-04	4.56E-06	9.54E-04	7.62E-06	9.24E-04	1.87E-05	8.13E-04
5.00E-05	1.71E-06	4.83E-04	4.00E-06	4.60E-04	9.02E-06	4.10E-04
1.00E-05	5.96E-07	9.40E-05	9.35E-07	9.07E-05	1.73E-06	8.27E-05
5.00E-06	3.36E-07	4.66E-05	3.81E-07	4.62E-05	1.01E-06	3.99E-05
1.00E-06	4.01E-08	9.60E-06	8.03E-08	9.20E-06	1.86E-07	8.14E-06
5.00E-07	2.24E-08	4.78E-06	3.96E-08	4.60E-06	5.85E-08	4.42E-06
1.00E-07	5.68E-09	9.43E-07	6.38E-09	9.36E-07	2.01E-08	7.99E-07
5.00E-08	2.55E-09	4.74E-07	3.73E-09	4.63E-07	9.19E-09	4.08E-07
1.00E-08	4.22E-10	9.58E-08	7.97E-10	9.20E-08	1.74E-09	8.26E-08
5.00E-09	1.82E-10	4.82E-08	4.02E-10	4.60E-08	1.19E-09	3.81E-08
1.00E-09	6.06E-11	9.39E-09	7.87E-11	9.21E-09	1.82E-10	8.18E-09
5.00E-10	3.35E-11	4.67E-09	4.25E-11	4.57E-09	9.87E-11	4.01E-09

CBC of Ni sorbed to HAO at pH 7 and 25°C

Time (h)	Total CPM	Final CPM	Ni ml	Add Zn	Total Ni M	CBC Ni	Ni Sorbed
0	0	0	0.0	0.00	0.00E+00	0.00E+00	0.000E+00
0.5	4238.1	400	5.2	0.00	2.60E-06	2.45E-07	2.355E-06
1	4238.1	382.25	5.2	0.00	2.60E-06	2.35E-07	2.365E-06
2	4238.1	402.83	5.2	0.00	2.60E-06	2.47E-07	2.353E-06
3	4238.1	399.52	5.2	0.00	2.60E-06	2.45E-07	2.355E-06
4	4238.1	398.75	5.2	1.00	2.60E-06	2.45E-07	2.355E-06
4.5	4993.26	394.02	6.2	1.00	3.10E-06	2.45E-07	2.855E-06
5	5767.75	414.89	7.2	0.00	3.60E-06	2.59E-07	3.341E-06
5.5	5767.75	392.14	7.2	0.50	3.60E-06	2.45E-07	3.355E-06
6	6161.38	422.13	7.7	0.00	3.85E-06	2.64E-07	3.586E-06
6.5	6161.38	391.74	7.7	0.40	3.85E-06	2.45E-07	3.605E-06
7	7145.65	434.58	8.1	0.00	4.05E-06	2.46E-07	3.804E-06
7.5	7145.65	430.54	8.1	0.30	4.05E-06	2.44E-07	3.806E-06
8	7602.43	438.16	8.4	0.10	4.20E-06	2.42E-07	3.958E-06
9	7800.01	449.51	8.5	0.10	4.25E-06	2.45E-07	4.005E-06
9.5	8003.35	461.29	8.6	0.05	4.30E-06	2.48E-07	4.052E-06
10	8120	460	8.7	0.05	4.33E-06	2.45E-07	4.080E-06
11	8211.42	462.41	8.7	0.05	4.35E-06	2.45E-07	4.105E-06
12	8470.35	507.23	8.8	0.00	4.38E-06	2.62E-07	4.113E-06
13	8470.35	491.05	8.8	0.00	4.38E-06	2.54E-07	4.121E-06
14	8470.35	474.29	8.8	0.05	4.38E-06	2.45E-07	4.130E-06
15	8725.13	494.22	8.8	0.00	4.40E-06	2.49E-07	4.151E-06
17	8777.64	488.71	8.8	0.05	4.40E-06	2.45E-07	4.155E-06
19	8992.66	521.27	8.9	0.00	4.43E-06	2.57E-07	4.168E-06
21	9000.76	512.45	8.9	0.00	4.43E-06	2.52E-07	4.173E-06
27	9000.7	520.49	8.9	0.00	4.43E-06	2.56E-07	4.169E-06
30	9000.7	524.71	8.9	0.00	4.43E-06	2.58E-07	4.167E-06
33	9000.7	517.5	8.9	0.00	4.43E-06	2.54E-07	4.171E-06
36	9000.7	508.38	8.9	0.00	4.43E-06	2.50E-07	4.175E-06
40	9000.7	525.14	8.9	0.00	4.43E-06	2.58E-07	4.167E-06
50	8982.16	526.39	8.9	0.00	4.43E-06	2.59E-07	4.166E-06
60	8982.16	531.45	8.9	0.00	4.43E-06	2.62E-07	4.163E-06
72	9010.2	528.11	8.9	0.00	4.43E-06	2.59E-07	4.166E-06
84	9084.16	526.03	8.9	0.00	4.43E-06	2.56E-07	4.169E-06
96	8995.28	520.93	8.9	0.00	4.43E-06	2.56E-07	4.169E-06
110	9000	523.19	8.9	0.00	4.43E-06	2.57E-07	4.168E-06
125	9000	522.65	8.9	0.00	4.43E-06	2.57E-07	4.168E-06
138	9000	519.85	8.9	0.00	4.43E-06	2.56E-07	4.169E-06
144	8984.53	520.49	8.9	-22.70	4.43E-06	2.56E-07	4.169E-06

CBC of Ni sorbed to HFO at pH 7 and 25°C

Time (h)	Total CPM	Final CPM	Ni ml	Add Zn	Total Ni M	CBC Ni	Ni Sorbed
0	0	0	0.0	0.00	0.00E+00	0.00E+00	0.000E+00
0.5	4238.1	180.29	5.2	0.00	2.60E-06	1.11E-07	2.489E-06
1	4238.1	177.31	5.2	0.00	2.60E-06	1.09E-07	2.491E-06
2	4238.1	174.78	5.2	0.00	2.60E-06	1.07E-07	2.493E-06
3	4238.1	176.38	5.2	0.00	2.60E-06	1.08E-07	2.492E-06
4	4238.1	174.5	5.2	0.50	2.60E-06	1.07E-07	2.493E-06
4.5	5170.28	183.26	5.7	0.30	2.85E-06	1.01E-07	2.749E-06
5	5542.44	187.6	6.0	0.20	3.00E-06	1.02E-07	2.898E-06
5.5	5999.06	197.12	6.2	0.20	3.10E-06	1.02E-07	2.998E-06
6	6396.2	202.45	6.4	0.40	3.20E-06	1.01E-07	3.099E-06
6.5	6925.25	205.27	6.8	0.60	3.40E-06	1.01E-07	3.299E-06
7	7760.04	213.11	7.4	0.10	3.70E-06	1.02E-07	3.598E-06
7.5	8017.29	214.66	7.5	0.10	3.75E-06	1.00E-07	3.650E-06
8	8202.21	216	7.6	0.10	3.80E-06	1.00E-07	3.700E-06
8.5	8438.1	220.75	7.7	0.10	3.85E-06	1.01E-07	3.749E-06
9	8614.26	221.03	7.8	0.10	3.90E-06	1.00E-07	3.800E-06
9.5	8624.01	221.36	7.9	0.00	3.95E-06	1.01E-07	3.849E-06
10	8600.5	220.2	7.9	0.10	3.95E-06	1.01E-07	3.849E-06
11	8784.91	223.01	8.0	0.05	4.00E-06	1.02E-07	3.898E-06
12	8894.61	226.17	8.1	0.00	4.03E-06	1.02E-07	3.923E-06
13	8880.15	228.87	8.1	0.10	4.03E-06	1.04E-07	3.921E-06
14	9000.12	245.13	8.2	0.00	4.08E-06	1.11E-07	3.964E-06
15	9000.12	244.4	8.2	0.00	4.08E-06	1.11E-07	3.964E-06
16	9000.12	238.33	8.2	0.00	4.08E-06	1.08E-07	3.967E-06
17	9000.12	221.48	8.2	0.10	4.08E-06	1.00E-07	3.975E-06
18	9256.17	232.26	8.3	0.00	4.13E-06	1.04E-07	4.021E-06
22	9256.17	227.67	8.3	0.10	4.13E-06	1.01E-07	4.024E-06
24	9508.32	288.31	8.4	0.00	4.18E-06	1.27E-07	4.048E-06
27	9480.24	308.83	8.4	0.00	4.18E-06	1.36E-07	4.039E-06
30	9512.37	282.17	8.4	0.00	4.18E-06	1.24E-07	4.051E-06
33	9540.16	310.27	8.4	0.00	4.18E-06	1.36E-07	4.039E-06
36	9484.16	310.66	8.4	0.00	4.18E-06	1.37E-07	4.038E-06
39	9480.78	320.19	8.4	0.00	4.18E-06	1.41E-07	4.034E-06
45	9503.26	302.79	8.4	0.00	4.18E-06	1.33E-07	4.042E-06
48	9510.83	298.76	8.4	0.00	4.18E-06	1.31E-07	4.044E-06
54	9480.18	308.64	8.4	0.00	4.18E-06	1.36E-07	4.039E-06
72	9524.36	296.26	8.4	0.00	4.18E-06	1.30E-07	4.045E-06
84	9447.13	277.14	8.4	0.00	4.18E-06	1.22E-07	4.053E-06
96	9484.01	318.35	8.4	0.00	4.18E-06	1.40E-07	4.035E-06
108	9517.22	347.46	8.4	0.00	4.18E-06	1.52E-07	4.023E-06
132	9501.27	307.37	8.4	0.00	4.18E-06	1.35E-07	4.040E-06
144	9492.45	292.67	8.4	0.00	4.18E-06	1.29E-07	4.046E-06
156	9503.17	316.17	8.4	0.00	4.18E-06	1.39E-07	4.036E-06
168	9521.46	323.17	8.4	0.00	4.18E-06	1.42E-07	4.033E-06
180	9506.25	295.57	8.4	0.00	4.18E-06	1.30E-07	4.045E-06
192	9440.16	287.75	8.4	-51.52	4.18E-06	1.27E-07	4.048E-06

CBC of Ni sorbed to HMO at pH 7 and 25°C

Time (h)	Total CPM	Final CPM	Zn ml	Add Zn	Total Ni M	Aqueous Ni	moles Ni sorbed/g HMO
0	0	0	0.000	0.0	0.00E+00	0.00E+00	0.000E+00
0.5	1288.45	36.28	2.700	0.0	1.35E-06	3.80E-08	1.312E-05
1	1288.45	30.05	2.700	0.0	1.35E-06	3.15E-08	1.319E-05
2	1288.45	31.18	2.700	0.0	1.35E-06	3.27E-08	1.317E-05
3	1368.77	30.45	2.700	0.0	1.35E-06	3.00E-08	1.320E-05
4	1368.77	30.79	2.700	0.4	1.35E-06	3.04E-08	1.320E-05
4.5	1995.23	40.5	3.100	0.4	1.55E-06	3.15E-08	1.519E-05
5	2374.13	39.01	3.500	0.3	1.75E-06	2.88E-08	1.721E-05
5.5	2600.09	44.12	3.800	0.3	1.90E-06	3.22E-08	1.868E-05
6	3092.41	48.3	4.100	0.3	2.05E-06	3.20E-08	2.018E-05
6.5	3501.16	46.19	4.400	0.4	2.20E-06	2.90E-08	2.171E-05
7	3950.04	50	4.800	0.3	2.40E-06	3.04E-08	2.370E-05
7.5	4303.18	51.01	5.100	0.2	2.55E-06	3.02E-08	2.520E-05
8	4698.65	54.37	5.300	0.2	2.65E-06	3.07E-08	2.619E-05
8.5	4945.02	56.8	5.500	0.1	2.75E-06	3.16E-08	2.718E-05
9	5148.12	61.18	5.600	0.3	2.80E-06	3.33E-08	2.767E-05
9.5	5589.25	60.47	5.900	0.3	2.95E-06	3.19E-08	2.918E-05
10	6086.2	63.6	6.200	0.1	3.10E-06	3.24E-08	3.068E-05
10.5	6209.75	62.98	6.300	0.1	3.15E-06	3.19E-08	3.118E-05
11	6477.09	65.01	6.400	0.2	3.20E-06	3.21E-08	3.168E-05
11.5	6622.17	68.26	6.600	0.1	3.30E-06	3.40E-08	3.266E-05
12	6814.45	67.84	6.700	0.1	3.35E-06	3.34E-08	3.317E-05
12.5	7048.52	70.46	6.800	0.0	3.40E-06	3.40E-08	3.366E-05
13	7048.52	65.3	6.800	0.1	3.40E-06	3.15E-08	3.369E-05
13.5	7200.6	67.11	6.900	0.1	3.45E-06	3.22E-08	3.418E-05
14	7459.52	68.05	7.000	0.1	3.50E-06	3.19E-08	3.468E-05
14.5	7666.13	68.46	7.100	0.2	3.55E-06	3.17E-08	3.518E-05
15	8074.27	75.04	7.300	0.1	3.65E-06	3.39E-08	3.616E-05
15.5	8201.35	69.48	7.400	0.1	3.70E-06	3.13E-08	3.669E-05
16	8195.19	68.8	7.500	0.2	3.75E-06	3.15E-08	3.719E-05
17	8462.21	70.38	7.700	0.6	3.85E-06	3.20E-08	3.818E-05
22	9141.02	70.04	8.300	0.2	4.15E-06	3.18E-08	4.118E-05
23	9515.66	70.54	8.500	0.1	4.25E-06	3.15E-08	4.218E-05
24	9723.04	71.7	8.600	0.2	4.30E-06	3.17E-08	4.268E-05
25	9965.53	70.99	8.800	0.2	4.40E-06	3.13E-08	4.369E-05
27	10348.22	71.37	9.000	0.2	4.50E-06	3.10E-08	4.469E-05
29	10688.12	72.39	9.200	0.3	4.60E-06	3.12E-08	4.569E-05
32	11129	75.59	9.500	0.2	4.75E-06	3.23E-08	4.718E-05
35	11400.16	74.03	9.700	0.2	4.85E-06	3.15E-08	4.819E-05
38	11626.9	73.92	9.900	0.2	4.95E-06	3.15E-08	4.919E-05
41	11901.25	74.49	10.100	0.2	5.05E-06	3.16E-08	5.018E-05
42	12196.24	74.31	10.300	0.3	5.15E-06	3.14E-08	5.119E-05
48	12607.19	74.62	10.600	0.1	5.30E-06	3.14E-08	5.269E-05
51	12822.67	76.01	10.700	0.2	5.35E-06	3.17E-08	5.318E-05
54	13252.04	77.09	10.900	0.2	5.45E-06	3.17E-08	5.418E-05
60	13466.24	77.34	11.100	0.2	5.55E-06	3.19E-08	5.518E-05
64	13689.18	78.56	11.300	0.3	5.65E-06	3.24E-08	5.618E-05

Time (h)	Total CPM	Final CPM	Zn ml	Add Zn	Total Ni M	Aqueous Ni	moles Ni sorbed/g HMO
72	13900.03	80.01	11.600	0.0	5.80E-06	3.34E-08	5.767E-05
78	13921.78	75.79	11.600	0.1	5.80E-06	3.16E-08	5.768E-05
84	14172.75	77.85	11.700	0.0	5.85E-06	3.21E-08	5.818E-05
87	14137.59	85.48	11.700	0.2	5.85E-06	3.54E-08	5.815E-05
98	14539.17	79.83	11.900	0.1	5.95E-06	3.27E-08	5.917E-05
114	15149.56	84	12.000	0.1	6.00E-06	3.33E-08	5.967E-05
125	15499.13	85.17	12.100	0.1	6.05E-06	3.32E-08	6.017E-05
138	15700.28	85.49	12.200	0.1	6.10E-06	3.32E-08	6.067E-05
150	15937.14	84.03	12.300	0.1	6.15E-06	3.24E-08	6.118E-05
162	16280.88	82.47	12.400	0.1	6.20E-06	3.14E-08	6.169E-05
174	16599	83.9	12.500	0.1	6.25E-06	3.16E-08	6.218E-05
189	16944.16	87.59	12.600	0.0	6.30E-06	3.26E-08	6.267E-05
204	17000.15	85.2	12.600	0.1	6.30E-06	3.16E-08	6.268E-05
216	17313.25	90.84	12.700	0.0	6.35E-06	3.33E-08	6.317E-05
240	17287.04	86.03	12.700	0.1	6.35E-06	3.16E-08	6.318E-05
252	17402.16	88.74	12.750	0.0	6.37E-06	3.25E-08	6.342E-05
270	17414.92	85.97	12.750	0.0	6.37E-06	3.15E-08	6.344E-05
288	17386.01	85.09	12.750	0.6	6.37E-06	3.12E-08	6.344E-05
314	15700.28	85.17	13.349	-9.4	6.67E-06	3.62E-08	6.638E-05

CBC Studies of Sr sorption to 1 g L^{-1} HAO at pH 7 and 25°C modeled wih pore diffusion model. Figure demonstrates pore diffusion may be not significant in amoprhous oxides.

$[Sr]_{bulk} = 2.6 \times 10^{-5}$ M maintained constant.

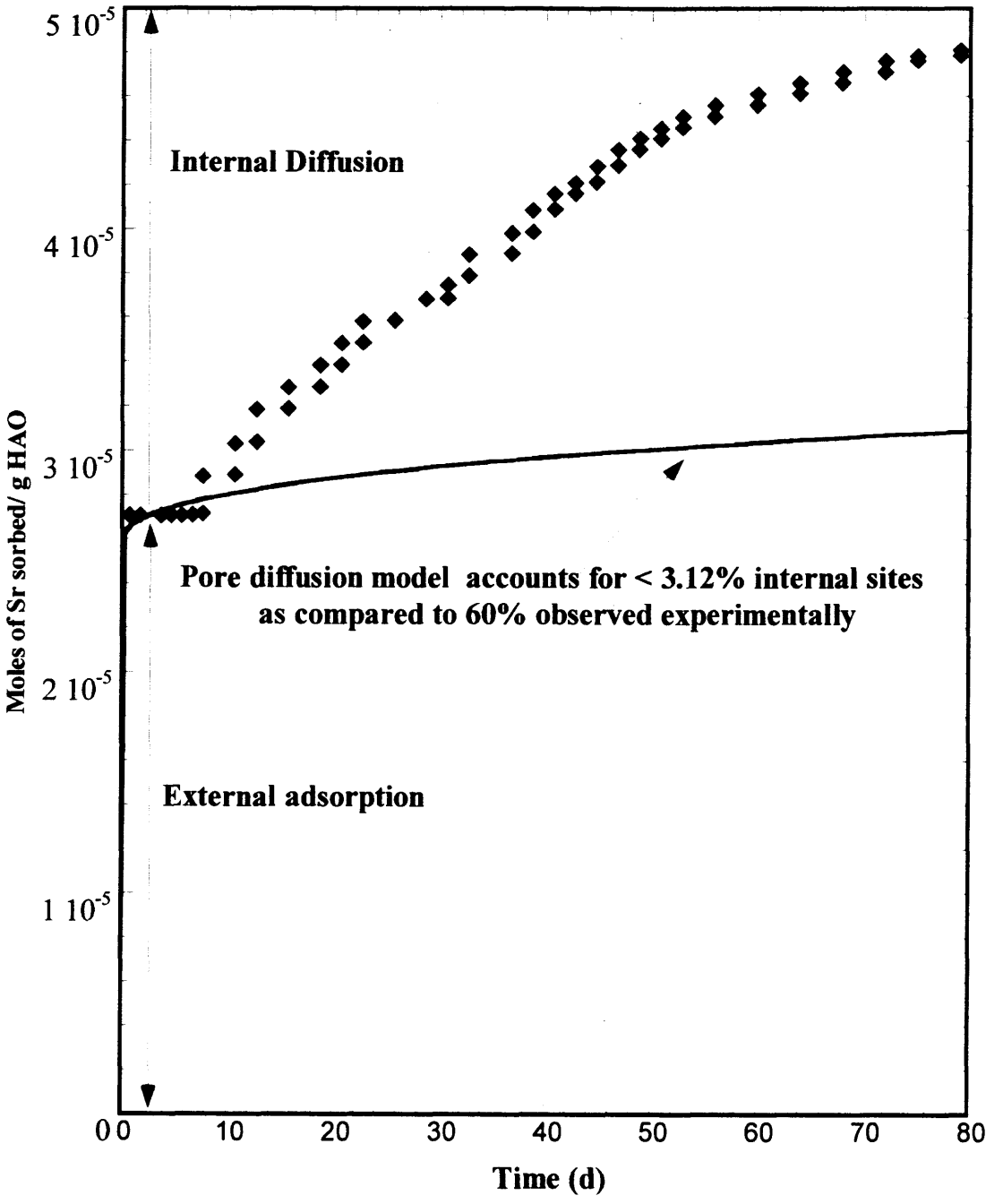

APPENDIX D

GOETHITE SORPTION STUDIES

Nickel Adsorption Studies

Nickel adsorption edges at 25°C

	Ionic Strength = 10^{-2}			Ionic Strength = 10^{-3}		
pH	total cpm	final cpm	%sorbed	total cpm	final cpm	%sorbed
4.11	167.43	165.77	0.991459	168.12	162.23	3.50345
4.57	167.43	150.25	10.261	168.12	149.15	11.28361
5.05	167.43	105.53	36.97067	168.12	106.88	36.42636
5.55	167.43	52.02	68.9303	168.12	50.77	69.80133
6.06	167.43	32.51	80.58293	168.12	30.51	81.85225
6.54	167.43	22.45	86.59141	168.12	23.3	86.14085
7	167.43	21.68	87.05131	168.12	20.22	87.97288
7.59	167.43	16.68	90.03763	168.12	14.18	91.56555
8.12	167.43	14.47	91.35758	168.12	16.97	89.90602
8.53	167.43	12.78	92.36696	168.12	14.94	91.11349
9.02	167.43	15.08	90.99325	168.12	13.21	92.14252
10	167.43	12.39	92.59989	168.12	12.13	92.78492
11.07	167.43	12.82	92.34307	168.12	12.47	92.58268

Nickel adsorption isotherms at pH 5 and 25°C (* marked samples were studied with 0.1 g/L goethite)

	Total CPM	Filtered CPM	Initial Conc.	Equilibrium Conc	Moles Ni/g Gt
	303.01	184.79	1.00E-09	6.10E-10	3.90E-10
	676.52	378.65	5.00E-09	2.80E-09	2.20E-09
	1322.21	892.60	1.00E-08	6.75E-09	3.25E-09
	3165.20	1836.13	2.00E-08	1.16E-08	8.40E-09
	3002.06	1888.30	4.00E-08	2.52E-08	1.48E-08
	2080.71	1203.14	1.00E-07	5.78E-08	4.22E-08
	345.50	216.34	2.00E-07	1.25E-07	7.48E-08
	647.91	468.56	5.00E-07	3.62E-07	1.38E-07
	594.72	459.00	1.00E-06	7.72E-07	2.28E-07
	2254.94	1801.40	2.00E-06	1.60E-06	4.02E-07
	3001.47	2457.50	4.00E-06	3.28E-06	7.25E-07
	362.49	284.77	1.00E-05	7.86E-06	2.14E-06
	656.22	614.81	2.00E-05	1.87E-05	1.26E-06
	635.75	611.25	4.00E-05	3.85E-05	1.54E-06
	1483.52	1448.82	1.00E-04	9.77E-05	2.34E-06
	3044.73	3008.26	2.00E-04	1.98E-04	2.40E-06
*	336.14	329.55	1.00E-05	9.80E-06	1.96E-06
*	641.18	634.00	2.00E-05	1.98E-05	2.24E-06
*	990.63	980.85	3.00E-05	2.97E-05	2.96E-06
*	1296.59	1289.00	4.00E-05	3.98E-05	2.34E-06
*	1313.93	1309.77	8.00E-05	7.97E-05	2.53E-06
*	3147.64	3141.02	1.00E-04	9.98E-05	2.10E-06
*	3072.50	3070.00	2.00E-04	2.00E-04	1.63E-06

Nickel adsorption isotherms at pH 6 and 25°C (* marked samples were studied with 0.1 g/L goethite)

	Total CPM	Filtered CPM	Initial Conc.	Eqlbm Conc	Ni/gGt
	356.96	85.54	1.00E-09	2.40E-10	7.60E-10
	660.79	125.26	5.00E-09	9.48E-10	4.05E-09
	1592.41	308.69	1.00E-08	1.94E-09	8.06E-09
	3335.46	663.86	2.00E-08	3.98E-09	1.60E-08
	3172.88	683.42	4.00E-08	8.62E-09	3.14E-08
	2052.49	384.66	1.00E-07	1.87E-08	8.13E-08
	376.60	78.19	2.00E-07	4.15E-08	1.58E-07
	672.75	152.27	5.00E-07	1.13E-07	3.87E-07
	537.09	204.51	1.00E-06	3.81E-07	6.19E-07
	2115.26	847.67	2.00E-06	8.01E-07	1.20E-06
	3043.50	1458.18	4.00E-06	1.92E-06	2.08E-06
	355.28	261.34	1.00E-05	7.36E-06	2.64E-06
	634.81	524.77	2.00E-05	1.65E-05	3.47E-06
	588.14	510.69	4.00E-05	3.47E-05	5.27E-06
	1601.86	1532.93	1.00E-04	9.57E-05	4.30E-06
	3341.10	3232.48	2.00E-04	1.93E-04	6.50E-06
*	328.96	310.00	1.00E-05	9.42E-06	5.76E-06
*	586.98	568.22	2.00E-05	1.94E-05	6.39E-06
*	986.13	961.25	3.00E-05	2.92E-05	7.57E-06
*	1390.20	1370.23	4.00E-05	3.94E-05	5.75E-06
*	1343.75	1332.74	8.00E-05	7.93E-05	6.55E-06
*	3404.15	3378.18	1.00E-04	9.92E-05	7.63E-06
*	3300.16	3290.91	2.00E-04	1.99E-04	5.61E-06

Nickel adsorption isotherms at pH 7 and 25°C (* marked samples were studied with 0.1 g/L goethite)

	Total CPM	Filtered CPM	Initial Conc.	Eqlbm Conc	Ni / g Gt
	100.67	12.05	1.00E-09	1.20E-10	8.80E-10
	304.98	34.76	5.00E-09	5.70E-10	4.43E-09
	311.55	41.30	2.00E-08	2.65E-09	1.73E-08
	320.69	37.24	4.00E-08	4.64E-09	3.54E-08
	103.27	10.03	1.00E-07	9.71E-09	9.03E-08
	186.97	30.81	2.00E-07	3.30E-08	1.67E-07
	279.25	40.11	5.00E-07	7.18E-08	4.28E-07
	477.35	53.94	1.00E-06	1.13E-07	8.87E-07
	181.89	24.29	2.00E-06	2.67E-07	1.73E-06
	462.32	69.74	4.00E-06	6.03E-07	3.40E-06
	104.54	47.85	1.00E-05	4.58E-06	5.42E-06
	143.64	86.39	2.00E-05	1.20E-05	7.97E-06
	184.92	150.47	5.00E-05	4.07E-05	9.31E-06
	458.36	408.76	1.00E-04	8.92E-05	1.08E-05
	1306.94	1226.96	2.00E-04	1.88E-04	1.22E-05
*	328.96	299.82	1.00E-05	9.11E-06	8.86E-06
*	644.15	629.56	2.00E-05	1.95E-05	4.53E-06
*	1004.02	966.78	3.00E-05	2.89E-05	1.11E-05
*	1338.76	1292.95	4.00E-05	3.86E-05	1.37E-05
*	1302.11	1264.45	8.00E-05	7.77E-05	2.31E-05
*	3160.14	3114.10	1.00E-04	9.85E-05	1.46E-05
*	3239.19	3218.80	2.00E-04	1.99E-04	1.26E-05

Nickel adsorption isotherms at pH 7 and 3.9°C

Total CPM	Filtered CPM	Initial Conc.	Equilibrium Conc	Moles Ni/g Gt
602.05	590.88	1.00E-08	9.81E-09	1.86E-10
1446.55	1434.50	2.00E-08	1.98E-08	1.67E-10
2564.23	2539.73	5.00E-08	4.95E-08	4.78E-10
3313.18	3291.60	1.00E-07	9.93E-08	6.51E-10
405.06	401.19	4.00E-07	3.96E-07	3.82E-09
917.09	908.76	1.00E-06	9.91E-07	9.08E-09
2435.06	2412.68	4.00E-06	3.96E-06	3.68E-08
2903.94	2878.90	4.00E-06	3.97E-06	3.45E-08
368.31	364.72	1.00E-05	9.90E-06	9.75E-08
499.19	494.63	2.00E-05	1.98E-05	1.83E-07
675.88	670.03	3.00E-05	2.97E-05	2.60E-07
938.61	930.93	4.00E-05	3.97E-05	3.27E-07

Nickel adsorption isotherms at pH 7 and 14°C

Total CPM	Filtered CPM	Initial Conc.	Equilibrium Conc	Moles Ni/g Gt
602.05	512.01	1.00E-08	8.50E-09	1.50E-09
1446.55	1206.37	2.00E-08	1.67E-08	3.32E-09
2564.23	2168.25	5.00E-08	4.23E-08	7.72E-09
3313.18	2806.00	1.00E-07	8.47E-08	1.53E-08
405.06	342.89	4.00E-07	3.39E-07	6.14E-08
917.09	780.12	1.00E-06	8.51E-07	1.49E-07
2435.06	2088.43	4.00E-06	3.43E-06	5.69E-07
2903.94	2440.82	4.00E-06	3.36E-06	6.38E-07
368.31	310.20	1.00E-05	8.42E-06	1.58E-06
499.19	440.34	2.00E-05	1.76E-05	2.36E-06
675.88	604.02	3.00E-05	2.68E-05	3.19E-06
938.61	848.22	4.00E-05	3.61E-05	3.85E-06

CBC studies of Nickel at pH 7 and 25°C (Run 1)

Time (h)	Total CPM	Final CPM	Ni ml	Add Zn	Total Ni M	CBC Ni	Ni Sorbed
0	0	0	0.0	0.00	0.00E+00	0.00E+00	0.00E+00
0.05	669.26	120.12	20.0	0.00	1.00E-06	1.79E-07	8.21E-07
1	669.26	90.75	20.0	0.00	1.00E-06	1.36E-07	8.64E-07
2	669.26	80.11	20.0	0.00	1.00E-06	1.20E-07	8.80E-07
2.5	669.26	77.54	20.0	0.00	1.00E-06	1.16E-07	8.84E-07
3	669.26	73.18	20.0	0.10	1.00E-06	1.09E-07	8.91E-07
3.5	694.35	64.03	20.1	0.30	1.01E-06	9.27E-08	9.12E-07
4	802.59	76.59	20.4	0.20	1.02E-06	9.73E-08	9.23E-07
4.5	852.59	83.79	20.6	0.10	1.03E-06	1.01E-07	9.29E-07
5	874.35	87.5	20.7	0.10	1.04E-06	1.04E-07	9.31E-07
5.5	890.52	93.21	20.8	0.00	1.04E-06	1.09E-07	9.31E-07
6	890.52	94.17	20.8	0.00	1.04E-06	1.10E-07	9.30E-07
7	890.52	91.55	20.8	0.00	1.04E-06	1.07E-07	9.33E-07
8	890.52	94.82	20.8	0.00	1.04E-06	1.11E-07	9.29E-07
9	890.52	97.93	20.8	0.00	1.04E-06	1.14E-07	9.26E-07
10	890.52	90.99	20.8	0.00	1.04E-06	1.06E-07	9.34E-07
11	890.52	95.95	20.8	0.00	1.04E-06	1.12E-07	9.28E-07
12	890.52	103.42	20.8	0.00	1.04E-06	1.21E-07	9.19E-07
13	890.52	93.26	20.8	0.00	1.04E-06	1.09E-07	9.31E-07
20	890.52	91.01	20.8	0.00	1.04E-06	1.06E-07	9.34E-07
22	890.52	94.79	20.8	0.00	1.04E-06	1.11E-07	9.29E-07
24	890.52	107.41	20.8	0.00	1.04E-06	1.25E-07	9.15E-07
27	890.52	103.5	20.8	0.00	1.04E-06	1.21E-07	9.19E-07
30	890.52	98.35	20.8	0.00	1.04E-06	1.15E-07	9.25E-07
33	890.52	96.21	20.8	0.00	1.04E-06	1.12E-07	9.28E-07
42	890.52	92.22	20.8	0.00	1.04E-06	1.08E-07	9.32E-07
48	890.52	93	20.8	0.00	1.04E-06	1.09E-07	9.31E-07

CBC studies of Nickel at pH 7 and 25°C (Run 2)

Time (h)	Total CPM	Final CPM	Ni ml	Add Zn	Total Ni M	CBC Ni	Ni Sorbed
0	0	0	0.0	0.00	0.00E+00	0.00E+00	0.00E+00
0.05	720.36	78.62	20.0	0.00	1.00E-06	1.09E-07	8.91E-07
1	720.36	77.16	20.0	0.00	1.00E-06	1.07E-07	8.93E-07
2	720.36	76.55	20.0	0.00	1.00E-06	1.06E-07	8.94E-07
3	720.36	75.79	20.0	0.00	1.00E-06	1.05E-07	8.95E-07
4	720.36	72.44	20.0	0.00	1.00E-06	1.01E-07	8.99E-07
6	720.36	76.47	20.0	0.00	1.00E-06	1.06E-07	8.94E-07
8	720.36	79.99	20.0	0.00	1.00E-06	1.11E-07	8.89E-07
10	720.36	72.24	20.0	0.10	1.00E-06	1.00E-07	9.00E-07
10.33	734.11	76.55	20.1	0.00	1.01E-06	1.05E-07	9.00E-07
12	734.78	81.39	20.1	0.00	1.01E-06	1.11E-07	8.94E-07
24	741.76	78.75	20.1	0.00	1.01E-06	1.07E-07	8.98E-07
35	741.76	81.01	20.1	0.00	1.01E-06	1.10E-07	8.95E-07
50	737.42	76.95	20.1	0.00	1.01E-06	1.05E-07	9.00E-07
60	737.42	80	20.1	0.00	1.01E-06	1.09E-07	8.96E-07
70	740	82.16	20.1	0.00	1.01E-06	1.12E-07	8.93E-07
81	728.25	77.25	20.1	0.00	1.01E-06	1.07E-07	8.98E-07
92	735.32	79.77	20.1	0.00	1.01E-06	1.09E-07	8.96E-07
104	756.18	79.5	20.1	0.00	1.01E-06	1.06E-07	8.99E-07
114	756.18	83.13	20.1	0.00	1.01E-06	1.10E-07	8.95E-07
126	742.04	85.33	20.1	0.00	1.01E-06	1.16E-07	8.89E-07
138	742.04	78.79	20.1	0.00	1.01E-06	1.07E-07	8.98E-07
188	733.5	79.99	20.1	0.00	1.01E-06	1.10E-07	8.95E-07
198	733.5	76.15	20.1	0.00	1.01E-06	1.04E-07	9.01E-07
238	745.52	78.41	20.1	0.00	1.01E-06	1.06E-07	8.99E-07
249	745.52	80.26	20.1	0.00	1.01E-06	1.08E-07	8.97E-07
264.5	731.68	77.45	20.1	0.00	1.01E-06	1.06E-07	8.99E-07
286	731.68	78.32	20.1	0.00	1.01E-06	1.08E-07	8.97E-07
300	736.25	81.75	20.1	0.00	1.01E-06	1.12E-07	8.93E-07
311	736.25	78.99	20.1	0.00	1.01E-06	1.08E-07	8.97E-07
337	743.32	79	20.1	0.00	1.01E-06	1.07E-07	8.98E-07
383.5	733.52	78.5	20.1	0.00	1.01E-06	1.08E-07	8.97E-07
416	729.5	79.12	20.1	0.00	1.01E-06	1.09E-07	8.96E-07
439	733.32	77.44	20.1	0.00	1.01E-06	1.06E-07	8.99E-07
456	733.32	80.56	20.1	0.00	1.01E-06	1.10E-07	8.95E-07
481	742.04	80.17	20.1	0.00	1.01E-06	1.09E-07	8.96E-07
510	742.04	80.5	20.1	0.00	1.01E-06	1.09E-07	8.96E-07
549	742.04	79.36	20.1	0.00	1.01E-06	1.07E-07	8.98E-07

Zinc Adsorption Studies

Zinc adsorption studies at 25°C

pH	$\mu = 10^{-3}$, [Zn] = 5×10^{-6}	pH	$\mu = 10^{-2}$, [Zn] = 5×10^{-6}	pH	$\mu = 10^{-2}$, [Zn] = 5×10^{-6}
3.54	14.771	3.61	12.342	3.83	14.013
4.08	18.327	4.17	16.679	4.18	16.685
4.54	22.085	4.53	21.284	4.38	22.315
5.08	32.237	5.23	33.9	5.18	35.134
5.54	40.227	5.63	46.063	5.31	50.336
6.01	66.157	6.28	69.107	6.19	66.443
6.58	72.327	6.68	74.44	6.68	93.289
7.01	88.71	7.11	81.93	7.25	97.315
7.53	92.137	7.65	87.85	7.41	96.604
8.24	92.369	8.19	92.078	8.06	99.329
8.92	92.722	8.68	96.094	8.72	99.329

Zinc adsorption isotherms at pH 5 and 25°C

[Zn]o	[Zn]o ppm	[S] ppb	[S] ppm	[S] M	C (Moles/g)
3.06E-04	2.00E+01	1.95E+04	1.95E+01	2.98E-04	7.94E-06
1.99E-04	1.30E+01	1.25E+04	1.25E+01	1.91E-04	7.95E-06
1.07E-04	7.00E+00	6.51E+03	6.51E+00	9.95E-05	7.49E-06
7.65E-05	5.00E+00	4.50E+03	4.50E+00	6.88E-05	7.64E-06
4.59E-05	3.00E+00	2.52E+03	2.52E+00	3.85E-05	7.34E-06
3.06E-05	2.00E+00	1.54E+03	1.54E+00	2.35E-05	7.03E-06
9.99E-06	6.54E-01	4.31E+02	4.31E-01	6.60E-06	3.40E-06
7.95E-06	5.20E-01	3.43E+02	3.43E-01	5.25E-06	2.70E-06
5.00E-06	3.27E-01	2.16E+02	2.16E-01	3.30E-06	1.70E-06
3.06E-06	2.00E-01	1.32E+02	1.32E-01	2.02E-06	1.04E-06
9.99E-07	6.54E-02	4.31E+01	4.31E-02	6.60E-07	3.40E-07
7.99E-07	5.23E-02	3.45E+01	3.45E-02	5.28E-07	2.72E-07

Zinc adsorption isotherms at pH 6 and 25°C

[Zn]o	[Zn]o ppm	[S] ppb	[S] ppm	[S] M	C (Moles/g)
3.06E-04	2.00E+01	1.93E+04	1.93E+01	2.95E-04	1.07E-05
1.99E-04	1.30E+01	1.23E+04	1.23E+01	1.88E-04	1.08E-05
1.07E-04	7.00E+00	6.26E+03	6.26E+00	9.57E-05	1.13E-05
7.65E-05	5.00E+00	4.25E+03	4.25E+00	6.50E-05	1.15E-05
4.59E-05	3.00E+00	2.30E+03	2.30E+00	3.52E-05	1.07E-05
3.06E-05	2.00E+00	1.46E+03	1.46E+00	2.23E-05	8.26E-06
9.99E-06	6.54E-01	3.79E+02	3.79E-01	5.80E-06	4.20E-06
7.95E-06	5.20E-01	3.02E+02	3.02E-01	4.61E-06	3.34E-06
5.00E-06	3.27E-01	1.90E+02	1.90E-01	2.90E-06	2.10E-06
3.06E-06	2.00E-01	1.16E+02	1.16E-01	1.77E-06	1.28E-06
9.99E-07	6.54E-02	3.79E+01	3.79E-02	5.80E-07	4.20E-07
7.99E-07	5.23E-02	3.03E+01	3.03E-02	4.64E-07	3.36E-07

Zinc adsorption isotherms at pH 7 and 25°C

[Zn]o	[Zn]o ppm	[S] ppb	[S] ppm	[S] M	C (Moles/g)
3.06E-04	2.00E+01	1.86E+04	1.86E+01	2.84E-04	2.14E-05
1.99E-04	1.30E+01	1.16E+04	1.16E+01	1.77E-04	2.22E-05
1.07E-04	7.00E+00	5.53E+03	5.53E+00	8.46E-05	2.25E-05
7.65E-05	5.00E+00	3.55E+03	3.55E+00	5.43E-05	2.22E-05
4.59E-05	3.00E+00	1.68E+03	1.68E+00	2.57E-05	2.02E-05
3.06E-05	2.00E+00	7.80E+02	7.80E-01	1.19E-05	1.87E-05
9.99E-06	6.54E-01	2.60E+02	2.60E-01	3.98E-06	6.02E-06
7.95E-06	5.20E-01	2.00E+02	2.00E-01	3.06E-06	4.89E-06
5.00E-06	3.27E-01	1.11E+02	1.11E-01	1.70E-06	3.30E-06
3.06E-06	2.00E-01	7.40E+01	7.40E-02	1.13E-06	1.93E-06
9.99E-07	6.54E-02	2.48E+01	2.48E-02	3.79E-07	6.20E-07
7.99E-07	5.23E-02	1.83E+01	1.83E-02	2.80E-07	5.20E-07

Zinc adsorption isotherms at pH 7 and 14°C

Total CPM	Filtered CPM	Initial Conc.	Equilibrium Conc	Moles Ni/g Gt
80.17	57.21	1.00E-08	7.14E-09	2.86E-09
188.53	144.03	5.00E-08	3.82E-08	1.18E-08
460.89	336.40	1.00E-07	7.30E-08	2.70E-08
1009.68	743.68	5.00E-07	3.68E-07	1.32E-07
1038.25	737.34	1.00E-06	7.10E-07	2.90E-07
2850.65	2005.01	4.00E-06	2.81E-06	1.19E-06
2721.51	1957.22	4.00E-06	2.88E-06	1.12E-06
151.04	111.49	1.00E-05	7.38E-06	2.62E-06
392.48	326.12	5.00E-05	4.15E-05	8.45E-06
717.22	627.54	8.00E-05	7.00E-05	1.00E-05
1520.56	1332.75	1.00E-04	8.76E-05	1.24E-05
2702.40	2496.75	2.00E-04	1.85E-04	1.52E-05

Zinc adsorption isotherms at pH 7 and 4.2°C

Total CPM	Filtered CPM	Initial Conc.	Equilibrium Conc	Moles Ni/g Gt
80.17	78.57	1.00E-08	9.80E-09	2.00E-10
188.53	185.50	5.00E-08	4.92E-08	8.04E-10
460.89	450.00	1.00E-07	9.76E-08	2.36E-09
1009.68	990.66	5.00E-07	4.91E-07	9.42E-09
1038.25	997.12	1.00E-06	9.60E-07	3.96E-08
2850.65	2768.19	4.00E-06	3.88E-06	1.16E-07
2721.51	2690.76	4.00E-06	3.95E-06	4.52E-08
151.04	147.91	1.00E-05	9.79E-06	2.07E-07
392.48	387.18	5.00E-05	4.93E-05	6.75E-07
717.22	707.04	8.00E-05	7.89E-05	1.14E-06
1520.56	1501.95	1.00E-04	9.88E-05	1.22E-06
2702.40	2672.88	2.00E-04	1.98E-04	2.18E-06

CBC studies of Zinc at pH 7 and 25°C

Time (h)	Total CPM	Final CPM	Ni ml	Add Zn	Total Ni M	CBC Ni	Ni Sorbed
0.001	0	0	0.0	0.00	0.00E+00	0.00E+00	0.00E+00
0.05	660.12	237.45	20.0	0.00	1.00E-06	3.60E-07	6.40E-07
0.10	660.12	227.8	20.0	0.00	1.00E-06	3.45E-07	6.55E-07
1	660.12	224.35	20.0	0.00	1.00E-06	3.40E-07	6.60E-07
2	660.12	224.77	20.0	0.00	1.00E-06	3.40E-07	6.60E-07
2.5	660.12	227.02	20.0	0.00	1.00E-06	3.44E-07	6.56E-07
3	660.12	222.67	20.0	0.10	1.00E-06	3.37E-07	6.63E-07
3.5	674.33	226.85	20.1	0.00	1.01E-06	3.38E-07	6.67E-07
4	674.33	225.9	20.1	0.00	1.01E-06	3.37E-07	6.68E-07
4.5	674.33	234.78	20.1	0.00	1.01E-06	3.50E-07	6.55E-07
5	674.33	227.29	20.1	0.00	1.01E-06	3.39E-07	6.66E-07
5.5	674.33	233.42	20.1	0.00	1.01E-06	3.48E-07	6.57E-07
6	674.33	232.17	20.1	0.00	1.01E-06	3.46E-07	6.59E-07
7	674.33	230.55	20.1	0.00	1.01E-06	3.44E-07	6.61E-07
8	674.33	228.62	20.1	0.00	1.01E-06	3.41E-07	6.64E-07
9	674.33	224.75	20.1	0.10	1.01E-06	3.35E-07	6.70E-07
10	688.56	236.51	20.2	0.00	1.01E-06	3.47E-07	6.63E-07
11	688.56	234.84	20.2	0.00	1.01E-06	3.44E-07	6.66E-07
12	688.56	240.11	20.2	0.00	1.01E-06	3.52E-07	6.58E-07
15	688.56	233.19	20.2	0.00	1.01E-06	3.42E-07	6.68E-07
20	688.56	229.02	20.2	0.10	1.01E-06	3.36E-07	6.74E-07
26	704.26	244.5	20.3	0.00	1.02E-06	3.52E-07	6.63E-07
32	704.26	238.75	20.3	0.00	1.02E-06	3.44E-07	6.71E-07
36	704.26	239.59	20.3	0.00	1.02E-06	3.45E-07	6.70E-07
42	704.26	240.31	20.3	0.00	1.02E-06	3.46E-07	6.69E-07
48	704.26	245.19	20.3	0.00	1.02E-06	3.53E-07	6.62E-07
57	704.26	240.26	20.3	0.00	1.02E-06	3.46E-07	6.69E-07
63	704.26	243.21	20.3	0.00	1.02E-06	3.51E-07	6.64E-07
72	704.26	239.78	20.3	0.00	1.02E-06	3.46E-07	6.69E-07
84	704.26	238.56	20.3	0.00	1.02E-06	3.44E-07	6.71E-07
96	704.26	240	20.3	0.00	1.02E-06	3.46E-07	6.69E-07
108	704.26	238.12	20.3	0.00	1.02E-06	3.43E-07	6.72E-07
120	704.26	238.7	20.3	0.00	1.02E-06	3.44E-07	6.71E-07
135	704.26	238	20.3	0.00	1.02E-06	3.43E-07	6.72E-07
150	704.26	238	20.3	0.00	1.02E-06	3.43E-07	6.72E-07
164	704.26	239.28	20.3	0.00	1.02E-06	3.45E-07	6.70E-07

Calcium Adsorption Studies

Calcium adsorption edges at 25°C

Ionic Strength = 10^{-3}

	Filterate Concentrations			
pH	In ppb	In ppm	In M	% Adsorbed
4	220.00	0.2200	5.39E-06	10.13
4.5	187.50	0.1875	4.60E-06	23.41
5.01	132.00	0.1320	3.24E-06	46.08
5.55	124.50	0.1245	3.05E-06	49.14
6.07	122.50	0.1225	3.00E-06	49.96
6.49	122.00	0.1220	2.99E-06	50.16
7.02	121.00	0.1210	2.97E-06	50.57
7.5	120.00	0.1200	2.94E-06	50.98
8.1	118.50	0.1185	2.90E-06	51.59
8.51	110.00	0.1100	2.70E-06	55.07
9.13	90.50	0.0905	2.22E-06	63.03
9.89	33.15	0.0332	8.13E-07	86.46

Ionic Strength = 10^{-2}

	Filterate Concentrations			
pH	In ppb	In ppm	In M	% Adsorbed
4.1	228.00	0.2280	5.59E-06	6.86
4.5	185.00	0.1850	4.53E-06	24.43
5.11	142.00	0.1420	3.48E-06	41.99
5.44	134.00	0.1340	3.28E-06	45.26
5.95	133.00	0.1330	3.26E-06	45.67
6.47	135.00	0.1350	3.31E-06	44.85
7.07	128.00	0.1280	3.14E-06	47.71
7.56	130.00	0.1300	3.19E-06	46.90
8.08	129.00	0.1290	3.16E-06	47.30
8.43	124.50	0.1245	3.05E-06	49.14
9.01	107.00	0.1070	2.62E-06	56.29
10.1	45.00	0.0450	1.10E-06	81.62

Calcium adsorption isotherms at pH 5 and 25°C (* marked samples were studied with 0.1 g/L goethite)

	Initial Concentration				S		C
	in M	in ppm	in ppb	in ppb	in ppm	in M	moles Ca/g Gt.
*	5.00E-03	200.00	200000	194000.00	194.00	4.85E-03	1.50E-03
*	4.00E-03	160.00	160000	153600.00	153.60	3.84E-03	1.60E-03
*	3.00E-03	120.00	120000	114000.00	114.00	2.85E-03	1.50E-03
*	2.00E-03	80.00	80000	74900.00	74.90	1.87E-03	1.28E-03
*	1.00E-03	40.00	40000	37800.00	37.80	9.45E-04	5.50E-04
*	8.00E-04	32.00	32000	30000.00	30.00	7.50E-04	5.00E-04
	5.00E-03	200.00	200000	141000.00	141.00	3.53E-03	1.48E-03
	4.00E-03	160.00	160000	108000.00	108.00	2.70E-03	1.30E-03
	1.00E-03	40.00	40000	22800.00	22.80	5.70E-04	4.30E-04
	5.00E-04	20.00	20000	10800.00	10.80	2.70E-04	2.30E-04
	3.00E-04	12.00	12000	6690.00	6.69	1.67E-04	1.33E-04
	1.00E-04	4.00	4000	2350.00	2.35	5.88E-05	4.13E-05
	5.00E-05	2.00	2000	1020.00	1.02	2.55E-05	2.45E-05
	2.50E-05	1.00	1000	524.00	0.52	1.31E-05	1.19E-05
	1.00E-05	0.40	400	218.00	0.22	5.45E-06	4.55E-06
	5.00E-06	0.20	200	108.00	0.11	2.70E-06	2.30E-06
	1.00E-06	0.04	40	21.00	0.02	5.25E-07	4.75E-07
	5.00E-07	0.02	20	11.00	0.01	2.75E-07	2.25E-07

Calcium adsorption isotherms at pH 6 and 25°C (* marked samples were studied with 0.1 g/L goethite)

	Initial Concentration				S		C
	in M	in ppm	in ppb	in ppb	in ppm	in M	moles Ca/g Gt.
*	5.00E-03	200.00	200000	191000.00	191.00	4.78E-03	2.25E-03
*	4.00E-03	160.00	160000	151600.00	151.60	3.79E-03	2.10E-03
*	3.00E-03	120.00	120000	111000.00	111.00	2.78E-03	2.25E-03
*	2.00E-03	80.00	80000	71400.00	71.40	1.79E-03	2.15E-03
*	1.00E-03	40.00	40000	37200.00	37.20	9.30E-04	7.00E-04
*	8.00E-04	32.00	32000	25200.00	25.20	6.30E-04	1.70E-03
	8.00E-03	320.00	320000	219000.00	219.00	5.48E-03	2.53E-03
	4.00E-03	160.00	160000	96000.00	96.00	2.40E-03	1.60E-03
	1.00E-03	40.00	40000	21330.00	21.33	5.33E-04	4.67E-04
	5.00E-04	20.00	20000	10400.00	10.40	2.60E-04	2.40E-04
	3.00E-04	12.00	12000	5225.00	5.23	1.31E-04	1.69E-04
	1.00E-04	4.00	4000	2130.00	2.13	5.33E-05	4.68E-05
	5.00E-05	2.00	2000	888.00	0.89	2.22E-05	2.78E-05
	2.50E-05	1.00	1000	494.00	0.49	1.24E-05	1.27E-05
	1.00E-05	0.40	400	204.00	0.20	5.10E-06	4.90E-06
	5.00E-06	0.20	200	104.00	0.10	2.60E-06	2.40E-06
	1.00E-06	0.04	40	19.00	0.02	4.75E-07	5.25E-07
	5.00E-07	0.02	20	10.00	0.01	2.50E-07	2.50E-07

Calcium adsorption isotherms at pH 7 and 25°C (* marked samples were studied with 0.1 g/L goethite)

	Initial Concentration				S		C
	in M	in ppm	in ppb	in ppb	in ppm	in M	moles Ca/g Gt.
*	5.00E-03	200.00	200000	188000.00	188.00	4.70E-03	3.00E-03
*	4.00E-03	160.00	160000	148800.00	148.80	3.72E-03	2.80E-03
*	3.00E-03	120.00	120000	110400.00	110.40	2.76E-03	2.40E-03
*	2.00E-03	80.00	80000	72000.00	72.00	1.80E-03	2.00E-03
*	1.00E-03	40.00	40000	37200.00	37.20	9.30E-04	7.00E-04
*	8.00E-04	32.00	32000	26400.00	26.40	6.60E-04	1.40E-03
	8.00E-03	320.00	320000	219000.00	219.00	5.48E-03	2.53E-03
	4.00E-03	160.00	160000	96000.00	96.00	2.40E-03	1.60E-03
	1.00E-03	40.00	40000	19200.00	19.20	4.80E-04	5.20E-04
	5.00E-04	20.00	20000	8570.00	8.57	2.14E-04	2.86E-04
	3.00E-04	12.00	12000	6180.00	6.18	1.55E-04	1.46E-04
	1.00E-04	4.00	4000	1560.00	1.56	3.90E-05	6.10E-05
	5.00E-05	2.00	2000	816.00	0.82	2.04E-05	2.96E-05
	2.50E-05	1.00	1000	472.00	0.47	1.18E-05	1.32E-05
	1.00E-05	0.40	400	192.00	0.19	4.80E-06	5.20E-06
	5.00E-06	0.20	200	96.00	0.10	2.40E-06	2.60E-06
	1.00E-06	0.04	40	19.00	0.02	4.75E-07	5.25E-07
	5.00E-07	0.02	20	9.00	0.01	2.25E-07	2.75E-07

Binary Systems

Reversibility studies in Ni-Zn systems: Ni added first, then aged 2 h, and then Zn added

Case 1: $[Ni]_o = 2 \times 10^{-4}$ M and $[Zn]_o = 1 \times 10^{-4}$ M

Time (min)	Total CPM	Filter CPM	Eqlbm Ni	Ni/g Gt	Total CPM	Filter CPM	Eqlbm Zn	Zn/g Gt
15	3456.12	3432.12	1.99E-04	1.389E-05				
30	3456.12	3432.05	1.99E-04	1.393E-05				
45	3456.12	3431.81	1.99E-04	1.407E-05				
60	3456.12	3431.26	1.99E-04	1.439E-05				
75	3456.12	3431.44	1.99E-04	1.428E-05				
90	3456.12	3431	1.99E-04	1.454E-05				
105	3456.12	3431.03	1.99E-04	1.452E-05				
120	3456.12	3432	1.99E-04	1.396E-05	2050.19	2040.03	9.95E-05	4.956E-06
135	3456.12	3432.78	1.99E-04	1.351E-05	2050.19	2039.05	9.946E-05	5.434E-06
150	3456.12	3433.06	1.99E-04	1.334E-05	2050.19	2037.81	9.94E-05	6.038E-06
165	3456.12	3432.75	1.99E-04	1.352E-05	2050.19	2037.47	9.938E-05	6.204E-06
180	3456.12	3432.84	1.99E-04	1.347E-05	2050.19	2037.24	9.937E-05	6.316E-06
195	3456.12	3432.91	1.99E-04	1.343E-05	2050.19	2037.2	9.937E-05	6.336E-06
210	3456.12	3432.98	1.99E-04	1.339E-05	2050.19	2037.28	9.937E-05	6.297E-06
225	3456.12	3433	1.99E-04	1.338E-05	2050.19	2036.96	9.935E-05	6.453E-06
240	3456.12	3432.95	1.99E-04	1.341E-05	2050.19	2037.13	9.936E-05	6.37E-06

Case 2: $[Ni]_o = 2 \times 10^{-4}$ M and $[Zn]_o = 2 \times 10^{-4}$ M

Time (min)	Total CPM	Filter CPM	Eqlbm Ni	Ni/g Gt	Total CPM	Filter CPM	Eqlbm Zn	Zn/g Gt
15	3456.12	3432.12	1.986E-04	1.389E-05				
30	3456.12	3432.05	1.986E-04	1.393E-05				
45	3456.12	3431.81	1.986E-04	1.407E-05				
60	3456.12	3431.26	1.986E-04	1.439E-05				
75	3456.12	3431.44	1.986E-04	1.428E-05				
90	3456.12	3431	1.985E-04	1.454E-05				
105	3456.12	3431.03	1.985E-04	1.452E-05				
120	3456.12	3432.29	1.986E-04	1.379E-05	4026.32	4010.25	1.992E-04	7.982E-06
135	3456.12	3434.65	1.988E-04	1.242E-05	4026.32	4008.52	1.991E-04	8.842E-06
150	3456.12	3437.08	1.989E-04	1.102E-05	4026.32	4006.84	1.990E-04	9.676E-06
165	3456.12	3438.98	1.990E-04	9.919E-06	4026.32	4005.62	1.990E-04	1.028E-05
180	3456.12	3439.2	1.990E-04	9.791E-06	4026.32	4005.09	1.989E-04	1.055E-05
195	3456.12	3439.08	1.990E-04	9.861E-06	4026.32	4004.77	1.989E-04	1.07E-05
210	3456.12	3438.89	1.990E-04	9.971E-06	4026.32	4004.36	1.989E-04	1.091E-05
225	3456.12	3439.13	1.990E-04	9.832E-06	4026.32	4004.2	1.989E-04	1.099E-05
240	3456.12	3439	1.990E-04	9.907E-06	4026.32	4004.31	1.989E-04	1.093E-05

Reversibility studies in Ni-Zn systems: Zn added first, then aged 2 h, and then Ni added

Case 1: $[Zn]o = 2 \times 10^{-4}$ M and $[Ni]o = 1 \times 10^{-4}$ M

Time (min)	Total CPM	Filter CPM	Eqlbm Ni	Ni/g Gt	Total CPM	Filter CPM	Eqlbm Zn	Zn/g Gt
15					4084.2	4043.05	1.98E-04	2.015E-05
30					4084.2	4042.64	1.98E-04	2.035E-05
45					4084.2	4042.03	1.98E-04	2.065E-05
60					4084.2	4041.51	1.98E-04	2.09E-05
75					4084.2	4041.29	1.98E-04	2.101E-05
90					4084.2	4041.4	1.98E-04	2.096E-05
105					4084.2	4041.5	1.98E-04	2.091E-05
120	3524.16	3517.96	9.982E-05	1.759E-06	4084.2	4045.13	1.98E-04	1.913E-05
135	3524.16	3510.84	9.962E-05	3.78E-06	4084.2	4049.07	1.98E-04	1.72E-05
150	3524.16	3508.32	9.955E-05	4.495E-06	4084.2	4050.85	1.98E-04	1.633E-05
165	3524.16	3505.28	9.946E-05	5.357E-06	4084.2	4052.37	1.98E-04	1.559E-05
180	3524.16	3504.11	9.943E-05	5.689E-06	4084.2	4053	1.98E-04	1.528E-05
195	3524.16	3502.63	9.939E-05	6.109E-06	4084.2	4053.84	1.99E-04	1.487E-05
210	3524.16	3500.9	9.934E-05	6.6E-06	4084.2	4054.98	1.99E-04	1.431E-05
225	3524.16	3500.32	9.932E-05	6.765E-06	4084.2	4055.42	1.99E-04	1.409E-05
240	3524.16	3500.59	9.933E-05	6.688E-06	4084.2	4055.31	1.99E-04	1.415E-05

Case 2: $[Zn]o = 2 \times 10^{-4}$ M and $[Ni]o = 2 \times 10^{-4}$ M

Time (min)	Total CPM	Filter CPM	Eqlbm Ni	Ni/g Gt	Total CPM	Filter CPM	Eqlbm Zn	Zn/g Gt
15					4084.2	4043.05	1.980E-04	2.015E-05
30					4084.2	4042.64	1.980E-04	2.035E-05
45					4084.2	4042.03	1.979E-04	2.065E-05
60					4084.2	4041.51	1.979E-04	2.09E-05
75					4084.2	4041.29	1.979E-04	2.101E-05
90					4084.2	4041.4	1.979E-04	2.096E-05
105					4084.2	4041.5	1.979E-04	2.091E-05
120	7368.25	7357.82	1.997E-04	2.831E-06	4084.2	4047.03	1.982E-04	1.82E-05
135	7368.25	7350.49	1.995E-04	4.821E-06	4084.2	4051.36	1.984E-04	1.608E-05
150	7368.25	7344.81	1.994E-04	6.362E-06	4084.2	4054.5	1.985E-04	1.454E-05
165	7368.25	7340.28	1.992E-04	7.592E-06	4084.2	4057.35	1.987E-04	1.315E-05
180	7368.25	7336.63	1.991E-04	8.583E-06	4084.2	4059.24	1.988E-04	1.222E-05
195	7368.25	7333.54	1.991E-04	9.422E-06	4084.2	4061.01	1.989E-04	1.136E-05
210	7368.25	7332	1.990E-04	9.84E-06	4084.2	4061.52	1.989E-04	1.111E-05
225	7368.25	7331.64	1.990E-04	9.937E-06	4084.2	4061.93	1.989E-04	1.091E-05
240	7368.25	7331.89	1.990E-04	9.869E-06	4084.2	4061.81	1.989E-04	1.096E-05

Ni-Zn competition as a function of concentration

Case 1: Ni concentration fixed and Zn concentration varied
Initial Ni added = 2×10^{-4} M

Initial Zn.	Total CPM	Filter CPM	Eqlbm Zn	Zn/g Gt	Total CPM	Filter CPM	Eqlbm Ni	Ni/g Gt
0.00E+00	0	0	0.00E+00	0.00E+00	3456.12	3429.03	1.9843E-04	1.6E-05
1.00E-04	2050.19	2037.13	9.94E-05	6.37E-06	3456.12	3432.95	1.9866E-04	1.3E-05
1.25E-04	2479.99	2464.18	1.24E-04	7.97E-06	3456.12	3434.67	1.9876E-04	1.2E-05
1.50E-04	3056.07	3037.25	1.49E-04	9.24E-06	3456.12	3436.22	1.9885E-04	1.2E-05
1.75E-04	3539.91	3519.67	1.74E-04	1.00E-05	3456.12	3437.75	1.9894E-04	1.1E-05
2.00E-04	4026.32	4004.31	1.99E-04	1.09E-05	3456.12	3439	1.9901E-04	9.9E-06
2.25E-04	4400.12	4377.05	2.24E-04	1.18E-05	3456.12	3439.34	1.9903E-04	9.7E-06

Case 2: Zn concentration fixed and Ni concentration varied
Initial Zn added = 2×10^{-4} M

Initial Ni.	Total CPM	Filter CPM	Eqlbm Ni	Ni/g Gt	Total CPM	Filter CPM	Eqlbm Zn	Zn/g Gt
0.00E+00	0	0	0.000E+00	0	4084.2	4042.36	1.980E-04	2E-05
1.00E-04	3524.16	3500.59	9.933E-05	6.7E-06	4084.2	4055.31	1.986E-04	1.4E-05
1.25E-04	4348.01	4320.72	1.242E-04	7.8E-06	4084.2	4057.16	1.987E-04	1.3E-05
1.50E-04	5200.58	5169.87	1.491E-04	8.9E-06	4084.2	4059.34	1.988E-04	1.2E-05
1.75E-04	6264.38	6230.87	1.741E-04	9.4E-06	4084.2	4060.95	1.989E-04	1.1E-05
2.00E-04	7368.25	7331.89	1.990E-04	9.9E-06	4084.2	4061.81	1.989E-04	1.1E-05
2.25E-04	8109.2	8073.25	2.240E-04	1E-05	4084.2	4063.18	1.990E-04	1E-05

Competitive Isotherms of Ni and Zn at pH 5

Initial Concentrations			At Equilibrium	
[M of Ni]	Total CPM	Filtered CPM	[Ni]eqlbm	Moles of Ni/g Gt
2.00E-04	3004.28	2999.98	1.997E-04	2.863E-06
1.50E-04	2396.45	2391.79	1.497E-04	2.917E-06
1.00E-04	1858.04	1852.89	9.972E-05	2.772E-06
5.00E-05	452.56	450.2	4.974E-05	2.607E-06
2.00E-05	333.33	329.85	1.979E-05	2.088E-06
1.00E-05	148.92	146.21	9.818E-06	1.820E-06
4.00E-06	3917.33	3807.84	3.888E-06	1.118E-06
2.00E-06	1500.16	1458.01	1.944E-06	5.619E-07
1.00E-06	1172.35	1134.42	9.676E-07	3.235E-07
8.00E-07	1800.63	1731.75	7.694E-07	3.060E-07
5.00E-07	2360.12	2280.12	4.831E-07	1.695E-07
2.00E-07	800.16	770.6	1.926E-07	7.389E-08
1.00E-07	540.33	520.56	9.634E-08	3.659E-08
5.00E-08	170.69	165.79	4.856E-08	1.435E-08
2.00E-08	120.26	116.1	1.931E-08	6.918E-09
1.00E-08	98.5	94.95	9.640E-09	3.604E-09

Initial Concentrations			At Equilibrium	
[M of Zn]	Total CPM	Filtered CPM	[Zn]eqlbm	Moles of Zn/g Gt
2.00E-04	1750.33	1746.8	1.996E-04	4.034E-06
1.50E-04	1430.21	1426.35	1.496E-04	4.048E-06
1.00E-04	1209.14	1204.29	9.960E-05	4.011E-06
5.00E-05	542.15	538.3	4.964E-05	3.551E-06
2.00E-05	390.12	384.25	1.970E-05	3.009E-06
1.00E-05	200.04	194.81	9.739E-06	2.614E-06
4.00E-06	2736.22	2636.94	3.855E-06	1.451E-06
2.00E-06	1388.39	1314.59	1.894E-06	1.063E-06
1.00E-06	700.85	667.72	9.527E-07	4.727E-07
8.00E-07	1850.41	1741.04	7.527E-07	4.728E-07
5.00E-07	1380.33	1309.58	4.744E-07	2.563E-07
2.00E-07	572.16	542.5	1.896E-07	1.037E-07
1.00E-07	282.39	267.75	9.482E-08	5.184E-08
5.00E-08	144.2	138.04	4.786E-08	2.136E-08
2.00E-08	100.35	94.62	1.886E-08	1.142E-08
1.00E-08	72.14	68.25	9.461E-09	5.392E-09

Competitive Isotherms of Ni and Zn at pH 6

Initial Concentrations			At Equilibrium	
[M of Ni]	Total CPM	Filtered CPM	[Ni]eqlbm	Moles of Ni/g Gt
2.00E-04	3001.63	2995.25	1.996E-04	4.251E-06
1.50E-04	2400.5	2393.75	1.496E-04	4.218E-06
1.00E-04	1880.33	1872.64	9.959E-05	4.090E-06
5.00E-05	825.45	819.52	4.964E-05	3.592E-06
2.00E-05	320.16	315	1.968E-05	3.223E-06
1.00E-05	151.65	147.98	9.758E-06	2.420E-06
4.00E-06	3907.24	3780.14	3.870E-06	1.301E-06
2.00E-06	1799.12	1725.95	1.919E-06	8.134E-07
1.00E-06	1002.26	957.9	9.557E-07	4.426E-07
8.00E-07	2800.77	2685.01	7.669E-07	3.307E-07
5.00E-07	2111.05	2014	4.770E-07	2.299E-07
2.00E-07	790.25	745.01	1.886E-07	1.145E-07
1.00E-07	412.88	394.44	9.553E-08	4.466E-08
5.00E-08	216.56	205.85	4.753E-08	2.473E-08
2.00E-08	133.4	127	1.904E-08	9.595E-09
1.00E-08	76.37	72.74	9.525E-09	4.753E-09

Initial Concentrations			At Equilibrium	
[M of Zn]	Total CPM	Filtered CPM	[Zn]eqlbm	Moles of Zn/g Gt
2.00E-04	1700.46	1695.5	1.994E-04	5.834E-06
1.50E-04	1344.29	1339.22	1.494E-04	5.657E-06
1.00E-04	970.75	965.55	9.946E-05	5.357E-06
5.00E-05	500.61	495.5	4.949E-05	5.104E-06
2.00E-05	190.12	186.01	1.957E-05	4.324E-06
1.00E-05	187.85	181.91	9.684E-06	3.162E-06
4.00E-06	2736.22	2636.94	3.855E-06	1.451E-06
2.00E-06	1388.39	1314.59	1.894E-06	1.063E-06
1.00E-06	700.85	667.72	9.527E-07	4.727E-07
8.00E-07	1850.41	1741.04	7.527E-07	4.728E-07
5.00E-07	1300.25	1215.84	4.675E-07	3.246E-07
2.00E-07	560.37	524.5	1.872E-07	1.280E-07
1.00E-07	272.45	255	9.360E-08	6.405E-08
5.00E-08	121.28	116.28	4.794E-08	2.061E-08
2.00E-08	80.35	74.92	1.865E-08	1.352E-08
1.00E-08	70.35	65.82	9.356E-09	6.439E-09

Competitive Isotherms of Ni and Zn at pH 7

Initial Concentrations			At Equilibrium	
[M of Ni]	Total CPM	Filtered CPM	[Ni]eqlbm	Moles of Ni/g Gt
2.00E-04	2971.18	2957.6	1.991E-04	9.141E-06
1.00E-04	1781.67	1765.34	9.908E-05	9.166E-06
5.00E-05	450.37	442.27	4.910E-05	8.993E-06
2.00E-05	320.21	309.15	1.931E-05	6.908E-06
4.00E-06	3808.94	3511.01	3.687E-06	3.129E-06
2.00E-06	1469.4	1341.5	1.826E-06	1.741E-06
1.00E-06	1138.08	999.99	8.787E-07	1.213E-06
8.00E-07	1812.35	1667.24	7.359E-07	6.405E-07
5.00E-07	2487.35	2227.45	4.478E-07	5.224E-07
2.00E-07	843.09	734.92	1.743E-07	2.566E-07
1.00E-07	549.02	482.1	8.781E-08	1.219E-07
5.00E-08	167.25	147.57	4.412E-08	5.883E-08
2.00E-08	111.23	97.35	1.750E-08	2.496E-08
1.00E-08	102.88	91.08	8.853E-09	1.147E-08

Initial Concentrations			At Equilibrium	
[M of Zn]	Total CPM	Filtered CPM	[Zn]eqlbm	Moles of Zn/g Gt
2.00E-04	1740.85	1731.36	1.989E-04	1.090E-05
1.00E-04	1393.09	1377.81	9.890E-05	1.097E-05
5.00E-05	563.87	551	4.886E-05	1.141E-05
2.00E-05	350.47	335.04	1.912E-05	8.805E-06
4.00E-06	2722.28	2460.25	3.615E-06	3.850E-06
2.00E-06	1520.85	1320.43	1.736E-06	2.636E-06
1.00E-06	1026.32	878.49	8.560E-07	1.440E-06
8.00E-07	2151.25	1858.66	6.912E-07	1.088E-06
5.00E-07	999.99	846.21	4.231E-07	7.689E-07
2.00E-07	574.4	490.28	1.707E-07	2.929E-07
1.00E-07	294.32	249.05	8.462E-08	1.538E-07
5.00E-08	154.85	134.19	4.333E-08	6.671E-08
2.00E-08	113.54	91.8	1.617E-08	3.829E-08
1.00E-08	76.63	65.75	8.580E-09	1.420E-08

Calcium-Nickel systems at pH 5 with 0.1 g/L goethite

At Equilibrium			Moles of Ca/g Gt		
[M of Ca]	[Ca] ppb	[Ca] M	1Ni:1Ca	1Ni:10Ca	1Ni:100Ca
2.00E-04	7525.50	1.881E-04	1.186E-04		
1.00E-04	3687.75	9.219E-05	7.806E-05		
5.00E-05	1806.80	4.517E-05	4.830E-05		
1.00E-05	378.83	9.471E-06	5.294E-06		
5.00E-06	183.20	4.580E-06	4.200E-06		
2.00E-03	75855.00	1.896E-03		1.036E-03	
1.00E-03	37312.50	9.328E-04		6.719E-04	
5.00E-04	18852.00	4.713E-04		2.870E-04	
1.00E-04	3770.25	9.426E-05		5.744E-05	
5.00E-05	1888.00	4.720E-05		2.800E-05	
2.00E-02	787800.00	1.970E-02			3.050E-03
1.00E-02	391050.00	9.776E-03			2.238E-03
5.00E-03	192800.00	4.820E-03			1.800E-03
1.00E-03	37650.00	9.413E-04			5.875E-04
5.00E-04	18880.00	4.720E-04			2.800E-04

Initial Concentrations		At Equilibrium				
[M of Ni]	Total CPM	Filtered CPM	[Ni]eqlbm	1Ni:1Ca	1Ni:10Ca	1Ni:100Ca
2.00E-04	3107.35	3104.91	1.998E-04	1.570E-06		
1.00E-04	1611.56	1609.06	9.984E-05	1.551E-06		
5.00E-05	875.75	873.42	4.987E-05	1.330E-06		
1.00E-05	150.16	149.21	9.937E-06	6.327E-07		
5.00E-06	3882.36	3852.29	4.961E-06	3.873E-07		
2.00E-04	3107.35	3104.78	1.998E-04		1.654E-06	
1.00E-04	1611.56	1608.94	9.984E-05		1.626E-06	
5.00E-05	875.75	873.5	4.987E-05		1.285E-06	
1.00E-05	150.16	149.27	9.941E-06		5.927E-07	
5.00E-06	3882.36	3853	4.962E-06		3.781E-07	
2.00E-04	3107.35	3105.36	1.999E-04			1.281E-06
1.00E-04	1611.56	1609.52	9.987E-05			1.266E-06
5.00E-05	875.75	873.61	4.988E-05			1.222E-06
1.00E-05	150.16	149.25	9.939E-06			6.060E-07
5.00E-06	3882.36	3853	4.962E-06			3.781E-07

Calcium-Nickel Systems at pH 6

Initial	At Equilibrium			Moles of Ca/g Gt	
[M of Ca]	[Ca] ppb	[Ca] M	1Ni:1Ca	1Ni:10Ca	1Ni:100Ca
2.00E-04	7369.50	1.842E-04	1.576E-04		
1.00E-04	3642.75	9.107E-05	8.931E-05		
5.00E-05	1836.00	4.590E-05	4.100E-05		
1.00E-05	360.00	9.000E-06	1.000E-05		
5.00E-06	186.00	4.650E-06	3.500E-06		
2.00E-03	75780.00	1.895E-03		1.055E-03	
1.00E-03	37305.00	9.326E-04		6.738E-04	
5.00E-04	18480.00	4.620E-04		3.800E-04	
1.00E-04	3682.50	9.206E-05		7.938E-05	
5.00E-05	1836.00	4.590E-05		4.100E-05	
2.00E-02	787500.00	1.969E-02			3.125E-03
1.00E-02	389250.00	9.731E-03			2.688E-03
5.00E-03	192400.00	4.810E-03			1.900E-03
1.00E-03	37125.00	9.281E-04			7.188E-04
5.00E-04	18400.00	4.600E-04			4.000E-04

Initial Concentrations		At Equilibrium				
[M of Ni]	Total CPM	Filtered CPM	[Ni]eqlbm	1Ni:1Ca	1Ni:10Ca	1Ni:100Ca
2.00E-04	3108.32	3100.38	1.995E-04	5.109E-06		
1.00E-04	1610.15	1601.94	9.949E-05	5.099E-06		
5.00E-05	870.87	863	4.955E-05	4.518E-06		
1.00E-05	153.33	149.97	9.781E-06	2.191E-06		
5.00E-06	3890.65	3775.23	4.852E-06	1.483E-06		
2.00E-04	3108.32	3100.24	1.995E-04		5.199E-06	
1.00E-04	1610.15	1602.23	9.951E-05		4.919E-06	
5.00E-05	870.87	862.79	4.954E-05		4.639E-06	
1.00E-05	153.33	150.09	9.789E-06		2.113E-06	
5.00E-06	3890.65	3776	4.853E-06		1.473E-06	
2.00E-04	3108.32	3101.49	1.996E-04			4.395E-06
1.00E-04	1610.15	1603.25	9.957E-05			4.285E-06
5.00E-05	870.87	863.94	4.960E-05			3.979E-06
1.00E-05	153.33	150.16	9.793E-06			2.067E-06
5.00E-06	3890.65	3775.59	4.852E-06			1.479E-06

Calcium-Nickel Systems at pH 7

At Equilibrium			Moles of Ca/g Gt		
[M of Ca]	[Ca] ppb	[Ca] M	1Ni:1Ca	1Ni:10Ca	1Ni:100Ca
2.00E-04	7170.00	1.793E-04	2.075E-04		
1.00E-04	3525.00	8.813E-05	1.188E-04		
5.00E-05	1788.00	4.470E-05	5.300E-05		
1.00E-05	363.20	9.080E-06	9.200E-06		
5.00E-06	176.40	4.410E-06	5.900E-06		
2.00E-03	73200.00	1.830E-03		1.700E-03	
1.00E-03	36075.00	9.019E-04		9.813E-04	
5.00E-04	18160.00	4.540E-04		4.600E-04	
1.00E-04	3615.00	9.038E-05		9.625E-05	
5.00E-05	1800.00	4.500E-05		5.000E-05	
2.00E-02	784500.00	1.961E-02			3.875E-03
1.00E-02	387750.00	9.694E-03			3.063E-03
5.00E-03	191200.00	4.780E-03			2.200E-03
1.00E-03	36000.00	9.000E-04			1.000E-03
5.00E-04	18400.00	4.600E-04			4.000E-04

Initial Concentrations		At Equilibrium				
[M of Ni]	Total CPM	Filtered CPM	[Ni]eqlbm	1Ni:1Ca	1Ni:10Ca	1Ni:100Ca
2.00E-04	3108.32	3093.66	1.991E-04	9.433E-06		
1.00E-04	1610.15	1594.78	9.905E-05	9.546E-06		
5.00E-05	870.87	857.51	4.923E-05	7.670E-06		
1.00E-05	153.33	147.44	9.616E-06	3.841E-06		
5.00E-06	3865.11	3684.12	4.766E-06	2.341E-06		
2.00E-04	3108.32	3094	1.991E-04		9.214E-06	
1.00E-04	1610.15	1595.24	9.907E-05		9.260E-06	
5.00E-05	870.87	857.99	4.926E-05		7.395E-06	
1.00E-05	153.33	147.57	9.624E-06		3.757E-06	
5.00E-06	3865.11	3682.85	4.764E-06		2.358E-06	
2.00E-04	3108.32	3096.12	1.992E-04			7.850E-06
1.00E-04	1610.15	1597.75	9.923E-05			7.701E-06
5.00E-05	870.87	858.48	4.929E-05			7.114E-06
1.00E-05	153.33	147.51	9.620E-06			3.796E-06
5.00E-06	3865.11	3687.02	4.770E-06			2.304E-06

Calcium-Zinc systems at pH 5

Initial	At Equilibrium			Moles of Ca/g Gt	
[M of Ca]	[Ca] ppb	[Ca] M	1Zn:1Ca	1Zn:10Ca	1Zn:100Ca
2.00E-04	7320.000	1.830E-04	1.700E-04		
1.00E-04	3682.500	9.206E-05	7.938E-05		
5.00E-05	1908.000	4.770E-05	2.300E-05		
1.00E-05	369.000	9.225E-06	7.750E-06		
5.00E-06	187.200	4.680E-06	3.200E-06		
2.00E-03	75600.000	1.890E-03		1.100E-03	
1.00E-03	37500.000	9.375E-04		6.250E-04	
5.00E-04	18680.000	4.670E-04		3.300E-04	
1.00E-04	3682.500	9.206E-05		7.938E-05	
5.00E-05	1856.000	4.640E-05		3.600E-05	
2.00E-02	789000.000	1.973E-02			2.750E-03
1.00E-02	390750.000	9.769E-03			2.313E-03
5.00E-03	192800.000	4.820E-03			1.800E-03
1.00E-03	37500.000	9.375E-04			6.250E-04
5.00E-04	18480.000	4.620E-04			3.800E-04

Initial Concentrations		At Equilibrium				
[M of Zn]	Total CPM	Filtered CPM	[Zn]eqlbm	1Zn:1Ca	1Zn:10Ca	1Zn:100Ca
2.00E-04	1740.15	1734.05	1.993E-04	7.011E-06		
1.00E-04	902.74	896.71	9.933E-05	6.680E-06		
5.00E-05	440.37	435.25	4.942E-05	5.813E-06		
1.00E-05	150.16	146.18	9.735E-06	2.651E-06		
5.00E-06	2725.33	2631.97	4.829E-06	1.713E-06		
2.00E-04	1740.15	1734.33	1.993E-04		6.689E-06	
1.00E-04	902.74	897.04	9.937E-05		6.314E-06	
5.00E-05	440.37	435.28	4.942E-05		5.779E-06	
1.00E-05	150.16	146.04	9.726E-06		2.744E-06	
5.00E-06	2725.33	2634.09	4.833E-06		1.674E-06	
2.00E-04	1740.15	1734.81	1.994E-04			6.137E-06
1.00E-04	902.74	897.3	9.940E-05			6.026E-06
5.00E-05	440.37	435.29	4.942E-05			5.768E-06
1.00E-05	150.16	145.71	9.704E-06			2.964E-06
5.00E-06	2725.33	2628.74	4.823E-06			1.772E-06

Calcium-Zinc systems at pH 6

Initial	At Equilibrium			Moles of Ca/g Gt	
[M of Ca]	[Ca] ppb	[Ca] M	1Zn:1Ca	1Zn:10Ca	1Zn:100Ca
2.00E-04	7350.000	1.838E-04	1.625E-04		
1.00E-04	3607.500	9.019E-05	9.813E-05		
5.00E-05	1864.000	4.660E-05	3.400E-05		
1.00E-05	373.600	9.340E-06	6.600E-06		
5.00E-06	184.400	4.610E-06	3.900E-06		
2.00E-03	75900.000	1.898E-03		1.025E-03	
1.00E-03	37875.000	9.469E-04		5.313E-04	
5.00E-04	18920.000	4.730E-04		2.700E-04	
1.00E-04	3615.000	9.038E-05		9.625E-05	
5.00E-05	1872.000	4.680E-05		3.200E-05	
2.00E-02	787500.000	1.969E-02			3.125E-03
1.00E-02	390000.000	9.750E-03			2.500E-03
5.00E-03	192400.000	4.810E-03			1.900E-03
1.00E-03	36450.000	9.113E-04			8.875E-04
5.00E-04	18200.000	4.550E-04			4.500E-04

Initial Concentrations		At Equilibrium				
[M of Zn]	Total CPM	Filtered CPM	[Zn]eqlbm	1Zn:1Ca	1Zn:10Ca	1Zn:100Ca
2.00E-04	1756.42	1748.08	1.991E-04	9.497E-06		
1.00E-04	912.79	904.17	9.906E-05	9.444E-06		
5.00E-05	450.03	442.88	4.921E-05	7.944E-06		
1.00E-05	138.17	133.25	9.644E-06	3.561E-06		
5.00E-06	2713.5	2581.38	4.757E-06	2.434E-06		
2.00E-04	1756.42	1748.2	1.991E-04		9.360E-06	
1.00E-04	912.79	904.45	9.909E-05		9.137E-06	
5.00E-05	450.03	443.08	4.923E-05		7.722E-06	
1.00E-05	138.17	132.84	9.614E-06		3.858E-06	
5.00E-06	2713.5	2575.22	4.745E-06		2.548E-06	
2.00E-04	1756.42	1749.42	1.992E-04			7.971E-06
1.00E-04	912.79	905.83	9.924E-05			7.625E-06
5.00E-05	450.03	443.28	4.925E-05			7.500E-06
1.00E-05	138.17	132.91	9.619E-06			3.807E-06
5.00E-06	2713.5	2588.72	4.770E-06			2.299E-06

Calcium-Zinc systems at pH 7

Initial	At Equilibrium		Moles of Ca/g Gt		
[M of Ca]	[Ca] ppb	[Ca] M	1Zn:1Ca	1Zn:10Ca	1Zn:100Ca
2.00E-04	7110.00	1.778E-04	2.225E-04		
1.00E-04	3555.00	8.888E-05	1.113E-04		
5.00E-05	1800.00	4.500E-05	5.000E-05		
1.00E-05	352.80	8.820E-06	1.180E-05		
5.00E-06	178.00	4.450E-06	5.500E-06		
2.00E-03	74400.00	1.860E-03		1.400E-03	
1.00E-03	36525.00	9.131E-04		8.688E-04	
5.00E-04	18400.00	4.600E-04		4.000E-04	
1.00E-04	3637.50	9.094E-05		9.063E-05	
5.00E-05	1816.00	4.540E-05		4.600E-05	
2.00E-02	786000.00	1.965E-02			3.500E-03
1.00E-02	387750.00	9.694E-03			3.063E-03
5.00E-03	190800.00	4.770E-03			2.300E-03
1.00E-03	37050.00	9.263E-04			7.375E-04
5.00E-04	18480.00	4.620E-04			3.800E-04

Initial Concentrations		At Equilibrium				
[M of Zn]	Total CPM	Filtered CPM	[Zn]eqlbm	1Zn:1Ca	1Zn:10Ca	1Zn:100Ca
2.00E-04	1708.54	1692.56	1.981E-04	1.871E-05		
1.00E-04	892.11	875.43	9.813E-05	1.870E-05		
5.00E-05	450.95	437.5	4.851E-05	1.491E-05		
1.00E-05	132.39	121.69	9.192E-06	8.082E-06		
5.00E-06	2702.28	2436.55	4.508E-06	4.917E-06		
2.00E-04	1708.54	1693.11	1.982E-04		1.806E-05	
1.00E-04	892.11	876.85	9.829E-05		1.711E-05	
5.00E-05	450.95	437.5	4.851E-05		1.491E-05	
1.00E-05	132.39	123.25	9.310E-06		6.904E-06	
5.00E-06	2702.28	2441.74	4.518E-06		4.821E-06	
2.00E-04	1708.54	1695.02	1.984E-04			1.583E-05
1.00E-04	892.11	878.21	9.844E-05			1.558E-05
5.00E-05	450.95	438.11	4.858E-05			1.424E-05
1.00E-05	132.39	122.09	9.222E-06			7.780E-06
5.00E-06	2702.28	2436.99	4.509E-06			4.909E-06

REFERENCES CITED

(1989) ATSDR-Public Health Statement, Cadmium.

(1989) ATSDR-Public Health Statement, Nickel.

(1989) ATSDR-Public Health Statement, Zinc.

(1996) National Emissions Standard for Hazardous Air Pollutants (NESHAPS), Radionuclides, Subpart I Recission Update, Office of Radiation and Indoor Air, U.S. EPA.

(1997) "Sample Analyses Report." Institute of Gas Technology, IL.

(1997) ATSDR/U.S. EPA Priority List of Top 20 Hazardous Substances for 1997, CERCLA Section 104 (i).

(1997) CERCLA Priority List of Hazardous Substances, Section 104 (i).

(1997) Section 112(b) List of Hazardous Air Pollutants, Division of Air Pollution, U.S. EPA.

(1999) Persistent, Bioaccumulative, and Toxic (PBT) Chemicals Initiative, Office of Pollution Prevention and Toxics, U.S. EPA.

Allison, J. D., Brown D. S., Novo-Gradac, K. J. (1991) MINTEQA2/PRODEFA2, A Geochemical Assessment Model for Environmental Systems, Center for Exposure Assessment Modeling, U.S. EPA.

Anderson, M. A., Ferguson, J. F., Gavis, J., (1976) *J. Colloid Interface Sci.* **54,** 391.

Anderson, M. A., Malotky D. T., (1979) 72, *J. Colloid Interface Sci.* **72,** 413.

Anderson, P, Benjamin, M. M., (1990) "Surface and Bulk Characteristics of Binary Oxide Suspensions" *Am. Chem. Soc.* **24**(5), 692.

Anderson, P. R., and Benjamin, M.M. (1985) "Effects of Silicon on the Crystallization and Adsorption Properties of Ferric Oxides" *Environ. Sci. Technol.* **19**, 1048.

Angove, M. J., Johnson, B. B., Wells, J. D., (1998) "The Influence of Temperature on the Adsorption of Cadmium(II) and Cobalt(II) on Kaolinite" *J. Colloid Interface Sci.* **204**, 93.

Ankomah, A.B. (1992) "Magnesium and pH Effect on Zinc Sorption by Goethite" *Soil Sci.* **154**(3) 26.

Apak, R., Atun, G., Güçlü, K., Tüten, E., Keskin, G., (1995) "Sorptive Removal of Cesium and Strontium-90 from Water by Unconventional Sorbents. I. Usage of Bauxite Wastes (Red Muds)" *J. Nucl. Sci. Technol.* **32**(10), 1008.

Apak, R., Güçlü, K., Turgut, M. H., (1998) "Modeling of Copper(II), Cadmium(II), and Lead(II) Adsorption on Red Mud" *J. Colloid Interface Sci.* **203**, 122.

ASTM C 699, Chemical Mass Spectrometric and Spectrochemical Analysis of, and Physical tests on, Beryllium Oxide Powder, Sections 105-113, Bulk and Real Densities, Porosity, and Pore size – Pore Volume Distribution Mercury – Penetration Porosimetry.

Atkinson, R.J., Posner, A.M., and Quirk, J.P. (1967) "Adsorption of Potential-Determining Ions at the Ferric Oxide-Aqueous Electrolyte Interface" *J. Phys. Chem.* **71**(3), 550.

Axe, L., Trivedi, P. (2001) "Sorption and Attenuation of Metal Contaminants to Iron Oxides, Amorphous versus Crystalline" in preparation for *J. Colloid Interface Sci.*

Axe, L., and Anderson, P. R. (1995) " Sr Diffusion and Reaction within Fe Oxides, Evaluation of the rate-limiting mechanism for sorption" *J. Colloid Interface Sci.* **175**, 157.

Axe, L., and Anderson, P. R., (1998), "Adsorption onto Oxides, The Role of Diffusion" Chapter 8 in Adsorption of Metals by Geomedia, Editor, Jenne, E., Academic Press, 193.

Axe, L., Anderson, P., (1995), "Sr Diffusion and Reaction within Fe Oxides, Evaluation of the Rate-Limiting Mechanism for Sorption" *J. Colloid Interface Sci.* **175**, 157.

Axe, L., Anderson, P., (1997), "Experimental and Theoretical Surface Diffusivities of Cd and Sr in hydrous Ferric Oxide" *J. Colloid Interface Sci.* **185**, 436.

Axe, L., Bunker, G. B., Anderson, P. R., Tyson, T., (1998) "An XAFS Analysis of Strontium at the Hydrous Ferric Oxide Surface" *J. Colloid Interface Sci.* **199**, 44.

Axe. L., Tyson, T., Trivedi, P., Morrison, T., (2000) "Local Structure Analysis of Strontium Sorption to Hydrous Manganese Oxide" *J. Colloid Interface Sci.* **224**, 408.

Balistrieri, L. S. and Murray, J. W. (1982) " The Adsorption of Cu, Pb, Zn, and Cd on Goethite from Major Ion Seawater" Geochim. *Cosmochim. Acta* **46**, 1253.

Baltpurvins, K. A., Burns, R. C., Lawrance, G. A., Stuart, A. D., (1996) "Effect of pH and Anion type on the Aging of Freshly Precipitated Iron(III) Hydroxide Sludges" *Environ. Sci. Technol.* **30**(3), 939.

Bargar, J. R., Brown Jr., G. E., Parks, G. A., (1997) "Surface Complexation of Pb(II) at Oxide-Water Interfaces, I. XAFS and Bond-Valence Determination of Mononuclear and Polynuclear Pb(II) Sorption Products on Aluminum Oxides" *Geochim. Cosmochim. Acta* **61**, 2617.

Bargar, J. R., Brown Jr., G. E., Parks, G. A., (1997) "Surface Complexation of Pb(II) at Oxide-Water Interfaces, II. XAFS and Bond-Valence Determination of Mononuclear Pb(II) Sorption Products and Surface Functional Group on Iron Oxides" *Geochim. Cosmochim. Acta* **61**, 2639.

Bargar, J. R., Brown Jr., G. E., Parks, G. A., (1998) "Surface Complexation of Pb(II) at Oxide-Water Interfaces, III. XAFS Determination of Pb(II) and Pb(II)-Chloro Adsorption Complexes on Goethite and Alumina" *Geochim. Cosmochim. Acta* **62**, 193.

Bargar, J. R., Persson, P., Brown, G. E. Jr., (1999) "Outer-sphere Adsorption of Pb(II)EDTA on Goethite" *Geochim. Cosmochim. Acta* **63**, 2957.

Barrow, N. J., Gerth, J Brümmer, G. W., (1989) "Reaction Kinetics of the Adsorption and Desorption of Ni, Zn, and Cd by Goethite, II Modeling the Extent and the Rate of Reaction" *J. Soil Sci.* **40**, 437.

Barrow, N.J., Bowden, J.W., Posner, A.M., and Quirk, J.P. (1981) "Describing the Adsorption of Copper, Zinc and Lead on a Variable Charge Mineral Surface" *Aust. J. Soil Res.* **19**, 309.

Benjamin, M, M., and Leckie, J. O. (1981) " Competitive Adsorption of Cd, Cu, Zn, and Pb on Amorphous Iron Oxyhydroxide" *J. Colloid Interface Sci.* **83**(2), 410.

Benjamin, M, M., and Leckie, J. O. (1981) " Multiple-Site Adsorption of Cd, Cu, Zn, and Pb on Amorphous Iron Oxyhydroxide" *J. Colloid Interface Sci.* **79**(1), 209.

Benyahya, L., Garnier, J., "Effect of Salicylic Acid Upon Trace-Metal Sorption (Cd^{II}, Zn^{II}, Co^{II}, and Mn^{II}) onto Alumina, Silica, and Kaolinite as a Function of pH" (1999) *Environ. Sci. Technol.* **33**, 1398.

Bolan, N. S., Naidu, R., Khan, M. A. R., Tillman. R. W., Syers, J. K., (1999) "The Effects of Anion Sorption on Sorption and Leaching of Cadmium" *Aust. J. Soil Res,* **37**, 445.

Borah, D.K. Banerjee, N. K., and R.K. Rattan, (1989) "Studies on Adsorption of Zinc by Soils" *J. Indian Soil Sci.* **38**, 27-33.

Bottero, J. Y., Arnaud, M., Michot, L. J., de Donato, P., François, M., (1993) "Surface and Textural Heterogeneity of Fresh Hydrous Ferric Oxides in Water and in the Dry States" *J. Colloid Interface Sci.* **159**, 45.

Boudart, M., (1968) "Kinetics of Chemical Processes" Prentice-Hall.

Brown, G. E. Jr., (1990) "Spectroscopic Studies of Chemisorption Reaction Mechanisms at Oxide/Water Interfaces" *in* "Mineral-Water Interface Geochemistry" (Eds. Hochella, M. F., White, A. F.), Mineralogical Society of America, **23**, 337.

Bunker, B., Sayers, D., (1988) "*X-ray Absorption, Principles, Applications, Techniques of EXAFS, SEXAFS, and XAFS*" (Koningsberger, D. C., Prins, R., Eds.) Wiley, NY.

Bunker, G., (1999) http,//gbxafs.iit.edu/trainingtutorials.html

Carroll, S. A., O'Day, P. A., Piechowski, M., (1998) "Rock-Water Interactions Controlling Zinc, Cadmium, and Lead Concentrations in Surface Waters and Sediments, U.S. Tri-State Mining District. 2. Geochemical Interpretation" *Environ. Sci.Tech.* **32,** 956.

Černík, M., Borkovec, M., "Affinity Distribution Description of Competitive Ion Binding to Heterogeneous Materials" *Langmuir* **12**, 6127.

Charlet, L., Manceau, A. A., (1992) "X-ray Absorption Spectroscopic Study of the Sorption of Cr(III) at the Oxide-Water Interface" *J. Colloid Interface Sci.* **148**, 443.

Charlet, L., Manceau, A. A., (1992) "X-Ray Absorption Spectroscopic Study of the Sorption of Cr(III) at the Oxide-Water Interface II. Adsorption, Coprecipitation, and Surface Precipitation on Hydrous Ferric Oxide" *J. Colloid Interface Sci.* **148**(2), 443.

Cheah, S., Brown, G. E. Jr., Parks, G. A., (1998) "XAFS Spectroscopy Study of Cu(II) Sorption on Amorphous SiO_2 and γ-Al_2O_3, Effect of Substrate and Time on Sorption Complexes" *J. Colloid Interface Sci.* **208**, 110.

Chen, C., Papelis, C., Hayes, K. F., (1998), "Extended X-ray Absorption Fine Structure (EXAFS) Analysis of Aqueous Sr^{II} Ion Sorption at Clay-Water Interfaces" in "Adsorption of Metals by Geomedia" (E.A. Jenne, Ed.), Academic Press.

Chisholm-Brause, C. J., Hayes, K. F., Roe, A. L., Brown Jr., G. E., Parks, G. A., Leckie, J. O., (1990) "Spectroscopic Investigation of Pb(II) complexes at the γ-Al_2O_3/Water Interface" *Geochim. Cosmochim. Acta* **54**, 1897.

Christl. I., and Kretzschmar, R. (1999) "Competitive Sorption of Copper and Lead at the Oxide-Water Interface, Implications for Surface Site Density" Geochim. *Cosmochim. Acta* **63**, 2929.

Christophi, C., and Axe, L. (2000) "Competition of Cd, Cu, and Pb Adsorption on Goethite" *J. Environ. Eng.* 66.

Christophi, C.A. (1998) "Competition of Copper, Lead and Cadmium Adsorption to Goethite" Dept. of Chemical and Environmental Science, New Jersey Institute of Technology, Newark, NJ 07102.

Clark, J. F., Chamberlin, R. M., Strauss, S. H., (1999) "Design and Use of Redox-Recyclable Organometallic Extractants for the Cationic Radionuclides $^{137}Cs^{+}$ and $^{90}Sr^{2+}$ from Waste Solutions" *Environ. Sci. Tech.* **33,** 2489.

Collins, C. R., Sherman, D. M., Ragnarsdottir, K. V., (1999) "Surface Complexation of Hg^{2+} on Goethite, Mechanism from EXAFS Spectroscopy and Density Functional Calculations" *J. Colloid Interface Sci.* **219**, 345.

Combes, J. M., Manceau, A., Calas, G., (1990) *Geochim. Cosmochim. Acta* **54**, 1897.

Coughlin, B. R., Stone, A. T., (1995) "Nonreversible Adsorption of Divalent Metal Ions (Mn^{II}, Co^{II}, Ni^{II}, Cu^{II}, and Pb^{II}) onto Goethite, Effects of Acidification, Fe^{II} Addition, and Picolinic Acid Addition" *Environ. Sci. Technol.* **29**, 2445.

Cowan, C. E., Zachara, J. M., and Resch, C. T. (1991) "Cadmium Adsorption on Iron Oxides in the Presence of Alkaline-Earth Elements" *Environ. Sci. Technol.* **25**, 437.

Crank, J., (1975) "The Mathematics of Diffusion." 2^{nd}. Ed., Clarendon.

Crawford, R. J., Harding, I. H., Mainwaring, D. E., (1993) "Adsorption and Coprecipitation of Single Heavy Metal Ions onto the Hydrated Oxides of Iron and Chromium" *Langmuir* **9,** 3050.

Cunningham, R. E., Williams, R. J. J., (1980) "Diffusion in Gases and Porous Media" Plenum Press, New York.

Dalba, G., Fornasini, P., Rocca, F., (1993) "Cumulant Analysis of the Extended X-ray Absorption Fine Structure of β-AgI" *Phys. Rev. B* **47**, 8502.

Davis, A. P., and Upadhyaya, M. (1996) "Desorption of Cadmium from Goethite (α-FeOOH)" *Wat. Res.* **30**(8), 1894.

de Boer, J.H., (1968) "The Dynamical character of Adsorption" Clarendon Press, Oxford.

Delaney. J. S., Dyar, M. D., Sutton, S. R., Bajt, S., (1998) "Redox Ratio with Relevant Resolution, Solving an Old Problem by Using the Synchrotron MicroXANES Probe" *Geology*, **26**(2), 139.

Dyer, J. A. (1998) "The Competitive Sorption of Metals on Iron Oxides" *Marine Organic Chemistry*1.

Dzombak D. A., Morel F. M. M., (1986) "Sorption of Cadmium on Hydrous Ferric Oxide at High Sorbate/Sorbent Ratios, Equilibrium, Kinetics, and Modeling" *J. Colloid Interface Sci.* **112**, 588.

Dzombak, D. A. and Morel, F. M. M. (1990) "Surface Complexation Modeling Hydrous Ferric Oxide" John Wiley & Sons, New York.

Elzinga, E. J., Sparks, D. L., (1999) "Nickel Sorption Mechanisms in a Pyrophyllite – Montmorillonite Mixture" *J. Colloid Interface Sci.* **213,** 506.

Farley, K. J., Dzombak, D. A., Morel, F. M. M., (1985) "A Surface Precipitation Model for the Sorption of Cations on Metal Oxides" *J. Colloid Interface Sci.* **106**, 226.

Fendorf, S., Eick, M. J., Grossl, P., Sparks, D. L., (1997) "Arsenate and Chromate Retention Mechanisms on Goethite. 1. Surface Structure" *Environ. Sci. Technol.* **31**(2), 315.

Fendorf, S., Jardine, P. P., Patterson, R. R., Taylor, D. L., Brooks, S. C.,(1999) "Pyrolussite Surface Transformations Measured in Real-Time During the Reactive Transport of Co(II)EDTA2-" *Geochim. Cosmochim. Acta* **63**(19/20), 3049.

Fogler, H. S. (1992) "Elements of Chemical Reaction Engineering" 2nd Ed., Prentice-Hall, Englewood Cliffs, N. J.

Fokkink, L. G. J., de Keizer, A., Lyklemma, J., (1990) *J. Colloid Interface Sci.* **135**, 118.

Forbes E. A., Posner, A. M., and Quirk, J. P. (1976) "The Specific Adsorption of Divalent Cd, Co, Cu, Pb, and Zn on Goethite" *J. Soil Sci.* **27**, 154.

Ford, R. G., Scheinost, A. C., Scheckel, K. G., Sparks, D. L., (1999) "The Link between Clay Mineral Weathering and the Stabilization of Ni Surface Precipitates" *Environ. Sci. Technol.* **33**, 3140.

Ford, R. G., Sparks, D. L., (2000) "The Nature of Zn Precipitates Formed in the Presence of Pyrophyllite" *Environ. Sci. Technol.* **34**, 2479.

Forstner U., (1994) "Metal Speciation and Contamination of Soil", Lewis Publishers.

Foster, A. L., Brown Jr., G. E., Parks, G. A., (1998) "X-ray Absorption Fine-Structure Spectroscopy Study of Photocatalyzed, Heterogeneous As(III) Oxidation on Kaolin and Anatase" *Environ. Sci. Tech.* **32,** 1444.

Foster, A. L., Brown Jr., G. E., Tingle, T. N., Parks, G. A., (1998) "Quantitative Arsenic Speciation in Mine Tailings Using X-ray Absorption Spectroscopy" *Am. Mineral.* **83**, 553.

Friedl, G., Wehrli, B., Manceau, A., (1997) "Solid Phases in the Cycling of Manganese in Eutrophic Lakes, New Insights from EXAFS Spectroscopy" *Geochim. Cosmochim. Acta* **61**, 275.

Fritsch, S., Post, J. E., Navrotsky, (1997) "Energetics of Low-Temperature Polymorphs of Manganese Dioxide and Oxyhydroxide" *Geochim. Cosmochim. Acta* **61**, 2613.

Froment, G. F., Bischoff, K. B., (1990) "Chemical Reactor Analysis and Design." Wiley Interscience.

Fuller, C.C., Davis, J. A., Waychunas, G. A., (1993) "Surface Chemistry of Ferrihydrite, Part 2. Kinetics of Arsenated Adsorption and Coprecipitation" *Geochim. Cosmochim. Acta* **57**, 2271.

Gadde, R. R., Laitinen, H. A., (1973) "Study of the Sorption of Lead by Hydrous Ferric Oxide" *Env. Lett.* **5** (4), 223.

Gadde, R. R., Laitinen, H. A., (1974) "Studies of Heavy Metal Adsorption by Hydrous Iron and Manganese Oxides" *Analytical Chemistry* **46**(13), 2022.

Gang, P., Liss, P. S., (1998) "Metastable-Equilibrium Adsorption Theory. 2. Experimental" *J. Colloid Interface Sci.* **201**, 77.

Ghose, S., (1963), "The Crystal Structure of Hydrozincite, $Zn_5(OH)_6(CO_3)_2$" *Acta Cryst.* **17**, 1051.

Goldberg, Sabine; Forster, H. S.; Godfrey, C. L. (1996) "Molybdenum Adsorption on Oxides Clay, Minerals, and Soils" *Soil Sci. Soc. Am. J.* **60**(2), 425.

Golden, D. C., Turner, F. T., Sittertz-Bhatkar, H., Dixon, J. B., (1997) "Seasonally Precipitated Iron Oxides in a Vertisol of Southeast Texas" *Soil Sci. Soc. Am. J.* **61**, 958.

Gray, M. J., (1981) "Manganese Dioxide as an Adsorbent for Heavy Metals" *Effluent and Water Treatment Journal* **21**, 201.

Gray, M. J., Malati, M. A., (1979) "Adsorption from Aqueous Solution by δ-Manganese Dioxide. II. Adsorption of Some Heavy Metal Cations" *J. Chem. Technol. Biotechnol.***29**(3), 135.

Greenberg, A.E., Trussell, R.R., Clesceri, L.S., Franson, M.H. (1995) "Standard Methods for the examination of water and wastewater" 19th edition, APHA, AWWA, WPCF, Washington D.C.

Green-Pedersen, H., Jensen, B.T., Pind, N., (1997) "Nickel Adsorption on MnO_2, $Fe(OH)_3$, Montmorillonite, Humic Acid, and Calcite, A Comparative Study" *Environ. Technol.* **18**, 807.

Gregg, S. J., Sing, K.S.W. (1982) "Adsorption, Surface Area and Porosity" 2nd edition, Academic Press Inc, Orlando, Florida.

Grossl, P. R., Sparks, D. L. (1995) "Evaluation of Contaminant Ion Adsorption/Desorption on Goethite Using Pressure-jump Relaxation Kinetics" *Geoderma* **67**(1-2), 87.

Grossl, P. R., Eick, M., Sparks, D. L., Ainsworth, C. C. (1997) "Arsenate and Chromate Retention Mechanisms on Goethite. 2. Kinetic Evaluation Using a Pressure–Jump Relaxation Technique" *Environ. Sci. Technol.* **31**, 321.

Grossl. P. R., Sparks, D. L., Ainsworth, C. C. (1994) "Rapid Kinetics of Cu(II) Adsorption/Desorption Kinetics on Goethite" *Environ. Sci. Technol.* **28**(8), 1422.

Gunneriusson, L. (1994) "Composition and Stability of Cd(II)-Chloro and –Hydroxo Complexes at the Goethite (α-FeOOH)/ Water Interface" *J. Colloid Interface Sci.* **163**, 484.

Hayes, K. F., Leckie, J. O. (1986) "Mechanism of Lead Ion Adsorption at the Goethite-Water Interface" in ACS Symposium Series 323(Geochemical Processes at Mineral Surfaces), 114.

Hesleitner, P., Babic, D., Kally, N., Matijevic E. (1987) "Adsorption at Solid/Solution Interfaces. 3. Surface Charge and Potential of Colloidal Hematite" *Langmuir* **3**, 815.

Hesterberg, D., (1998) "Biogeochemical Cycles and Processes Leading to Changes in Mobility of Chemicals in Soils" *Ecosyst. Environ.* **67**, 121.

Hesterberg, D., Sayers, D. E., Zhou, W., Plummer, G. M., Robarge, W. P., (1997) "X-ray Absorption Spectroscopy of Lead and Zinc Speciation in a Contaminated Groundwater Aquifer" *Environ. Sci. Technol.* **31**(10), 2840.

Hilton, J., Nolan, L., Jarvis, K. E., (1997) "Concentrations of Stable Isotopes of Cesium and Strontium in Freshwaters in Northern England and their Effect on Estimates of Sorption Coefficients (K_d)"*Geochim. Cosmochim. Acta* **61**, 1115.

Hsu, P. H., (1989) "Aluminum Hydroxides and Oxyhydroxides" *in* "Minerals in Soil Environment" (J. B. Dixon, S. B. Weed, Eds.), Soil Society of America Book Series No. 1, SSSA, Madison, WI.

Huang, C., Cheng, W. P., (1997) "Thermodynamic Parameters of Iron-Cyanide Adsorption onto γ-Al_2O_3" *J. Colloid Interface Sci.* **188**, 270.

IGT (1997) Institute of Gas Technology, Sample Analyses Report, IL.

Israelachvilli, J., (1997)"Intermolecular & Surface Forces" Academic Press, 2nd Ed.

Jackson, R. E., Inch, K. J., (1989) "The *In-situ* Adsorption of 90Sr in a Sand Aquifer at the Chalk River Nuclear Laboratories" *J. Contaminant Hydrol.* **4**, 27.

Jain, J. S., and Snoeyink, V. L. (1973) "Adsorption from Bisolute Systems on Active Carbon" *J. Water Pollution Control Federation*, **45**, 2463.

Jenkins, R., and Snyder, R.L. (1996) "Introduction to X-ray Powder Diffractometry" John Wiley & Sons Inc, NY.

Jenne, E. A., (1968) "Controls on Mn, Fe, Co, Ni, Cu, and Zn Concentrations in Soils and Water, the Significant Role of Hydrous Mn and Fe Oxides" *in* "Trace Inorganics in Water" (R. F. Gould, Ed.), ACS Advances in Chemistry, Am. Chem. Soc., Washington, **73**, 337.

Jenne, E. A., (1998) *in* "Adsorption of Metals by Geomedia" (E. A. Jenne, Ed.), Academic Press.

Johnson, B., (1990) "Effect of pH, Temperature, and Concentration on the Adsorption of Cadmium on Goethite" *Environ. Sci. Technol.* **24**, 112.

Kanungo, S. B., (1994) "Adsorption of Cations on Hydrous Oxides of Iron. I. Interfacial Behavior of Amorphous FeOOH and β-FeOOH (Akagenite) in Different Electrolyte Solutions" *J. Colloid Interface Sci.* **162**, 103.

Kanungo, S. B., (1994) "Adsorption of Cations on Hydrous Oxides of Iron. II. Adsorption of Mn, Co, Ni, and Zn onto Amorphous FeOOH from Simple Electrolyte Solutions as Well as from a Complex Electrolyte Solution Resembling Seawater in Major Ion Content" *J. Colloid Interface Sci.* **162**, 86.

Kanungo, S. B., (1994) "Adsorption of Cations on Hydrous Oxides of Iron. III. Adsorption of Mn, Co, Ni, and Zn on β-FeOOH from Simple Electrolyte Solutions as Well as from a Complex Electrolyte Solution Resembling Seawater in Major Ion Content" *J. Colloid Interface Sci.* **162**, 93.

Kärger, J., Ruthven, D. M., (1992) "Diffusion in Zeolites and Other Microporous Solids" John Wiley & Sons.

Kinniburgh, D. G., Jackson, M. L., Syers, J. K., (1976) "Adsorption of Alkaline Earth, Transition, and Heavy Metal Cations by Hydrous Oxide Gels of Iron and Aluminum" *Soil Sci. Soc. Am. J.* **40**, 796.

Koretsky, C. M., Sverjensky, D. A., Sahai, N., (1998) "A Model of Surface Site Types on Oxide and Silicate Minerals Based on Crystal Chemistry, Implications for Site Types and Densities, Multi-Site Adsorption, Surface Infrared Spectroscopy, and Dissolution Kinetics" *Sci. Am. J.* **298**, 349.

Kraepiel, A. M. L., Keller, K., Morel, F. M. M., (1999) "A Model for Metal Adsorption on Montmorillonite" *J. Colloid Interface Sci.* **210**, 44.

Ku, H. H., (1966) "Notes on the Use of Propagation of Error Formulas" *Journal of Research of the National Bureau of Standards – C. Engineering and Instrumentation*, **70**C(4), 263.

Lead, J. R., Hamilton-Taylor, J., Davison, W., Harper, M., (1999) "Trace Metal Sorption by Natural Particles and Coarse Colloids" *Geochim. Cosmochim. Acta* **63**, 1661.

Lee, P. A., Citrin, P. H., Eisenberger, P., Kincaid, B. M., (1981) "Extended X-ray Absorption Fine Structure – its Strengths and Limitations as a Structural Tool" *Rev. Mod. Phys.* **53**(4), 769.

Lee, S., Allen, H. E., Huang, C. P., Sparks, D. L., Sanders, P. F., Peijnenburg, W. J. G. M., (1996) "Predicting Soil-Water Partition Coefficients for Cadmium" *Environ. Sci.Tech.* **30**, 3418.

Lide D. R., and Frederikse, H. P. R. (1998) "CRC Handbook of Chemistry and Physics – A Ready Book of Chemical and Physical Data" 78th Edition, CRC Press, New York, NY.

Lin, Z., "Mineralogical and Chemical Characterization of Wastes From the Sulfuric Acid Industry in Falun, Sweden" *Environ. Geology* **30**(3/4), 152.

Lion, L. W., Altmann, R. S., Leckie, J. O., (1982) "Trace-Metal Adsorption Characteristics of Estuarine Particulate Matter, Evaluation of Contributions of Fe/Mn Oxide and Organic Surface Coatings" *Environ. Sci. Technol.* **16**, 660.

Lion, L. W., Nelson, Y. M., Shuler, M. L., Ghiorse, W. C., (1999) "Lead Binding to Metal Oxide and Organic Phases of Natural Aquatic Biofilms" *Limnol.Oceanography.*

Lo Shang-Lien, Jeng, H., and Lai, C. (1997), "Characteristics and Adsorption Properties of Iron-Coated Sand" *Wat. Sci. Technol.* **35**(7), 63.

Lo, K. S. L., Leckie, J. O., (1993) "Kinetic Studies of Cd and Zn onto Al_2O_3/Solution Interfaces" *Wat. Sci. Tech.* **28**, 39.

Lothenbach, B., Furrer, G., Schärli, H., Schulin, R., (1999) " Immobilization of Zinc and Cadmium by Montmorillonite Compounds, Effects of Aging and Subsequent Acidification" *Environ. Sci. Technol.* **33**, 2945.

Lumsdon, D. G. and Evans, L. J. (1994) "Surface Complexation Model Parameters for Goethite (α-FeOOH)" *J. Colloid Interface Sci.* **164**, 119.

Lützenkirchen, J., (1997) "Ionic Strength Effects on Cation Sorption to Oxides, Macroscopic Observations and Their Significance in Microscopic Interpretation" *J. Colloid Interface Sci.* **195**, 149.

Magini, M., Licheri, G., Paschina, G., Piccaluga, Pinna, G., *X-ray Diffraction of Ions in Aqueous Solutions, Hydration and Complex Formation*, CRC Press Inc., **1988**

Mahara, Y., (1993) "Heavy Metals in the Environment, Storage and Migration of Fallout Strontium-90 and Cesium-137 for Over 40 Years in the Surface Soil of Nagasaki" *J Environ. Qual.* **22**, 722.

Malati, M. A., (1987) "The Role of the Hydration of Cations in Their Adsorption on Oxides" *Surf. Coat. Technol.* **30**(3), 317.

Manceau, A., Boisset, M-C. Sarret, G., Hazemann, J-L., Michel, M., Cambier, P., Prost, R., (1996) "Direct Determination of Lead Speciation in Contaminated Soils" *Environ. Sci. Tech.* **31**, 2954.

Manceau, A., Charlet, L., (1992) "X-ray Absorption Spectroscopic Study of the Sorption of Cr(III) at the Oxide/Water Interface. I. Molecular Mechanism of Cr(III) Oxidation on Mn Oxides" *J. Colloid Interface Sci.* **148**, 425.

Manceau, A., Charlet, L., (1994) "The Mechanism of Selenate Adsorption on Goethite and Hydrous Ferric Oxide" *J. Colloid Interface Sci.* **168**, 87.

Manceau, A., Combes, J. M., (1988) "Structure of Mn and Fe Oxides and Oxyhydroxides, A Topological Approach by EXAFS" *Phys. Chem. Minerals* **15**, 283.

Manceau, A., Gorshkov, A. I., Drits, V. A. (1992) "Structural Chemistry of Mn, Fe, Co, and Ni in Manganese Hydrous Oxides, Part I. Information from XANES Spectroscopy" *Am. Mineral.* **77**,1133.

Manceau, A., Gorshkov, A. I., Drits, V. A. (1992) "Structural Chemistry of Mn, Fe, Co, and Ni in Manganese Hydrous Oxides, Part II. Information from EXAFS Spectroscopy and Electron and X-ray Diffraction" *Am. Mineral.* **77**,1144.

Manceau, A., Schlegel, M. L., Musso, M., Sole, V. A., Gauthier, C., Petit, P. E., Trolard, F., (2000) "Crystal Chemistry of Trace Elements in Natural and Synthetic Goethite" *Goechim. Cosmochim. Acta* **64** (21), 3643.

Manning, B. A., and Goldberg, S. (1996) "Modeling Competitive Adsorption of Arsenate with Phosphate and Molybdate on Oxide Minerals" *Soil Sci. Soc. Am. J.* **60**, 121.

Manning, B. A., Fendorf S. E., Goldberg, S., (1998) "Surface Structures and Stability of Arsenic(III) on Goethite, Spectroscopic Evidence for Inner-Sphere Complexes" *Environ. Sci.Tech.* **32**(16), 2383.

Manning, B. A., Goldberg, S., (1997) "Surface Structures and Stability of Arsenic(III) at the Clay-Mineral Interface" *Environ. Sci.Tech.* **31**, 2005.

Martinez, C. E., Mc Bride, M. B., (1999) "Solubility of Cd^{2+}, Cu^{2+}, Pb^{2+}, and Zn^{2+} in Aged Coprecipitates with amorphous Iron Hydroxides" *Environ. Sci. Technol.* **33**, 745.

McKenzie, R. M., (1989) "Manganese Oxides and Hydroxides" *in* "Minerals in Soil Environment" (J. B. Dixon, S. B. Weed, Eds.), Soil Society of America Book Series No. 1, SSSA, Madison, WI.

McBride, M. B. (1989) "Surface Chemistry of Soil Minerals" *Minerals in Soil Environments*, second edition, SSSA Book Series no.1 WI USA, Soil Science of America, 35.

McCarty, D. K., Moore, J. N., Marcus, W. A., (1998) "Mineralogy and Trace Element Association in an Acid Mine Drainage Iron Oxide Precipitate; Comparison of Selective Extractions" *Appl. Geochem.* **13**, 165.

McKenzie, R. M., (1980) "The Adsorption of Lead and Other Heavy Metals on Oxides of Manganese and Iron" *Aust. J. Soil. Res.* 18, 61.

Meima, J. A., Zomeren, A. V., Comans, R. N. J., (1999) "Complexation of Cu with Dissolved Organic Carbon in Municipal Solid Waste Incinerator Bottom Ash Leachates" *Environ. Sci.Tech.* **33**, 1424.

Meng, X., Letterman, R. D., (1993) "Effect of Component Oxide Interaction on the Adsorption Properties of Mixes Oxides" *Environ. Sci.Tech.* **27**, 970.

Mesuere, K., and Fish, W. (1992) "Chromate and Oxalate Adsorption on Goethite. 2. Surface Complexation Modeling of Competitive Adsorption" *Environ. Sci. Technol.* **26**(12), 2365.

Misak, N. Z., Ghonemy, G. H., Morcos, T. N., (1996) "Adsorption of Co^{2+} and Zn^{2+} Ions on Hydrous Fe(III), Sn(IV), and Fe(III)/Sn(IV) Oxides. II. Thermal Behavior of Loaded Oxides, Isotopic Exchange Equilibria, and Percentage Adsorption-pH Curves" *J. Colloid Interface Sci.* **106**, 226.

Mishra, S. P., Singh, V. K., Tiwary, D., (1997) "Inorganic Particulates in Removal of Toxic Heavy Metal Ions, Efficient Removal of Cadmium Ions from Aqueous Solutions by Hydrous Zirconium Oxide" *Radiochimica Acta* **76**, 97.

Mishra, S. P., Tiwary, D., (1995) "Inorganic Particulates in Removal of Toxic Heavy Metal Ions, Efficient Removal of Strontium Ions from Aqueous Solutions by Hydrous Manganese Oxide" *Radiochimica Acta* **69**, 121.

Mishra, S. P., Tiwary, D., (1998) "Inorganic Particulates in Removal of Toxic Heavy Metal Ions, Efficient Removal of Cadmium Ions from Aqueous Solutions by Hydrous Manganese Oxide" *Radiochimica Acta* **80**, 213.

Miyazaki, A., Matsuo, M., Tsurumi, M., (1996) "Surface Complex Formation Between Zn ions and Amorphous Aluminosilicate in Aquatic Systems" *J. Colloid Interface Sci.* **177**, 335.

Morel, F.M.M., and Hering, J.G. (1993) "Principles and Applications of Aquatic Chemistry" John Wiley & Sons, Inc.

Morgan, J., Stumm W., (1964) "Colloid Chemical Properties of Manganese Dioxide" *Journal of Colloid Science* **19**, 347.

Morgan, J., Stumm W., "Aquatic Chemistry, An Introduction Emphasizing Chemical Equilibria in Natural Waters" John Wiley Interscience Publishing.

Murray, J. W., (1974) "Surface Chemistry of Hydrous Manganese Dioxide" *J. Colloid Interface Sci.* **46**, 357.

Murray, K. S., Cauvet, D., Lybber, M., Thomas, J. C., (1999) "Particle Size and Chemical Control of Heavy Metals in Bed Sediment from the Rouge River, Southeast Michigan" *Environ. Sci.Tech.* **33**, 987.

Myneni, S. C. B., Tokunaga, T. K., Brown J., G. E., (1997) "Abiotic Selenium Redox Transformations in the Presence of Fe(II,III) Oxides" *Science* **278**, 1106.

Nelson, Y. M., Lion, L. W., Ghiorse, W. C., Shuler, M. L., (1999) "Production of Biogenic Mn Oxides by Leptothrix discophora SS-1 in a Chemically Defined Growth Medium and Evaluation of their Pb Adsorption Characteristics" *Appl. Environ. Microbiol.* **65**(1), 175.

Newville, M., (1995) http,//krazy.phys.washington.edu/papers/x8-feffit/node1.html

Nightingale, Jr., E. R., (1959) *J. Can. Phy. Chem.* **63**, 1381.

Nilsson, K., Jensen, B. S., Carlsen, L., (1985) "The Migration Chemistry of Strontium" *European Appl.Res.- Nucl. Sci. Technol.* 7(1), 149.

Nowack, B., and Sigg, L. (1996) "Adsorption of EDTA and Metal-EDTA Complexes onto Goethite" *J. Colloid Interface Sci.* **177**, 106.

Nowack, B., and Stone, A. T. (1999) "The Influence of Metal Ions on the Adsorption of Phosphonates onto Goethite" *Environ. Sci. Technol.* **33**, 3627.

Nowack, B., Lützenkirchen, J., Phillippe, B., and Sigg, L. (1996) "Modeling the Adsorption of Metal-EDTA Complexes onto Oxides" *Environ. Sci. Technol.* **30**, 2397.

Numako, C., Nakai, I., (1999)"XAFS Analysis of Coprecipitation of Zn by Sulfide Ions in an Acidic Solution" *Spectrochimica Acta:B* **54**, 133.

O'Day, P. A., Brown, G. E. Jr., Parks, G. A., (1994) "EXAFS Study of Aqueous Co(II) Sorption Complexes on Kaolinite" *J. Colloid Interface Sci.* **165**(2), 269.

O'Day, P. A., Brown, G. E. Jr., Parks, G. A., (1994) "Molecular Structure and Binding Sites of Co(II) Sorption Complexes on Kaolinite From X-ray Absorption Spectroscopy", *Clays Clay Miner.* **42**(3), 337.

O'Day, P. A., Carroll, S. A., Waychunas, G. A., (1998) "Rock-Water Interactions Controlling Zinc, Cadmium, and Lead Concentrations in Surface Waters and Sediments, U.S. Tri-State Mining District. 1. Molecular Identification Using X-ray Absorption Spectroscopy" *Environ. Sci. Tech.* **32**, 943.

O'Day, P. A., Chisholm-Brause, C. J., Towle, S. N., Parks, G. A., Brown, G. E. Jr., (1996) "X-ray Absorption Spectroscopy of Co(II) Sorption Complexes on Quartz (α-SiO_2) and Rutile(TiO_2)" *Geochim. Cosmochim. Acta* **60**(14), 2515.

Oakley, S. M., Nelson, P. O., Williamson, K.J., (1981) "Model of Trace-Metal Partitioning in Marine Sediments" *Environ. Sci. Tech.* **15**(4), 474.

Ohtsuka, Y., Takebe, S., (1990) "Migration Behavior of Radionuclides (^{60}Co, ^{85}Sr, and ^{137}Cs) in Aerated Sandy Soil Layer" *J. Nucl. Sci. Tech.* **27**, 62.

Okazaki, M., Takamidoh, K., Yamane, I., (1986) "Adsorption of Heavy Metal Cations on Hydrated Oxides and Oxides of Iron and Aluminum with Different Crystallinities" *Soil Sci. Plant Nutr.* **32**(4), 523.

Ostergren, J. D., Brown, G. E. Jr., Parks, G. A., Tingle, T. N., (1999) "Quantitative Speciation of Lead in Selected Mine Tailings from Leadville, CO" *Environ. Sci.Tech.* **33**, 1627.

Östhols, E., Manceau, A., Farges, F., Charlet, L., (1997) "Adsorption of Thorium on amorphous Silica, An EXAFS Study" *J. Colloid Interface Sci.* **194**, 10.

Palmqvist, U., Ahlberg, E., Lövgren, L., and Sjöberg S. (1997) "*In Situ* Voltammetric Determinations of Metal Ions in Goethite Suspensions, Single Metal Ion System" *J. Colloid Interface Sci.* **196**, 254.

Palmqvist, U., Ahlberg, E., Lövgren, L., and Sjöberg S. (1999) "Competitive Metal Ion Adsorption in Goethite Using *In Situ* Voltammetric Methods and Potentiometry" *J. Colloid Interface Sci.* **218**, 388.

Pan, G. and Liss, P.S. (1998) "Metastable-Equilibrium Theory II. Experimental" *J. Colloid Interface Sci.* **201**, 77.

Pandya, K. I., O'Grady, W. E., Corrigan, D. A., McBreen, J., Hoffman, R. W., (1990) "Extended X-Ray Absorption Fine Structure Investigation of Nickel Hydroxides" *J. Phys. Chem.* **94**, 21.

Pandya, K. I., Russell, A. E., McBreen, J., O'Grady, W. E., (1995) "XAFS Investigations of Zn(II) in Concentrated Aqueous Hydroxide Solutions" *J. Phys. Chem.* **99**, 11967.

Papelis, C., (1995) "X-ray Photoelectron Spectroscopic Studies of Cadmium and Selenite Adsorption on Aluminum Oxides" *Environ. Sci. Technol.* **29**, 1526.

Papelis, C., Brown, G. E. Jr., Parks, G. A., Leckie, J. O., (1995) "X-ray Absorption Spectroscopic Studies of Cadmium and Selenite Adsorption on Aluminum Oxides" *Langmuir* **11**(6), 2041.

Papelis, C., Roberts, P. V., Leckie, J. O., (1995) "Modeling the Rates of Cadmium and Selenite Adsorption on Micro- and Mesoporous Transition Aluminas" *Environ. Sci. Tech.* **29**, 1099.

Parkman, R. H., Charnock, J. M., Livens, F. R., Vaughan, D. J., (1998) "A Study of the Interaction of Strontium Ions in Aqueous Solution with the Surfaces of Calcite and Kaolinite" *Geochim. Cosmochim. Acta* **62**(9), 1481.

Parks G. A., De Bruyn. L., (1962), "The Zero Point of Charge of Oxides" *J. Phy. Chem.* **66**, 967.

PCPDFWIN Version 2.0, (1998) Powder Diffraction File, PDF# 29-713, International Centre for Diffraction Data, PA.

Pedersen-Green, H., Jensen, B. T., Pind, N., (1997) "Nickel Adsorption on MnO_2, $Fe(OH)_3$, Montmorillonite, Humic Acid and Calcite, A Comparative Study" *Environ. Technol.* **18**, 807.

Perry, R.H., Green, D.W., Maloney, J. O., (1984) Perry's Chemical Engineer's Handbook, McGraw Hill International Editions, 6th Ed.

Pertlik, F. (1985) "Structures of Hydrothermally Synthesized Cobalt(II) and Nickel(II) Carbonate" *Acta Crsytallogr.* **C42**, 4.

Peterson, M. L., Brown Jr., G. E., Parks, G. A., Stein, C. L., (1997) "Differential Redox and Sorption of Cr(III/IV) on Natural Silicate and Oxide Minerals, EXAFS and XANES Results" *Geochim. Cosmochim. Acta* **61**, 3399.

Pivarov, S. (1998) "Acid-Base Properties and Heavy and Alkaline Earth Metal Adsorption on the Oxide-Solution Interface, Non-Electrostatic Model" *J. Colloid Interface Sci.* **206**, 122.

Porta, P., Minelli, G., Botto, I. L., Baran, E. J., (1991) "Structural, Magnetic, and Optical Investigation of Ni_6MnO_8" *J. Solid State Chem.* **92**, 202.

Posselt, H. S., Weber, W. J. Jr. in (1974) "Removal of Cadmium from Waters and Wastes by Sorption on Hydrous Metal Oxides for Water Treatment" in "Symposium on the Chemistry of Water Supply, Treatment, and Distribution" Ann Arbor Science (Rubin, A. J. Ed.), 89.

Post, J. E., "Manganese oxide minerals, Crystal structures and Economic and Environmental Significance" *Proc. Natl. Acad. Sci. (USA)* **96**, 3447.

Post, J. E., Appleman, D. E., (1988) "Chalcophanite $ZnMn_3O_7 \cdot 3H_2O$, New crystal structure determinations" *Amer. Mineral.* **73**, 1401.

Potter, H. A. B., Yong, R. N., (1997) "Influence of Amorphous Oxides on the Fate of Heavy Metals" *Geoenviron. Eng., Ground Proc.* 141.

Radke, C. J., and Prausnitz, J. M. (1972) "Thermodynamics of Multi-Solute Adsorption from Dilute Liquid Solutions" *AIChE J.* **18**, 761.

Radovanovic, H., Koelmans, A. A., (1998) "Prediction of Trace Metal Distribution Coefficients (K_d) for Aerobic Sediments" *Environ. Sci. Technol.* **32**, 753.

Raven, K. P., Jain, A., Loeppert, R. H., (1998) "Arsenite and Arsenate Adsorption on Ferrihydrite, Kinetics, Equilibrium, and Adsorption Envelopes" *Environ. Sci.Tech.* **32**, 344.

Richens, D. A., (1997) "The Chemistry of Aqua Ions, Synthesis, Structure, and Reactivity. A Tour Through the Periodic Table of Elements" John Wiley & Sons, New York.

Roberts, D. R., Scheidegger, A. M., Sparks, D. L., (1999) "Kinetics of Mixed Ni-Al Formation on a Soil Clay Fraction" *Environ. Sci. Technol.* **33**, 3749.

Roberts, P. V., Cunningham, J. A., (1998) "Kinetics of Mixed Ni-Al Precipitate Formation on a Soil Clay Fraction" *Wat. Res.* **34**, 1415.

Rodda, D. P., Johnson, B. B., Wells, J. D., (1996) "Modeling the Effect of Temperature on Adsorption of Lead(II) and Zinc(II) onto Goethite at Constant pH" *J. Colloid Interface Sci.* **184**, 365.

Rodda, D. P., Johnson, B. B., Wells, J. D., (1996) "Modeling the Effect of Temperature on Adsorption of Lead(II) and Zinc(II) onto Goethite at Constant pH" *J. Colloid Interface Sci.* **168**(1), 87.

Rodda, D. P., Johnson, B.B., and Wells, J. D. (1993) "The Effect of Temperature and pH on Adsorption of Copper(II), Lead(II), and Zinc(II) onto Goethite" *J. Colloid Interface Sci.* **161**, 57.

Rose, A.W., and Bianchi-Mosquera, G.C. (1993) "Adsorption of Cu, Pb, Zn, Co, Ni, and Ag on Goethite and Hematite, A Control on Metal Mobilization from Red Beds into Stratiform Copper Deposits" *Economic Geology* **88**, 1226.

Rose, J., Manceau, A., Bottero, J., Masion, A., Garcia, F., (1996) "Nucleation and Growth Mechanisms of Fe Oxyhydroxide in the Presence of PO4 Ions. 1. Fe K-Edge EXAFS Study" *Langmuir* **12**, 6701.

Ross, S. M., (1994) "Retention, Transformation, and Mobility of Toxic Metals in Soils" *in* "Toxic Metals in Soil-Plant Systems" (S. M. Ross, Ed.), John Wiley & Sons Ltd., 63.

Ross, S. M., (1994) "Toxic Metals, Fate and Distribution in Contaminated Ecosystems" *in* "Toxic Metals in Soil-Plant Systems" (S. M. Ross, Ed.), John Wiley & Sons Ltd., 189.

Rubin, S. E., (1999) "Toxic Releases from Power Plants" *Environ. Sci. Tech.* **33**, 3062.

Sahai, N., Carroll, S. A., Roberts, S., O'Day, P. A., (2000) "X-ray Absorption Spectroscopy of Strontium(II) Coordination II. Sorption and Precipitation at Kaolinite, Amorphous Silica, and Goethite Surfaces" *J. Colloid Interface Sci.* **222**, 198.

Sayers, D. E., Bunker, B. A., (1988) "Data Analysis (EXAFS)" *Chem. Anal. (N.Y.)* **92**, 211.

Scheidegger, A. M., Lamble, G. M., Sparks, D. L., (1996) "Investigation of Ni Sorption on Pyrophyllite, An XAFS Study" *Environ. Sci. Technol.* **30**(2), 548.

Scheidegger, A. M., Strawn, D. G., Lamble, G. M., Sparks, D. L., (1998) "The Kinetics of mixed Ni-Al Hydroxide Formation on Clay and Aluminum Oxide Minerals, A Time-Resolved Study" *Geochim. Cosmochim. Acta* **62**(13), 2233.

Scheinost, A. C., Abend, S., Pandya, K. I., Sparks, D. L., (2001) "Kinetic Controls on Cu and Pb Sorption by Ferrihydrite" *Environ. Sci. Technol.***35**(6), 1090.

Scheinost, A. C., Ford, R. G., Sparks, D. L., (1999) "The Role of Al in the Formation of Secondary Ni Precipitates on Pyrophyllite, Gibbsite, Talc, and Amorphous Silica, A DRS Study" *Geochim. Cosmochim. Acta* **63**(19/20), 3193.

Schlegel, M. L., Charlet, L., Manceau, A., (1999) "Sorption of Metal Ions on Clay Minerals II Mechanism of Co Sorption on Hectorite at High and Low Ionic Strength and Impact on the Sorbent Stability" *J. Colloid Interface Sci.* **220**, 392.

Schlegel, M. L., Manceau, A., Charlet, L., (1997) "EXAFS Study of Zn and Zn EDTA Sorption at the Goethite (α-FeOOH)/Water Interface" *J. Phy. IV France* 7 823.

Schwertmann, U., and Cornell, R. M. (1991) "Iron oxides in the Laboratory Preparation and Characterization" VCH, NY.

Schwertmann, U., and Taylor, R.M. (1989) "Iron oxides" *Minerals in Soil Environments*, 2nd edition, Soil Science of America, SSSA Book Series no. 1, WI, USA, 379.

Schwertmann, U., Friedl., J., Stanjek, H., "From Fe(III) Ions to Ferrihydrite and then to Hematite" *J. Colloid Interface Sci.* **209**, 215.

Schwertmann, U., Taylor, R. M., (1989) "*Iron Oxides*" Minerals in Soil Environments, 2nd Ed., Soil Science of America, SSSA Book Series No. 1, WI, USA, 379.

Shuman, L.M., (1977) "Adsorption of Zn by Fe and Al Hydrous Oxides as Influenced by Aging and pH" *Soil Sci. Soc. Am. J.* **41**, 703.

Sigg. L., Mason, Y., Ammann, A. A., Ulrich, A., (1999) "Behavior of Heavy Metals, Nutrients, and Major Components during Roof Runoff Filtration" *Environ. Sci. Technol.* **33**, 1588.

Simpson, T. W., Wen, Q., Yu, N., Clarke, D. R., (1998) "Kinetics of the Amorphous to γ to α Transformations in Aluminum Oxides, Effect of Crystallographic Orientation" *J. Am. Ceramic Soc.* **81**, 61.

Smith, J. M., Van Ness, H. C., "Introduction to Chemical Engineering Thermodynamics" 4th Ed., McGraw-Hill Book Co., N.Y.

Spadini, L., Manceau, A., Schindler, P.W., and Charlet, L. (1994) "Structure and Stability of Cd^{2+} Surface Complexes on Ferric Oxides, 1. Results from EXAFS Spectroscopy" *J. Colloid Interface Sci.* **168**, 73.

Sposito, G., (1986) "Geochemical Processes at Mineral Surface" (Eds. Davis, J. A., Hayes, K. F.), ACS symposium Series 323, Am. Chem. Soc. 217.

Sposito, G., (1998) "On Points of Zero Charge" *Environ. Sci. Technol.* **32**(19), 2815.

Stahl, R. S., James, B. R., (1991) "Zinc Sorption by Manganese-Oxide-Coated Sand as a Function of pH" *Soil. Sci. Soc. Am. J.* **55**, 1291.

Stern, E. A., (1976) "The Analysis of Materials by X-ray Absorption" *Sci. Am. Appl.* **23** (4), 96.

Stern, E. A., Ma, Y., Hanske-Petitpierre, O., Bouldin, C. E., (1992) Radial Distribution Function in X-ray Absorption Fine Structure, *Phys. Rev. B, Condens. Matter,* **46** (2), 687.

Strauss R., Brümmer, G.W., and Barrow, N.J. (1997) "Effects of Crystallinity of Goethite, I. Preparation and Properties of Goethites of Differing Crystallinity" *Eur. J. Soil Sci.* **48**, 87.

Strawn, D. G., Scheidegger, A. M., Sparks, D. L., (1998) "Kinetics and Mechanisms of Pb(II) Sorption and Desorption at the Aluminum Oxide-Water Interface" *Environ. Sci. Tech.* **32**, 2596.

Strawn, D. G., Sparks, D.L., (1999) "The Use of XAFS to Distinguish between Inner- and Outer-Sphere Lead Adsorption Complexes on Montmorillonite" *J. Colloid Interface Sci.* **216**, 257.

Stumm, W., (1992) "Chemistry of the Solid-Water Interface." Wiley, New York.

Stumm, W., and Morgan, J. (1996) "Aquatic Chemistry" 3rd Ed., Wiley, New York.

Stumm, W., Huang, C. P., Jenkins, S. R., (1970) "Specific Chemical Interaction Affecting the Stability of Dispersed Systems" *Croatica Chemica Acta* **42**, 223.

Swallow, C. K., Hume, D.N., and Morel F. M. M. (1980) "Sorption of Lead and Copper by Hydrous Ferric Oxide" *Environ. Sci. Technol.* **11**,1326.

Szulczewski, M. D., Helmke, P. A., Bleam, W. F., (1997) "Comparison of XANES Analyses and Extractions to Determine Chromium Speciation in Contaminated Soils" *Environ. Sci. Technol.* **31**, 2954.

Tamura, H., Furuichi, R., (1997) "Adsorption Affinity of Divalent Heavy Metal Ions for Metal Oxides Evaluated by Modeling with the Frumkin Isotherm" *J. Colloid Interface Sci.* **195**, 241.

Tamura, H., Katayama, N., Furuichi, R., (1996) "Modeling of Ion-Exchange Reactions on Metal Oxides with the Frumkin Isotherm. 1. Acid-Base and Charge Characteristics of MnO_2, TiO_2, Fe_3O_4, and Al_2O_3 Surfaces and Adsorption affinity of Alkali Metal Ions" *Environ. Sci. Tech.* **30**, 1198.

Tamura, H., Katayama, N., Furuichi, R., (1997) "The Co^{2+} Adsorption Properties of Al_2O_3, Fe_2O_3, Fe_3O_4, TiO_2, and MnO_2 Evaluated by Modeling with the Frumkin Isotherm" *J. Colloid Interface Sci.* **195**, 192.

Theis, T. L., Iyer, R., Ellis, S. K., (1992) "Evaluating a New Granular Iron Oxide for Removing Lead From Drinking Water" *J. AWWA* 101.

Tiller, K. G., Gerth, J., and Brümmer, G. (1984) "The Relative Affinities of Cd, Ni, and Zn for Different Soil Clay Fractions and Goethite" *Geoderma* **34**, 17.

Toran, L., Bryant, S., Saunders, J., Wheeler, A. F., (1998) "A Two-Tiered Approach to Reactive Transport, Application to Sr Mobility Under Variable pH" *Ground Water* **36**, 404.

Towle, S. N., Bargar, J. R., Brown Jr., G. E., Parks, G. A., (1997) "Surface Precipitation of Co(II)(aq) on Al_2O_3" *J. Colloid Interface Sci.* **187**, 62.

Towle, S. N., Bargar, J. R., Brown Jr., G. E., Parks, G. A., (1999) *J. Colloid Interface Sci.* **217**, 312.

Towle, S.N., Brown, G. E. Jr., Parks, G. A., (1999) "Sorption of Co(II) on Metal Oxide Surfaces I. Identification of Co(II)(aq) Adsorption Sites on the (110) and (001)

Surfaces of TiO_2 by Grazing-Incidence XAFS Spectroscopy" *J. Colloid Interface Sci.* **217**, 299.

Towle, S.N., Brown, G. E. Jr., Parks, G. A., (1999) "Sorption of Co(II) on Metal Oxide Surfaces II. Identification of Co(II)(aq) Adsorption Sites on the (0001) and (1102) Surfaces of α-Al_2O_3 by Grazing-Incidence XAFS Spectroscopy" *J. Colloid Interface Sci.* **217**, 312.

Trainor, T. P., Brown, G. E. Jr., Parks, G. A., (2000) "Adsorption and Precipitation of Aqueous Zn(II) an Alumina Powders" *J. Colloid Interface Sci.* **231**, 359.

U.S. EPA (1997) *Cleaning Up the Nation's Waste Sites, Markets and Technology Trends*, EPA 542-R-96-005A, Washington, DC.

Vaník, K., and Jedináková, V. (1986) "Adsorption of Ba ions on α-FeOOH" *J. Colloid Interface Sci.* **111**, 106.

Vulava, V. M.; Kretzschmar, R.; Rusch, U.; Grolimund, D.; Westall, J. C.; Borkovec, M. (2000) "Cation Competition in a Natural Subsurface Material, Modeling of Sorption Equilibria" *Environ. Sci. Technol.* **34**(11), 2149.

Waite, T. D., Davis, J. A., Payne, T. E., Waychunas, G. A., Xu, N., (1994) "Uranium(VI) Adsorption to Ferrihydrite, Application of a Surface Complexation Model" *Geochim. Cosmochim. Acta* **58**(24), 5465.

Waychunas, G. A., Rea, B. A., Fuller, C. C., David, J. A., (1993) "Wide Angle X-ray Scattering (WAXS) Study of "Two-line" Ferrihydrite Structure, Effect of Arsenate Sorption and Counterion Variation and Comparison with EXAFS Results" *Geochim. Cosmochim. Acta* **57**, 2251.

Weesner, F. J., Bleam, W. F., (1998) "Binding Characteristics of PB2+ on Anion-Modified and Pristine Hydrous Oxide Surfaces Studied by Electrophoretic Mobility and X-Ray Absorption Spectroscopy" *J. Colloid Interface Sci.* **205**, 380.

Weidler, G.P., Degovics, G., and Laggner, P. (1998) "Surface Roughness Created by Acidic Dissolution of Synthetic Goethite with SAXS and N_2 – Adsorption Isotherms" *J. Colloid Interface Sci* **197**, 1.

Wen, X., Qing, D., Tang, H., (1998) "Surface Complexation Model for the Heavy Metal Adsorption on Natural Sediment" *Environ. Sci. Technol.* **32**, 870.

Wilcke, W., Kaupenjohann, M., (1998) "Heavy Metal Distribution Between Soil Aggregate Core and Surface Fractions Along Gradients of Deposition from the Atmosphere" *Geoderma* **83**, 55.

Wong, J., (1986) "Extended X-ray Absorption Fine Structure, A Modern Structural Tool in Materials Science" *Matl. Sci. Eng.* **80**, 107.

Wyckoff, R. W. G., (1963) "*Crystal Structures, Volume 1*" 2nd Ed. John Wiley & Sons, New York.

Zachara, J. M., Smith S. C., and Fredrickson, J. K. (2000) "The Effect of Biogenic Fe(II)on the Stability and Sorption of Co(II)EDAT2- to Goethite and a Subsurface Sediment" *Geochim. Cosmochim. Acta* **64**(8), 1345.

Zasoki, R. J., and Burau, R. G. (1988) "Sorption and Sorptive Interactions of Cadmium and Zinc on Hydrous Manganese Oxide" *Soil Sci. Soc. Am. J.* **52**, 81.

Zeverbergen, C., Bradley, J. P., Reeuwijk, L. P. V., Shyam, A. K., Hjelmar, O., Comans, R. N. J., (1999) "Clay Formation and Metal Fixation During Weathering of Coal Fly Ash" *Environ. Sci.Tech.* **33**, 3405.